DISSERTATION

RESILIENCE OF TRANSPORTATION NETWORK DURING POST-EARTHQUAKE EMERGENCY RESPONSE AND RECOVERY STAGES

Submitted by

Yangyang Wu

Department of Civil and Environmental Engineering

In partial fulfillment of the requirements

For the Degree of Doctor of Philosophy

Colorado State University

Fort Collins, Colorado

Summer 2023

Doctoral Committee:

Advisor: Suren Chen

Thomas Bradley
Hussam Mahmoud
Gaofeng Jia

ABSTRACT

RESILIENCE OF TRANSPORTATION NETWORK DURING POST-EARTHQUAKE EMERGENCY RESPONSE AND RECOVERY STAGES

Earthquakes can cause casualty, injuries, and extensive infrastructure damages and significantly disrupt transportation networks. Disrupted transportation networks resulting from damaged bridges or debris may cause delays on emergency response activities and impact traffic efficiency and safety during the post-earthquake recovery stage. A functioning post-hazard transportation network is the backbone to support the effective emergency response and maintain efficient post-hazard recovery plans of the whole community. The main purpose of this dissertation is to model and improve the resilience performance of transportation networks during both post-earthquake emergency response and recovery stages. It is expected that the proposed methodologies in this dissertation will help making risk-informed decisions in terms of pre-hazard mitigation planning, emergency medical service management, and post-earthquake restoration planning to enhance the resilience of transportation networks. A suite of novel methodologies is proposed to evaluate and enhance the resilience performance of transportation networks subjected to major earthquakes in this dissertation. Firstly, a resilience modeling framework of traffic networks is developed to simulate the transportation performance during post-earthquake emergency medical response considering interactions between infrastructures, people, and hazard. Secondly, a new approach is proposed to quantify the comprehensive redundancy of transportation networks during post-earthquake emergency

medical response considering search-and-rescue efforts and life vitality decay. Thirdly, a methodology is proposed to evaluate the resilience performance of traffic networks in private-vehicle-based post-earthquake emergency medical response considering bridge failure, building debris, and emergency traffic flow. Fourthly, a novel methodology is proposed to assess the post-earthquake resilience of transportation networks considering link functionality, travel time and traffic safety. Finally, a model to simulate time-dependent resilience of degraded transportation networks during post-hazard recovery period is developed to incorporate the time-evolving travel demand of the community.

ACKNOWLEDGEMENTS

First, I want to express my great gratitude to my advisor, Professor Suren Chen, for offering me the precious opportunity to attend CSU and for his consistent guidance and support throughout my PhD study. This dissertation could not have been finished without his invaluable advice and assistance. Whenever I was struggling with my studies, Dr. Chen was always patient and supportive to help maintain my interest in research and critical thinking. I believe I will greatly benefit from such experience in the future.

I would also like to thank the esteemed committee members, Dr. Thomas Bradley, Dr. Hussam Mahmoud, and Dr. Gaofeng Jia. Their indispensable suggestions and comments have significantly elevated the quality of this dissertation.

I would also like to thank both my past and present fellow graduate students at Colorado State University, Dr. Yufen Zhou, Dr. Xiaoxiang Ma, Luke Chen, Dr. Guangyang Hou, Dr. Qiling Zou, Kaisen Yao, Ziluo Xiong, et al. They have provided me immense support in various aspects of my life, studies, and work. Collaborating and learning alongside them has been a great pleasure and honor.

I also like to acknowledge the financial support for my research provided by the Center for Risk-based Community Resilience Center sponsored by National Institute of Standards and Technology (NIST) (Award No. 70NANB15H044), and the Mountain-Plains Consortium, a University Transportation Center funded by the U.S. Department of Transportation.

Last but not the least, I wish to express my heartfelt appreciation to my family for their unwavering emotional support and continual encouragement. I am deeply grateful for their love throughout my journey.

TABLE OF CONTENTS

LIST OF TABLES

LIST OF FIGURES

CHAPTER 1 INTRODUCTION

1.1 Background

Disastrous natural hazards can cause extensive property damages, casualty, and injuries during very short time periods (Lu et al., 2019; and Liu et al., 2020). Following an earthquake, for example, some of the vulnerable buildings are destroyed or damaged and those residents who are severely injured may need immediate medical assistance and evacuation (Coburn et al. 1992). A functioning post-hazard transportation network is the backbone to support the effective emergency response, recovery efforts and resilience of the whole community. Disrupted transportation networks following hazards, such as damaged bridges or roadways, may reduce the accessibility and cause delay on emergency response efforts. Such delay can be extremely critical to those who suffer from severe injuries with dire needs of immediate medical assistance. Thus, more rational post-hazard performance assessment and planning of emergency medical services (EMS) through a disrupted transportation network become vital.

In the meantime, the blacked-out traffic signals may turn signalized intersections into all-way stops because of extensive power outages. Even worse, there can be a considerable amount of emergency traffic generated by dislocated residents and emergency response efforts. Therefore, compared to normal time, a realistic scenario of typical transportation systems following major earthquakes often exhibits some unique challenges such as considerable emergency traffic, degraded transportation infrastructures, and extensive "all-way stop intersections". All these challenges will cause severe delays in transporting injured people to hospitals and greatly hinder the emergency response efforts, particularly for those using private vehicles. Transporting injured residents using private vehicles has been found to be the most used method during post-earthquake emergency medical responses (Djalali et al., 2011; Kang et al., 2015; Hwang et al., 2001; Nia et al., 2008). Unlike emergency medical service (EMS) vehicles with travel privileges, private vehicles usually do not have the same privilege, limiting themselves to be part of regular post-hazard traffic. For these private vehicles, to avoid being jammed on few accessible routes following the "first-come, first-serve" rule at every blacked-out traffic signal, the existence of alternative or redundant routes is essential for transporting injured people to hospitals in a timely manner. Apparently, to appropriately evaluate and further improve the redundancy and resilience of the post-earthquake transportation networks by considering the above-mentioned unique challenges is critical to saving more lives following major earthquakes.

Moreover, post-earthquake transportation systems often experience various disruptions. Severely damaged links will totally obstruct the traffic, while mildly damaged links may cause traffic capacity reduction. In addition to increased trips to hospitals, post-earthquake traffic also exhibits other unique characteristics: (1) a considerable amount of trips by dislocated people following earthquakes; (2) numerous uncertainties associated with hazard intensity, bridge damage, and building debris, which can cause significant computational complexity on related quantifications. To make risk-informed decisions and planning of EMS efforts, an efficient approach to assess the traffic resilience performance during the post-disaster emergency response stage is needed to address the unique characteristics of post-earthquake traffic. To better simulate the traffic during the emergency medical response after earthquakes, it is significant to assess various disruptions and their impact on the emergency medical response efforts by the disrupted transportation network, particularly injuries transported by private vehicles.

Disruption of transportation systems will not only affect the emergency and rescue operations immediately after hazards, but also impact the transportation experience of the community residents during the recovery stage. Following an earthquake, for example, some vulnerable transportation infrastructures such as bridges can be severely damaged, which may lose partial to full functionality. One example was during the 2008 Wenchuan earthquake when extensive highway and bridge damages were reported in Sichuan Province, China (Hu et al. 2014). The extensive repairs of disrupted transportation infrastructures usually take months or even years following earthquakes to finish, making the transportation network in the region remain partially disrupted over an extended period during the long-term recovery stage (Blackman et al. 2017; Yi and Fu 2018). A timely recovery of a disrupted transportation network is of utmost importance because it cannot only help improving the traffic efficiency of the affected community, but also more importantly, expedite long-term recovery efforts of other critical infrastructures, e.g., communication, energy, and water systems, that are heavily dependent on effective transportation. Moreover, partially disrupted traffic networks over extended durations of repairs will create multiple work zones with considerably elevated vehicle crash risks, threatening the safety of both general drivers and those drivers involved in post-hazard recovery efforts (Yang et al. 2015). To strategically plan the long-term post-hazard recovery of disrupted transportation infrastructures requires rational performance modeling of disrupted transportation infrastructure networks and consideration of impacts on both traffic efficiency and safety.

Moreover, earthquakes may have significant and long-term impacts on the population and infrastructure of modern communities, both of which substantially affect the performance of the transportation networks. Major earthquakes often cause changes in population size and distribution in the communities, which may affect the travel demand and origin-destination (OD) conditions accordingly. For example, after an earthquake, some residents may have to be dislocated to other cities because of the damaged dwelling units and the lack of necessary living resources (Hazus 2020). These people may move back to the community along with the recovery of the lodging units, water, power, etc. The change in the population size can significantly affect the total travel demand of the community (Chang et al. 2012). In addition to those residents dislocated to other cities, some residents may be displaced to the short-term or long-term shelters located at different zones in the community and move back to their pre-hazard zones when their dwelling units are repaired. As a result, the community population is being redistributed extensively during the post-earthquake recovery stage, which may considerably affect the traffic OD conditions of the community. So, it is significant to incorporate the time-evolving feature of the travel demand when simulating the resilience performance of transportation networks during the post-earthquake recovery stage.

Thus, a rational post-hazard resilience performance assessment of disrupted transportation networks during post-earthquake emergency response and recovery stages is so significant that the stakeholders can make risk-informed decisions in terms of effective mitigation, emergency management, and reconstruction measures to protect transportation systems and further improve the resilience of the whole community. In the following section, a literature review of related topics will be made.

1.2 Literature review

The following literature review will include three parts: (1) resilience modeling of transportation network during post-earthquake emergency response stage; (2) resilience modeling of transportation network during post-earthquake recovery stage; and (3) risk-informed decision-making to increase transportation resilience.

1.2.1 Resilience modeling of transportation network during post-earthquake emergency response stage

1.2.1.1 Characteristics of post-earthquake emergency response stage

Other than the injured residents needing immediate medical assistance and extensively blacked-out traffic signal lights as introduced in Section 1.1, an urban traffic system exhibits unique characteristics in both capacity and demand perspectives immediately following major hazards like earthquakes (Liu et al. 2021; Liu et al. 2022; Somy et al. 2021; Zou & Chen 2021). On the one hand, natural hazards often cause damage and failure to various types of infrastructures, such as bridges, roads, residential buildings, and hospitals. The damaged bridges as well as building debris will significantly affect not only the road capacity, but also the traffic efficiency, such as travel time and speed, in a sophisticated way (Hou et al., 2022; Wang et al. 2022). Traditional traffic simulation tools and data-driven approaches, primarily developed for normal and intact roads, cannot provide reliable results of post-hazard disrupted traffic networks due to the lack of appropriate tools and sufficient site-specific data during the emergency response stage. Rationally predicting the traffic performance of disrupted road networks with reduced capacity has become a substantial challenge attracting considerable attention and efforts in recent years (Hou et al., 2022). On the other hand, following hazards like earthquakes, many people may be forced to relocate to other places, e.g., friends' homes and shelters, because of losing inhabitable areas and necessities such as dwelling units, drinking water, and electricity (Tamima and Chouinard 2016). In addition to the traffic involving these dislocated people, emergency response traffic, such as those for emergency medical service, firefighters, and emergency repair and recovery teams, will be on the roads right after the hazards and remain for an extended time with the progress of the emergency response and recovery efforts. Moreover, employees, students, shoppers, and people that are traveling for other purposes may return to their homes immediately after the earthquake (Kilanitis and Sextos 2019a). As a result, the traffic immediately following a major hazard often consists of emergency response traffic, and those by dislocated people and people with other immediate traveling demands, rather than typical commuting traffic in normal situations. Another unique characteristic in contrast to normal and long-term recovery traffic is that the traffic conditions in the emergency response stage change faster over time with higher uncertainties.

The injured residents caused by building damage who may need immediate medical assistance are typically transported to hospitals or emergency medical centers using two modes of transportation: EMS vehicles and private vehicles. There are two main differences between the two modes in terms of the transportation performance: EMS vehicles have driving privileges of passing road segments and traffic signal lights; and private vehicles can transport injured people to hospitals with a one-way trip. Emergency medical response using EMS vehicles is not affected by blacked-out signal lights, partially damaged road segments, and the traffic in the network. A well-connected network full of short paths is essential in the scenario of emergency medical response using EMS vehicles. On the contrary, emergency medical response based on private vehicles can be significantly affected by all the traffic disruptions: blacked-out traffic signals may turn signalized intersections into all-way stops; and roads with various disruptions and the considerable amount of emergency traffic may worsen the situation.

1.2.1.2 Transportation resilience focusing on connectivity

Although commendable progress (e.g., Wen et al. 2022; Wang and Yuen 2022; Yeh et al. 2021) has been made on studies of other transportation modes (e.g., airline, railway, maritime, etc.), the following discussions will mainly focus on road transportation. Most existing studies on resilience modeling of transportation networks focused on the network performance quantification. As an important performance index, transportation network reliability defines the probability that a traffic system can meet a specified level of performance under a certain condition (Wakabayashi and Iida 1992). Most of the existing research efforts on traffic networks primarily focused on the reliability of intact networks during nonemergency circumstances by investigating travel time (e.g., Mahmassani et al. 2013; Guo and Williams 2015; Clark and Walting 2005; Wu and Zhang 2016), connectivity (e.g., Guo and Williams 2015; D'este and Taylor 2003; Husdal 2004, Wakabayashi and Iida 1992; Jenelius et al. 2006; Kondo et al. 2012; Qian et al. 2012; Viriyasitavat et al. 2011; Beamon & Kotleba 2006; Horner & Widener 2011; Day 2014), traffic capacity (e.g., Chen et al. 2002), accessibility (e.g., Nicholson 2003; Kondo et al. 2012), and trip cost (e.g., Bell 2000).

There are some existing studies related to emergency response and post-hazard traffic systems, in which the connectivity level of the system was used as the primary performance indicator evaluated in a similar way as non-emergency connectivity studies (e.g., Aydin et al., 2018; Guo et al., 2015; Hadjidemetriou et al. 2021; Scott et al. 2006; Viriyasitava et al. 2011; Du and Nicholson 1997; Zhang et al. 2018; Merschman et al. 2020; Li and Zhou 2020). Mete and Zabinsky (2010) developed a stochastic optimization model of medical supply location and distribution and EMS vehicle transportation plan in disastrous conditions. Dalal and Üster (2017) and Üster and Dalal (2017) presented an emergency network design model that integrated relief and evacuation considering the uncertainties in disaster location and intensity. Nogal et al. (2015, 2016, 2017) proposed some frameworks for the resilience assessment of transportation networks against extreme weather events and perturbations. Cost increment, user stress level, system impedance and fragility curves of the traffic network were considered in the methodology. They also studied the uncertainties in the traffic demand, local vulnerability and capacity of user response and developed the early warning system, and decision support tools for the quick restoration of networks. Ganin et al. (2017) defined the transportation network resilience as the change in the average annual delay per peak-period auto commuter resulting from roadway disruptions and compared the scenarios of different cities. Liao and Hu (2018) proposed a framework to assess the transportation resilience based on traffic conditions and emergency management and derived the prioritization in the preparedness and recovery activities under budget constraints. Edrissi et al. (2015) proposed a disaster-based transportation network model based on connectivity and travel time and used death toll as the performance indicator. Zhou et al. (2019) proposed the concepts of "global connectivity" and "local connectivity" to consider both the connection extent of the whole transportation network and the distance between each node to its neighbors and evaluated the system efficiency using percolation theory. Boakye et al. (2022) proposed a framework to evaluate the role of transportation network in terms of natural disasters' impact on communities. They quantified the community well-being and distributive social justice and defined an indicator based on the network's capability to "maintain health". The metrics were defined based on the connectivity theory and the shortest path between injured people and medical resources. Wu and Chen (2019) proposed a framework to assess the accessibility of injured residents to hospitals or EMS centers, considering the interactions among hazards, infrastructure, and EMS efforts. They used the total transportation network usage time from the beginning to the end of the EMS efforts to develop the resilience index and link importance indicator. Also, they investigated the optimal location for an extra EMS center based on the proposed metrics.

1.2.1.3 Transportation resilience focusing on network redundancy and emergency traffic

Rapidity, robustness, redundancy, and resourcefulness were popular indexes when simulating community resilience (e.g., Wang and van de Lindt, 2021; Wang et al. 2021; Cimellaro et al. 2010; Zou and Chen 2019). Other than the studies focusing on the connectivity and accessibility of transportation networks, there have been some interesting studies focusing on the network redundancy and even the traffic flow during the emergency response following hazards like earthquakes. Cimellaro et al. (2010) developed the resilience model of the acute care facilities based on the normalized waiting time and the distinction between the waiting time before and after the disaster happens and extended the resilience concept to the hospital network at the community level. Ip and Wang (2011) and Zhang and Wang (2016) proposed a new network performance metric called weighted independent pathway that can consider the redundancy level of roadways in a network. Their models considered network topology, traffic demands, and the uncertainties in infrastructure fragility, demonstrating considerable merits in redundancy quantification. However, the independent pathway is not sufficient to consider the effect of every single link/roadway on the network performance. Except for independent paths without any shared edges, those paths with shared edges can also provide extra redundancy to the system. Wu and Chen (2023a) introduced a methodology to fully consider the redundancy of transportation systems during the emergency response period based on the equivalent resistance theory and applied the emergency medical demand of different zones as the weighing factor. Feng et al. (2020) proposed a scenario-based methodology to model the performance of a transportation network during the post-earthquake emergency response stage using an agent-based model. The model considered abrupt destination changes, driving behavior after a major earthquake, lack of traffic information, and decreased traffic capacity due to infrastructure damages.

1.2.2 Resilience modeling of transportation network during post-earthquake recovery stage

The recovery stage is a vital stage after hazards, and some progress has been made in terms of the resilience modeling of transportation networks during this stage with focuses on general traffic simulation (e.g., Chang et al. 2012), infrastructure deterioration (e.g., Alipour and Shafei 2016), microscopic simulation and travel safety (e.g., Wu et al. 2021), OD-grid capacity (e.g., Pan et al. 2022), elaborated recovery optimization and time-dependent index (e.g., Zhang et al. 2022; Li et al. 2019), metro system (e.g., Zheng et al. 2022), large networks (e.g., Wandelt et al. 2021) and link importance factors (e.g., Gauthier et al. 2018), etc. Among the many studies focusing on the post-disaster performance modeling of transportation networks (e.g., Kozin and Zhou 1990; Wakabayashi & Kameda 1992; Chang and Nojima 2001; Zamanifar & Seyedhoseyni 2017; and Sun et al 2020), some of them paid attention to the resilience analysis and modeling of critical transportation infrastructures. Akiyama et al. (2020) investigated the importance of bridges considering both independent and interrelated hazards on bridges by developing a life-cycle reliability and risk approach to assess bridge and networks under various hazards like earthquakes, tsunami, and corrosion. Dong & Frangopol (2015) estimated the risk and resilience of bridges under earthquakes by proposing an approach to improve bridge mitigation under hazards. Besides the mainshocks, they also investigated the impact of aftershocks on the bridge resilience, and concluded aftershocks have significant effects on bridge repair loss and residual functionality. Argyroudis et al. (2020) proposed an integrated framework to account for the nature and sequence of multiple hazards and their effects and to quantify the resilience of critical transportation infrastructures subjected to hazards considering the structural vulnerability and recovery rapidity.

In recent years, more and more researchers incorporated travel demand and traffic assignment methods into their works when simulating the resilience and performance of transportation networks during post-earthquake recovery period. Kameshwar et al. (2020) developed a bridge restoration model based on decision trees to assess the performance of regional road networks under extreme events to provide a detailed assessment of bridge functionality and traffic restriction and derived the traffic capacity of disrupted links based on the Highway Capacity Manual. Wu et al. (2021) introduced a resilience indicator by considering both travel time and safety for assessing transportation networks during the extended recovery phase following an earthquake. The researchers examined the impact of partially closed links resulting from severe bridge damage on travel time and traffic safety. They employed static traffic assignment and the Poisson regression model to derive the travel time and traffic accident frequency. The study assumed that the travel demand during the long-term recovery stage is the same as the pre-hazard level. Some researchers suggested deriving the travel demand during the post-earthquake recovery stage by applying modification factors based on seismic intensity, building damage, or network capacity (Kiremidjian et al. 2007; Shinozuka et al. 2008; and Zhou et al. 2010). These travel demand modification methods have been followed by some studies when simulating transportation resilience. Alipour and Shafei (2016) examined the influence of deteriorating components on network resilience. They developed a framework that considered the degradation of components over time and its consequential impact on the network functionality. By applying this framework to the transportation network in San Francisco Bay Area, they utilized historical seismic activity data along with current estimates of component deterioration. They used reduction ratios for different trip purposes as functions of peak ground accelerations.

Chang et al. (2012) introduced an in-depth exploration of modeling approaches for assessing transportation networks in the aftermath of earthquakes. The authors delved into various methodologies for damage assessment, network performance evaluation, and recovery planning. They introduced modification factors for trip production and attraction based on different functionalities and hazard scenarios of the zones. They also adopted the classic gravity model to estimate the changed travel demand during the post-earthquake stage. Most of these studies were based on the modified but fixed travel demand of the network and did not capture the time-evolving nature of the travel demand during the recovery stage. Some studies considered the time-evolving feature of travel demand during the post-earthquake recovery stage (Zhou et al. 2010; Kilanitis and Sextos 2019b). Kilanitis and Sextos (2019b) investigated the effects of earthquake-induced bridge damage and time-varying traffic demand on the resilience of road networks when simulating post-earthquake transportation network resilience. The study focused on the interaction between the network capacity and the trip generation during post-earthquake scenarios, based on which they introduced a trip reduction factor to simulate the time-evolving travel demand.

1.2.3 Risk-informed decision-making to increase transportation resilience

1.2.3.1 Pre-earthquake mitigation planning

There have been some efforts on improving community resilience through pre-hazard mitigation (e.g., Zhang et al. 2018; Wang and Jia 2020; Zhang and Alipour 2020). Freckleton et al. (2012) and Edrissi et al. (2015) proposed a methodology to help decision-makers identify specific weaknesses within the network so that pre-disaster improvement projects are prioritized appropriately. Chandrasekaran and Banerjee (2016) applied a multi-objective evolutionary algorithm to determine the optimal retrofit design considering resilience and limited budget, with which different retrofit methods were investigated on bridges suffering multiple hazards. Zhang and Wang (2016) developed a project ranking methodology to prioritize transportation network retrofit projects and built a decision-making model to select the optimal new construction plan based on their proposed resilience metric. Wu and Chen (2019) proposed a link importance factor based on the performance of traffic networks during the emergency medical response to prioritize the most significant links to the network. Merschman et al. (2020) prioritized the bridge repair using three performance measures: total travel distance and time, bridge importance based on connectivity, and a social measure in terms of the accessibility to emergency facilities. The bridge importance measure is defined from the topology of the network and shortest paths. Wang & Jia (2019) proposed an efficient sample-based approach to estimate a probabilistic sensitivity measure of the network that yields bridge importance rankings for pre-earthquake risk mitigation priorities. The methodology incorporated the uncertainties in hazards and bridge damage states and enabled effective search of the mitigation strategies within a small subset. Also, they considered the partial functionality of disrupted links by assuming different levels of capacity according to damage states.

1.2.3.2 Post-earthquake reconstruction planning

In addition to studies focusing on pre-hazard mitigation planning, there have also been some studies focusing on post-hazard reconstruction planning. Most of the studies optimized the post-earthquake restoration based on the network performance or resilience and information about infrastructure repair time, limited resources, and contractors (e.g., Chen and Tzeng 1999; Cho et al., 2000; Orabi et al., 2009, 2010; and El-Anwar et al., 2015). Bocchini & Frangopol (2012a) presented an optimization for the repair activities of the bridges in a transportation network that were severely damaged by an earthquake. The study adopted three conflicting objectives: maximizing network resilience, minimizing the time and total costs, and provided an entire set of Pareto solutions to the optimization. Bocchini & Frangopol (2012b) built a model to prioritize the intervention of bridges along a highway segment by incorporating both travel time and distance into the resilience indicator and conducting the optimization with two conflicting objectives: resilience and cost. Zhao & Zhang (2020) proposed a bi-objective and bi-level optimization framework to optimize the transportation infrastructure restoration plan. They took the unmet demand and total travel time as performance measures and solved the optimization using elastic user equilibrium and a modified active set algorithm. Liu et al. (2020) considered the reduced traffic carrying capacity of damaged links and proposed a modified network robustness index as the resilience measure to prioritize the network recovery using a two-stage optimization method. The traffic capacities of damaged links were assumed to be determined through communication with stakeholders.

1.3 Current research gaps

1.3.1 Interactions between infrastructure, people, EMS, and hazards during post-earthquake emergency medical response

There are some limitations of most existing studies in Section 1.2.1 (Novak and Sullivan 2014): (1) the complex interactions between vulnerabilities of transportation infrastructure, people, EMS and hazards have not been systematically modeled; (2) the limited resources during emergency response, such as personnel and vehicles, have not been realistically incorporated; (3) most of the existing studies focused on recovery with limited information of critical links, which are substantial to the pre-hazard mitigation or reinforcement prioritization in the prevention stage (Edrissi et al. 2015; Holguín-Veras et al. 2014, Miller-Hooks et al. 2012).

1.3.2 Holistic model to simulate full redundancy of transportation network to support post-earthquake emergency medical response

Most studies as discussed in Section 1.2.1 cannot be used to simulate the realistic disrupted scenarios introduced in Section 1.2.1. Holistic models were not available to support the post-earthquake emergency medical response by considering these disrupted scenarios. For the realistic scenarios as discussed previously, extensive blacked-out traffic signals, considerable emergency traffic, and a high number of private-vehicle-based hospitalization trips may happen simultaneously during the emergency response stage. For the commonly used static traffic assignment models, it is challenging for them to simulate the unstable traffic demand and the "all-way stop intersections". Although the accessibility and connectivity methods can help recognize the shortest paths, the existence of alternative/redundant routes may be more critical during the emergency medical response. The weighted independent pathway theory improved the redundancy quantification, but it did not consider the impact of the connecting/bridging links between independent pathways on system redundancy. The dynamic traffic assignment (DTA) methods may be used to model the unstable traffic demand. However, the application with DTA is so complex that only scenario-based analysis is feasible so far (Feng et al. 2020).

1.3.3 Travel demand estimation and traffic flow simulation during post-earthquake emergency medical response

Although EMS vehicles play an essential role in people's daily life and some disastrous events, private-vehicle-based injury transporting has been recognized as the primary mode during the emergency response periods following major natural hazards like earthquakes (Djalali et al., 2011; Kang et al., 2015; Hwang et al., 2001; Nia et al., 2008). Unlike emergency vehicles with driving privileges, personal cars will become part of regular post-disaster traffic in the emergency response stage. EMS efforts based on private vehicles deserve more attention partly because of the relatively significant role in the overall EMS efforts and higher vulnerability of experiencing more delay, which can be substantially affected by various traffic disruptions. As summarized in Section 1.2.1, existing studies on transportation performance resilience during the emergency response stage did not reasonably estimate the emergency travel demand and simulate the traffic flow, especially when the traffic in the emergency response stage experiences considerable variations over time.

1.3.4 Link functionality quantification and work zone traffic simulation during post-earthquake recovery stage

Most studies as summarized in Section 1.2.2 have several major limitations: (1) most of the studies considered either fully closed or fully opened links in terms of the functionality of traffic networks following hazards. As discussed earlier, the time-progressive restoration processes of infrastructures (e.g., severely damaged bridges or roads) following earthquakes usually take rather long time. It is very common that some roads or bridges may only remain open for some lanes for certain time periods, especially given the common shortage of available restoration resources. Assumptions of instantaneous repair and recovery made in many existing studies were not realistic, which directly affect the accuracy and rationality of related traffic performance assessment and prioritization decisions during the long-term recovery stage. Although some studies have related the bridge traffic restrictions to the bridge functionality levels based on the Highway Capacity Manual (Kameshwar et al. 2020), they didn't consider the effects of bridge length and flow merging and diverging on link travel time, which are very important for simulating the traffic performance of partially closed links. A methodology to rationally assess the traffic performance on transportation networks with various levels of disruptions between a fully closed and fully opened stages is still lacking; (2) as discussed earlier, a partially disrupted transportation network (e.g., bridges and roads with limited lanes open) not only affects travel time, but also creates multiple work-zone scenarios and results in merging and diverging of link traffic flows, which considerably increase vehicle crash risks. (Yang et al. 2015). Therefore, for traffic planning in the long-term recovery stage following earthquakes, both travel time and safety risks should be appropriately considered for partially disrupted traffic networks; (3) uncertainties associated with hazards and bridge fragility affect the long-term recovery stage, which have been rarely incorporated into the existing studies of traffic performance (e.g., time and safety). In addition, post-disaster repair priority of the vulnerable bridges is related not only to the network topology and infrastructure location but also to the seismic uncertainty, travel demand, traffic efficiency and safety. So, for the traffic performance assessment and post-disaster restoration prioritization, uncertainties should be carefully incorporated.

1.3.5 Time-dependent transportation resilience based on time-evolving travel demand during post-earthquake recovery stage

Most of these studies summarized in Section 1.2.2 either used the pre-hazard travel demand or applied a reduction or modification factor to quantify the number of trips during the post-earthquake recovery stage. These simplifications may differ from reality when simulating the performance of transportation networks, especially during the post-earthquake recovery stage after disastrous hazards. After major earthquakes, the time-evolving community population and travel demand may change drastically, which may differ significantly from the pre-hazard community. Thus, transportation resilience modeling and reconstruction planning based on a specific ratio of the pre-hazard travel demand may not reflect the unique characteristics of the transportation during the recovery stage. It would be desirable to incorporate the time-dependent OD demand into the simulation to rationally assess the transportation performance and resilience during the post-earthquake recovery stage. Moreover, the reconstruction planning of damaged transportation infrastructures was not properly conducted. As mentioned above, the reconstruction planning should focus on meeting the actual demands of the current/remaining and future/recovering residents like urban planning.

However, the reconstruction plans in existing studies were based on approximated travel demands as a certain ratio of the pre-hazard OD demand instead of using reasonably estimated time-evolving data.

1.4 Research objectives of this dissertation

Disruption of transportation systems by earthquakes will impact the post-earthquake emergency response and long-term recovery of the attacked community. Transportation systems are easily degraded in the link level (e.g., traffic capacity and safety) and network level (e.g., network connectivity, network redundancy, and travel demand) during both the emergency response and the recovery stages. Also, a reasonably estimated travel demand during both stages is significant for transportation resilience. As discussed in Section 1.3, previous studies to assess transportation resilience in these stages are not sufficient given their limitations in modeling methodologies. Therefore, this dissertation will focus on developing resilience simulation frameworks of transportation networks subjected to earthquakes during the two stages. It aims to (1) develop traffic resilience performance assessment frameworks to simulation multiple interactions, comprehensive network redundancy, and emergency travel demand during the emergency response stage; (2) develop transportation resilience assessment frameworks to simulate link functionality with work zones and the time-evolving travel demand of the attacked community during the recovery stage. Specifically, the research objectives of the current dissertation are as follows:

The first objective is to develop a resilience modeling framework for traffic network in post-earthquake emergency medical response considering interactions between infrastructures, people, and hazard. This framework can help assess the transportation resilience performance during EMS vehicle-based emergency medical response and derive link importance factor for pre-hazard mitigation planning.

The second objective is to develop a resilience modeling methodology for transportation network during the post-earthquake emergency medical response with consideration of the extensively blacked-out traffic signal lights and private-vehicle-based injury transportation. The proposed methodology can quantify the comprehensive network redundancy and derive pre-hazard mitigation planning to support post-earthquake emergency medical response.

The third objective is to develop a traffic resilience modeling framework for post-earthquake emergency medical response and planning considering disrupted infrastructure, dislocated residents, and the services from both EMS and private vehicles. The developed methodology can help estimate emergency travel demand and investigate the reasonable number of EMS vehicles.

The fourth objective is to develop a post-earthquake resilience assessment model during the long-term recovery stage, considering link functionalities and work zone travel safety. The new model incorporates infrastructure damage uncertainties and can be used for long-term restoration prioritization of transportation networks.

The fifth objective is to develop a time-dependent transportation resilience modeling framework based on time-evolving travel demand during the post-earthquake recovery period. The proposed model can help people understand the importance of simulating community population and travel demand changes and can support post-earthquake bridge reconstruction planning.

1.5 Outline of the dissertation

The outline of the dissertation is as follows:

Chapter 1 provides the research background for this dissertation and presents the literature review on the related research topics. Meanwhile, the current research gaps for these research topics are identified, followed by the research objectives of this dissertation.

In Chapter 2, a transportation network's resilience-related performance following an earthquake is modeled with a focus on emergency medical services based on EMS vehicles. The model incorporates fragility information for buildings and bridges to assess the number and locations of individuals requiring emergency medical assistance and potential disruptions to network links. Two resilience performance indicators are introduced to evaluate the relative importance of different links within the traffic network and the overall efficiency of emergency medical response for the entire network. Subsequently, the proposed framework is demonstrated in a virtual community affected by a seismic event. A parametric study is conducted to examine the impact of critical model parameters under two earthquake intensity scenarios. Furthermore, the potential inclusion of a new EMS medical center is analyzed to identify optimal locations and potential outcomes.

In Chapter 3, a comprehensive methodology is developed to assess the resilience performance of a transportation network and facilitate pre-hazard mitigation planning, focusing on post-earthquake emergency medical response based on private vehicles. The model incorporates seismic fragility information of infrastructure and utilizes the Monte Carlo Sampling method to account for uncertainties, enabling the quantification of residents who may require emergency medical services and potential damage scenarios to network links. A novel resilience performance indicator is introduced to evaluate the efficiency, redundancy, and overall emergency medical response performance of the entire transportation network. The effectiveness of the proposed methodology is demonstrated in Shelby County, Tennessee. A parametric study is conducted to examine the effects of Richter magnitude on the injured population, saved population, and resilience index. Additionally, an optimization process is employed to strengthen bridges prior to hazards, considering the detailed budget information and resilience index.

In Chapter 4, a framework is developed to model the resilience performance of transportation systems during the emergency medical response phase following an earthquake, specifically from the perspective of emergency medical services based on both EMS and private vehicles. The framework considers the impact of emergency dislocation traffic and infrastructure disruption. To capture various uncertainties in ground motion, infrastructure damage states, debris distribution, and road disruption, the study incorporates the seismic fragility of infrastructures and utilizes the Latin Hypercube Sampling method to generate numerous potential scenarios. This chapter adopts a dynamic traffic assignment method to simulate the flow of emergency traffic and the time-dependent delays in the injury transport system, which relies on private vehicles. A new resilience indicator is introduced to assess the efficiency of the transportation network and the performance of the emergency medical response within the affected community. Finally, the proposed model is demonstrated in a virtual community, and a comparative study is conducted to examine the differences between the dynamic and static traffic assignment methods.

In Chapter 5, a framework is developed to model the resilience-related performance of a transportation network, considering both travel time and traffic safety perspectives. The model considers uncertainties in earthquake information and bridge fragility to simulate realistic earthquake scenarios, including potential bridge disconnections or partial functionality. An introduced resilience performance indicator evaluates the overall travel time and safety performance of the entire network, while a bridge restoration prioritization index assesses the relative priorities for restoring different bridges within the traffic network. Finally, the proposed framework is demonstrated in a hypothetical community located in earthquake-prone areas.

In Chapter 6, a framework is developed to model the time-dependent resilience performance of transportation networks during the recovery stage following an earthquake, with a specific focus on enhancing the transportation experience for both current and future residents of the affected community. To account for uncertainties in bridge damage scenarios, the study incorporates the seismic attenuation law, bridge fragility functions, and employs the Latin Hypercube sampling method to generate multiple disruption scenarios within the network. Additionally, building fragility functions, recovery information, community demographics, and the Metropolitan Planning Organization model are utilized to estimate the evolving community population and travel demand over time. To simulate traffic efficiency and travel safety during the recovery stage, a modified Bureau of Public Roads function for work zones, the static traffic assignment method, and a work-zone traffic accident model are employed, specifically considering the morning rush hour traffic. A novel time-dependent resilience index is introduced to assess the transportation performance experienced by the evolving community residents throughout the recovery period. Finally, the proposed methodology is demonstrated in Shelby County, Tennessee, and a comparative analysis is conducted during the reconstruction planning phase to examine the impact of optimal reconstruction plans on transportation resilience in the post-earthquake recovery stage.

Chapter 7 concludes the dissertation by highlighting the major findings and suggesting some future research directions.

CHAPTER 2 RESILIENCE MODELING FRAMEWORK OF TRAFFIC NETWORK IN POST-EARTHQUAKE EMERGENCY MEDICAL RESPONSE CONSIDERING INTERACTIONS BETWEEN INFRASTRUCTURES, PEOPLE AND HAZARD0F[1]

2.1 Introduction

An efficient and timely rescue of injured people by emergency medical services (EMS) is essential to saving as many lives as possible following disasters. Disrupted traffic networks due to the failures of transportation infrastructure (e.g., bridges) following major hazards like earthquakes affect the accessibility and travel time of the disrupted transportation network during the emergency response stage. A rational prediction of the traffic network resilience performance in terms of EMS cannot only help implementing optimized post-disaster medical response plan, but also identify the most cost-effective preventive measures before the occurrence of disasters. Post-hazard EMS transportation highly depends on both medical needs of the vulnerable group and the serviceability of the disrupted traffic network. A framework to assess the resilience performance of a typical traffic network in terms of post-earthquake EMS is developed by considering the complex interactions between building infrastructures, injured people, vulnerable medical centers, EMS vehicles, disrupted traffic network and natural hazards. Two resilience performance indicators are introduced characterizing the relative importance of different links in a traffic network and overall EMS resilience for the whole network. A virtual community is selected as the prototype to demonstrate the proposed framework, which is followed by a parametric study of the earthquake magnitude, different types

---

[1] This chapter is adapted from a published paper by the author (Wu and Chen. 2019) with permission from Taylor & Francis.

of bridges, location and number of medical centers, and optimal location for a new medical center facility. The proposed framework and resilience performance indicators can help establishing more efficient pre-disaster improvement plan of critical links, prioritizing post-disaster recovery, and optimizing the strategic placement and resource allocation of EMS medical center.

This chapter aims to build a framework to assess the resilience performance of a typical traffic network in terms of post-earthquake EMS by comprehensively capturing the interactions between building infrastructures, injured people who may need EMS, disrupted traffic network, limited EMS resources and specific hazard. Two resilience performance indicators are introduced to evaluate the relative importance of different links in a traffic network and overall emergency medical response resilience for the whole network. With the two indicators, both post-hazard recovery strategies and pre-hazard prevention measures with the constraints of limited resources can be made. The proposed framework is demonstrated through a traffic network system with 20 zones, 33 links and 9 bridges in earthquake-prone areas, followed by detailed parametric analyses.

2.2 Model description

As shown in Fig 2.1, the proposed framework adopts the fragilities of bridges and buildings to obtain the failure rates of those structures following the occurrence of the hazard to derive the information about the network connectivity ("supply") and the number and locations of vulnerable people who need medical assistance ("demand"), respectively. The states of a traffic network after a disaster and the corresponding probability of occurrence for each state are calculated based on the failure rates of bridges. Similarly, the number and distribution of injured people that need EMS are estimated based on the failure probability of buildings as well as associated injury severities of each zone. In the proposed model, two resilience performance indicators specific to emergency response planning, evaluation and improvements are introduced: total rescue time of the network and link importance values. These resilience matrices for emergency medical response can be applied in several stages of disaster response, such as prevention, emergency response and recovery.

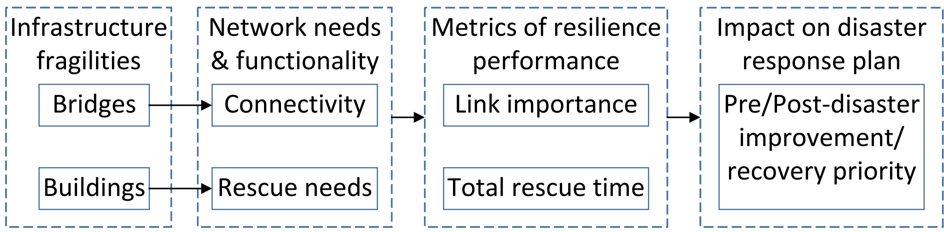

Figure 2.1 Flowchart of the modeling process

2.2.1 Seismic fragility of structures

The seismic fragility functions provide the conditional probability of exceeding a specified performance level given a set of seismic intensity measures e.g., peak ground acceleration (PGA), spectral acceleration (SA), spectral displacement (SD), etc. The failure in terms of a limit state is defined as an excess of the limiting value of the performance indicator, such as stress and displacement of structures. There are many sources of uncertainties affecting the accuracy of the structural capacity and in turn the ground acceleration capacity for structures significantly. As a result, the seismic fragility of structures is usually presented as fragility curve(s) with an assigned probability to describe the confidence level associated with the estimation of fragility for each limit state.

For bridges, there are typically several different limit (damage) states, for example, no damage or slight/ minor damage, moderate damage, extensive damage, and complete damage (e.g., Choi et al. 2004). For each damage state, its probability is the difference between fragility curves corresponding to different limit state functions. In a region with different types of bridges (e.g., multi-span continuous slab/ concrete/

steel bridges, and reinforced concrete columns), the fragilities are also different for different bridge types (e.g., Choi et al. 2004, Gardoni et al. 2002 & 2003, Neilson and DesRoches 2007). From the perspective of emergency response of traffic networks involving bridges, a linkage needs to be built between the emergency management decision of a bridge (e.g., closure, partial closure or open) and the physical damage state.

In addition to bridges, researchers have conducted extensive studies on the seismic fragility of typical buildings in a similar way (e.g., Reinhorn et al. 2001, Jaiswal et al. 2011). The seismic fragility of typical buildings can be used to estimate the injury severities of people residing in these buildings. The failures of the residential, commercial, and industrial buildings are further related to the injured population with existing knowledge about the occupancy, trapped and injured people. The details will be introduced in the next section.

2.2.2 Estimation of vulnerable people who may need EMS

According to some existing studies (e.g., Coburn et al. 1992), the injured population of a building zone is related to the building collapse rate, occupancy rate, trapped rate and injury rate. The failure rate of buildings under a given earthquake can be obtained through their seismic fragility performance as introduced in the previous section. The injured group of people can be quantified based on the population, average occupancy, building failure rate, trapped rate and injury rate (Coburn et al. 1992):

$$\mathrm{b_z} = \sum_u \mathrm{Pop_z} * \mathrm{P_u} * \mathrm{M_1^z} * \mathrm{M_2^u} * \mathrm{M_3^u} \tag{2.1}$$

where $\mathrm{b_z}$ is the number of injured people of a given zone z; $\mathrm{Pop_z}$ is the population of a given community or zone z; $\mathrm{P_u}$ is the collapse probability of buildings type u. $\mathrm{M_1^z}$ is the average building occupancy of zone z and $\mathrm{M_2^u}$ is the trapped rate of occupants in the collapse of building type u. $\mathrm{M_3^u}$ is the injury rate among the trapped population of building type u. M_1^z is related to the condition of the zone and different time during a day. For instance, for residential zones, the occupancy rates are relatively low at daytime, but high at nighttime, while they are opposite for the non-residential zones in urban places. M_2^u and M_3^u are related to the building type and the earthquake intensity. Usually, the higher intensity the earthquake is, the higher trapped and injury rates are of the same type of buildings.

2.2.3 Resilience index and link importance values

After an earthquake has occurred, the rescue time is an important factor to evaluate the effectiveness and success of emergency response efforts. The longer time it takes to rescue all the injured people, the higher potential death toll may be. Therefore, the total rescue time of the network is used as the performance indicator of the traffic system in terms of emergency medical response, which needs to be minimized. The total rescue time is defined here as the total travel time on the roads of the round trip between the medical center and the site to pick up injuries. It does not include the delay time during the EMS process (e.g., temporary on-site medical care, and transporting patients out of the buildings), which is assumed to be the same for all EMS trips in this study. After an earthquake, there are typically several damage states for a traffic system ranging from various damages of bridges or roadways, etc. In this framework, only the bridge and medical center failures are considered as damage states of the traffic system and each bridge will be in either "no failure" or "failure" states. Also, the medical centers are vulnerable under earthquakes and each medical center will be in either "full functionality" or "close for maintenance". If there are $n1$ bridges and $n2$ medical centers in the system, there will thus be totally $2^{(n1+n2)}$ possible states of the traffic system after an earthquake.

The emergency response performance can be assessed with optimizations on the total rescue time made for every possible state after an earthquake.

Objective: $$\mathrm{T_s} = \min_{\boldsymbol{x}}\{\max_{\mathrm{p}}[\mathrm{T_s^p}(\boldsymbol{x})]\} \tag{2.2}$$

Constraints: $$\mathrm{T_s^p}(\boldsymbol{x}) = \sum_{\mathrm{z}}\left(\frac{\boldsymbol{x}_{\mathrm{s}}^{\mathrm{p,z}}}{\mathrm{N_p}} \cdot \mathrm{t_s^{p,z}}\right) \tag{2.3}$$

$$\sum_{\mathrm{z}} \boldsymbol{x}_{\mathrm{s}}^{\mathrm{p,z}} \leq \mathrm{w_p} \quad \forall \mathrm{p,z} \in \boldsymbol{N} \tag{2.4}$$

$$\sum_{\mathrm{p}} \boldsymbol{x}_{\mathrm{s}}^{\mathrm{p,z}} = \mathrm{b_z} \quad \forall \mathrm{p,z} \in \boldsymbol{N} \tag{2.5}$$

$$\boldsymbol{x}_{\mathrm{s}}^{\mathrm{p,z}} \geq 0 \text{ and } \boldsymbol{x}_{\mathrm{s}}^{\mathrm{p,z}} \in \boldsymbol{Z} \tag{2.6}$$

where $\mathrm{T_s}$ is the optimal rescue time of the system under a certain state $\mathrm{s} \in \mathrm{K}$ (K is the set of possible network states after an earthquake); $\max_{\mathrm{p}}[\mathrm{T_s^p}(\boldsymbol{x})]$ is the longest rescue time among all the EMS centers and is defined as the rescue time of the system under network state s; $\mathrm{T_s^p}$ is the rescue time of EMS medical center in zone p under network state s; $\mathrm{t_s^{p,z}}$ is the round trip travel time from zone p to zone z under a certain network state s. $\mathrm{x_s^{p,z}}$ is the number of injured people being picked up from zone z and transported to the EMS medical center in zone p and $\mathrm{w_p}$ is the capacity of the EMS medical center located in zone p. $\mathrm{N_p}$ is the number of EMS vehicles for EMS medical center in zone p and $\boldsymbol{Z}$ is the set of integer numbers. The objective of this optimization is to minimize the total rescue time of the whole system. Eqs. (2.2-2.6) ensure that (1) the injured people are distributed to different medical centers in a balanced way so that every medical center can finish rescuing effort around similar time, and (2) the overall rescue process is as quick as possible to save most lives.

Based on the optimization results from Eqs. (2.2)-(2.6), the resilience index of the traffic system is defined as:

$$\mathrm{RI}(\varepsilon) = \sum_{s=1}^{|K|} \mathrm{P}\left\{\frac{\mathrm{T}_0}{\mathrm{T}_s} \geq \varepsilon\right\} \tag{2.7}$$

where T_0 is the optimal rescue time of the system when all the links are intact, and all of the medical centers remain full serviceability. ε is the level of functionality (LOF) criterion of the traffic system after an earthquake, which is a ratio between 0 and 1 to assess whether the reduced emergency response performance due to possible infrastructure disruptions is acceptable. ε is usually specified by the stakeholders as a subjective criterion.

In addition to the overall emergency response performance indicator, link importance value is very useful in terms of identifying the critical links from the perspective of EMS. Such information can be used to prioritize the reinforcement of the links before a hazard occurs or emergency repair of damaged bridges immediately following the hazard to maximize the emergency response efficiency. The link importance of any link may be defined as the impact on the resilience index if that link fails. The more the resilience index drops once a link fails, the more critical that the link is to the EMS. To derive the link importance factor I_{ij} , the sample space of T_s is divided into subset ① where link (i, j) works and subset ② where link (i, j) fails (Edrissi et al. 2015). RI_{+ij} and RI_{-ij} are the resilience indices of subsets ① and ② respectively. Considering that $\mathrm{RI}_{+ij} \geq \mathrm{RI}_{-ij}$ and the link importance is negatively related to $\frac{\mathrm{RI}_{-ij}}{\mathrm{RI}_{+ij}}$, the link importance value of link (i, j) is defined as:

$$\mathrm{I}_{ij} = 1 - \frac{\mathrm{RI}_{-ij}}{\mathrm{RI}_{+ij}} \tag{2.8}$$

which ensures that the link importance value $0 \leq \mathrm{I}_{ij} \leq 1$.

2.3 Case study of transportation network of Centerville

Fig. 2.2 shows the basic traffic network of a virtual community called Centerville, which has been used as a virtual test bed for several studies (Ellingwood et al. 2016). To demonstrate the proposed network under seismic hazards, this community is assumed to be in seismic-intensive regions. Some basic information of this network is shown in Table 2.1 and Table 2.2 and the length of each link is calculated from the longitudes and latitudes of the two nodes. For post-earthquake emergency response, the posted speed limits usually become irrelevant for privileged emergency vehicles. We assume conservatively the driving speeds of EMS vehicles are 30 mph for all the roads since there might be some debris, obstacles or partial damage on the roads following the earthquake that may lower the actual driving speeds of EMS vehicles. It is apparent more accurate driving speeds that are specific to road conditions, if available, can be easily applied to the proposed framework in the future. The travel time for each link is obtained based on the link length and the driving speed of EMS vehicles. Each of the 20 nodes forms a zone in the whole community. It is assumed there are two medical centers offering EMS in the network that locate in zone $\mathrm{R3}$ and zone $\mathrm{R5}$ (marked with stars in Fig. 2.2) and are in relatively central locations of the community with proximity to most of the nodes in the network. The two medical centers are special buildings and are considered as mid-rise concrete shear walls according to Hazus 1997. It is assumed in this study that a medical center will be closed for at least days if it experiences extensive or complete damages. Or it will remain full functionality. Zones $\mathrm{I1}-\mathrm{I7}$ are mainly residential areas and the rest zones are mainly non-residential areas: zones $\mathrm{P1}-\mathrm{P6}$ are mainly commercial areas and zones $\mathrm{R1}-\mathrm{R7}$ are mainly industrial areas. In this study, only bridge damage may cause the links being totally disconnected. The full closure caused by roadway damage due to earthquake is deemed rare and not considered in this study. Some possible minor or local damages on the roadways are reflected on relatively lower driving speeds of EMS vehicles throughout the network as introduced above. Nine out of thirty-three roads/links are therefore vulnerable to earthquakes due to the existence of bridges on these links (marked with the bridge symbols in Fig. 2.2). There are three types of bridges in the community: multi-span continuous (MSC) slab, concrete, and steel bridges. Given emergency medical response often occurs before transportation authorities can conduct comprehensive inspections of damaged bridges, it is conservatively assumed in this study that a bridge will be closed to traffic if it experiences extensive or complete damages as defined by the limit states. This is based on the understanding that a bridge may not remain opened either due to apparent impassable nature caused by severe physical damages or decisions made by drivers based on the observations of extensive damages on the bridges out of caution.

The parameters in Table 2.2 are determined based on the zonal information. There are two different types of building materials in the community, namely masonry and concrete. For residential buildings, masonry structures are more popular while concrete structures are more popular for non-residential buildings like commercial and industry buildings. We randomly generated the percentage of masonry building between 50%-100% for the residential zones and between 0-50% for the non-residential zones. Since this demonstrative example focuses on the movements of EMS vehicles, instead of the medical service capacity of medical centers, it is assumed that the total number of people that the two medical centers can accommodate is always higher than the total number of injured people being delivered by EMS vehicles. In other words, each medical center will accommodate every patient being delivered by EMS vehicles. According to the national ambulance statistics, there were 48,384 ambulances in US in 2008 when the population was 304.1 million in the United States (EMS Statistics, 2017; Population in the U.S. 2017).

To consider realistic emergency response resources, the total number of available EMS vehicles (Table 2.2) of the community is assumed based on its population with the same national ratio as illustrated above. The EMS vehicles are assigned to the two EMS medical centers roughly proportional to their capacities (total number of patients they can accommodate) so that all medical centers have the same "pick-up capability" (number of EMS vehicles/capacity).

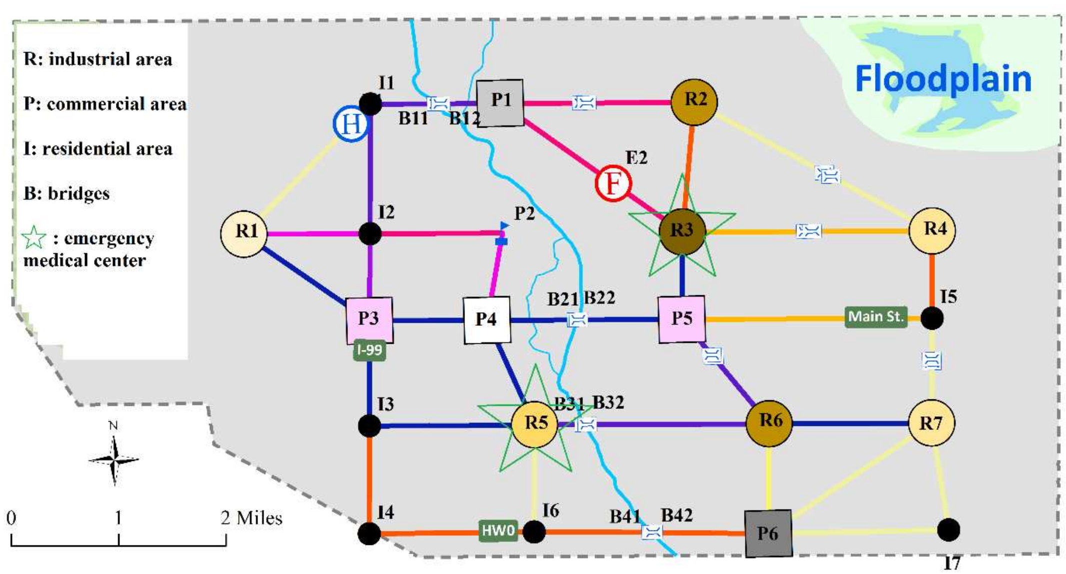

Figure 2.2 Traffic network of Centerville

Table 2.1 Link characteristics

Link#	Start zone	End zone	Length (km)	Travel time(min)	Bridges
1	I1	I2	1.9445	2.4306	0
2	I1	P1	1.594	1.9925	1 MSC-Slab
3	I1	R1	2.4817	3.1022	0
4	I2	P2	1.6246	2.0308	0
5	I2	P3	1.3118	1.6397	0
6	I2	R1	1.548	1.935	0
7	I3	I4	1.6205	2.0256	0
8	I3	P3	1.5741	1.9677	0

9	I3	R5	2.0231	2.5288	0
10	I4	I6	2.0231	2.5288	0
11	I5	P5	3.0653	3.8316	0
12	I5	R4	1.3118	1.6397	0
13	I5	R7	1.5741	1.9677	1 MSC-Concrete
14	I6	P6	2.8818	3.6023	1 MSC-Steel
15	I6	R5	1.605	2.0063	0
16	I7	P6	2.2073	2.7591	0
17	I7	R7	1.62	2.025	0
18	P1	R2	2.3757	2.9696	1 MSC- Slab
19	P1	R3	2.969	3.7113	0
20	P2	P4	1.324	1.6551	0
21	P3	P4	1.4407	1.8009	0
22	P3	R1	2.0321	2.5401	0
23	P4	P5	2.3909	2.9887	1 MSC- Concrete
24	P4	R5	1.6801	2.1001	0
25	P5	R3	1.3118	1.6397	0
26	P5	R6	1.9077	2.3847	1 MSC- Steel
27	P6	R6	1.6513	2.0641	0
28	P6	R7	2.5838	3.2297	0
29	R2	R3	1.9489	2.4362	0
30	R2	R4	3.5194	4.3993	1 MSC- Slab
31	R3	R4	3.0653	3.8317	1 MSC- Concrete
32	R5	R6	2.8813	3.6017	1 MSC- Steel
33	R6	R7	1.9924	2.4905	0

Table 2.2 Zone characteristics

Zone	Pop_z (person)	Masonry building	Concrete building	EMS	No. of EMS
I1	8423	59.442	40.558	-----	-----

I2	10256	45.819	54.181	-----	-----
I3	9389	52.313	47.687	-----	-----
I4	6960	61.32	38.68	-----	-----
I5	9454	59.307	40.693	-----	-----
I6	14310	62	38	-----	-----
I7	15140	56.91	43.09	-----	-----
P1	4174	0.01	99.99	-----	-----
P2	7666	37.5	62.5	-----	-----
P3	5545	40.102	59.898	-----	-----
P4	5007	31.714	68.286	-----	-----
P5	3695	34.497	65.503	-----	-----
P6	7347	33.996	66.004	-----	-----
R1	7549	19.859	80.141	-----	-----
R2	8499	30.859	69.141	-----	-----
R3	7875	8.2284	91.772	182	6
R4	10129	32.697	67.303	-----	-----
R5	6768	0.012	99.988	304	10
R6	7727	14.117	85.883	-----	-----
R7	3674	0.3455	99.654	-----	-----

Assuming the depth of the epicenter in this study is 10 kilometers, we employed the seismic attenuation law developed by Atkinson and Boore (1995) for the mean PGA ($\mathrm{cm/s^2}$):

$$\log(\mathrm{PGA}) = c_1 + c_2(M_L - 6) + c_3(M_L - 6)^2 - \log R - c_4 R \tag{2.9}$$

where M_L is the Richter magnitude; R is the epicentral distance (km); c_1, c_2, c_3, and c_4 are parameters from regression analysis. According to the study by Atkinson and Boore (1995), following parameters are selected: $c_1 = 3.79$, $c_2 = 0.298$, $c_3 = -0.0536$, $c_4 = 0.00135$.

To study the bridge failure risks during the occurrence of earthquakes, the fragility curves of similar bridges in a high seismic zone are adopted from an existing study (Neilson and DesRoches 2007). In the work by Neilson and DesRoches (2017), a bridge's fragility is defined as the probability that the seismic-induced demand meets or exceeds the seismic capacity of the bridge. The relationship between PGA and the extensive damage rates of the three types of bridges are shown in Fig 3. Since the extensive damage limit state in Fig. 2.3 includes extensive and higher damage limits, the extensive damage rate can be used as the seismic failure rate of bridges for both extensive and complete damage limit states.

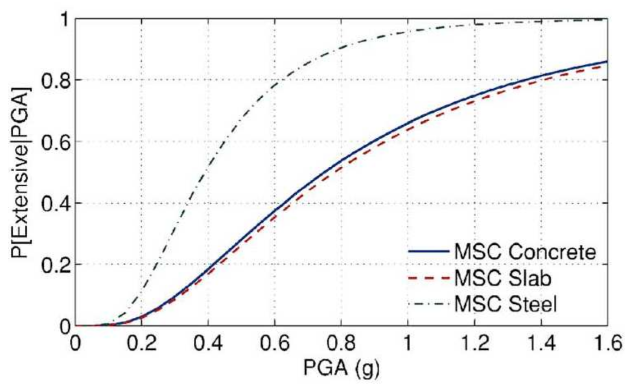

Figure 2.3 Seismic fragility curves for typical bridge types (Neilson and DesRoches 2007)

In the work by Neilson and DesRoches (2017), the probability of each damage state is:

$$P[Damage\ State\ i\ or\ greater|PGA] = \Phi[\frac{\ln(PGA) - \ln(med_i)}{\zeta_i}] \tag{2.10}$$

where med_i is the median PGA value of damage state i; ζ_i is the dispersion of damage state i. The median and dispersion values for seismic fragility curves of the three bridge types are presented in Table 2.3. According to Hazus (1997), Eq. (2.10) also works for special buildings like medical centers with median and dispersion values of 1.24g and 0.64 respectively.

Table 2.3 Median and dispersion values for seismic fragility of five bridge classes

	Median PGA values (g)

Bridge Class	Extensive med_i	Dispersion ζ_i
MSC slab	0.78	0.7
MSC concrete	0.75	0.7
MSC steel	0.39	0.55

In this study, the failure of buildings is defined as the collapse since the number of injured population caused by building collapse is the primary concern for EMS. Jaiswal et al. (2011) provided the relationship between Modified Mercalli Intensity (MMI) and the collapse fragility of several different types of buildings, which is:

$$\mathrm{P_u(I_{mm}) = A_u \times 10^{(B_u/(I_{mm}-C_u))}} \tag{2.11}$$

where $\mathrm{A_u}$, $\mathrm{B_u}$, and $\mathrm{C_u}$ are the scale, shape, and location parameters for building type u. The values of parameters A, B and C are 0.85, -2.35, and 5.9 for precast concrete frame and 9.52, -4.89, and 5.32 for masonry buildings, respectively. $\mathrm{I_{mm}}$ is the seismic intensity related to the MMI scale. Wald et al. (1999) proposed the relation between PGA (g) and $\mathrm{I_{mm}}$ based on the analysis of earthquakes in California, which is

$$\mathrm{I_{mm} = 3.66\log(PGA) - 1.66 \quad for \ \ V \leq I_{mm} \leq VIII} \tag{2.12}$$

Based on Equations (11) and (12), the relationship between PGA and building collapse fragility can be derived:

$$\mathrm{P_u(PGA) = A_u \times 10^{(B_u/(3.66\log(PGA)-1.66-C_u))} \qquad for \ \ V \leq I_{mm} \leq VIII} \tag{2.13}$$

Coburn et al. (1992) studied the occupancy rate ($\mathrm{M_1^z}$) of urban residential and nonresidential buildings (Fig. 2.4a) during a day and the occupants trapped rate by collapse for different macroseismic intensities with scale Medvedev–Sponheuer–Karnik (MSK). Musson et al. (2009) compared different macroseismic intensity scales including MSK and Modified Mercalli Intensity (MMI). Both MMI and MSK have twelve intensity levels from I to XII. According to the study of Musson, any given ground motion has the same intensity level in terms of scales of MMI and MSK and thus they are practically interchangeable. In this demonstrative example, for the convenience of presentation, the occupants' trapped rates of masonry buildings based on MSK by Coburn et al. (1992) are converted to those based on MMI, as shown in Fig. 2.4b. The trapped rate of concrete buildings under near field earthquakes is 0.5. Fig. 2.5 shows the distribution of different injury severities (i.e., light injury, hospitalization, severe injury and dead) among people trapped by the collapse of masonry buildings and reinforced concrete buildings (Coburn et al. 1992).

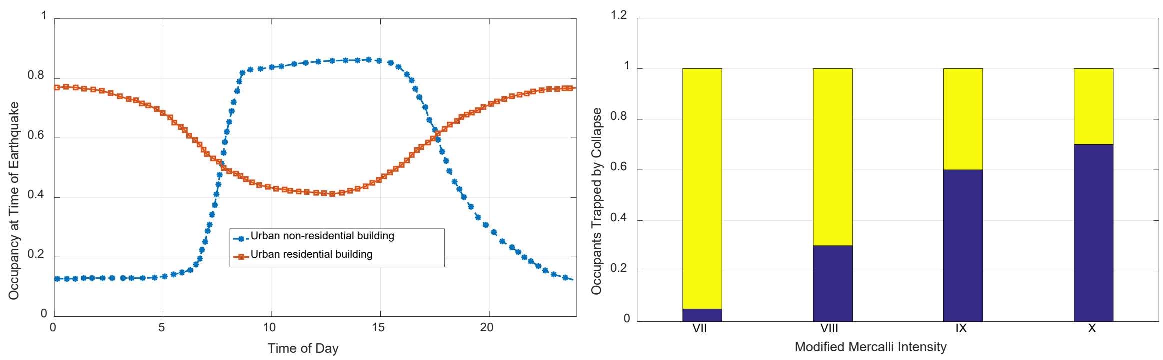

a. Occupancy rate of urban buildings b. Trapped rate by collapse of masonry buildings

Figure 2.4 Occupancy and trapped rates by collapse (Coburn et al. 1992)

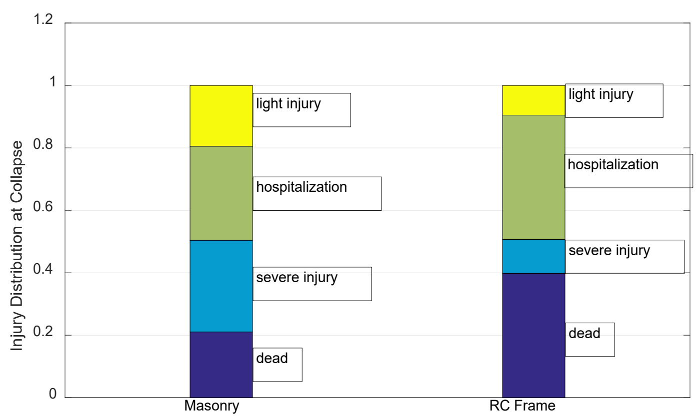

Figure 2.5 Injury distribution among trapped people (Coburn et al. 1992)

For EMS, the focus is apparently on those who were considerably injured but remained alive after the earthquake. Among all the injured people, those with severe injury and hospitalization levels in Fig. 5 may need immediate medical care and will receive the priority of EMS. The scenario earthquake is assumed to happen at 10:00AM, and the average occupancy of residential and non-residential buildings can be obtained from Fig. 2.4a. Similarly, the other parameters under two different earthquake magnitudes can be calculated with Eqs. (2.9-2.13) and the details are summarized in Table 2.4.

Table 2.4 Model parameters derived from Richter magnitudes

Richter magnitude	6.5	7.25
PGA (g)	0.2988	0.4486
I_{mm}	7.37	7.93
P_u of RC frame	0.0213	0.059
P_u of masonry	0.039	0.127
Failure rate of MSC-slab	0.08	0.19
Failure rate of MSC-concrete	0.09	0.21
Failure rate of MSC-steel	0.31	0.56
M_1^z of residential zones	0.42	0.42
M_1^z of nonresidential zones	0.85	0.85
M_2^u of masonry	0.143	0.282
M_2^u of concrete	0.5	0.5
M_3^u of masonry	0.6	0.6
M_3^u of concrete	0.5	0.5

As discussed earlier, there are nine vulnerable links in the traffic system with bridges involved and two vulnerable medical centers. Any of the nine links and the two medical centers is possible to fail during an earthquake, so the total number of possible states K for the traffic network after an earthquake equals 2^{11}. The depth of the epicenter and the epicentral distance are assumed to be 10 km and 26.5 km respectively. Considering both are much bigger than the linear size of the community, it is assumed that the whole community shares the same PGA and other seismic characteristics. In this study, the graph theory and Dijsktra's shortest route algorithm (Dijsktra 1959) are applied to analyze the shortest routes between nodes for each possible state after hazard. Let the LOF $\varepsilon = 0.85$ and $M_L = 6.5$, the link importance values and system indicators are calculated with the framework introduced above and the results are listed in Table 2.5 and Fig. 2.6. Genetic Algorithm and Sequential Quadratic Programming are used to optimize the total rescue time (Eq. (2.2)) with integer constraints for variables on a desktop computer with 3.2GHz processor and 16GB RAM and the computational time is about 7 minutes.

Fig. 2.6 shows considerable difference among the importance values of different links from the EMS perspective is found to be the most important link while link 18 and 30 are the least ones in the network. As shown in Fig. 2.2, it is apparent that link 18 and 30 are redundant and there are better alternative routes that can bring the EMS vehicle to the EMS medical center from the same area.

Table 2.5 System indicators when $M_L = 6.5$

	$M_L = 6.5$
Rescue time (min)	264.3
RI	0.9317
T_0 (min)	207.1

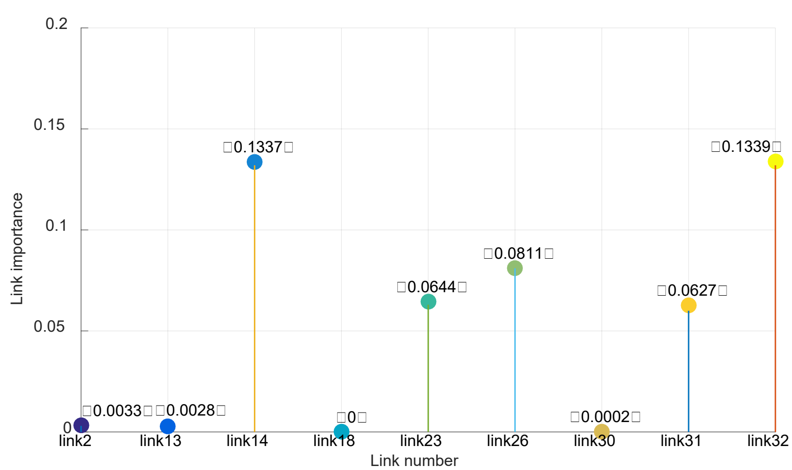

Figure 2.6 Link importance values when $M_L = 6.5$

2.4 Parametric analysis

Parametric analyses are conducted with the proposed framework on different parameters, such as level of functionality, Richter magnitude, bridge types, number and location of EMS medical center and possible new addition of EMS medical center.

2.4.1 Level of functionality $\boldsymbol{\varepsilon}$

As introduced previously, the stakeholders may specify the level of functionality as a type of subjective performance expectation and such a value may have influence on the resilience index and link importance values. The influence of the LOF ε on network indicators is analyzed and the results of several selected links are shown in Figs. 2.7-2.10. Figs. 7-9 show that link 2, 13, 14, 23, 26, 31, 32 are most sensitive to the value of LOF ε and link 18 and 30 are the least. It is consistent with what has been observed from Fig. 2.2 that link 18 is always redundant in the system. There are several peaks in Fig. 2.9. Taking link 18 as an example, when the LOF is larger than 0.7, the failure or functionality of link 18 has little impact on the acceptability of the network performance for all possible network damage states. When the LOF ε is around 0.67, link 18 has moderate effect for some network damage states. In Fig. 2.10, a relatively faster reduction in network reliability is observed when LOF increases. It is because most values of T_s concentrate within a narrow range around T_0. This phenomenon is caused by the relatively low failure probability of the medical centers and bridges especially for the MSC slab and MSC concrete bridges under $M_L = 6.5$, and the complexity of the traffic network. When a network becomes more complex, a link is more likely to have alternative links with similar travel time in the network.

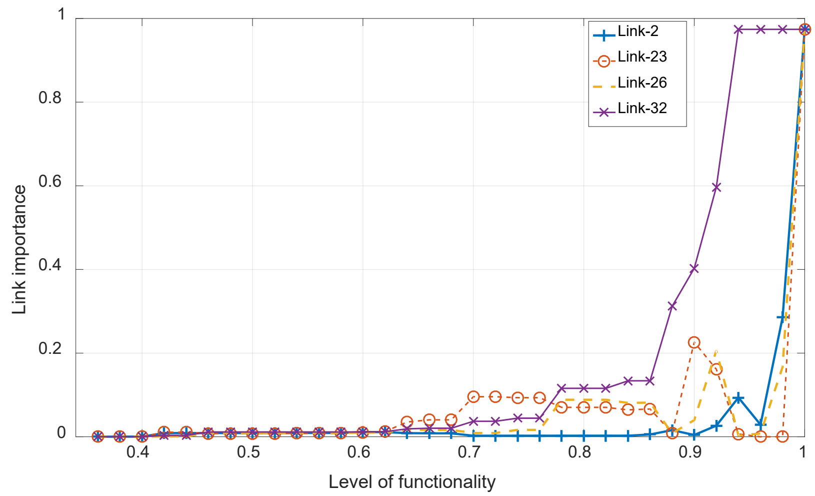

Figure 2.7 Link importance values (link 2, 23, 26, 32) as a function of the level of functionality

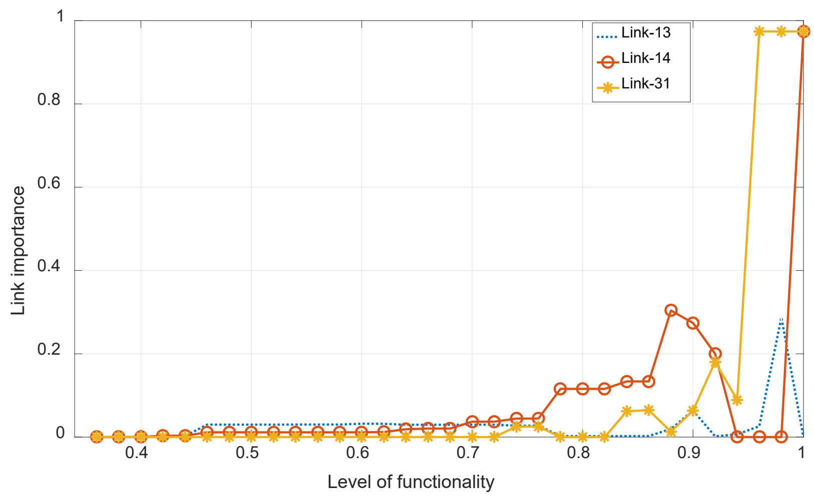

Figure 2.8 Link importance values (link 13, 14, 31) as a function of the level of functionality

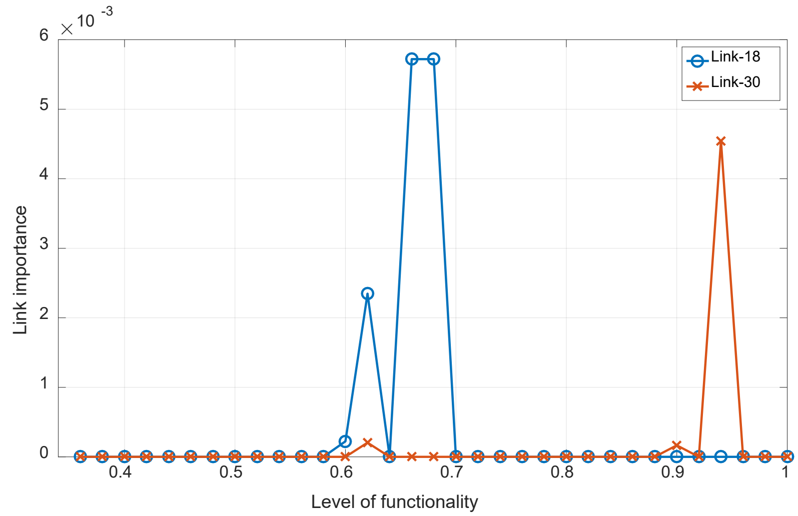

Figure 2.9 Link importance values (link 18, 30) as a function of the level of functionality

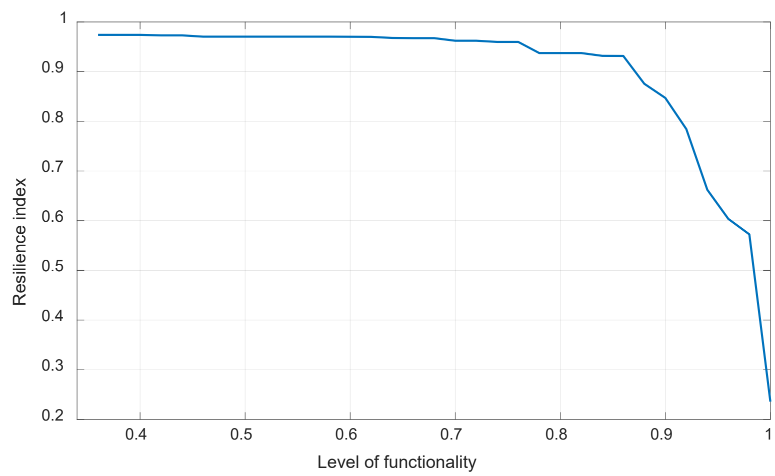

Figure 2.10 Resilience index as a function of the level of functionality

2.4.2 Richter magnitude

The influence of Richter magnitude on the system is based on its influence on the fragilities of residential buildings and bridges. In this study, another Richter magnitude is also applied to make a comparison, i.e., $\mathrm{M_L} = 7.25$. When $\mathrm{M_L} = 7.25$, the failure probabilities of buildings, MSC slab bridges, MSC concrete bridges and MSC steel bridges get higher. As a result, the higher the Richter magnitude is, the more injured people and also the more vulnerable links (i.e., bridges) of the traffic network will be. In reality, the EMS capacity of a medical center may not be sufficient for a higher number of injured people that all need immediate medical attention during a very short time period under a high seismic magnitude like 7.25. In this case, additional overflow or temporary medical center is assumed to be made available in zone $I1$ and it is also a mid-rise concrete shear wall. It is assumed the overflow or temporary medical center in zone $I1$ has the same "pick-up capability" as the original medical centers and the "pick-up capability" of a medical center is the ratio of its number of EMS vehicles to its capacity. The link importance values and the comparison of the rescue time and reliability are shown in Fig. 2. 11 and Table 2.6.

By comparing Fig. 2.6 ($M_L = 6.5$) and Fig. 2.11 ($M_L = 7.25$), it is found that the link importance values change considerably under different seismic intensities. Different from the case with $M_L = 6.5$ (Fig. 2.6), when $M_L = 7.25$, link 2 becomes the most significant one and link 18 is no longer the least important one (Fig. 2.11). Thanks to the change in the medical resources/supply condition caused by the overflow or temporary medical center at zone $I1$, link 2 becomes very critical and link 18 is no longer redundant. Table 2.6 lists the results of the total rescue time and resilience index under two magnitudes. It shows that magnitude has a significant effect on the system resilience and the rescue time in a complex way since different magnitudes of earthquakes affect both "supply" (connectivity and travel time due to possible bridge failure) and "demand" (injury caused by the building damage) of the system. Therefore, post-earthquake EMS planning may have different optimal strategies when earthquakes with different intensities occur.

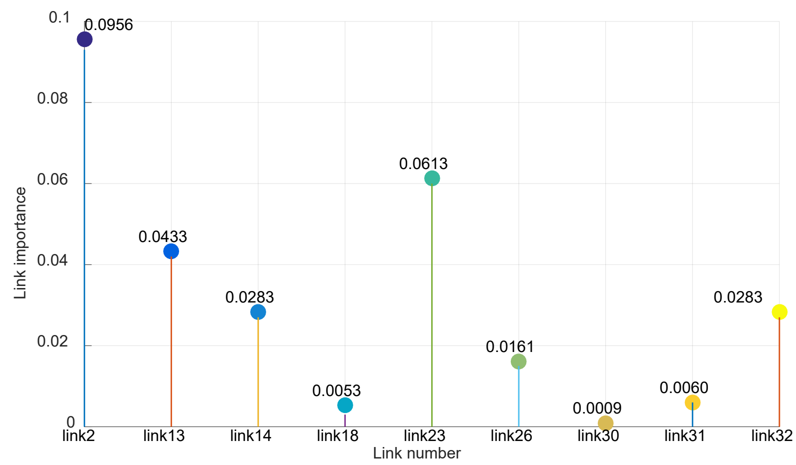

Figure 2.11 Link importance values when $M_L = 7.25$

Table 2.6 Comparison of system indicators at different magnitudes

	$M_L = 6.5$	$M_L = 7.25$
rescue time (min)	264.3	574.9
RI	0.9317	0.8451

2.4.3 Bridge types

Three types of bridges have been considered in this study with certain ratios of composition. Apparently, different kinds of typical bridges have different seismic responses and failure probability. Accordingly, the connectivity conditions of the system will also change. Three special cases are studied for comparison purposes: case 1- all bridges are MSC slab ones; case 2- all bridges are concrete girder ones; and case 3- all bridges are steel ones. The three cases are analyzed under seismic with both $M_L = 6.5$ and $M_L = 7.25$. The total rescue time results are listed in Fig. 2.12.

Fig 2.12 shows that at both Richter magnitude and the composition of different bridge types have considerable influences on the network efficiency and total rescue time. Compared to that when $M_L = 6.5$, larger difference exists among different bridge composition scenarios when $M_L = 7.25$. The results suggest that detailed classification of bridge types with considerably different seismic fragilities may be more critical for areas experiencing higher seismic intensities than lower intensities. Comparatively, the adoption of more MSC slab or girder bridges may potentially reduce the total rescue time or increase the system emergency response reliability. Steel bridges may cause the largest impact on increasing the total rescue time. More general conclusions, however, can only be made based on studies of more traffic networks with site-specific details. But this type of information, if available to a specific community, can be very helpful to the planning efforts of future pre-hazard bridge strengthening, post-hazard repair prioritization and the design of new bridges when post-earthquake EMS performance is of concern.

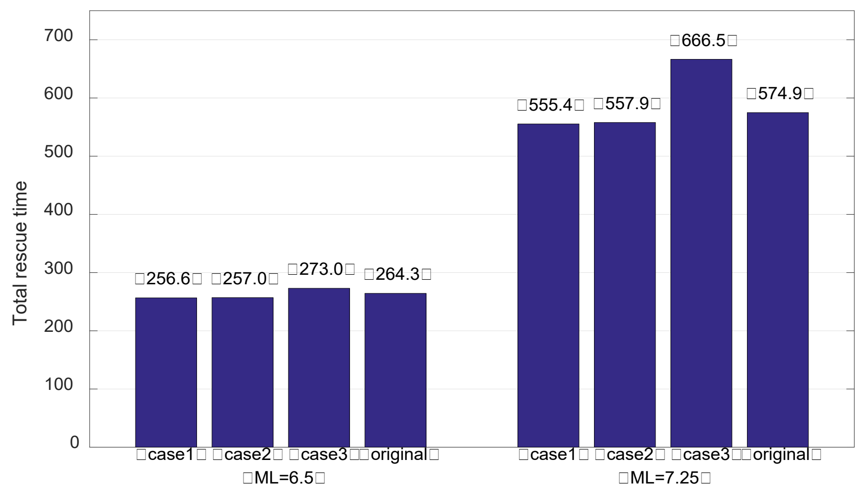

Figure 2.12 Total rescue time (min) in different cases/ magnitudes

2.4.4 Location/number of EMS medical centers

The location and number of medical centers supporting EMS in a community are apparently important decisions, and a strategic and optimized planning can achieve the best balance between saving more rescue time and economic efficiency. In the proposed framework, such parameters deserve further investigations since they can directly affect the "supply" of emergency medical response. To make more insightful observation of the impacts from these parameters, it is assumed there is only a centralized EMS medical center in the community in this section. With only one EMS medical center, a wide range of possible locations of the centralized EMS medical center in the network can be investigated to disclose the effect of the location of EMS medical center on emergency medical response performance as well as possible optimal locations. For parametric and comparative study purposes, the total demand of the EMS traffic (i.e., total patients need to be transported), the community's total medical center capacity and the number of total EMS vehicles remain the same as the ones in the previous sections. Each of the 20 zones is studied as a possible candidate of the centralized EMS medical center, so the system indicators of 20 different potential medical center locations are compared. Figs. 2.13-14 list the resulted link importance values and total rescue time.

Fig. 2.13 suggests that the locations and number of EMS medical centers affect the importance values of individual links significantly. For some medical center locations (e.g., I1, I6, R4, R6), the link importance values of one or two links become very critical, justifying higher priority of enhancement or maintenance on those links before and restoration after an earthquake. For some medical center locations, such as I2 and I3, the link importance values of most links are similar, indicating almost even contributions to the emergency response of the whole network. As discussed earlier, link importance is only one side of the coin by showing the relative relations of different links. The other important performance indicator is about the total rescue time of the network, which directly defines the overall emergency response performance of the whole network.

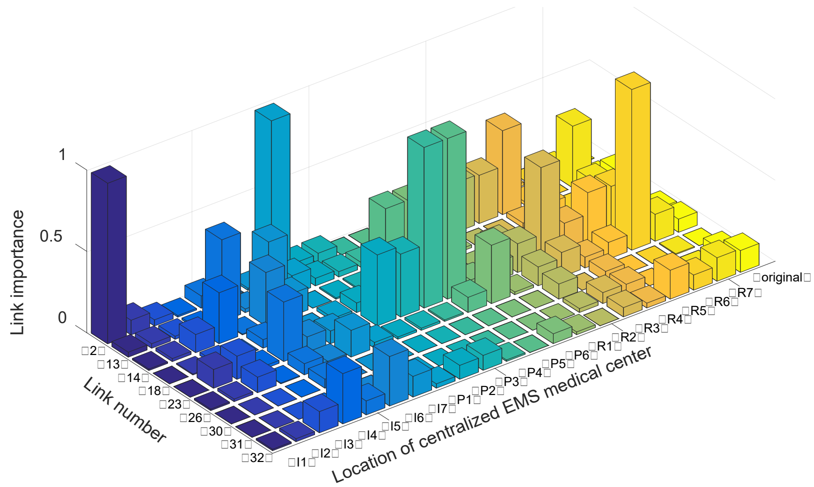

Figure 2.13 Comparison of link importance for different location/number of EMS medical center(s)

Fig. 2.14 shows that there is big difference between the rescue time results when the location of centralized EMS medical center changes. When the centralized medical center is located at P4 or P5 zone, the community is most efficient in terms of total rescue time. It is due to the relatively central locations of the two zones and there is only one or two vulnerable links (with bridge) connected to them. Locating the centralized EMS medical center at I7 zone leads to the highest total rescue time since I7 is at a corner of the community and surrounded by 4 vulnerable links (with bridges reducing the accessibility of the system). When compared to the original case, all the comparison cases show higher total rescue time, and it is apparent that an additional EMS medical center in the original case can greatly increase their accessibility for the entire system. It is noted that the analysis in this section is for demonstration purposes of the proposed methodology. If site-specific data for a particular community is available, a detailed analysis can be made following the same procedure introduced above to provide important planning information of the EMS medical center.

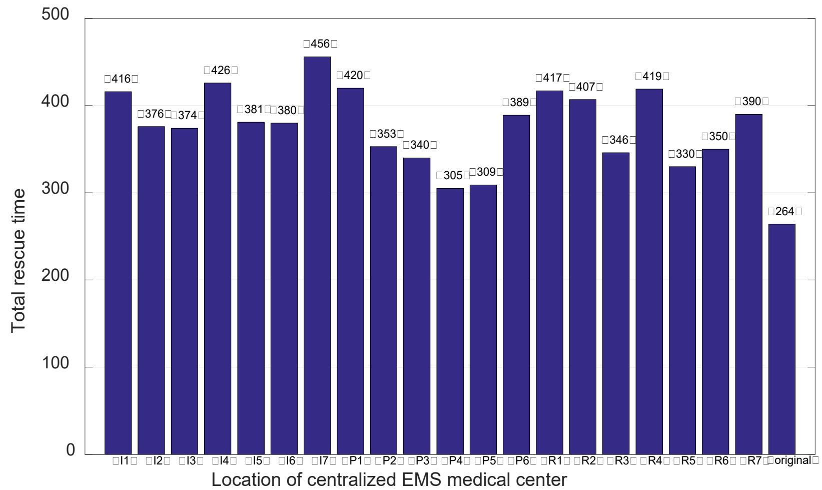

Figure 2.14 Comparison of total rescue time (min) for different location/number of EMS medical center(s)

2.4.5 Best location of a new additional EMS medical center

For a community with population growth over time or simply to improve the emergency response reliability of the community, sometimes it is warranted to build a new EMS medical center. In this study, if people build a third EMS medical center in one of the rest zones, the accessibility of the whole network may increase, and in turn, so does the resilience of the traffic system. In this section, investigations are made to identify the optimal locations of the new facility and possible impacts to the emergency response performance of the whole community. Suppose that each zone is a possible candidate of the third EMS medical center except zone R3 and R5 (already have EMS medical centers) and it is assumed that the new EMS medical center can accommodate 90 people with 3 EMS vehicles. The resulted link importance values and total rescue time of each candidate are calculated and shown in Figs. 2.15-16.

Fig. 2.15 shows that the location of the new medical center has a great influence on the link importance. There are some locations with new EMS medical center, such as I7, P6, R6 and R7 that will cause overall reduced link importance of the whole network. This can be interesting information for the traffic management and public health authorities to evaluate the current link conditions or decide between focusing the limited recovery/ resources on the functionality of several critical links and spreading the resources to more links with less dependency on individual ones. Fig. 2.16 shows that there is big difference among the rescue time of different medical center candidates. When the new additional EMS medical center is located at zone I7, P6, R6 or R7, the traffic system is most efficient in terms of rescue time. The four zones located at a corner of the community and all the links connecting these zones to the rest of the community are more vulnerable. By considering both the results of link importance and total rescue time, building a new EMS medical center among the four zones (i.e., I7, P6, R6 or R7) has the most significant impact on the EMS performance of the whole community.

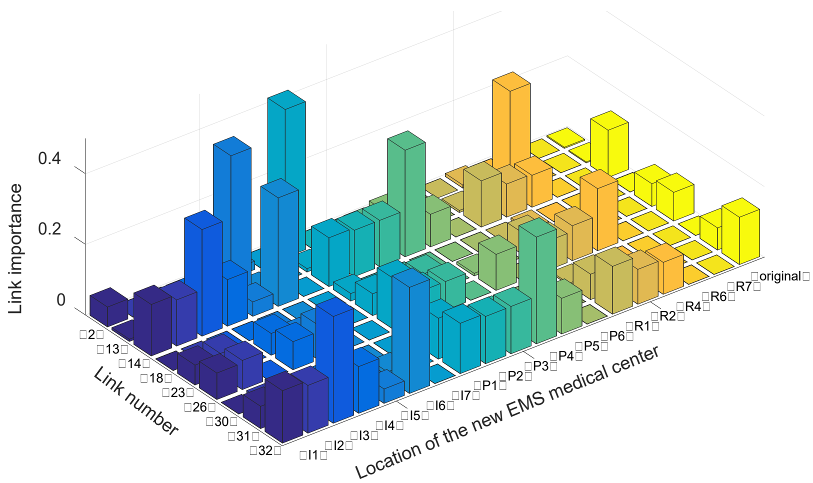

Figure 2.15 Comparison of link importance for different location of the new EMS medical center

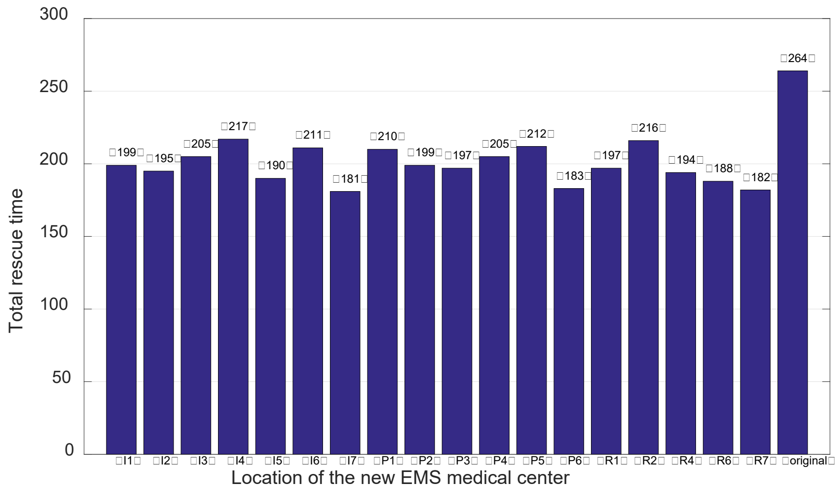

Figure 2.16 Comparison of total rescue time (min) for different location of the new EMS medical center

2.5 Conclusion

Emergency response is a very critical stage following any major hazard or incident. A framework of modeling resilience-related performance of a transportation network following an earthquake was developed from an emergency medical service perspective. In the model, fragility information of both the buildings and bridges were adopted to quantify the number and locations of people who may need emergency medical assistance and possible disruptions of the links, respectively. Two resilience performance indicators were introduced to evaluate the relative importance of different links in a traffic network as well as the overall emergency medical response efficiency for the whole network. The importance information of links can be used on developing more efficient pre-disaster improvement plan and post-hazard emergency recovery strategy by keeping those links with higher importance robust and passable in both preparation and emergency response stages. In the meantime, the overall emergency medical response resilience can assist on evaluating the emergency response performance of the whole community, conducting performance-based intervention and design optimization, and developing more rational emergency response plan for a community. Finally, the proposed framework was demonstrated in a virtual community following a seismic event. A parametric study was conducted to study the impacts of several important parameters of the model under two scenario earthquake intensities. The possible addition of new EMS medical center was also studied to find out the optimal locations and possible outcome. The results show that the seismic magnitudes considerably affect the number of severely injured people needing emergency medical assistance and at the same time, change the network connectivity. The proportion of different bridge types has a great influence on the connectivity and total rescue time of the network. The locations and number of the EMS medical centers affect the total rescue time notably since they impact the accessibility of the EMS. The best location for a new EMS medical center is sensitive to the site-specific vulnerability of infrastructure in the community and requires a case-by-case study to maximize the impact. Although this study was demonstrated through an earthquake hazard, the proposed framework can also be extended and applied to more diverse scenarios with different hazards or incidents.

This study is not free of limitations: (1) only full closure of bridges was considered and no special case of limited passage such as by emergency vehicles on bridges was considered; (2) due to the scope limit, EMS facility capacity reduction following hazards was not considered in this study. More realistic medical service capacity variations of each individual medical center due to for example, medical infrastructure damage or power outrage during earthquakes, can be considered in the future studies; (3) possible debris, obstacles or damages on roads were reflected only on relatively lower driving speeds of all EMS vehicles, which are the same throughout the whole network. With road-specific speed characterization with possible debris, the EMS vehicle driving speeds may be adaptive to the specific disruption scenarios of the road in the future studies; and (4) the proposed framework was demonstrated with limited damage states of infrastructures in a moderately sized community. For very large and complex community with higher number of limit states, more efficient optimization algorithms may be required to maintain reasonable computational efforts.

CHAPTER 3 RESILIENCE MODELING AND PRE-HAZARD MITIGATION PLANNING OF TRANSPORTATION NETWORK TO SUPPORT POST-EARTHQUAKE EMERGENCY MEDICAL RESPONSE1F[2]

3.1 Introduction

Earthquakes can cause traffic network disruption, extensive blacked-out traffic signals, considerable dislocation trips, and numerous injuries. To avoid injury-transporting private vehicles jamming on few routes on a first-come, first-served basis, existence of redundant routes is essential for transporting injured people to hospitals in a timely manner. To save as many lives as possible, a resilient transportation network with redundant paths between injured people and hospitals is crucial following major earthquakes. This study aims to support the emergency medical response through improving system resilience with a focus on redundancy by integrating post-hazard emergency response and pre-hazard mitigation planning holistically.

First, a new methodology to quantify the resilience of transportation networks is developed with two main contributions: incorporating infrastructure fragility, seismic uncertainty, search-and-rescue activity, and life vitality decay of injured people to quantify the urgency of hospitalization trips; and introducing equivalent resistance theory to model the redundancy of road networks. Second, the feasibility of developing a resilience-based pre-hazard mitigation strategy of vulnerable infrastructures to proactively support post-earthquake emergency medical response is investigated. A comparison with existing resilience

---

[2] This chapter is adapted from a published paper by the author (Wu and Chen 2023a) with permission from Elsevier.

metrics is conducted to reveal the advantage of the proposed methodology. Shelby County, Tennessee, is selected as the prototype community to demonstrate the proposed framework.

Aiming to address these challenges, this chapter will propose a new methodology that can reasonably quantify the resilience of the realistic scenario following major hazards with a focus on network redundancy and incorporate the seismic uncertainties using sampling methods efficiently. Meanwhile, it helps quantify the urgency of transporting injured people by introducing the life vitality decay on linked edges. Inspired by the effectiveness of pre-hazard planning and the vital importance and challenges associated with emergency medical response following earthquakes, this study aims to tackle this problem with an innovative concept by integrating both post-hazard emergency response and pre-hazard mitigation planning holistically. Specifically, in addition to directly improving post-hazard emergency response efforts, the proposed study will also investigate the feasibility of indirectly contributing to the post-hazard emergency response efforts by proactively carrying out optimal pre-hazard mitigation planning of vulnerable infrastructures.

The proposed holistic framework to improve post-hazard emergency medical response following earthquakes will lead to a new and more realistic resilience performance assessment methodology and proactive pre-hazard mitigation planning strategy of transportation networks. Specifically, the new methodology will assess the resilience performance with a focus on the redundancy during the post-hazard emergency response stage by considering the search-and-rescue (SAR) activity and emergency traffic demand of the network with the following novel contributions: (1) the survival function of injured people is incorporated to reflect the urgency of emergency medical service and quantify the life vitality decrease on the way to hospitals; (2) uncertainties in the ground intensity and the bridge fragility are incorporated to provide an accurate resilience quantification of the system that includes sufficient and realistic representation of possible scenarios; (3) the equivalent resistance theory originally developed in electrical engineering is adopted here to quantify the full redundancy of the network, based on which a new resilience performance index is introduced to evaluate the overall efficiency of the emergency medical response for the community. Based on the new resilience metric developed from the proposed resilience assessment methodology, the feasibility of conducting optimal pre-disaster mitigation planning through infrastructure reinforcement is investigated with a heuristic algorithm. The proposed framework is demonstrated through Shelby County in Tennessee as a part of earthquake-prone areas, followed by detailed parametric analyses.

3.2 Methodology

The emergency medical response following earthquakes in this study aims to (1) search-and-rescue (SAR) the injured people trapped by damaged buildings, and (2) transport them to designated hospitals. The proposed holistic resilience analysis and hazard mitigation framework include the following components: firstly, ground motion attenuation theories are applied to obtain the ground intensities at the sites of buildings and bridges, with which seismic fragility analyses of residential buildings, hospitals and bridges in the region are conducted; secondly, the seismic fragility results are applied to estimate the rescue demands such as the number of people in need of hospitalization and network functionality by considering the degradation scenarios of the road network; thirdly, based on the equivalent resistance theory from electrical engineering, a new system resilience indicator is proposed to simulate the functionality of the post-hazard transportation system with a focus on redundancy; lastly, the feasibility of developing a pre-hazard risk mitigation planning on bridge reinforcement with a limited budget is developed based on the new resilience index using the Genetic Algorithm. Fig. 3.1 summarizes the main parts of the proposed methodology and Tables 3.1 and 3.2 present the lists of notation and acronyms used in this study.

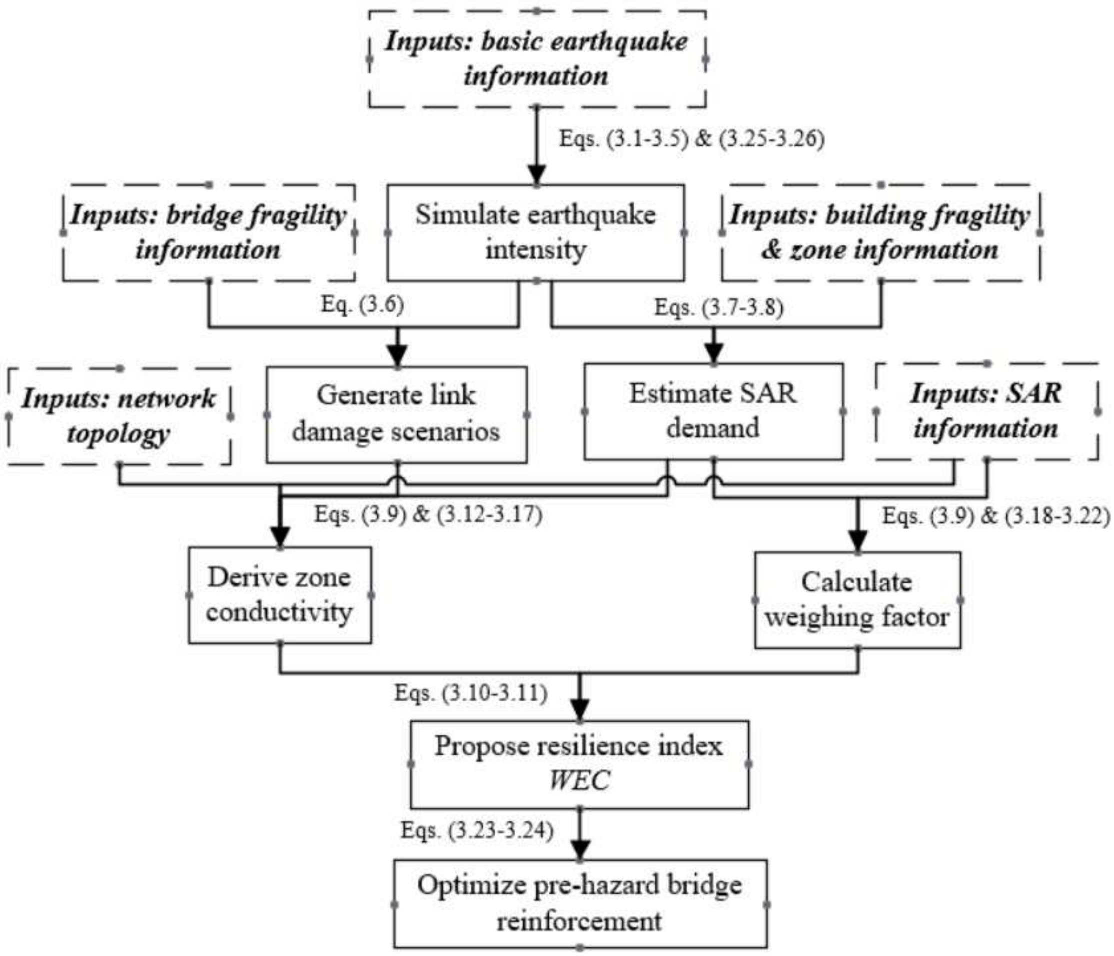

Figure 3.1 Flowchart of the proposed framework

Table 3.1 List of notations

Variables	Description
a	Additional time for rescue one more victim
A	Array of reinforcement costs for different maintenance methods
Avg_z	Average household size of zone z
b	Base time to rescue the first victim from the site
b_z^a	Population with injured severity a in zone z
b_t	Total budget for the pre-hazard bridge maintenance planning
c_i	Equivalent "conductivity" of node/zone i

E	Set of linked edges in a network
$f(i)$	The SAR speed for zone i
$F_s(T)$	Site coefficient at period T
G	Road network
H	Epicenter depth
I	Current
M	Richter magnitude
N	Number of sampled network damage scenarios
med_i	Median PGA value of damage state i
$M_{l,ds}^a$	Injured rate of severity a of building type l with damage state ds
$P_{l,ds}$	Probability of damage state ds of buildings type l
$P(s)$	Probability of occurrence of network damage state s
P_z	Total number of households of zone z
$q(l,s)$	Probability of occurrence (safe or fail) of link l under state s
R	Epicentral distance
$r(i)$	Equivalent resistance between zone i and its designated hospital(s)
$r(i,j,s)$	Equivalent resistance between zone i and its designated hospital j under state s
$R(h,k,s)$	Integrated resistance of link (h,k) over time under damage scenario s
$R'(h,k,t)$	Temporal resistance of link (h,k) at time t
SA_{BR}	Spectral acceleration for the bedrock
$S_{l,z}$	Percentage of building type l in zone z
$S(t)$	Survival function of people severely injured by hazards
T	Natural period of structure
T_0	Time for all SAR operations being completed
$T(h,k)$	Travel time of link (h,k)
n_{vic}	Number of victims rescued
V	Voltage
$V1, V2$	Electric potentials before and after a resistor
$v1(i)$	SAR speed of trained and voluntary teams
$v2(i)$	Self-rescue speed of injured people
$v(i,t)$	SAR speed of alive people with injury severity 2 and 3 at node/zone i
VN	Set of nodes/zones in a network
w_i	Weighting factor applied to individual node/zone i
Y	Rescue time needed per dwelling unit by one SAR team
ξ_s, ξ_f	Zero-mean normal random variables
β_i, ζ_i	Dispersions of infrastructure damage state i
Ω_i	Total number of severely injured people found and saved by SAR team for zone i

Table 3.2 List of acronyms

Acronym	Expansion
1SWF	1-story wood frame
2SWF	2-story wood frame
BR	Bedrock
EMS	Emergency medical service
MSC	Multi-span continuous
MSSS	Multi-span simple supported
PA	Peak acceleration in bedrock
PGA	Peak ground acceleration
RI	Resilience index
SA	Spectral acceleration
SAR	Search-and-rescue
SD	Spectral displacement
STD	Standard deviation
TDP	Total daytime population
WEC	Weighted equivalent "conductivity"
WIP	Weighted independent pathway

3.2.1 Ground intensity

Ground intensity (e.g., peak ground acceleration) is often used to simulate the impact of an earthquake on a given site as a function of the earthquake magnitude, epicentral distance, and depth of the earthquake source. The peak acceleration (PA) and spectral acceleration (SA) for the bedrock (BR) can be derived by the attenuation laws in terms of magnitude (M), epicentral distance (R), epicenter depth (H), and the natural period (T) of the structures on site (Huo and Hwang 1996).

$$Ln(SA_{BR}\ or\ PA) = f_1(M, R, H, T)\ ) + \xi_s \tag{3.1}$$

where PA is the peak acceleration for the bedrock; SA_{BR} is the spectral acceleration for the bedrock; f_1 represents the function of seismic attenuation laws; ξ_s is a zero-mean normal random variable to simulate the uncertainty of ground motion.

For different site categories, the site coefficient F_s is defined as:

$$Ln(F_s(T)) = f_2(PA, T) + \xi_f \tag{3.2}$$

where $F_s(T)$ is the site coefficient at period T; f_2 represents the function of $F_s(T)$; T is the natural period of structures on site. ξ_f is a zero-mean normal random variable like ξ_s. The peak ground acceleration (PGA), spectral acceleration (SA) and spectral displacement (SD) for a given T are defined as (Huo and Hwang 1996):

$$PGA = PA * F_s(T) \tag{3.3}$$

$$SA = SA_{BR} * F_s(T) \tag{3.4}$$

$$SD = SA * \left(\frac{T}{2\pi}\right)^2 \tag{3.5}$$

3.2.2 Seismic fragility

The seismic fragility of a given structure is used to describe the probability of a specific structural failure type under a given earthquake intensity. It is usually presented as a function of seismic parameters, e.g., PGA and SA. The failure in terms of a limit state is defined as an excess of the threshold value of a performance indicator, such as stress, displacement, acceleration, etc. There are many sources of uncertainties in the structural capacity and ground motions, which affect the seismic performance of structures significantly. As a result, the seismic fragility of structures is usually presented with fragility curve(s) with an assigned probability to describe the confidence level associated with the estimation of vulnerability for each limit state. For bridges, typically, there are several different damage states: no or slight damage, moderate damage, extensive damage, and complete damage (Nielson and DesRoches 2007; Hazus 1997). The probability of each damage state is defined as:

$$P[Damage\ State\ i\ or\ greater|PGA] = \boldsymbol{\Phi}\left[\frac{ln(PGA) - ln(med_i)}{\zeta_i}\right] \tag{3.6}$$

where med_i is the median PGA value of the damage state i; Φ is the standard normal cumulative distribution function; ζ_i is the dispersion of damage state i. According to the investigation results by Padget and DesRoches (2007), a moderately or less damaged bridge maintains partial or full capacity to carry traffic soon after the earthquake, while an extensively damaged or completely damaged bridge cannot carry traffic within seven days after the earthquake. Therefore, only bridges and hospitals that have suffered from extensive or more severe damages are deemed failed in this study based on the observation that the emergency response stage is typically shorter than a week.

Similarly, there are several different damage states for buildings: no damage, slight damage, moderate damage, extensive damage, and complete damage. Complete damage can be divided into two types: non-collapsed complete damage and collapse. The probability of damage state *i* or greater is defined as (Hazus 1997):

$$P[Damage\ State\ i\ or\ greater|SD] = \Phi\left[\frac{1}{\beta_i}\ln\left(\frac{SD}{SD_i}\right)\right] \tag{3.7}$$

where SD is the spectral displacement defined in Eq. (3.5); Φ is the standard normal cumulative distribution function; SD_i is the median standard deviation value of damage state i; β_i is the dispersion of damage state i. The seismic fragility of typical residential buildings can be used to estimate the failure rates of the buildings. Building failures are further related to the injured population, which will be introduced in the next section.

3.2.3 Estimation of injuries

According to Hazus (1997), the injured population of a community is related to the building damage states, occupancy rate, and injured rate. The failure rate of buildings under a given earthquake can be obtained through their seismic fragility performance as introduced in previous sections. Based on Eqs. (3.1-3.7), the injured population can be defined as:

$$b_z^a = \sum_l \sum_{ds} P_z * S_{l,z} * P_{l,ds} * Avg_z * M_{l,ds}^a \tag{3.8}$$

where b_z^a is the population with injured severity a in zone z; P_z is the total number of households of zone z; $S_{l,z}$ is the percentage of building type l in zone z; $P_{l,ds}$ is the probability of damage state ds of buildings type l. Avg_z is the average household size of zone z and $M_{l,ds}^a$ is the injured rate of severity a of building type l with damage state ds.

According to Hazus (1997), there are four levels of injury severities: severity 1 means people are just slightly injured and only need basic medical aid; severity 2 requires a greater degree of medical care but might not be life-threatening; severity 3 is a life-threatening condition that calls for immediate medical treatment; severity 4 is instantaneously killed or mortally injured. In this study, it is assumed that people with severity 2 and 3 would need emergency medical service (EMS), including both search and rescue (SAR) and transport. Those people who need immediate hospitalization are further divided into two groups: unburied and buried. The unburied people are injured by non-collapsed building damages, and the buried people are caused by building collapses.

3.2.4 Search-and-Rescue (SAR) operations

For the buried and unburied injuries, there are different search and rescue plans. According to the study of the 1995 Hanshin-Awaji earthquake (Murakami et al. 2000), there were three groups of people carrying out the SAR: the trained rescue teams (e.g., fire department and police department), voluntary teams from local inhabitants and self-rescue by unburied people. The fire department performs SAR operations with professional skills and equipment. Voluntary teams use their own tools but have the highest number of personnel. They are also the main rescue force during the emergency medical response stage. Studies show that local inhabitants conducted almost 67% of the rescue during the SAR operation in Kobe City (Murakami et al. 2000). People performing self-rescue are the ones injured in damaged buildings without collapse so that they can walk or crawl out by themselves.

Among all the three groups, the self-rescued people usually have the highest rescue speed because they do not need to remove any rubble to get out. For a heavily damaged building with impediments (e.g., broken stairwell, fallen non-structural parts, injured occupants), the evacuation time for 100% of the occupants can be around 30 minutes in the worst case (e.g., no external rescuing powers available) (Liu et al. 2016). Trained and voluntary teams usually rescue the injured people from the collapsed buildings and are relatively slow because they need to remove the rubbles to save the buried people. After investigating around 1,900 cases of SAR operations, Murakami et al. (2000) estimated the SAR time using multiple regression analyses and presented the SAR time as:

$$Y = a(n_{vic} - 1) + b \tag{3.9}$$

where Y is the amount of time (in minutes) spent for the SAR of a housing unit; n_{vic} is the number of victims rescued; b is the base time to rescue the first victim from the site; and a is the additional time for rescue of the second, third, and more victims. Both b and a are parameters that differ with building types (e.g., wooded detached, wooden apartment). Since Murakami et al. (2000) did not specify the rescue power working on a unit, this study defines Y as the rescue time needed per dwelling unit by one SAR team.

Also, the building size was not included in their research because b and a are parameters only related to building types. So, this study assumes buildings of similar types have similar sizes. Due to the lack of site-specific SAR data, this study will evenly distribute the trapped injuries (Eq. (3.8)) to the collapsed buildings (Eq. (3.7)). When the building types, number of trapped injuries, and available SAR teams of a zone are provided, the SAR speed of the area can be estimated with Eq. (3.9).

3.2.5 New system resilience index

3.2.5.1 <u>Definition of resilience index</u>

For those people who are severely injured (severity 2 and 3) from building damages, a timely SAR and efficient transport are usually necessary. As introduced above, earthquakes can cause traffic network degradation, extensive blacked-out traffic signals, and considerable emergency trips at the same time. Compared to all hospitalization trips jammed on the shortest path, the existence of multiple alternative routes can be more efficient. A new system resilience index is introduced to quantify transportation resilience during the emergency medical response, focusing on network redundancy.

In an electric circuit, every resistor, whether series, parallel or compound, will impact the system resistance. So, similar concept is applied in this study to simulate the full redundancy of the transportation network. For severely injured people, any delay on the way to the hospital may cause their life vitality to drop and impact their chances of survival. In this study, the loss of life vitality on the road is considered as the “resistance to be saved”. If the resistance between an injured resident and the hospital is high, it is hard for the resident to access the hospital quickly. The resilience index of the community is defined based on the overall resistance of the transportation network. The resilience index is small if the “resistance” is large, or the “conductivity” is small. Redundancy is reflected in the proposed resilience index because every alternative route, whether independent or not, is going to make a difference. The resilience index (RI) of the system is defined as:

$$RI = WEC(G) \tag{3.10}$$

where $WEC(G)$ is the weighted equivalent "conductivity" (WEC) of the community.

Let $G = (VN, E)$ denote the road network, where $VN = \{1, 2, \ldots n\}$ is the set of nodes that represent major nodes/zones in a community and $E = \{1, 2, \ldots m\}$ is the set of linked edges that represent roads either without or with bridges. $WEC(G)$ is defined as:

$$WEC(G) = \sum_{i=1}^{n} w_i c_i \tag{3.11}$$

where w_i (defined by Eqs. (3.18-3.22)) is the weighting factor applied to individual node/zone $i \in V$, and c_i (defined by Eqs. (3.12-3.17)) is the equivalent "conductivity" of node/zone i, which is defined as:

$$c_i = \frac{1}{r(i)} \tag{3.12}$$

$$r(i) = \begin{cases} \int_1^N r(i,j,s)P(s)ds, & if\ hospital\ j\ works \\ \int_1^N r(i,j,s)P(s)ds + \int_1^N r(j,j',s)P(s)ds, & if\ hospital\ j\ fails \end{cases} \tag{3.13}$$

where $r(i)$ is the equivalent resistance between zone i and its designated hospital(s). $r(i,j,s)$ is the equivalent resistance between zone i and its designated hospital j under state s, N is the number of all sampled network damage scenarios after hazards, and j' is the collaborative hospital of j. If hospital j is damaged in the earthquake, all the injured residents will be triaged to hospital j' upon arrival of hospital of j. $r(i)$ is the expected transportation performance index between the injured residents and their hospitals that considers numerous possible network damage states caused by bridge damage and hospital damage. $P(s)$ is the probability of occurrence of state s:

$$P(s) = \prod_{\forall\, l \in A} q(l, s) \tag{3.14}$$

where $q(l, s)$ is the probability of occurrence (safe or fail) of link l under state s. In this study, only extensive or severe damages of bridges may result in the failure of their links. For any network damage state s, it is a combination of the bridge/link damage scenarios that represent a new network topology. The seismic vulnerability of bridges will affect the conductivity of the network. If a bridge is robust to earthquake, its link is more likely to stay intact under earthquakes, may become a segment of extra paths, and contribute to network redundancy and resilience.

$r(i, j, s)$ in Eq. (3.13) is defined as:

$$r(i, j, s) = F_{cn\forall\, adjacent\; h,k \in A}\big(R(h, k, s)\big) \tag{3.15}$$

where F_{cn} is the function of calculating the equivalent resistance between two nodes in an arbitrary network (Kagan 2015). In an electric circuit, the equivalent resistance concept can help evaluate the contribution made by any component. Same concept is applied to traffic network to fully consider the network redundancy that incorporates the effect of every single linked edge.

$R(h, k, s)$ is the integrated resistance of link (h, k) over time under network damage state s, and it is defined as

$$R(h, k, s) = \begin{cases} \infty, & if\;\; link(h, k)\; fails\; in\; state\; s \\ \int_0^{T_0} R'(h, k, t)dt & if\;\; link(h, k)\; works\; in\; state\; s \end{cases} \tag{3.16}$$

where $R'(h, k, t)$ is the temporal resistance of link (h, k) at time t, and T_0 is the time for all SAR operations being completed. This study integrates $R'(h, k, t)$ to get $R(h, k, s)$ because a vehicle carrying injured residents may drive through a link (h, k) at any time during the emergency medical response stage. The integration can quantify the overall link resistance over the emergency medical response process.

For any link (h, k), $R'(h, k, t)$ is defined as:

$$R'(h, k, t) = S(t) - S\big(t + T(h, k)\big) \tag{3.17}$$

where $T(h, k)$ is the travel time of link (h, k) and $S(t)$ is the survival function of people severely injured by hazards (e.g., building collapse, etc.).

In Eq. (3.17), $S(t)$ is the survival function value/life vitality of the injured people when they enter link (h, k). $S\big(t + T(h, k)\big)$ is the survival function/life vitality of the injured people when they exit link (h, k). So, the temporal resistance of link (h, k) is the life vitality drop on the link. This study defines it as the resistance of injured people from being saved when they are transported through the link. To maintain a minimum/satisfying current in an electrical circuit, a network of many parallel and low-value resistors can significantly reduce the voltage requirement or the electric potential drop. Similarly, the existence of multiple and short paths between injured people and their hospitals may considerably reduce the life vitality drop on the way to hospitals, especially when there is a considerable amount of traffic made by post-hazard dislocating residents and emergency response staff (Tamima and Chouinard 2016).

Table 3.3 shows the analogy between the $R'(h, k, t)$ and an electrical resistor. In Table 3.3, just like the electrical resistance being proportional to the electric potential difference/drop, the "resistance" proposed in this study is proportional to the life vitality drop. In Table 3.3, V is voltage; I means current; and $V1$ and $V2$ are the electric potentials before and after the resistor.

Table 3.3 Analogy between the temporal resistance and electric resistance

Electric resistance	This study
$\frac{V}{I} = Resistance$	$S(t) - S\big(t + T(h, k)\big) = R'(h, k, t)$
$V = V1 - V2$	

Fig. 3.2 shows the survival function of people severely injured in the earthquake (Edrissi et al. 2015). The survival rate or life vitality index is 0.8 with injury in contrast to 1.0 for healthy people. The survival rate decreases with time because of the lack of food and water and the worsening of injury if the injured people are not rescued immediately.

$R'(h,k,t)$ is the survival rate change on link (h,k). When link travel time is very short compared to maximum survival time of injured people, the curve between $[t, t+T(h,k)+T(k,\ldots)]$ can be deemed as a short straight line. That means the total "resistance" of two connecting road segments can be considered as equal to the sum of their resistances if the link travel time is negligible as compared to the maximum survival time. For a typical local transportation network, it only takes up to several minutes to drive through a link between neighboring intersections. On the contrary, buried injured people may survive for hours to days. Considering two different time scales, $R'(h,k,t)$ has the property of electric resistance when in series. However, $R'(h,k,t)$ does not have the parallel property of electric resistance, especially for minimal traffic when the shortest path controls. A redundant link can increase traffic efficiency and reduce traffic stress for the real-life scenario introduced above. Although $R'(h,k,t)$ of a redundant link does not satisfy the parallel theory, it has the similar effect as an electric resistor. So, it is rational for this study to adopt the equivalent resistance theory to quantify the network resilience.

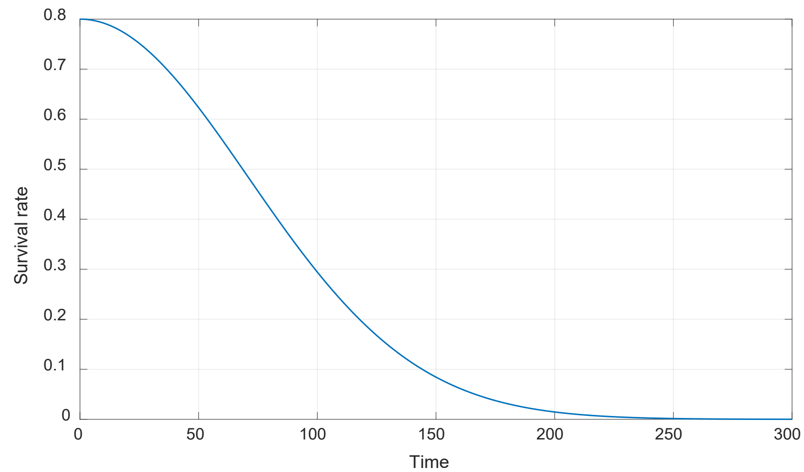

Figure 3.2 Survival function of injured people (Reproduced from Edrissi et al. 2015)

The weighting factor w_i for zone i in Eq. (3.11) is defined based on the number of severely injured people in the zone that are found and saved on site by the SAR teams. The more people are found and saved in each zone, the more weight it has according to the definition. w_i is therefore defined as:

$$w_i = \frac{\Omega_i}{\sum_a \sum_z b_z^a} \tag{3.18}$$

where b_z^a is the population with injured severity a in community z derived in Eq. (3.8). Ω_i is the total number of severely injured people that are found and saved by the rescue team on site for zone i, which can be obtained from Eq. (3.19):

$$\Omega_i = \int_0^{T_0} v(i,t)dt \tag{3.19}$$

where $v(i,t)$ is the SAR speed of alive people with injury severity 2 and 3 at node/zone i.

$$v(i,t) = f(i).S(t) \tag{3.20}$$

where $S(t)$ is the survival function of people severely injured by the hazard. The SAR speed for zone i, $f(i)$, is defined as:

$$f(i) = v1(i) + v2(i) \tag{3.21}$$

where $v1(i)$ is the SAR speed of trained and voluntary teams; $v2(i)$ is the self-rescue speed. $v1(i)$ can be derived by Eq. (3.9) when the building types, number of victims, and available SAR teams are provided.

Combining Eqs. (3.18)-(3.20), the weighting factor of zone i can be derived as:

$$w_i = \frac{\int_0^{T_0} f(i).S(t)dt}{\sum_a \sum_z b_z^a} \tag{3.22}$$

3.2.5.2 Comparison with existing studies

The main difference between WEC and existing studies is the consideration of network redundancy, and it is helpful to evaluate the proposed WEC approach by comparing with other state-of-the-art models. Two popular models from existing studies are selected for comparison: traditional connectivity theory with shortest path as the index (Wu and Chen 2019; Day 2014; Edrissi et al. 2015) and the weighted independent pathway (WIP) with the number of independent pathways as the index (Ip and Wang 2011; Zhang and Wang 2016). Fig. 3.3 shows a simple example with three different networks for comparison purposes. Compared to network (a), network (b) has an extra link AB_2. Compared to network (b), network (c) has an extra link BC_2. A comparative analysis of these three networks based on the connectivity theory, weighted independent pathway (WIP), and the proposed WEC is conducted to evaluate the performance indexes between nodes A and C with results presented in Table 3.4. As shown in Table 3.4, t_{AB1} and t_{BC1} are the travel time between AB and BC in network (a), respectively; $r_{AC}^{(a)}$, $r_{AC}^{(b)}$ and $r_{AC}^{(c)}$ are the equivalent resistance between A and C for networks (a), (b) and (c), respectively. Table 3.4 suggests the connectivity theory cannot consider network redundancy since the performance indexes are the same for all the three networks. The WIP theory can tell the difference between network (a) and network (c), but not the one between network (a) and network (b). So, it can only consider partial network redundancy. Based on Section

3.2.5.1, we can tell $r_{AC}^{(a)} > r_{AC}^{(b)} > r_{AC}^{(c)}$. When comparing network (a) and network (b), the extra link AB_2 does make a difference and can improve the network resilience, especially when there is considerable traffic, as introduced above. So, the proposed WEC model with equivalent resistance as the index provides a new way to consider network resilience with superior performance in terms of modeling redundancy than the other two popular approaches.

Although the proposed resilience index is a new way to consider network resilience during post-earthquake emergency medical response with unique advantages over existing methodologies, it can also be treated as a more general case which can be reduced to traditional connectivity in some circumstances. In the case of the network in Fig. 3.3(a), the WEC will become a connectivity-based variable because there is no extra redundancy. A similar situation is when all road segments fail in the network. The methodology will remain the same as the connectivity-based one until redundant routes between zones and hospitals start showing up.

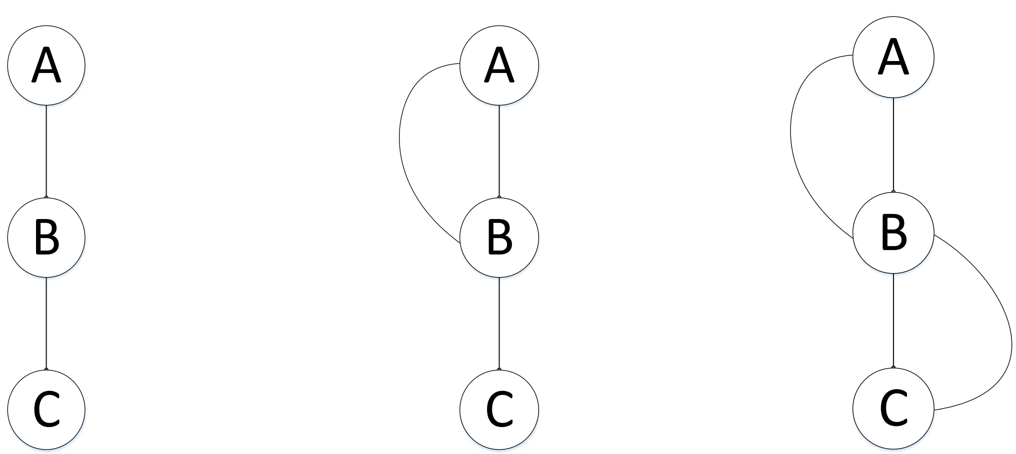

(a) (b) (c)

Figure 3.3 Comparison networks

Table 3.4 Comparison of existing models based on Fig. 3.3

Models	Index description	Network (a)	Network (b)	Network (c)
Connectivity	Shortest path (t_{min} for connected, ∞ for disconnected)	$t_{AB1} + t_{BC1}$	$t_{AB1} + t_{BC1}$	$t_{AB1} + t_{BC1}$
WIP	Number of independent pathways	1	1	2
WEC	Equivalent resistance	$r_{AC}^{(a)}$	$r_{AC}^{(b)}$	$r_{AC}^{(c)}$

3.2.6 Pre-hazard bridge reinforcement planning

After major earthquakes, transportation degradation and emergency medical response happen at the same time. A well-functioning transportation network can increase efficiency of post-earthquake emergency medical response and enhance the accessibility to medical resources. Based on the definition of the proposed *WEC* resilience index in Section 3.2.5, if there are multiple short routes for every zone to access its designated hospital(s), the transportation network is deemed resilient. To improve the resilience of the transportation network, it is significant that as many vulnerable links are intact as possible. Since bridge damage is the only cause of a failed linked edge in this study, the robustness of bridges is important to transportation resilience during the post-earthquake emergency medical response. So, it is essential to reinforce the vulnerable bridges proactively before the hazard to reduce their failure probability, and in turn boost the system resilience during the post-hazard emergency response stage. There could be several possible restrictions for pre-hazard bridge reinforcement planning, among which a popular one is the limited available resources or budget. This study will explore the optimal pre-hazard bridge reinforcement plan with the proposed resilience index under limited budget, which is demonstrated under a specific earthquake scenario.

Given the limited resources available, it is apparently not practical to strengthen all vulnerable bridges during the pre-hazard mitigation planning stage in the foreseeable future. Instead, reinforcement planning needs to be developed to prioritize the bridge strengthening efforts and enumerate the reinforcement cost. A sensible strengthening plan should consider both the importance of the bridge to the transportation network and the reinforcement cost and outcome. In this study, we will optimize the pre-hazard bridge reinforcement plan based on the resilience index as proposed above. A detailed bridge deterioration case will be assumed according to the real-world data, and the effect of the reinforcement on the bridges in terms of seismic fragility is predictable and quantifiable (Padgett et al. 2010). When applying the resource limitations, the optimal bridge reinforcement plan can be developed through the following optimization:

$$\text{Objective:} \quad \text{Max (RI)} \tag{3.23}$$

$$\text{Subjected to:} \quad A * x \leq b_t \tag{3.24}$$

where RI is the resilience index as defined in Eq. (3.10). A is the array of reinforcement costs for different maintenance methods; x is a binary array (either 0 or 1) to imply if bridge i is going to be strengthened ($x_i = 1$) or not ($x_i = 0$); b_t is the total budget for the pre-hazard bridge maintenance planning.

3.3 Demonstrative study

3.3.1 Shelby County

Shelby County in Tennessee is one of the typical earthquake-prone zones in the central and eastern United States. There are 37 zip codes in Shelby County, and the demographics of each zip code area are available at U.S. Census Bureau (Figs. 3.4-3.5). This study does not consider zip codes 38054, 38058, 38131, and 38132 because they are not deemed residential communities (e.g., P.O. box, local airport). The residential buildings in Shelby County are largely 1-2 story wood frames (Steelman & Hajjar 2008), and the information for the zip codes is shown in Table 3.5. To balance the modeling details and complexness, the intersections of the main road network are considered as a single node/ zone (Fig. 3.6) and the main road network is composed of 78 nodes and 115 links. The demographic data of each zip code are evenly distributed to the nodes within the corresponding area. Among all the links, it is assumed 31 of them have bridges classified into five different types: multi-span continuous (MSC) concrete, MSC slab, MSC steel girder bridges, multi-span simple supported (MSSS) concrete girder, and MSSS steel girder bridges (Fig. 3.7).

In this study, it is assumed only bridges suffering extensive and complete damages (Eq. (3.6)) may cause the failures of links since less severe damages usually do not cause extended bridge closure in practice. 31 out of 115 links are, therefore, vulnerable to earthquakes due to the existence of bridges (*B1-B31*) on these links (marked with symbols in Fig. 3.7). The hospitals are treated as special building structures with high-code seismic levels (Hazus 1997), and they will lose functionality if suffering extensive or higher structural damage states. According to Hassan and Mahmoud (2019), there are about 30 factors affecting the functionality of hospitals, including staff availability, elevator/stair functionality, water and power facilities' functionality, transportation performance, and ambulance availability, etc. When assessing the functionality of hospitals, this study only focuses on the functionality of hospital buildings without considering other factors. It is assumed all hospitals are one-story buildings, have enough backup resources and supplies, and are fully staffed. The geographic information of the nodes and bridges is available through Google Maps and ArcGIS, and all the nodal and bridge information is presented in Tables 3.6-3.7. Considering that residents may prefer close-by hospitals in case of emergency, each node is assigned one primary hospital for emergency medical response based on distance. Every primary hospital has its collaborative hospital for triage purposes in case of extensive structural damages. Following major earthquakes, for the prototype network as an example, at least thousands of injured residents may need prompt hospitalization, while the number of emergency medical service vehicles is typically limited. As a result, the transportation efficiency would become poor and many injured residents would die from lacking timely medical treatment, highlighting the critical importance of effective emergency medical response following earthquakes.

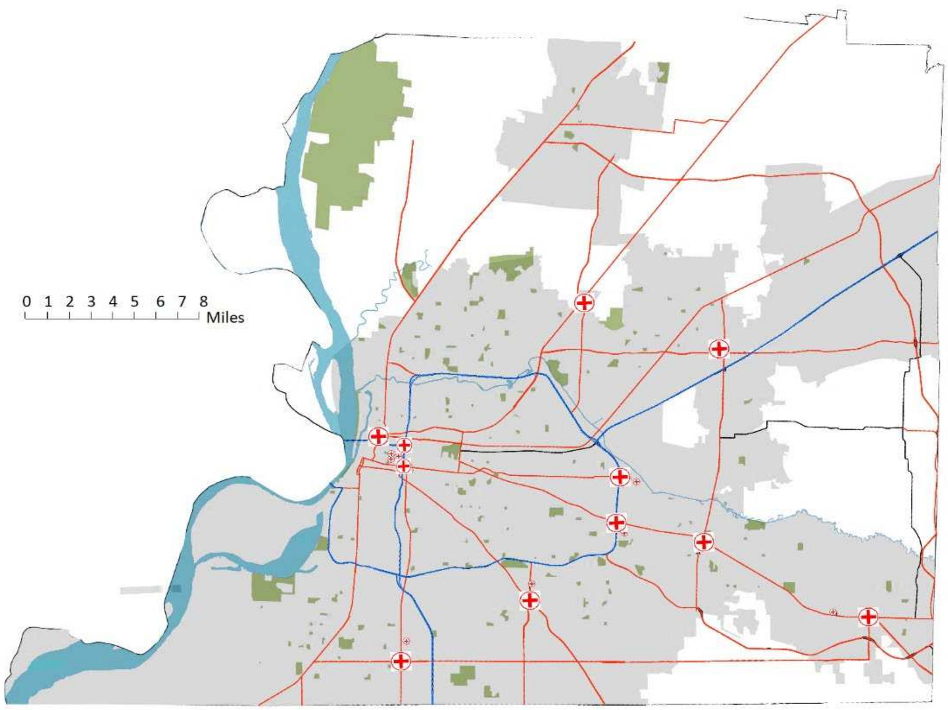

Figure 3.4 Main Road network and emergency hospitals of Shelby County

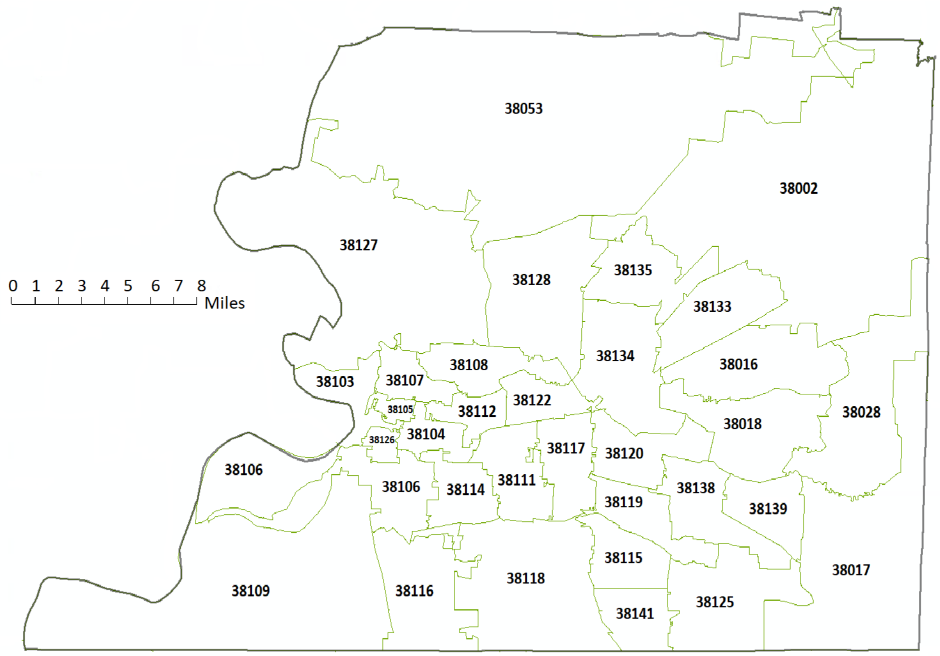

Figure 3.5 Zip code border of Shelby County

Table 3.5 Zip code information of Shelby County

Zip codes	TDP[1]	Avg[2]	Households	Hospitals	1 story %[3]	2 story%[4]
38002	25802	1.84	14053		0.388	0.612
38016	33445	1.78	18801		0.461	0.539
38017	48012	2.67	17980	1	0.503	0.497
38018	29209	2.04	14317		0.553	0.447
38028	4696	1.77	2646		0.638	0.362
38053	23981	2.29	10490		0.492	0.508
38103	35566	5.08	7005	1	0.554	0.446
38104	37758	3.02	12517	3	0.403	0.597
38105	17336	6.48	2676	3	0.437	0.563
38106	28019	2.69	10429		0.446	0.554
38107	15159	2.14	7073		0.406	0.594
38108	19164	2.85	6729		0.667	0.333
38109	43959	2.59	16989		0.628	0.372
38111	38634	2.16	17860		0.478	0.522
38112	18764	2.75	6826		0.393	0.607
38114	25507	2.4	10624		0.403	0.597
38115	37249	2.32	16053		0.472	0.528
38116	43802	2.96	14793	1	0.659	0.341

38117	37887	3.15	12029		0.376	0.624
38118	101321	7.21	14062	1	0.369	0.631
38119	28514	2.83	10065	1	0.432	0.568
38120	42874	6.28	6827	2	0.516	0.484
38122	23456	2.34	10044		0.535	0.465
38125	33446	2.27	14722		0.571	0.429
38126	10891	4.18	2607		0.492	0.508
38127	35673	2.33	15320		0.584	0.416
38128	35595	2.21	16080	1	0.453	0.547
38133	35919	4.67	7689	1	0.630	0.370
38134	42981	2.86	15053		0.522	0.478
38135	18557	1.66	11170	1	0.450	0.550
38138	34024	3.37	10082	1	0.608	0.392
38139	10335	1.84	5629		0.374	0.626
38141	19847	2.58	7678		0.681	0.319

Note: [1]TDP means total daytime population, including daytime workers and daytime residents; [2]Avg means average daily household size; [3]1 story % and [4]2 story % are the assumed percentages of 1 story buildings and 2 story buildings in the zip code area, respectively.

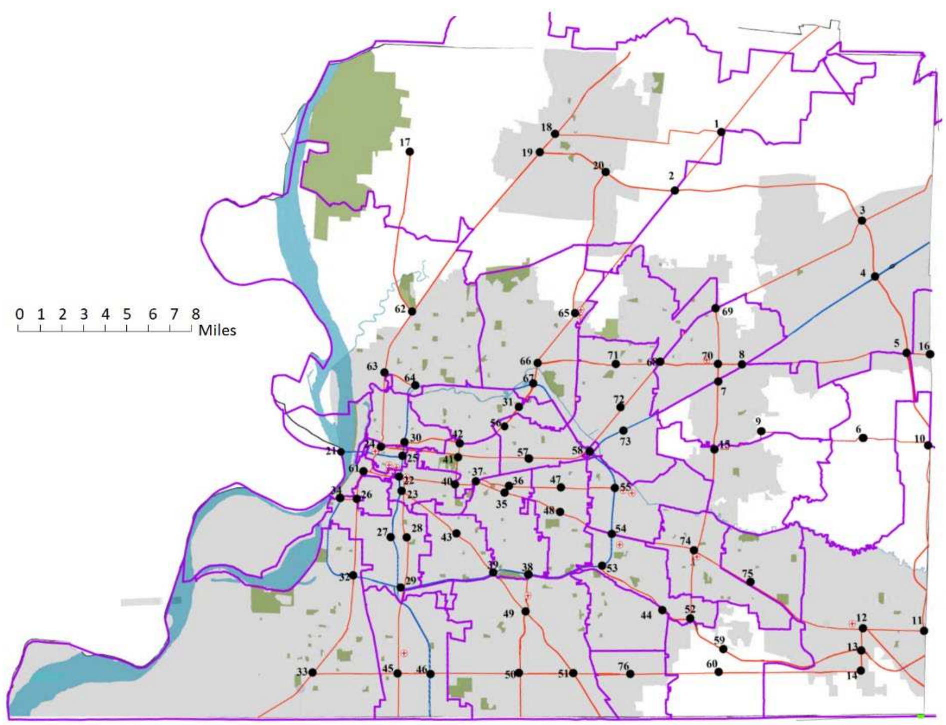

Figure 3.6 Nodes/ zones distribution of Shelby County

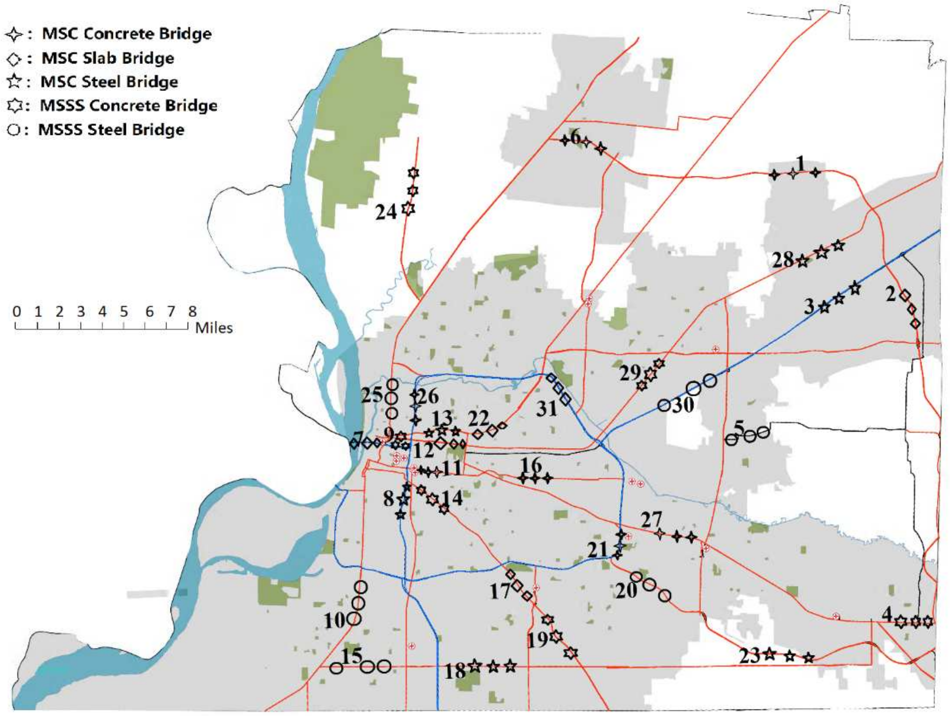

Figure 3.7 Bridge locations and types of Shelby County

Table 3.6 Node/ Zone information

Nodes	Latitude	Longitude	#HP[1]	CP[2]	AP[3]	HH[4]	Soil[5]	#TT[6]	#VT[7]
1	35.343022	-89.788899			65	3513	D	0	1
2	35.308079	-89.822665			65	2098	D	0	1
3	35.288887	-89.686639			65	3513	D	0	1
4	35.2561	-89.676892			55	3513	D	0	1
5	35.210145	-89.653792			55	3513	D	0	1
6	35.158731	-89.694493			54	1323	D	0	1
7	35.195068	-89.792187			70	9401	D	0	2
8	35.20436	-89.77236			70	2563	D	0	1
9	35.156498	-89.774194			54	9401	D	0	2
10	35.156446	-89.638166			54	3596	D	0	1
11	35.044817	-89.637635			12	3596	D	0	1
12	35.046272	-89.689285	1	55	12	3596	D	0	1
13	35.033613	-89.689272			12	3596	D	0	1
14	35.020894	-89.689143			12	3596	D	0	1
15	35.157881	-89.794974			55	14317	D	1	1
16	35.211229	-89.63495			55	1323	D	0	1
17	35.332123	-90.015529			24	2098	E	0	1

18	35.34534	-89.906004			25	2098	E	0	1
19	35.331266	-89.920981			25	2098	E	0	1
20	35.319164	-89.873442			65	2098	D	0	1
21	35.153188	-90.059146			24	7005	E	0	1
22	35.137466	-90.024084	3	22	22	6259	D	0	2
23	35.130376	-90.023955			22	6259	D	1	1
24	35.155747	-90.037473	1	25	24	3537	D	0	2
25	35.151606	-90.040735	3	25	25	2676	D	0	1
26	35.124652	-90.054897			22	2086	E	0	1
27	35.10264	-90.029534			22	2086	E	0	1
28	35.103061	-90.019985			22	2086	E	0	1
29	35.071525	-90.023332			45	2086	E	0	1
30	35.158338	-90.020242			25	3537	D	0	1
31	35.182929	-89.932609			25	6729	E	0	1
32	35.07939	-90.057321			45	8495	E	0	2
33	35.020647	-90.08822			45	8495	D	0	2
34	35.124294	-90.067707			22	2086	E	0	1
35	35.131173	-89.956728			22	5953	D	0	2
36	35.133559	-89.956127			22	5953	D	0	2
37	35.135243	-89.968143			22	1707	D	0	1
38	35.079982	-89.930549			49	5953	D	0	2
39	35.080578	-89.955869			22	5312	D	0	2
40	35.133766	-89.984064			22	1707	D	0	1
41	35.150891	-89.98136			25	1707	D	0	1
42	35.158259	-89.980416			25	1707	E	0	1
43	35.108035	-89.98827			22	5312	D	0	2
44	35.057674	-89.833646			74	16053	D	1	2
45	35.021095	-90.025306	1	22	45	7397	D	0	2
46	35.020989	-90.002561			45	7397	D	0	2
47	35.131269	-89.901452			55	6015	D	0	2
48	35.11449	-89.901795			22	6015	D	1	1
49	35.057248	-89.932866	1	22	49	4687	D	0	2
50	35.021407	-89.937372			49	4687	D	1	1
51	35.020528	-89.898062			49	4687	D	0	1
52	35.052222	-89.812832			74	5033	D	0	1
53	35.084536	-89.878106			54	5033	D	0	1
54	35.101952	-89.870081	1	55	54	3414	D	0	1
55	35.130947	-89.867721	2	55	55	3414	E	0	1
56	35.171825	-89.943552			25	3348	E	0	1
57	35.149089	-89.927158			25	3348	D	0	1
58	35.152387	-89.884629			25	3348	D	0	1

59	35.037425	-89.795708			74	7361	D	1	1
60	35.020556	-89.795966			12	7361	D	0	1
61	35.142383	-90.051141			25	2607	D	0	1
62	35.236202	-90.014406			24	5107	E	0	1
63	35.199458	-90.034662			24	5107	E	1	1
64	35.191005	-90.016037			25	5107	E	0	1
65	35.235393	-89.895316	2	65	65	4020	D	0	2
66	35.205276	-89.923297			65	4020	E	0	2
67	35.192791	-89.926172			25	4020	E	1	1
68	35.205485	-89.834333			70	11170	D	1	1
69	35.237388	-89.793563			70	2563	D	0	1
70	35.204362	-89.791932	1	65	70	2563	D	0	1
71	35.204642	-89.867163			65	3763	D	0	1
72	35.180442	-89.860168			55	3763	D	0	2
73	35.168234	-89.85416			55	3763	D	0	2
74	35.093018	-89.808541	1	55	74	10082	D	0	2
75	35.075809	-89.774767			74	5629	D	0	1
76	34.994567	-89.84841			49	7678	D	0	1
77	35.207011	-89.894558			65	4020	D	0	1
78	35.169095	-89.90233			55	3763	D	0	1

Note: [1]#HP stands for the number of hospitals in the zone; [2]CP represents location of the collaborative hospital; [3]AP means the locations of assigned hospitals for the zone; [4]HH is the number of households in the zone; [5]Soil defines the seismic site class (D for stiff soil, and E for soft clay soil) of the zone (Fig. 3.8); [6]#TT is the number of trained rescue teams in the zone; [7]#VT refers to the number of voluntary rescue teams in the zone.

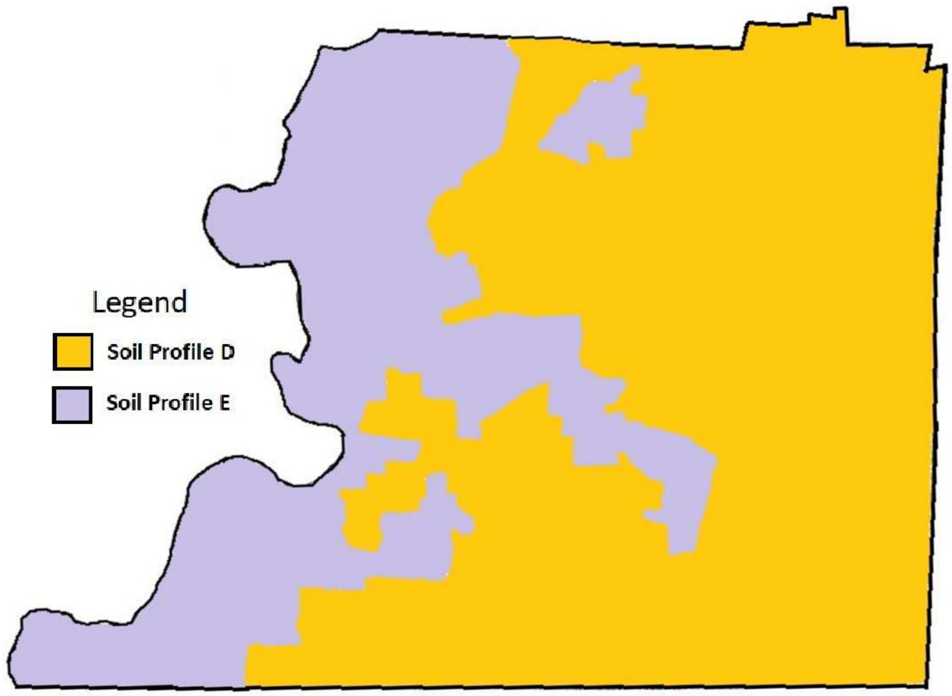

Figure 3.8 Soil Classification in Shelby County (reproduced from Huo & Hwang 1996)

Table 3.7 Bridge types and geographic information

#	Linked edges	Bridge type	Latitude	Longitude
1	(2,3)	MSC concrete	35.310937	-89.744193
2	(4,5)	MSC slab	35.233253	-89.659217
3	(4,8)	MSC steel	35.246915	-89.695855
4	(11,12)	MSSS concrete	35.045511	-89.662113
5	(9,15)	MSSS steel	35.156043	-89.776514
6	(19,20)	MSC concrete	35.314482	-89.865053
7	(21,24)	MSC slab	35.153178	-90.05445
8	(23,27)	MSC steel	35.123137	-90.025811
9	(24,30)	MSSS concrete	35.155959	-90.042432
10	(32,33)	MSSS steel	35.054171	-90.060664
11	(22,40)	MSC concrete	35.135788	-90.005511
12	(30,41)	MSC slab	35.15393	-90.01548
13	(30,42)	MSC steel	35.158315	-90.014235
14	(23,43)	MSSS concrete	35.1226	-90.010316
15	(33,45)	MSSS steel	35.021105	-90.062014
16	(36,47)	MSC concrete	35.13159	-89.920537
17	(39,49)	MSC slab	35.06855	-89.944091
18	(46,50)	MSC steel	35.021045	-89.973089

19	(49,51)	MSSS concrete	35.046231	-89.920253
20	(44,53)	MSSS steel	35.07499	-89.861721
21	(53,54)	MSC concrete	35.089844	-89.870991
22	(42,56)	MSC slab	35.160008	-89.963941
23	(13,59)	MSC steel	35.030062	-89.711567
24	(17,62)	MSSS concrete	35.288598	-90.023812
25	(24,63)	MSSS steel	35.215395	-90.031278
26	(30,64)	MSC concrete	35.196909	-90.023514
27	(3,69)	MSC steel	35.273335	-89.704086
28	(68,72)	MSSS concrete	35.187827	-89.852946
29	(7,73)	MSSS steel	35.176214	-89.834316
30	(54,74)	MSC concrete	35.100944	-89.854158
31	(67,78)	MSC slab	35.175003	-89.906512

3.3.2 Data Analysis

With Eqs. (3.1-3.6), peak ground acceleration, spectral acceleration and spectral displacement can be estimated from seismic attenuation laws. Huo and Hwang (1996) and Hwang et al. (1997) derived the seismic attenuation law for Memphis and Shelby County area, which can be applied to earthquakes with magnitudes M (5.0-7.5) and epicentral distances R (5-200km). Their seismic attenuation law is adopted here to derive the spectral acceleration and peak ground acceleration at the sites of the infrastructures:

$$Ln(SA_{BR}\ or\ PA) = C1 + C2M + C3Ln\left[\sqrt{R^2+H^2} + 0.06e^{0.7M}\right] + C4\sqrt{R^2+H^2} \tag{3.25}$$

$$Ln[F_s(T)] = C5(T)PA + C6(T) \tag{3.26}$$

where $C1$, $C2$, $C3$, $C4$, $C5$, and $C6$ are the parameters from regression analyses. Their values for the 1-story wood frame (1SWF), 2-story wood frame (2SWF), peak acceleration (PA) in the bedrock, and different soil types, and the values of the standard deviations (STD) of $Ln(SA_{BR})$ and $Ln[F_s(T)]$ are presented in Tables 3.8(a)-3.8(b). Based on the study by Hafeez et al. (2018), this study selected 0.1 seconds and 0.2 seconds as the natural periods of 1-story wood frame and 2-story wood frame, respectively.

Table 3.8 Regression parameters

Table 3.8(a) Regression parameters 1 (Huo & Hwuang 1996)

	C1	C2	C3	C4	STD ($Ln(SA_{BR})$)
1-story wood frame	-2.312	0.924	-1.233	-0.00317	0.311
2-story wood frame	-2.968	0.952	-1.219	-0.0024	0.326
PA in the bedrock	-2.904	0.926	-1.271	-0.00302	0.309

Table 3.8(b) Regression parameters 2 (Huang et al. 1997)

	Soil Type	C5	C6	STD ($Ln(F_s(T))$)
1-story wood frame	D	-4.038	1.046	0.533
	E	-4.457	1.112	0.427
2-story wood frame	D	-2.741	1.226	0.393
	E	-3.239	1.462	0.374
PGA	D	-2.075	1.001	0.323
	E	-3.014	1.187	0.273

For Eqs. (3.6-3.7), the seismic fragility parameters of bridges (Nielson & DesRoches 2007), hospitals, and wood frame buildings (Hazus 1997) are presented in Table 3.9 (a-b). Table 3.9(c) shows the indoor casualty rates (Eq. (3.8)) of wood-frame buildings for different damage states (Hazus 1997).

Table 3.9 Fragility and casualty information

Table 3.9(a) Median and dispersion values for seismic fragility of bridges and hospitals

Bridge Class	Extensive med_i	Dispersion ζ_i
MSC concrete	0.75	0.7
MSC slab	0.78	0.7
MSC steel	0.39	0.55
MSSS concrete	0.83	0.65
MSSS steel	0.56	0.5
Hospitals	1.76	0.64

Table 3.9(b) Median and dispersion values for seismic fragility of buildings (inch)

	Slight		Moderate		Extensive		Complete	
	Median	Beta	Median	Beta	Median	Beta	Median	Beta
1 story	0.5	0.8	1.51	0.81	5.04	0.85	12.6	0.97
2 story	0.86	0.81	2.59	0.88	8.64	0.9	21.6	0.83

Table 3.9(c) Casualty rates of severity 2 and 3 for all building damage states

	Slight		Moderate		Extensive		No collapse		Collapse*	
	S2 (%)	S3 (%)	S2 (%)	S3 (%)	S2 (%)	S3 (%)	S2 (%)	S3 (%)	S2 (%)	S3 (%)
1 story	0	0	0.03	0	0.1	0.001	1	0.01	20	3
2 story	0	0	0.025	0	0.1	0.001	1	0.01	20	5

*No collapse and collapse are two subtypes of damage state "complete" and collapse rate is 3% of all the complete damage 1-2 story wood frame buildings (Hazus 1997).

Like voluntary SAR teams, it is assumed in this study that enough self-organized and voluntary staff, e.g., neighbors and roommates, will help send the injured residents to designated hospitals. To be conservative, it is assumed all the self-rescue activities are completed within 1 hour after the earthquake according to Liu et al. (2016), and the parameters of Eq. (3.9) are listed in Table 3.10 (Murakami et al. 2000). According to the demographics of Shelby County (Census profile 2018), 70% of the units are single-family houses (wooden detached). Assuming the buried injuries are evenly distributed among all collapsed units, the weighted SAR speed for the buried cases can be derived with the results summarized in Table 3.10.

Table 3.10 Parameters of SAR Speed (Murakami et al. 2000)

	Wooden detached	Wooden apartment	Weighted
slope, a	19.2	25.9	21.21
constant, b	83.4	93.9	86.55

3.3.3 Results

Two scenario earthquakes are studied here with Richter magnitude of 7.0 and 7.5, respectively. Both have the same hypocenter, which is 10km deep with longitude and latitude of -89.940678 and 35.107757, respectively. The survival function is defined as $S(t) = 0.8e^{-0.00015t^2}$ following the study by Edrissi et al. (2015). To consider uncertainties, Monte Carlo simulation is employed to model the failure scenarios of the bridges for 1,000,000 times. Dijkstra's algorithm (Dijsktra 1959) and equivalent resistant theory (Kagan 2015) are applied to solve the system's graph theory problem and equivalent resistances. The simulation is conducted using Matlab 2020 with a personal computer (processor of 3.2GHz and 16GB RAM).

The results from Eqs. (3.8) and (3.18) are plotted in Figs. 3.9-3.10, showing the comparison results between the numbers of injured people and rescued people of each node/zone under M7.0 and M7.5 earthquakes respectively. It is found that some nodes have high rescue rates because they have more trained rescue teams and/or voluntary teams as compared to their collapsed buildings and injured populations. The others have low rescue rates due to the lack of enough rescuing resources. With Eq. (3.10), the system resilience indexes at M7.0 and M7.5 are calculated, which are 60.4446 and 48.917, respectively. The resilience index of M7.5 is lower than that of M7.0, which corroborates existing findings (e.g., Zhang and Wang 2016) and common understanding. Compared to M7.5, fewer bridges would fail at M7.0. When more roads are intact, the transportation network apparently has a higher redundancy level leading to higher resilience indexes at M7.0.

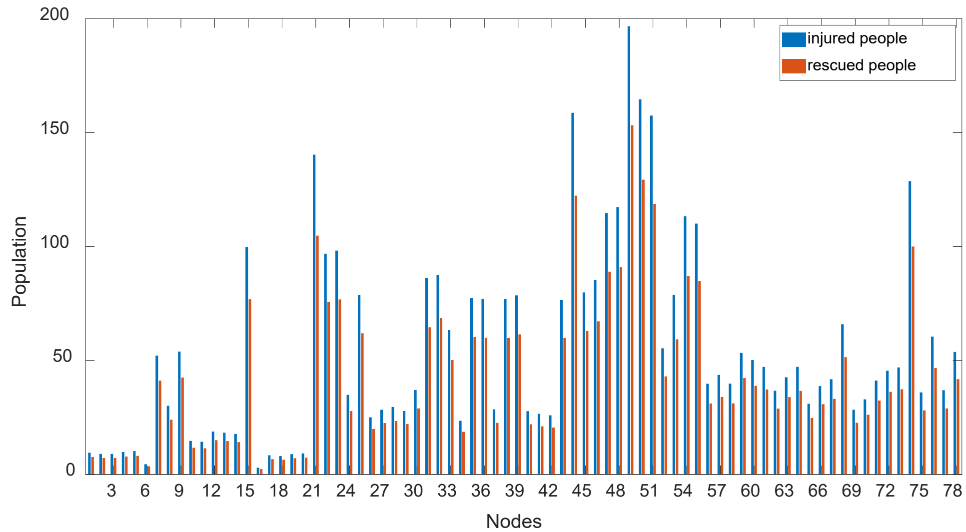

Figure 3.9 Number of injured people and rescued people when M=7.0

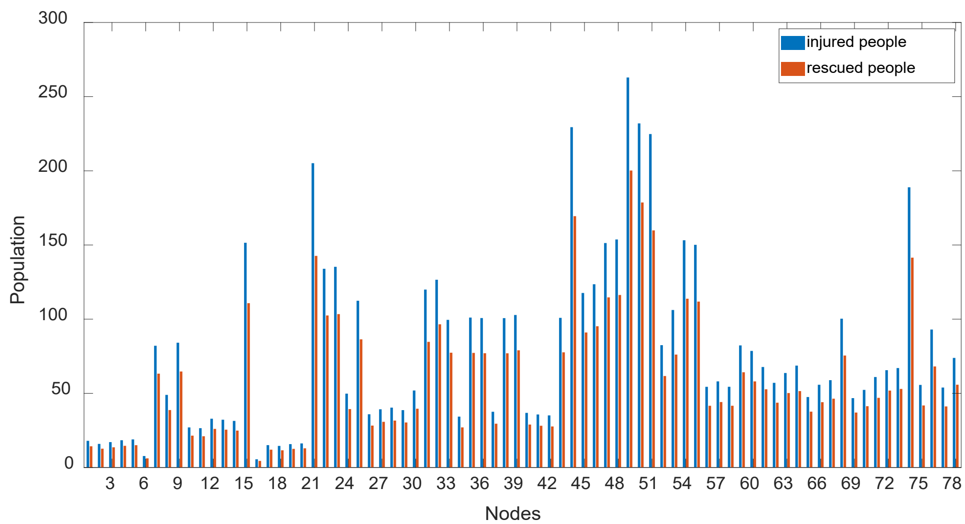

Figure 3.10 Number of injured people and rescued people when M=7.5

Fig. 3.11 illustrates the comparison between the conductivity of nodes to their designated hospitals for two different earthquake magnitudes. As defined in Eq. (3.12), "conductivity" is the reciprocal of a node's equivalent "resistance" to its designated hospitals. Higher conductivity means lower resistance and easier access to hospitals. The conductivity of M7.0 is higher than that of M7.5 for most nodes, which is caused by the significantly increased failure rates of various bridges and the reduced redundancy level of the network caused by more bridge failures when the Richter Magnitude is 7.5. Nodes 17 and 33 have the lowest conductivities because the only link (17, 62) between node 17 and the rest part of the community was vulnerable to earthquakes (Figs. 3.6-3.7); similarly, both links (32, 33) (33, 45) connecting node 33 to the rest of the community were susceptible to earthquakes. Nodes 3 and 4 had low conductivities under M7.5 because they were isolated by vulnerable links (2, 3), (3, 69), (4, 5), and (4, 8), which had relatively high failure probabilities under M7.5. All these nodes with low conductivities share the same characteristics: they either don't have alternative independent routes to hospitals, or all the routes to hospitals are vulnerable to earthquakes. Such phenomenon corroborates the findings by Zhang and Wang (2016).

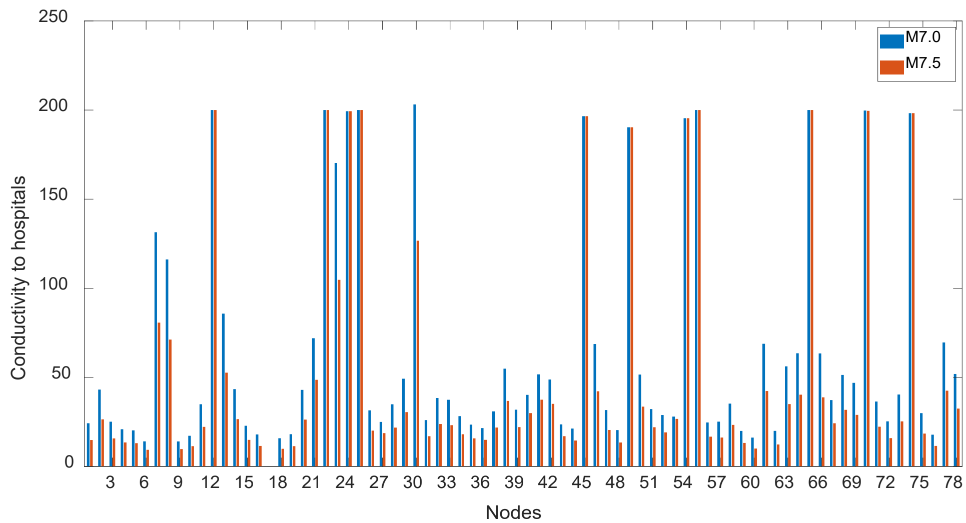

Figure 3.11 Conductivity of nodes to their designated hospitals

Fig. 3.12 presents the number of total injured and rescued people of the community varying with the Richter magnitude to study the impacts of earthquake intensity. It is found that the number of injured people increases with the increase of the magnitude considerably, and the ratio of the rescued population to the injured population gets smaller when the Richter magnitude increases. It may be caused by the fact that the professionally trained and voluntary teams remained the same in this study while the collapsed buildings and injured population increased with the magnitude. It usually takes longer time for the rescue team to reach the increased number of trapped residents when the earthquake magnitude increases. As a result, many people cannot stay alive long enough to be searched and rescued. To study the relationship between the resilience index and the magnitude of earthquakes, a wide range of earthquake magnitudes are studied under which the corresponding network resilience indexes are calculated as shown in Fig. 3.13. It is found from Fig. 3.13 that the resilience index decreases quickly in lower Richter magnitudes and then only vary slowly when Richter magnitudes are between M7.0 to M8.0.

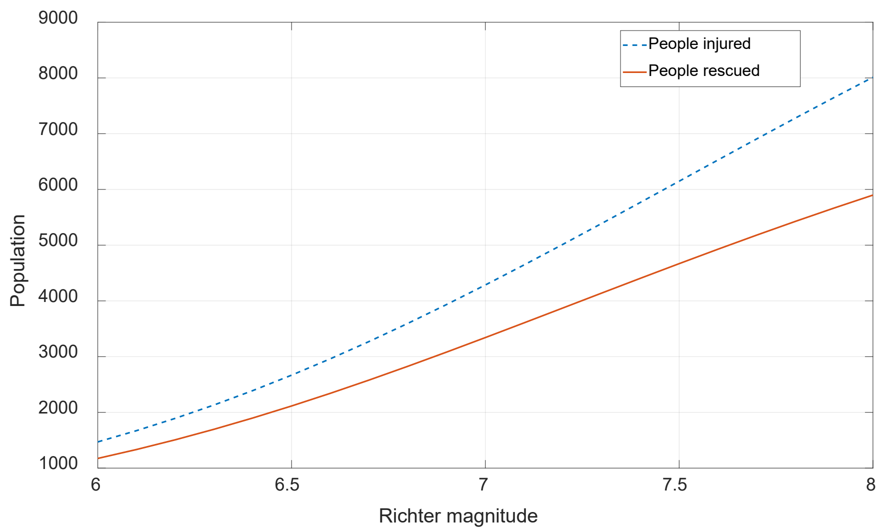

Figure 3.12 Community total injured and rescued population as a function of magnitude

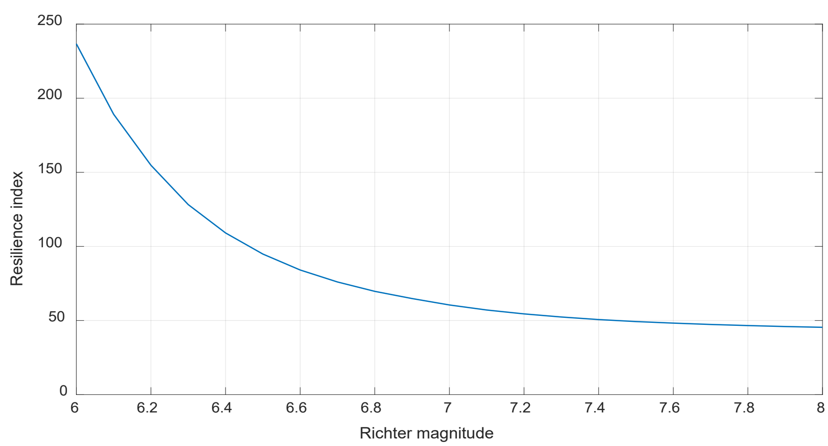

Figure 3.13 Resilience index as a function of magnitude

3.4 Feasibility study of developing optimal pre-hazard bridge reinforcement plan

In this section, the feasibility study of developing optimal pre-hazard bridge reinforcement plan is conducted. Given the high diversity of bridges between regions and site-specific hazard and infrastructure characteristics, some assumptions need to be made to avoid losing generality. To demonstrate a more general scenario, all bridges in this study are assumed not specifically designed against earthquakes, so that typical bridge seismic fragility and reinforcement data can be applied as reliable generic data source. In other words, these bridges just followed typical national bridge design guidelines like most regions in the country without following special and elevated local seismic design guidelines. As shown in Fig. 3.7, there are 31 vulnerable links in the network. Due to the limited bridge maintenance data for multi-span continuous slab bridges and their relatively high seismic robustness according to Table 3.9(a), it is assumed MSC slab bridges don't need reinforcement in this study and the rest 25 groups of bridges will be considered in the reinforcement plan. Padgett and DesRoches (2009) studied the effects of five retrofit methods on the seismic fragility of different bridge types. These methods include full height circular steel jackets to strengthen bridge columns, steel restrainer cables to carry half of the weight of the superstructure, elastomeric isolation bearings to increase the fundamental period in bridge longitudinal direction, transverse shear keys to limit the force transferred to the columns, and seat extenders to provide extra support beyond the bent beam. They concluded the effect of each retrofit method on the seismic fragility of every bridge type as a modification factor for median PGA (med_i) shown in Table 3.9(a) (Padgett and DesRoches 2009). For the different bridge reinforcement methods introduced above, Padgett et al. (2010) also investigated the corresponding costs of all reinforcement methods. Due to the lack of more site-specific data in the studied network, the published data by Padgett and DesRoches (2009) and Padgett et al. (2010) will be used to demonstrate the feasibility of developing optimal pre-hazard bridge performance reinforcement plan. Although these data may not exactly represent the specific scenarios in the prototype area, the publicly accessible data is believed to be general and transparent enough for anyone to repeat the results and follow the proposed methodology with their available site-specific data.

Table 3.11 lists the abbreviated names of different retrofit methods, their maintenance costs, and reinforcement effects on the bridge fragilities derived from Padgett and DesRoches (2009) and Padgett et al. (2010). Due to the lack of site-specific information, these retrofit plans are randomly assigned to different bridge groups in the prototype region for demonstration purposes. As shown in Table 3.11, the total cost to strengthen all bridges is $1,537,308.3. For demonstration purposes, the available budget is set to be $750,000, and the hazard mitigation planning is based on an earthquake with Richter Magnitude of 7.5. The pre-earthquake risk mitigation planning is optimized using the Genetic Algorithm based on Eqs. (3.23-3.24). After repeated calibration experiments, the algorithm parameters are selected as: population size=150, maximum generation=150, crossover rate=0.7, and mutation rate=0.04. The results show when bridge groups 4, 6, 8-11, 15, 18, 24, 26, and 28-29 are repaired, the system has the maximum resilience index of 49.34 at a total cost of $716,599. Twelve groups of bridges are strengthened, most of which are located around the hospitals, e.g., Bridges 8, 9, and 10. Apparently, it is found the reinforcement of these bridges will significantly increase the accessibility to medical resources and the network redundancy. The rest six groups of bridges are on the critical links between some nodes and their designated hospital(s). For example, Bridge 24 is on the link (17, 62), which is the only link connecting node 17 and the rest of the community. The reinforcement of Bridge 28 can increase the accessibility of the "isolated" nodes 3 and 4 to hospitals (Figs. 3.6-3.7).

Table 3.11 Bridge retrofit costs and effects

Bridges	Link	Need retrofit?	Suggest retrofit	Cost $	MF1*
1	(2,3)	Yes	steel column jacket	108000	1.17
2	(4,5)	No	0	0	1
3	(4,8)	Yes	steel column jacket	108000	1.14
4	(11,12)	Yes	steel column jacket	108000	1.33
5	(9,15)	Yes	steel column jacket	108000	1.07
6	(19,20)	Yes	elastomeric isolation bearing	65736	1.21
7	(21,24)	No	0	0	1
8	(23,27)	Yes	elastomeric isolation bearing	104938.95	1.27
9	(24,30)	Yes	elastomeric isolation bearing	42955.35	1.05
10	(32,33)	Yes	elastomeric isolation bearing	60923.85	1.37
11	(22,40)	Yes	steel restrainer cable	33840	1.01
12	(30,41)	No	0	0	1
13	(30,42)	Yes	steel restrainer cable	33840	1.11
14	(23,43)	Yes	steel restrainer cable	33840	1.1
15	(33,45)	Yes	steel restrainer cable	33840	1.04
16	(36,47)	Yes	transverse shear key	69750	0.99
17	(39,49)	No	0	0	1
18	(46,50)	Yes	transverse shear key	69750	1.13
19	(49,51)	Yes	transverse shear key	69750	0.92
20	(44,53)	Yes	transverse shear key	69750	0.98
21	(53,54)	Yes	seat extender	27000	1
22	(42,56)	No	0	0	1
23	(13,59)	Yes	seat extender	27000	1
24	(17,62)	Yes	seat extender	27000	1.02
25	(24,63)	Yes	seat extender	27000	1
26	(30,64)	Yes	elastomeric isolation bearing	65736	1.21
27	(3,69)	Yes	elastomeric isolation bearing	104938.95	1.27
28	(68,72)	Yes	elastomeric isolation bearing	42955.35	1.05
29	(7,73)	Yes	elastomeric isolation bearing	60923.85	1.37
30	(54,74)	Yes	steel restrainer cable	33840	1.01
31	(67,78)	No	0	0	1

Note: *MF1 means modification factors for med_i when calculating extensive damage rate with Eq. (3.6).

Fig. 3.14 outlines the resilience index as a function of the reinforcement budget to investigate the effect of available budget on the system resilience index. It shows the resilience index increases fast with the available reinforcement budget when the budget level remains low and becomes stable when the reinforcement budget further increases. Since the most important links for the network are to be reinforced first, the reinforcement is found to greatly increase the resilience index even with relatively low total budget levels. The resilience index peaks before the reinforcement budget reaches the total cost to strengthen all the bridges, which is $1,537,308.3. There are two reasons for this phenomenon: (1) some retrofit methods don't have obvious positive impacts or even have adverse impacts on the bridge seismic fragilities as shown in Table 3.11 (Padgett and DesRoches 2009); (2) some bridges, such as bridge group 6, locate on relatively insignificant links in terms of emergency medical services and the reinforcements on those groups only have trivial impacts on the network performance. Since the reinforcement budget is commonly insufficient, the tradeoffs will be made between the available budget and the desired RI to achieve by the stakeholders. The results suggest that the pre-hazard bridge reinforcement is an effective mitigation measure to increase the network resilience effectively and proactively in terms of emergency medical response. The specific results, apparently, depend on more site-specific traffic network, bridge inventories and fragility performance data against earthquakes. From the demonstrative study shown above, it is found feasible and promising to use the proposed framework to provide quantitative measures to assist stakeholders to make more informed decisions including proactive pre-hazard mitigation to support emergency medical response.

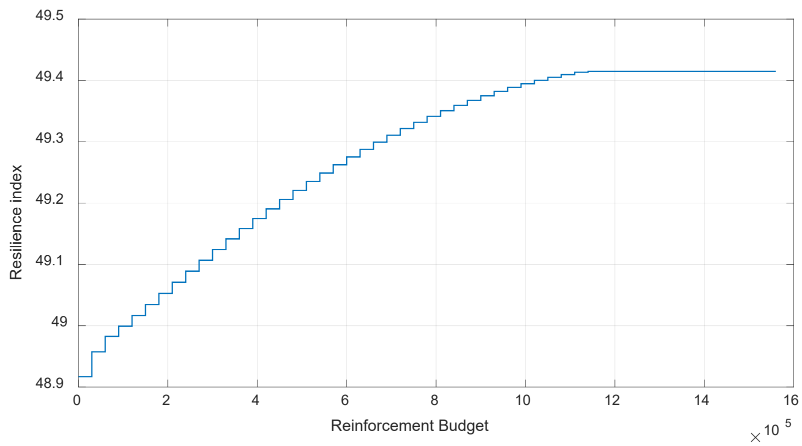

Figure 3.14 Resilience index as a function of reinforcement budget

3.5 Conclusion

The emergency medical response is very critical following disastrous hazards, like earthquakes. A holistic methodology to assess the resilience performance of a transportation network and further conduct pre-hazard mitigation planning was developed from the post-earthquake emergency response perspective. To quantify the number and locations of residents who may need emergency medical services and possible damage scenarios of the links, the seismic fragility information of infrastructure and the Monte Carlo Sampling method were applied in the model to incorporate essential uncertainties. This study introduced a new resilience performance indicator to evaluate the efficiency and full redundancy of the transportation network, as well as the overall performance of the emergency medical response of the whole community. The incorporation of uncertainties into the road damage states made the resilience performance modeling more realistic and reliable. The resilience index is used to develop effective pre-hazard bridge reinforcement and improvement plans, given the limited monetary budget and constantly increasing reinforcement costs. Finally, the proposed methodology was demonstrated in a real-world community-Shelby County, Tennessee, representing a typical earthquake-prone area in the United States. A parametric study was conducted to investigate the impacts of Richter magnitude on the injured population, saved population, and resilience index. The pre-hazard bridge strengthening planning was optimized based on the resilience index given the detailed budget information. The results show that the Richter magnitude considerably affects the number of injured people who may need immediate hospitalization, the number of people that can be saved, and network redundancy. As a result, the seismic magnitude has a notable influence on the conductivity between different zones and their designated hospitals and the overall performance of the emergency medical response.

This study introduced a new approach to consider the full redundancy when quantifying the resilience performance of transportation networks during the emergency medical response. Also, it considered the life vitality loss of injured people when transporting them to hospitals. In practice, the methodology can be implemented to support future emergency medical response with site-specific hazard information, infrastructure data, and demographic information of the community. This study has several limitations: (1) the search-and-rescue operation was simplified because of lacking more refined data and information during the emergency response stage; (2) bridge damage was considered as the only cause of degradation of the traffic network due to the lack of reliable and well-accepted fragility data of other transportation infrastructures under earthquakes. In fact, other than bridge damages, debris, obstacles, and pavement damages may also impact the connectivity of links during the emergency response stage, which may be incorporated in the future when the data becomes available; (3) the feasibility study of pre-hazard mitigation planning used the published generic bridge retrofitting options and cost data because of the lack of site-specific data and the goal of not losing generality; (4) this study did not consider uncertainties and spatial correlations of earthquake excitations in the region because of the scope limit, which may be improved in the future studies.

There are several recommendations for the continuation of the work: (1) building a more advanced post-hazard search-and-rescue model once some essential data becomes available; (2) incorporating all types of link damages to simulate the network degradation more accurately; and (3) developing a more accurate and efficient pre-hazard mitigation optimization program that is capable of computing thousands of bridges with site-specific retrofitting information. Finally, although this study was about earthquakes, the proposed methodology can be easily adapted and applied to more diverse scenarios of emergency medical response involving other hazards or incidents if the post-hazard disruptions are similar.

CHAPTER 4 TRAFFIC RESILIENCE MODELING FOR POST-EARTHQUAKE EMERGENCY MEDICAL RESPONSE AND PLANNING CONSIDERING DISRUPTED INFRASTRUCTURE AND DISLOCATED RESIDENTS2F[3]

4.1 Introduction

Quick access to hospitals is essential for severely injured people during post-earthquake emergency medical response. In addition to emergency medical vehicles, most injured residents are often transported to hospitals by private vehicles. Unlike emergency vehicles, private vehicles carrying injured people don't have the driving privilege and therefore become part of regular traffic. Meanwhile, there is usually considerable traffic from dislocated people subjected to various levels of road disruptions following earthquakes. A realistic and efficient assessment of the resilience performance of the disrupted transportation network during the emergency medical response is crucial to saving as many lives as possible through optimal emergency response planning. This study proposes a new methodology to quantify the resilience of disrupted transportation networks during the emergency response stage considering private-vehicle-based injury transport and evacuation traffic. The proposed methodology simulates the traffic during the emergency medical service using the dynamic traffic assignment method by considering various road disruptions. A resilience index is proposed based on the traffic efficiency of the hospitalization trips and uncertainties in earthquakes and infrastructure vulnerability. Finally, the reasonable number of EMS vehicles is investigated from the optimal emergency medical transportation perspective.

[3] This chapter is adapted from a published paper by the author (Wu and Chen 2023b) with permission from Elsevier.

This chapter is to investigate the resilience performance of EMS efforts following major hazards based on the traffic performance assessment of the disrupted traffic networks to close existing research gaps. The contributions of this study include (1) modeling more realistic traffic demand as well as capacity following hazards; (2) adopting dynamic traffic assignment techniques to capture the time-dependent nature of traffic during the emergency response stage with high uncertainties; (3) focusing on private vehicle-based EMS efforts which have become more important yet being rarely studied; and (4) investigating an important yet unanswered question: with the assistance of private vehicles, what is the reasonable number of EMS vehicles needed in a community to carry out efficient emergency medical response. Specifically, in this study the travel demand is composed of the hospitalization trips of severely injured people and the trips by dislocated residents resulting from earthquake-induced building damages. In the meantime, the reduced traffic capacity of the disrupted roads caused by bridge damages and roadside debris is appropriately modeled.

4.2 Methodology

This study proposes a methodology to evaluate the transportation network resilience during the post-disaster emergency response period considering hazard-induced traffic capacity reduction because of road degradation, dislocated population, and private-vehicle-based emergency medical response. As outlined in Fig.1, the proposed methodology starts with earthquake simulation, with which the damage scenarios of buildings and bridges are estimated using seismic attenuation law and infrastructure fragility (Atkinson and Boore 2006; Neilson and DesRoches 2007). The debris distribution on the roads is simulated based on the building damage scenarios using probabilistic methods (Moya et al. 2020), while the numbers of dislocated residents and injured populations are further estimated based on building damage scenarios (Hazus 2020).

In this study, dislocated residents and injured people being transported to hospitals are the main travel demand of the community during the emergency medical response. Based on the estimated travel demand and road degradation information, the traffic simulation during the post-disaster emergency response period is conducted using the dynamic traffic assignment (DTA) method (Han et al., 2019). The traffic efficiency of transporting injured residents is of utmost importance during the emergency response stage and is therefore used as the resilience index of the EMS efforts in the community. Finally, traffic efficiency will be used to estimate the reasonable number of EMS vehicles to support emergency management. Figure 4.1 summarizes these key steps along with corresponding equations, and Table 4.1 lists the notations of main variables used in this study.

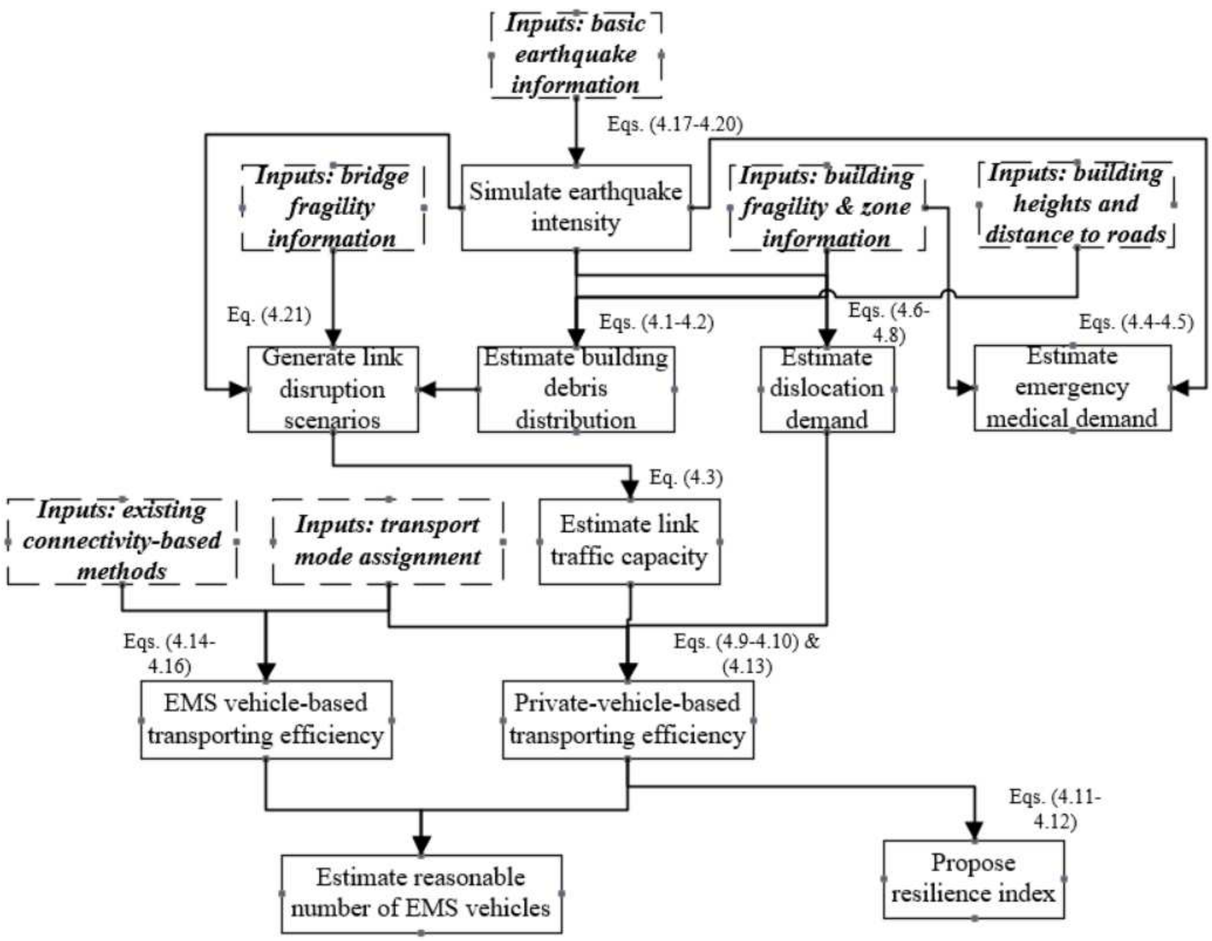

Figure 4.1 Flowchart of the proposed methodology

Table 4.1 List of notations

Variables	Description
AOD	Mean ambulance offload delay
c_r	Traffic capacity of roads with work zones
d	Debris extent
DH_i	Number of the dislocated household of zone i
f_{HV}	Adjustment factor for heavy vehicles
h	Height of building
HH_i	Total number of households for zone i
inj_i	Number of injured people of a given zone i
M_1^i	Average building occupancy of zone i
M_2^{bt}	Trapped rate of occupants in the collapse of building type bt
M_3^{bt}	Severely injured rate among the trapped population of building type bt
med_i	Median peak ground acceleration value of damage state i
$\%MF_i$	Parameter related to the structural damage states

$\%MFC_i$	Probabilities for multi-family residential buildings suffering complete damage
$\%MFE_i$	Probabilities for multi-family residential buildings suffering extensive damage
$\%MFM_i$	Probabilities for multi-family residential buildings suffering moderate damage
MFU_i	Total numbers of dwelling units for multiple families for zone i
M_L	Richter magnitude
$n_{i,j}^{a}$	Maximum number of transport rounds
$n_{i,j}^{Ev}$	Demand of EMS vehicle transport from zone i to hospital j
$n_{i,j}^{t0}$	EMS vehicle demand from zone i to hospital j per unit time
n_{SAR}^{i}	Number of rescue teams available in zone i
$n_{t,p}^{ij}$	Number of injured people transported from zone i to hospital j at time t through path p by private vehicles
N_{EV}	Total number of injured people using EMS vehicles
$N_{i,j}^{Ev}$	Available number of EMS vehicles from zone i to hospital j
$N_{i,j}^{T_0}$	Total number of injured residents in zone i that choose to go to hospital j using EMS vehicles
N_{lanes}	Number of lanes through the work zone
P_{bt}	Collapse probability of building type bt
PGA	Mean peak ground acceleration
P_{ij}	Set of all OD pairs
Pop_i	Population of zone i
$\mathrm{R_e}$	Epicentral distance
RI	Resilience indicator
RI_s	Resilience indicator of the system under network damage state s
R_{ramp}	Adjustment for on-ramps in or near the work zone
$R(\varepsilon)$	Reliability of the transportation system
S	Factor for soil sites
$\%SF_i$	Parameter related to the structural damage states
$\%SFC_i$	Probabilities for single-family residential buildings suffering complete damage
$\%SFE_i$	Probabilities for single-family residential buildings suffering extensive damage
$\%SFM_i$	Probabilities for single-family residential buildings suffering moderate damage
SFU_i	Total numbers of dwelling units for single families for zone i
t	Traffic departure time
$t_{i,j}^{0}$	Shortest-path free-flow travel time from zone i to hospital j
$t_{i,j}^{Mean}$	Mean transporting time per injured resident from zone i to hospital j using EMS vehicle
TA_{ij}	Target arrival time of OD pair (i,j)
T_0	Defined study time horizon
TH_0	Pre-hazard total travel time of hospital trips of the community using private vehicles
TH	Post-hazard total travel time of hospital trips of the community using private vehicles
t_{mean}^{Ev}	Mean transporting times of an injured resident to a designated hospital using EMS vehicles
t_{mean}^{pv}	Mean transporting times of an injured resident to a designated hospital using private vehicles

$T_{t,p}^{ij}$	Travel time from zone i to hospital j at time t through path p
v_{SAR}	Search-and-rescue speed per rescue team
WI	Adjustment factor for type and intensity of work activity
W_{MFC}	Default value for complete damage probability for multi-family homes
W_{MFE}	Default value for extensive damage probability for multi-family homes
W_{MFM}	Default value for moderate damage probability for multi-family homes
W_{SFC}	Default value for complete damage probability for single-family homes
W_{SFE}	Default value for extensive damage probability for single-family homes
W_{SFM}	Default value for moderate damage probability for single-family homes
ζ_i	Dispersion of damage state i
μ_h	Mean value of building heights
σ	Variance of building heights
$\psi_p(t,h)$	Travel cost of path p at departure time t and departure rate h

4.2.1 Traffic capacity of disrupted infrastructures

The seismic fragility of typical structures offers the probability of exceeding specified structural performance indicators, such as stress and displacement, for specified seismic intensity measures, e.g., peak ground acceleration (Casotto et al., 2015). Because of the uncertainties in structural capacity and seismic intensities affecting the accuracy of structural failure, typical structures' seismic fragility is often expressed as probabilities of specified structural damage states as functions of structural intensities (Muntasir Billah and Shahria Alam, 2015).

4.2.1.1 Link closure caused by bridge damages

There are five typical seismic damage states for bridges: no damage, slight damage, moderate damage, extensive damage, and complete damage (e.g., Choi et al. 2004). Seismic fragilities for various bridge types (e.g., concrete bridges and steel bridges) are usually different, and so are the fragilities for different damage states of the same bridge (e.g., Choi et al. 2004; Gardoni et al. 2003; Neilson and DesRoches 2007). When simulating the transportation network during the emergency response stage, a linkage needs to be built between bridge functionality (e.g., closure, partial closure, or fully open) and damage states (Wu and Chen, 2019). According to Padgett and DesRoches (2007), bridges suffering extensive or higher damages cannot carry any traffic immediately after the disaster. Some existing studies (Mackie and Stojadinović 2006; Yoon et al. 2021) also suggest bridges with extensive damage may lose most of their traffic carrying capacity. Because emergency response often occurs before transportation authorities can conduct comprehensive inspections of damaged bridges, it is conservatively assumed in this study that the transportation department will close a whole link if such a link has a bridge experiencing extensive or higher levels of damages as defined by the limit states. This is based on common observations that a bridge with extensive or worse damages usually exhibits apparent impassable features like settlement, bent bolts, or considerable cracks on decks, beams, or piers (Choi et al. 2004; Hsu and Fu 2004).

4.2.1.2 Debris distribution and link capacity

In addition to bridges, extensive studies have been conducted on damages and collapse of residential, commercial, and special buildings (e.g., hospitals) (Reinhorn et al. 2001; Jaiswal et al. 2011; Wang and van de Lindt, 2022). When vulnerable buildings are tall and adjacent to the roads, their damages may result in debris on the roads, which may reduce the road functionality if the debris blocks some lanes or even the whole road segment. The probability that the debris will block a certain width of a street is mainly a function of building height, the distance from the building edge to the road edge, and the width of the street (Tamima and Chouinard 2017; Moya et al., 2020).

According to Moya et al. (2020), the probabilities that a collapsed building of a given height h produces the debris extent D greater than or equal to d are defined as the following respectively:

$$P(D > d|H = h \,\&\, collapse) = \int_d^{\infty} P(D = d|H = h \,\&\, collapse)dx \qquad (4.1)$$

$$P(D = d|H = h \,\&\, collapse) = \begin{cases} 1.5e^{-0.43h}, & d = 0 \\ (1 - 1.5e^{-0.43})\left(\frac{1}{\sqrt{2\pi\sigma}}\exp\left[-\frac{(d-\mu_h)^2}{2\sigma^2}\right]\right) & d > 0 \end{cases} \quad (4.2)$$

where μ_h and σ are the mean value and the variance of the building heights (Moya et al., 2020).

Existing studies (e.g., Stein and Neuman 2007) suggest that arterial roads are not deemed safe to get through if the lane width is less than 3 meters. In this study, both single- and double-lane roads will be deemed fully closed if the clear width of the road is less than 3 meters due to debris blockage. For a given direction on a road segment, a double-lane road will be degraded into a single-lane road if the clear width of the road is between 3 and 6 meters. Otherwise, a road will be deemed fully open in the direction if the clear width is more than 3 and 6 meters for single- and double-lane roads, respectively. The detailed decision flowchart to assess the road degradation level for single-lane and double-lane roads is presented in Fig. 4.2.

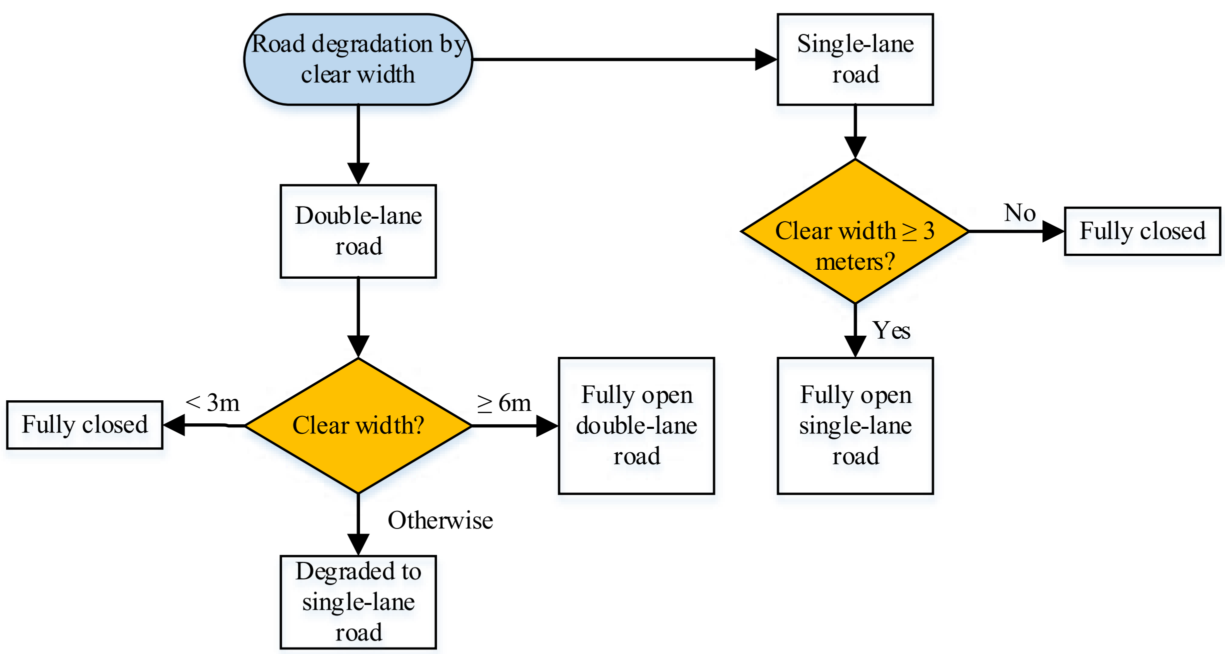

Figure 4.2 Road degradation by clear width

For multi-lane roads with two or more lanes in one direction, one lane blocked by debris will create a short-term “work zone” on the road by debris. The “work zone” can significantly change the link's traffic flow and traffic pattern. According to the Highway Capacity Manual (Manual, 2010), short-term work zones may reduce the traffic capacity and the reduced capacity c_r (veh/h) can be estimated by:

$$c_r = (1600 + WI) \cdot f_{HV} \cdot N_{lanes} - R_{ramp} \tag{4.3}$$

where WI is the adjustment factor for the type and intensity of work activity (pc/h/ln) ranging between ±160 pc/h/ln; f_{HV} is the adjustment factor for heavy vehicles, and $f_{HV} = 1$ when the truck percentage is negligible; N_{lanes} is the number of lanes through the work zone, and R_{ramp} is the adjustment for on-ramps in or near the work zone (veh/h), which is only applicable to freeways. In this study with a focus on urban roads, it is assumed the truck percentage is negligible during the emergency response stage and the ramp adjustment is ignored. In addition, considering the actual speed limits during the emergency response stage are either unavailable or not well followed, a greatly reduced speed limit at half its original value is adopted following the assumptions and observations in existing studies (Costa et al., 2020).

4.2.2 Traffic demand during emergency response stage

In this study, the hospitalization trips of injured residents and the dislocation trips by evacuated residents generate the primary travel demand during the emergency response stage. The seismic fragilities of buildings introduced previously will be used to estimate the damages of residential buildings and the resulting injuries to the residents. The building fragilities will also be used to simulate the damage states of medical facilities and the available post-earthquake medical resources, e.g., hospitals (Coburn et al., 1992; Hazus 2020), whose failure will affect the transporting destination choices of the injured people.

4.2.2.1 *Hospital trips and mode choice*

The injured people can be estimated based on the population, average occupancy, building failure rate, trapped rate, and severely injured rate (Coburn et al. 1992; Hazus 2020):

$$inj_i = \sum_{bt} Pop_i * P_{bt} * M_1^i * M_2^{bt} * M_3^{bt} \tag{4.4}$$

where inj_i is the number of injured residents of a given zone i; Pop_i is the population of zone i; P_{bt} is the collapse probability of building type bt; M_1^i is the average building occupancy of zone i and M_2^{bt} is the trapped rate of occupants in the collapse of building type bt; M_3^{bt} is the severely injured rate among the trapped population of building type bt.

When the injured residents are rescued from the damaged buildings, the hospitalization trips of zone i during the study time T_0 can be estimated:

$$N_h^i = n_{SAR}^i * v_{SAR} * T_0 \tag{4.5}$$

where n_{SAR}^i is the number of SAR teams available in zone i; v_{SAR} is the rescue speed per rescue team (unit: person/hour); N_h^i is the number of hospitalization trips of zone i.

According to Tani et al. (2004), the search and rescue (SAR) teams can rescue about 85% of trapped people on-site at a relatively high and steady speed, while the rescue of the rest 15% of trapped residents would take a very long time. T_0 is the study period of the EMS activity, which starts from the beginning of the EMS activity till 85% of injured residents have been rescued. Hazus (2020) states that most severely injured residents who need immediate hospitalization are caused by building collapse. It is assumed in this study that all the severely wounded residents are trapped and need to be searched and rescued for demonstrative purposes.

There are various emergency transport methods for injured people, including on foot, public transportation, private vehicles, ground EMS vehicles, and air ambulances. Considering public transit may be severely impacted without providing normal service under severe earthquakes, this study focuses on ground transportation of emergency medical response in two modes: using private vehicles and using EMS vehicles. According to some recent studies on post-hazard rescue efforts, most injured people were transported to hospitals by private vehicles (Djalali et al., 2011; Kang et al., 2015). Tanaka et al. (1998) found around 74% of the injured residents were sent to hospitals by private vehicles during the 1995 Hanshin-Awaji Earthquake. So, for communities without site-specific data, it will be a reasonable assumption that 75% of the injured residents are transported using private vehicles. Since the traffic on the road typically will not yield to these private vehicles transporting injured people, these hospital trips by private vehicles would experience similar delays as other regular vehicles on the same routes at that time. Due to the lack of reliable data, no special driving behavior of those private vehicles transporting injured people is considered.

4.2.2.2 Traffic demands from dislocated population

Earthquakes can cause residential building damages, drinking water shortages, and power outages, resulting in dislocated households. These households may need temporary shelters like friends' houses or public shelters. According to Hazus (2020), the number of dislocated households after earthquakes can be estimated by the following equation:

$$DH_i = (SFU_i \times \%SF_i + MFU_i \times \%MF_i) * (\frac{HH_i}{SFU_i + MFU_i}) \tag{4.6}$$

where DH_i is the number of the dislocated household of zone i; SFU_i and MFU_i are the total numbers of dwelling units for single and multiple families for zone i, respectively; HH_i is the total number of households for zone i; $\%SF_i$ and $\%MF_i$ are parameters related to the structural damage states (Hazus 2020), which are defined as:

$$\%SF_i = W_{SFM} \times \%SFM_i + W_{SFE} \times \%SFE_i + W_{SFC} \times \%SFC_i \tag{4.7}$$

$$\%MF_i = W_{MFM} \times \%MFM_i + W_{MFE} \times \%MFE_i + W_{MFC} \times \%MFC_i \tag{4.8}$$

where $\%SFM_i$, $\%SFE_i$, and $\%SFC_i$ are the probabilities for single-family residential buildings suffering moderate, extensive, and complete damage states, respectively. Similarly, $\%MFM_i$, $\%MFE_i$, and $\%MFC_i$ are the probabilities for multi-family situations for the three damage states, respectively. W_{SFM}, W_{SFE}, W_{SFC}, W_{MFM}, W_{MFE}, and W_{MFC} are the default values for damage state probabilities which are 0, 0, 1, 0, 0.9, and 1, respectively. In this study, it is assumed the evacuation will conclude within the study horizon T_0, considering the low possibility for anyone to live in damaged buildings without drinking water, food supplies, and power.

4.2.3 Traffic performance modeling and resilience assessment

4.2.3.1 Dynamic traffic assignment

As discussed previously, to handle varying traffic characteristics during the emergency response stage, real-time traffic simulation is critical to estimating the travel time of hospitalization trips with different departure time and origin-destination situations. The emergency travel demand can be estimated as introduced in Section 4.2.2. However, the information about the distribution of these trips during the emergency response period is still lacking. So, it will be recognized as a fixed-demand traffic simulation in this study, for which the fixed-demand Dynamic User Equilibria model proposed by Han et al. (2019) is applied to conduct the dynamic traffic assignment (DTA) during the emergency response period. The effective delays of paths are defined as:

$$\psi_p(t,h) = D_p(t,h) + \begin{cases} 0.8(t + D_p(t,h) - TA_{ij})^2 \;\; if\; t + D_p(t,h) < TA_{ij} \\ 1.2(t + D_p(t,h) - TA_{ij})^2 \;\; if\; t + D_p(t,h) \geq TA_{ij} \end{cases} \qquad p \in P_{ij} \tag{4.9}$$

where $\psi_p(t,h)$ is the travel cost of path p at the departure time t and departure rate h; TA_{ij} is the target arrival time of OD pair (i,j); and P_{ij} is the set of all OD pairs (Han et al. 2019). As indicated by its name, the travel demand between each OD pair is fixed according to the study of Han et al. (2019). For trips between each OD pair, a target arrival time TA_{ij} needs to be assigned to calculate the travel cost.

4.2.3.2 Post-earthquake traffic performance and resilience indicators

The efficiency of transporting injured people to hospitals is a key factor in evaluating the success of emergency response efforts. Therefore, the total travel time of private-vehicle-based hospital trips of the community is proposed to reflect the efficiency of the transportation network, which is defined as:

$$TH = \sum_{ij} \sum_p \int_0^{T_0} n_{t,p}^{ij} \cdot T_{t,p}^{ij} dt \tag{4.10}$$

where TH is the total travel time of hospital trips of the community using private vehicles; T_0 is the study time horizon, which is defined as the time limit for rescuing 85% of the injured people in this study; $n_{t,p}^{ij}$ is the number of injured people transported from zone i to hospital j at time t through path p by private vehicles; and $T_{t,p}^{ij}$ is the travel time from zone i to hospital j at time t through path p. For any given earthquake scenario, the hospitalization travel demand stays the same. So, the smaller TH is, the more efficient the network will be during the emergency response. The resilience indicator (RI) of the transportation network is defined as:

$$RI = \frac{TH_0}{TH} \tag{4.11}$$

where TH_0 and TH are the travel time for the pre-hazard and post-hazard periods, respectively. To evaluate the expected performance of the transportation network, the reliability of the transportation system $R(\varepsilon)$ to maintain a given level of performance ε is expressed as:

$$R(\varepsilon) = \sum_{s=1}^{M} P\{RI_s \geq \varepsilon\} \tag{4.12}$$

where RI_s is the resilience indicator of the system under network damage state s caused by link closure or degradation and hospital failure; M is the number of sampled network damage states; ε is the level of performance (LOP) criterion of the transportation network during emergency response stage, which is usually specified by the stakeholders; ε is between 0 and 1 being used as a criterion set by stakeholders for acceptable performance.

4.2.4 The Reasonable number of EMS vehicles

For emergency transportation of people with life-threatening injuries, the efficiency of transport is the key factor for their survival (Meisel et al. 2011; Radun et al. 2022; Wandling et al. 2018). This study will compare the transport efficiency between private and EMS vehicles to investigate the reasonable number of EMS vehicles. Private vehicles of injured people, their families, and neighbors are assumed to be sufficient and immediately available as needed, given the high popularity of private vehicle ownership in the U.S. As mentioned previously, private vehicles will become part of the post-earthquake emergency traffic and may experience traffic delays. In comparison, EMS vehicles can avoid traffic delays because of their driving privilege. However, EMS vehicles may not be immediately available if the demand is larger than the supply, and an injured people may need to wait till the next available EMS vehicle arrives. Assuming all EMS vehicles depart from the hospitals, the travel time can be approximated as the free-flow time given the privilege. An injured resident may experience twice the free-flow travel time (round trip) between the hospital and hazard zone if sufficient EMS vehicles are available. If the SAR speed is fast enough that the EMS demand becomes larger than the number of available EMS vehicles, except for those people being transported in the first round, everyone else must wait for extra time that can be as long as several transport rounds. Each transport round includes a zone-hospital roundtrip and the offloading time at the emergency department of the hospital. It takes time for the EMS vehicles to unload patients at the hospital emergency department and prepare for the subsequent transport (Cooney et al. 2013; Li et al. 2019). So, the ambulance offload delay (AOD) should be included in the calculation of the efficiency of EMS vehicles if the demand is larger than the supply. The supply of a zone is defined as the number of EMS vehicles being assigned to that zone, while the demand in any zone is defined as the number of severely injured residents rescued by SAR teams over one transport round that choose to be transported by EMS vehicles. So, the supply-demand relationship of a zone can be recognized as the EMS vehicle number-SAR speed relationship. For this situation, the mean transporting time of EMS vehicles can be estimated using the first-in and first-out queueing model (Mannering & Washburn 2020). In this study, the transport time is defined as the period from the moment when a patient is ready to be transported on site until the patient is transported to the designated hospital. The mean transporting time of an injured resident using private and EMS vehicles (Mannering & Washburn 2020) is respectively defined as:

$$t_{mean}^{pv} = \frac{TH}{\sum_{ij}\sum_{p}\int_{0}^{T_0} n_{t,p}^{ij}\,dt} \tag{4.13}$$

$$t_{mean}^{Ev} = \frac{\sum_{i.j} t_{i,j}^{Mean} n_{i,j}^{Ev}}{\sum_{i,j} n_{i,j}^{Ev}} \tag{4.14}$$

$$t_{i,j}^{Mean} = \begin{cases} 2t_{i,j}^0, & if\ n_{i,j}^{t0} \le N_{i,j}^{Ev} \\ 2t_{i,j}^0 + \dfrac{AOD[n_{i,j}^a(N_{i,j}^{T_0} - \frac{T_0}{2t_{i,j}^0} N_{i,j}^{Ev}) - \frac{n_{i,j}^a(n_{i,j}^a - 1)}{2} N_{i,j}^{Ev})]}{N_{i,j}^{T_0}}, & if\ n_{i,j}^{t0} > N_{i,j}^{Ev} \end{cases} \quad (4.15)$$

$$n_{i,j}^a = \left\lceil \frac{N_{i,j}^{T_0} - \frac{T_0}{2t_{i,j}^0} N_{i,j}^{Ev}}{N_{i,j}^{Ev}} \right\rceil \quad (4.16)$$

where t_{mean}^{pv} and t_{mean}^{Ev} are the mean transporting time per injured resident using private and EMS vehicles, respectively. $t_{i,j}^{Mean}$ is the mean transporting time per injured resident from zone i to hospital j using EMS vehicle; $n_{i,j}^{Ev}$ is the demand of EMS vehicle transport from zone i to hospital j; $t_{i,j}^0$ is the shortest-path free-flow travel time from zone i to hospital j; AOD is the mean ambulance offload delay; $n_{i,j}^a$ is the maximum number of transport rounds that the last round of injured people need to wait; $n_{i,j}^{t0}$ is EMS vehicle demand from zone i to hospital j per unit time, which is the number of rescued people by SAR teams during the period of $2t_{i,j}^0$ in zone i that choose to go to hospital j using EMS vehicles; $N_{i,j}^{Ev}$ is the available number of EMS vehicles from zone i to hospital j; $N_{i,j}^{T_0}$ is the total number of injured residents in zone i that choose to go to hospital j using EMS vehicles, and its value is $n_{i,j}^{t0} \frac{T_0}{2t_{i,j}^0}$. The reasonable number of EMS vehicles is defined based on their efficiency. If t_{mean}^{Ev} is shorter than t_{mean}^{pv} in more than 50% of the sampled network disruption scenarios, the EMS vehicles are considered as more efficient, and the number of EMS vehicles is deemed reasonable.

4.3 Case study

4.3.1 Transportation network of Centerville

Fig. 4.3 presents the basic transportation network of a virtual community called Centerville, which has been used as a virtual testbed for many studies (Ellingwood et al. 2016). This virtual community is assumed to be in earthquake-prone areas to demonstrate the proposed network under seismic hazards. The network has 20 nodes (I1-I7, P1-P6, and R1-R7), each representing the centroid of a zone (e.g., traffic analysis zone) in the community. The average household size of the community is set as 2.51, according to the average household size of the U.S. in 2021 (Statista 2022). There are eight types of buildings in the community: one-story wood-frame (W1), two-story wood-frame (W2), low-rise steel moment frame (S1L), mid-rise steel moment frame (S1M), low-rise concrete moment frame (C1L), mid-rise concrete moment frame (C1M), low-rise concrete shear wall (C2L), and mid-rise concrete shear wall (C2M). The percentages of these building types in different zones are shown in Table 4.2.

During the emergency response period after major earthquakes, the speed limits were set to be half of their original values (Costa et al., 2020). For Centerville, the speed limit during the emergency response stage for all the roads is set as 20 miles/hour, which is about half the typical speed limits of main roads in a small- or medium-sized city. It is assumed that two hospitals in the network are in zone R3 and zone R5 (marked in Fig. 4.3). The two medical centers are special buildings classified as mid-rise buildings with concrete shear walls, as defined by Hazus (2020). It is assumed a medical center will be closed if it experiences extensive or complete damages. Otherwise, it will remain at its full functionality. In this study, only bridge damage and building debris may cause any link to be fully or partially closed. Nine out of thirty-three roads/links have bridges on them in this community (Fig. 4.3). The bridge types and fragility parameters are listed in Table 4.5. Six links are identified to be vulnerable to building debris because the buildings on both sides of those roads are vulnerable to earthquakes, tall and close to the roads. The information of the six links with possible debris blockage is presented in Table 4.4. This study assumes the buildings on both sides of the six links are wood-frame buildings, so the debris scattering models under earthquakes by Moya et al. (2020) can be applied.

Since Centerville is a small city, the distance may not be the primary concern for residents to choose hospitals in normal conditions. Without introducing unnecessary complexity for this virtual community, it is assumed the residents of each zone evenly select the two hospitals in normal daily life, who will keep the same preference during the emergency response stage. The only community shelter is in zone I7 (marked in Fig. 4.3) to provide temporary accommodation for the dislocated residents. It is assumed the shelter has enough space and resource to accept all the dislocated people and remains robust enough against earthquakes. Therefore, zone I7 will be the destination of all the dislocation trips.

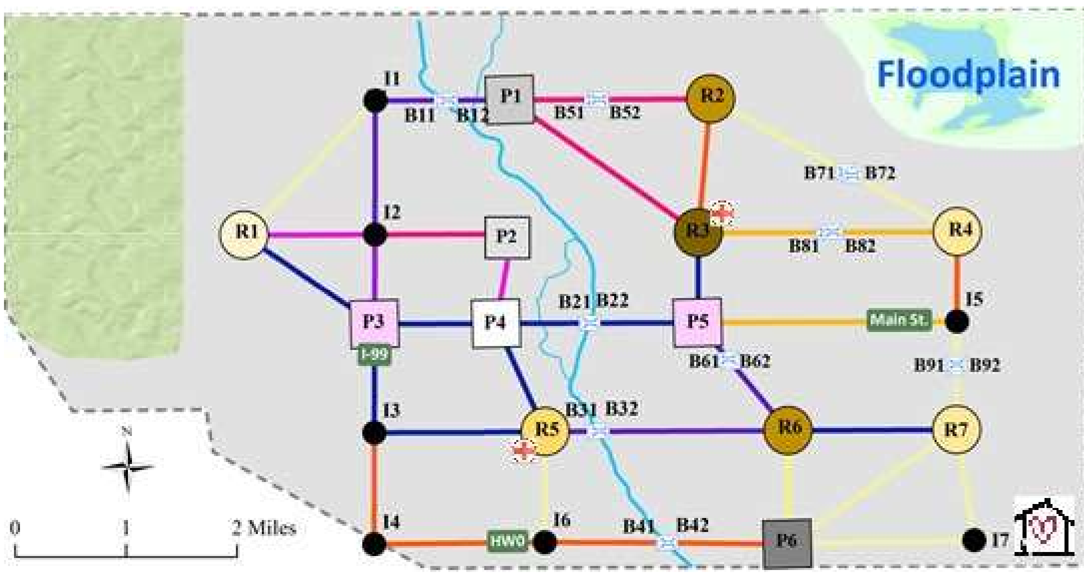

Figure 4.3 Traffic network of Centerville

Table 4.2 Zone information

Zone	Longitude	Latitude	#HH	W1 %	W2 %	S1L %	S1M %	C1L %	C1M %	C2L %	C2M %
I1	-97.48847	35.25686	1836	0.122	0.125	0.126	0.134	0.121	0.119	0.131	0.122
I2	-97.48904	35.23938	1740	0.136	0.107	0.124	0.113	0.136	0.117	0.137	0.13
I3	-97.48989	35.21343	1775	0.111	0.135	0.11	0.123	0.121	0.107	0.144	0.149
I4	-	35.1988	184	0.11	0.13	0.108	0.109	0.103	0.102	0.133	0.195

	97.49037	6	4	1	9						
I5	-97.41353	35.22570	1941	0.14	0.105	0.148	0.123	0.105	0.117	0.1	0.162
I6	-97.46811	35.19846	1673	0.128	0.107	0.14	0.118	0.12	0.101	0.139	0.147
I7	-97.41214	35.19706	1903	0.143	0.118	0.122	0.122	0.101	0.117	0.137	0.14
P1	-97.47092	35.25643	982	0.118	0.124	0.108	0.123	0.114	0.128	0.128	0.157
P2	-97.47116	35.23894	932	0.122	0.113	0.124	0.118	0.134	0.12	0.143	0.126
P3	-97.48943	35.22758	969	0.137	0.127	0.116	0.106	0.128	0.14	0.136	0.11
P4	-97.47357	35.22719	1146	0.123	0.114	0.119	0.107	0.118	0.133	0.149	0.137
P5	-97.44726	35.22654	913	0.123	0.136	0.118	0.116	0.1	0.141	0.131	0.135
P6	-97.49008	35.20760	889	0.104	0.128	0.108	0.111	0.136	0.119	0.141	0.153
R1	-97.50608	35.23979	832	0.1	0.128	0.129	0.133	0.141	0.127	0.135	0.107
R2	-97.44477	35.25578	947	0.134	0.118	0.117	0.125	0.102	0.133	0.149	0.122
R3	-97.44687	35.23834	533	0.109	0.118	0.103	0.117	0.118	0.14	0.104	0.191
R4	-97.41313	35.23749	848	0.122	0.105	0.101	0.123	0.1	0.114	0.15	0.185
R5	-97.46763	35.21289	900	0.141	0.115	0.131	0.143	0.145	0.105	0.109	0.111
R6	-97.43593	35.21210	712	0.117	0.125	0.11	0.145	0.142	0.11	0.127	0.124
R7	-97.41401	35.21155	960	0.133	0.115	0.108	0.128	0.101	0.15	0.141	0.124

Table 4.3 Link characteristics

Link#	Start zone	End zone	Length (km)	No. of lanes
1	I1	I2	1.945	1
2	I1	P1	1.594	1
3	I1	R1	2.482	1

4	I2	P2	1.625	1
5	I2	P3	1.312	1
6	I2	R1	1.548	1
7	I3	I4	1.621	1
8	I3	P3	1.574	1
9	I3	R5	2.023	2
10	I4	I6	2.023	1
11	I5	P5	3.065	2
12	I5	R4	1.312	1
13	I5	R7	1.574	1
14	I6	P6	2.882	1
15	I6	R5	1.605	1
16	I7	P6	2.207	1
17	I7	R7	1.620	1
18	P1	R2	2.376	1
19	P1	R3	2.969	1
20	P2	P4	1.324	2
21	P3	P4	1.441	2
22	P3	R1	2.032	1
23	P4	P5	2.391	2
24	P4	R5	1.680	2
25	P5	R3	1.312	2
26	P5	R6	1.908	2
27	P6	R6	1.651	1
28	P6	R7	2.584	1
29	R2	R3	1.949	1
30	R2	R4	3.519	1
31	R3	R4	3.065	1
32	R5	R6	2.881	2
33	R6	R7	1.992	1

Table 4.4 Information of links with debris blockage risks

Link	# Lanes	[1]LW	[2]BLW	[3]BTRD	[4]Bd longitude	Bd latitude	[5]Mean h	[6]Std h	# Bd
I5-P5	2	3.3	0	3	-97.44726	35.22654	10.4	2.4	20
P1-R3	1	3.3	2	3	-97.47092	35.25643	10.2	2	10
P2-P4	2	3.3	2	3	-97.47237	35.23307	10.2	2.2	55
P3-P4	2	3.3	0	3	-97.48150	35.22739	10.3	2.3	60
P4-R5	2	3.3	2	3	-97.47357	35.22719	10.1	2.2	30
P6-R6	1	3.3	2	3	-97.49008	35.20760	10.4	2.4	10

Note: [1]LW is for lane width; [2]BLW is for bike lane width and values are assumed based on FHWA (2002); [3]BTRD is for building-to-road distance and value assumed according to Municode Library (2022); [4]Bd is for building; [5]Mean h is for mean height of buildings; [6]Std h is for standard deviations of building heights.

4.3.2 Data analysis

Assuming a scenario earthquake with a Richter magnitude of 7.0, epicentral depth of 10 km, and epicenter location at the latitude and longitude of (35.15, -97.15) has attacked Centerville. We employ the seismic attenuation law developed by Atkinson and Boore (2006) for the mean peak ground acceleration (PGA):

$$\log(\mathrm{PGA}) = c_1 + c_2 M_L + c_3 {M_L}^2 + (c_4 + c_5 M_L) f_1 + (c_6 + c_7 M_L) f_2 + (c_8 + c_9 M_L) f_0 + c_{10} R_e + S \tag{4.17}$$

$$f_0 = \max\left(\log\left(\frac{10}{R_e}\right), 0\right) \tag{4.18}$$

$$f_1 = \min(\log R_e, \log 70) \tag{4.19}$$

$$f_2 = \max\left(\log\left(\frac{R_e}{140}\right), 0\right) \tag{4.20}$$

where M_L is the Richter magnitude; R_e is the epicentral distance (km); $c_1 - c_{10}$ are the parameters from regression analysis; and S is the factor for soil sites and $S = 0$ for hard-rock sites. Centerville is assumed to be located at a hard-rock site. According to the study by Atkinson and Boore (2006), the following parameters are selected: $c_1 = 0.907$, $c_2 = 0.983$, $c_3 = -0.066$, $c_4 = -2.7$, $c_5 = 0.159$, $c_6 = -2.8$, $c_7 = 0.212$, $c_8 = -0.301$, $c_9 = -0.0653$, $c_{10} = -4.48\mathrm{E}-04$.

In the work by Neilson and DesRoches (2007), the probability of a certain infrastructure damage state i or greater is estimated as:

$$P[Damage\ State\ i\ or\ greater|PGA] = \Phi[\frac{\ln(PGA)-\ln(med_i)}{\zeta_i}] \quad (4.21)$$

where med_i and ζ_i are the median PGA and dispersion of damage state i, respectively.

The values of med_i and ζ_i for different bridges and building types are presented in Table 4.5 and Table 4.6, respectively. The moderate med_i, extensive med_i, and complete med_i in Tables 4.5-4.6 are the median PGA values (Eq. (4.21)) that correspond to moderate, extensive, and complete damages, respectively. According to Hazus (2020), Eq. (4.21) also applies to special buildings like hospitals and medical centers. They are mid-rise buildings with concrete shear walls experiencing median PGA and dispersion values of 1.24g and 0.64, respectively. Table 4.7 shows the indoor casualty rates of various building types for different damage states (Hazus 2020).

Table 4.5 Bridge fragility information (Nielson & DesRoches 2007)

Bridge #	Bridge Class	Extensive med_i (g)	Dispersion (g)	Longitude	Latitude
B11-B12	MSC concrete	0.75	0.7	-97.479543	35.256638
B21-B22	MSC slab	0.78	0.7	-97.461509	35.226897
B31-B32	MSC steel	0.39	0.55	-97.460889	35.212719
B41-B42	MSSS concrete	0.83	0.65	-97.452268	35.197926
B51-B52	MSSS concrete box	1.19	0.75	-97.459936	35.256156
B61-B62	MSSS slab	0.94	0.75	-97.443390	35.221606
B71-B72	MSSS steel	0.56	0.5	-97.427446	35.245770
B81-B82	SS concrete	2.62	0.9	-97.430203	35.237922
B91-B92	SS steel	1.52	0.55	-97.413721	35.220139

Table 4.6 Building fragility information (Hazus 2020)

Building type	Moderate med_i (g)	Extensive med_i (g)	Complete med_i (g)	Dispersion (g)
W1	0.43	0.91	1.34	0.64

W2	0.35	0.64	1.13	0.64
S1L	0.22	0.42	0.8	0.64
S1M	0.21	0.44	0.82	0.64
C1L	0.23	0.41	0.77	0.64
C1M	0.21	0.49	0.89	0.64
C2L	0.3	0.49	0.87	0.64
C2M	0.26	0.55	1.02	0.64

Table 4.7 Injury probabilities of severity 2 and 3 for different building types

	Moderate		Extensive		No collapse*		Collapse*		P(col)*
	S2 (%)	S3 (%)	S2 (%)	S3 (%)	S2 (%)	S3 (%)	S2 (%)	S3 (%)	%
W1	0.03	0	0.1	0.001	1	0.01	20	3	3
W2	0.025	0	0.1	0.001	1	0.01	20	5	3
S1L	0.025	0	0.1	0.001	1	0.01	20	5	8
S1M	0.025	0	0.1	0.001	1	0.01	20	5	5
C1L	0.03	0	0.1	0.001	1	0.01	20	5	13
C1M	0.03	0	0.1	0.001	1	0.01	20	5	10
C2L	0.03	0	0.1	0.001	1	0.01	20	5	13
C2M	0.03	0	0.1	0.001	1	0.01	20	5	10

* Damage state “complete” has two subtypes: no collapse and collapse. P(col) is the collapse rates for complete building damage (Hazus 2020).

From Eqs. (4.6-4.8 & 4.17-4.21) and the community information shown in Table 4.2 and Table 4.6, the evacuation travel demand of each zone can be estimated. The evacuation trips for different zones are presented in Fig. 4.4, and Zones I5 and I7 have the most evacuation demands because of large populations and proximity to the epicenter. Zone R1 has the smallest evacuation demand, which is in accordance with its small population and relatively long distance to the epicenter.

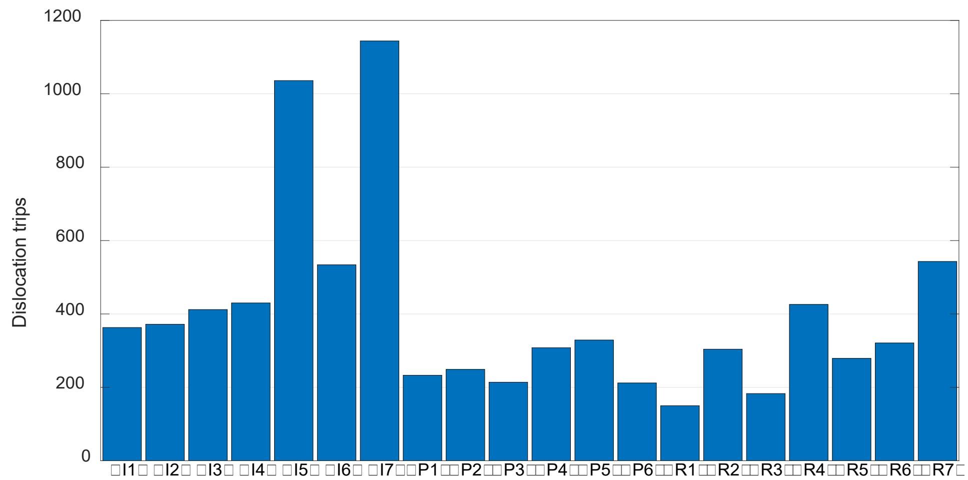

Figure 4.4 Evacuation travel demand of different zones

According to Tani et al. (2004), the average search-and-rescue (SAR) speed for one rescue team is around 16-23 persons/hour for the first 85% of trapped injured residents. The SAR speed of the rest 15% of the trapped injured residents is much lower than that for the first 85% of trapped injured residents. Considering it takes extended time to rescue the last 15% of trapped injured residents during which the usage of ambulances will be way below the peak demand. Therefore, this study assumes there will be sufficient ambulances for the last 15% of the trapped injured residents because of the immediate availability and expected much shorter turnaround time due to driving privilege. This study is focused on the period (T_0) from the beginning of SAR to rescuing 85% of the injured residents. Due to the lack of information on the emergency dislocation timetable, this study assumes most of the dislocation will be completed during the study time frame (T_0). The rescue speed is assumed to be 23 persons/hour/team according to Tani et al. (2004), and the rescue power is equivalent to 2 SAR teams in the community. The rescue power consists of trained SAR teams like those from fire departments and voluntary SAR teams like neighbors, family members, and roommates, and the latter is usually accounted for most of the SAR efforts due to their dominant quantity (Murakami et al. 2000). It is ideally assumed the total rescue power of the community is proportionally assigned to different zones according to their respective populations. So, the SAR of the first 85% of the injured people will be completed within similar time durations for all the zones.

Based on Eqs. (4.4-4.5 & 4.17-4.21), Table 4.2 and Tables 4.6-4.7, the injured people that need immediate medical care can be estimated. It takes about 6 hours to rescue 85% of the severely injured people who need immediate medical treatment according to the above-mentioned rescue speed. Tanaka et al. (1998) found around 74% of the injured residents were sent to hospitals by private vehicles during the 1995 Hanshin-Awaji Earthquake. So, in this study without site-specific data, 75% of the severely injured residents during the period (T_0) are assumed to be transported to hospitals by private cars, and the numbers of these trips for different zones are shown in Fig. 4.5. Like the evacuation trips in Fig. 4.4, the hospitalization trips for different zones share similar characteristics.

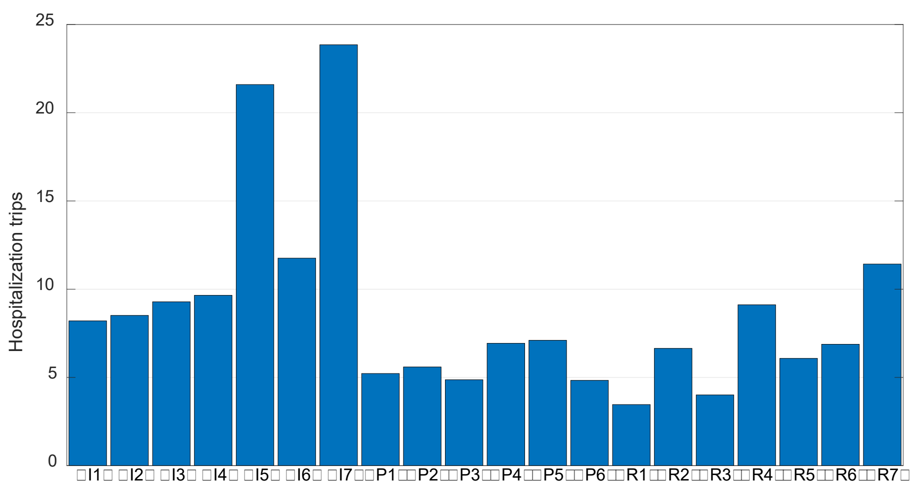

Figure 4.5 Hospitalization trips using private vehicles of different zones

4.3.3 Results

Considering the urgency for the residents who have lost living necessities to dislocate as soon as possible, this study takes the first 6 hours after the earthquake as the time horizon, which means both the evacuation trips and hospital trips in Figs. 4.4-4.5 will be finished during that period. The target arrival times TA_{ij} (Eq. (4.9)) for the evacuation trips of different zones are randomly generated during the study time horizon. As introduced earlier, there are nine vulnerable links in the traffic system with bridges, six vulnerable links with possible debris blockage, and two vulnerable medical centers. According to Adachi and Ellingwood (2007), PGA is assumed to follow a lognormal distribution with a coefficient of variance of 0.6. Based on Eqs. (4.1-4.2) and (4.17-4.21), Latin Hypercube sampling is adopted to simulate bridge damage, debris blockage, and hospital damage scenarios with 10,000 samples. The samples are generated based on 100 data points of PGA and 100 infrastructure damage samples per PGA point.

Based on the estimated travel demand and the fixed-demand dynamic user equilibria, the traffic simulation is conducted on the post-hazard network using the dynamic traffic assignment algorithms (Eq. (4.9)) coded with MATLAB. The mean and shortest travel times between several zone-hospital pairs are presented in Figs. 4.6-4.7. The mean travel time is the average travel time of the 10 shortest paths between each OD pair. The 10 shortest paths won't remain the same since the network topology varies with link degradations. The shortest travel time is the travel time for the optimal path throughout the study period, which may be derived based on multiple paths since the optimal path changes with the fluctuations in travel demand. Both Figs. 4.6-4.7 suggest that the travel time of different zone-hospital origin-destination (OD) pairs peaks at different time instants, which is caused by different target arrival times for all the zones. When people in different zones start to evacuate, the traffic can become heavy on several main routes. If these busy routes or road segments happen to be on the paths of some zone-hospital pairs, the zone-hospital travel time may surge. As a result, heavy traffic causes peaks in some specific OD directions. Similarly, the flat lines mean the traffic is not heavy in that OD direction. Since zone I7 is the location of shelters, the dislocation traffic flows to zone I7 will concentrate at the southeast corner of the community (Fig. 4.3). It is reasonable that if a link is on the south or east border of the network, there may be significant traffic on the link in the direction to zone I7. For instance, links R4-I5, I5-R7, I4-I6, and I6-P6 can be busy if residents living in the northeast part of the community are evacuating to the public shelter in zone I7. This can explain the longer travel time of OD pairs (I4, R3) and (R4, R5). Similarly, paths from R1 to R3 and P1 to R5 will avoid the busiest road segments, resulting in relatively short and steady travel time. Besides the traffic flow, road vulnerability may further exacerbate the congestion. For OD pair (R4, R5), R4 is surrounded by vulnerable links, and the same situation applies to hospital R5 except for link I6-R5. This will significantly impair the accessibility through the pre-hazard shortest routes since some of them may not be accessible anymore due to the potential closure of the vulnerable links on the routes.

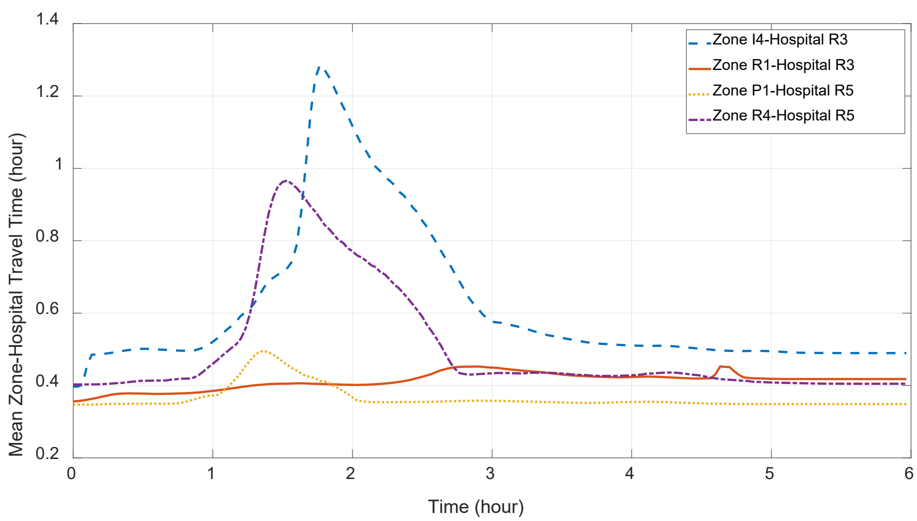

Figure 4.6 Mean travel time for hospitalization trips for selected ODs

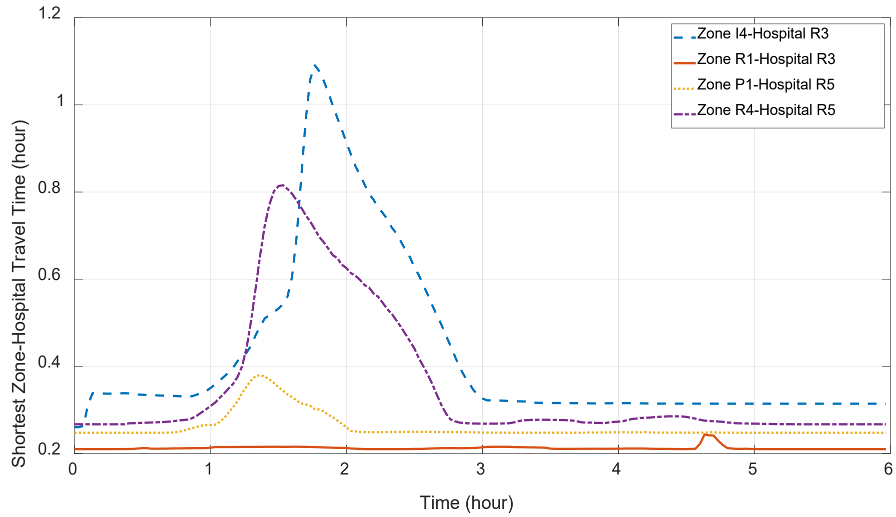

Figure 4.7 Shortest travel time for hospitalization trips for selected ODs

The distributions of total travel time (TH) and the resilience index are shown in Figs. 4.8-4.9. Fig. 4.8 suggests that the post-hazard TH values for most sample scenarios are concentrated between 50 and 100 hours. As shown in Fig. 4.8, the mean TH is 82.8433 hours for the post-hazard network. The pre-hazard network is a special case in all the sampled scenarios when no link fails, and it has a total travel time (TH_0) of 49.2254 hours. There is about a 68% increase in the total travel time of post-hazard hospitalization trips from that before hazard. Apparently, the disruption of the transportation network caused by earthquakes should be blamed for such an increase, and the emergency traffic further aggravates such impact. Almost half of the links in the network are vulnerable to the earthquake in this study. Other related links may expect increased traffic congestion under significant network travel demand when some critical links are fully or partially closed due to bridge damage or debris blockage. Fig. 4.9 shows the cumulative distribution of the system resilience index has little change, a rapid increase, and a slow increase when the resilience index varies between 0.1 to 0.4, 0.5 to 0.7, and 0.7 to 1, respectively. Since the resilience index is based on TH, similar phenomena can also be observed in Fig. 4.8.

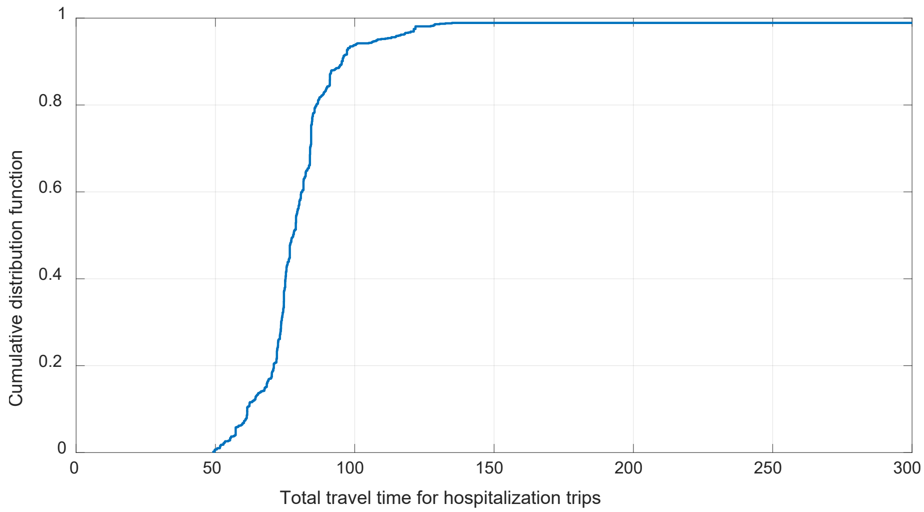

Figure 4.8 Cumulative distribution of total hospitalization travel time (hour)

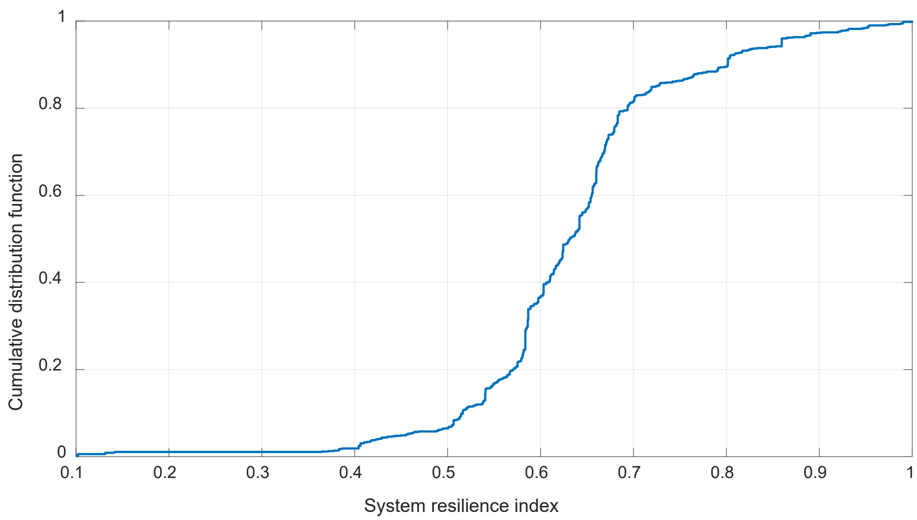

Figure 4.9 Cumulative distribution of system resilience index

The impact of LOP on system reliability is studied with the result presented in Fig. 4.10. It is found that the system reliability remains stable around 1 when LOP is below 0.5. It is because the network remains at a certain level of performance, even with fully or partially closed links and considerable travel demand. So, the network meets the low functionality expectation in almost all sampled scenarios. The system reliability decreases almost linearly with the LOP in the range of (0.5, 0.7) because more and more severely damaged scenarios can no longer meet the increasing LOP requirements. The closure or partial closure of some essential links will reduce the network performance and keep it below the expected level of performance. The selection of LOP value in this interval is found reasonable to demonstrate the impact of link failures on the system performance.

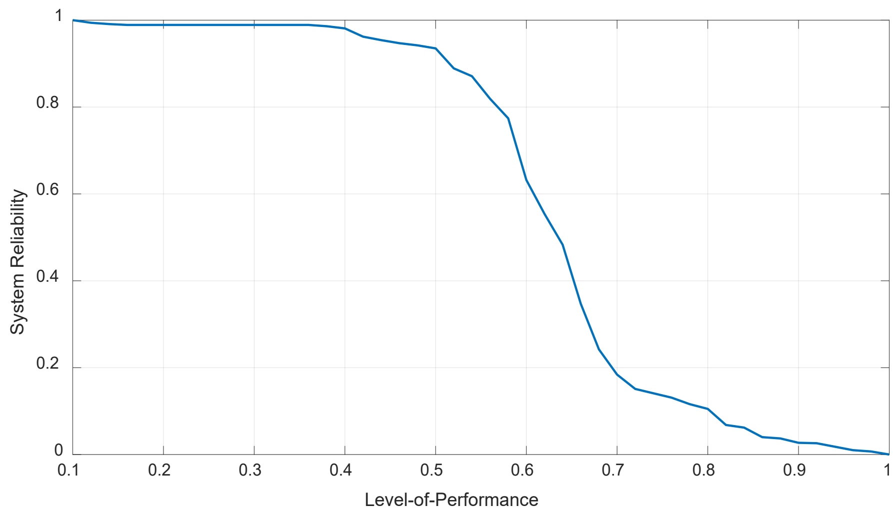

Figure 4.10 System reliability as a function of level-of-performance

4.3.4 Comparison with static traffic assignment results

For comparison purposes, a counterpart model based on static traffic assignment (STA) is set up to explore the advantages of using dynamic traffic assignment (DTA) under the same scenario as introduced in this study. Unlike the DTA that can continuously simulate the traffic, STA was conducted for every 30-minute time segment during the study time horizon. The travel demand during each time segment is estimated from the dislocation trips and target arrival times of different zones. Other than different travel demands, both DTA and STA models use the same link travel time and capacity information. The travel time of several typical OD pairs is presented in Fig. 4.11. By comparing Fig. 4.11 with Fig. 4.6, it is found that the travel time is similar for DTA and STA for the most time, although the DTA results exhibit a relatively higher level of congestion, especially for I4-R3 and R4-R5. It may be caused by the fact that STA would not relay to neighboring time instants by propagating congestion. Although strict comparison with real traffic data is not possible for this virtual community, the DTA method should provide more realistic results in this study given its well-known advantage compared to STA.

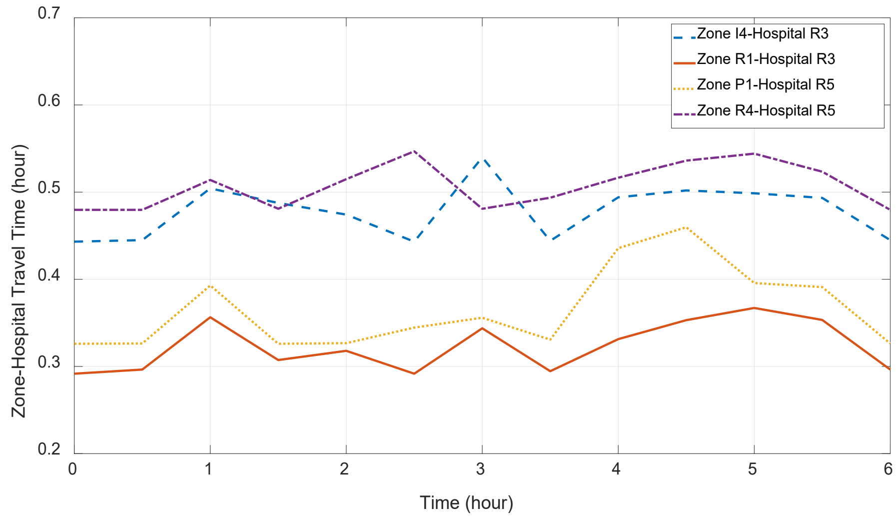

Figure 4.11 Travel time for hospitalization trips for selected ODs using STA

4.4 Investigation of the reasonable number of EMS vehicles

As introduced in Section 4.2.4, unlike private vehicles, EMS vehicles enjoy the driving privilege of having other vehicles yielding to them, but also with their limitations during emergency medical response. Unlike private vehicles that can transport injured residents on one-way trips, EMS vehicles always need to arrive at the site first upon request, transport a patient to the hospital, offload the patient, and then head to another location. Injured people must wait for the EMS vehicles when the demand is high enough that EMS vehicles become insufficient following major hazards. According to the national ambulance statistics, there were 73,500 EMS vehicles in the U.S. in 2020 when the population was 329.5 million in the United States (National Association of State EMS Officials 2020; U.S. Population 2022). Assuming Centerville has the same EMS vehicle-population ratio as the national one, there are 14 EMS vehicles in the community, and their transporting power is proportionally assigned to all the zones according to their demands. According to Eckstein and Chan (2004), the median ambulance offload delay (AOD) for their 21,240 investigation cases was 27 minutes. This study assumes the two hospitals in Centerville have similar efficiency in terms of receiving and admitting patients at both emergency departments, and the AOD is 27 minutes per EMS vehicle. Based on Dijkstra's shortest route algorithm (Dijkstra 1959), the distributions of t_{mean}^{EMSv} and t_{mean}^{pv} for all sampled scenarios are shown in Fig. 4.12, with the median values of 0.3391 and 0.4451 hours, respectively. As shown in Fig. 4.12, t_{mean}^{EMSv} is not only more efficient, but also less deviated. Therefore, the number of EMS vehicles seems reasonable in terms of the transporting efficiency given Centerville's specific post-earthquake emergency response situation in this study. This study also investigated the changing of t_{mean}^{EMSv} with the number of EMS vehicles, and the results are demonstrated in Fig. 4.13. In comparison, t_{mean}^{pv} is also plotted on the same figure to find the minimum reasonable number of EMS vehicles. Considering the hospital trips are negligible as compared to the dislocation traffic following earthquakes, their impact on t_{mean}^{pv} was deemed minimal. Fig. 4.13 shows t_{mean}^{EMSv} drops quickly at the beginning, then slows down, and stays the same when the number of EMS vehicles reaches 5. It implies that when 5 or more EMS vehicles are available in the community, the supply of EMS vehicles will be more than the demand. Therefore, Fig. 4.13 suggests the minimum reasonable number of EMS vehicles is about 4 for Centerville based on the median travel time.

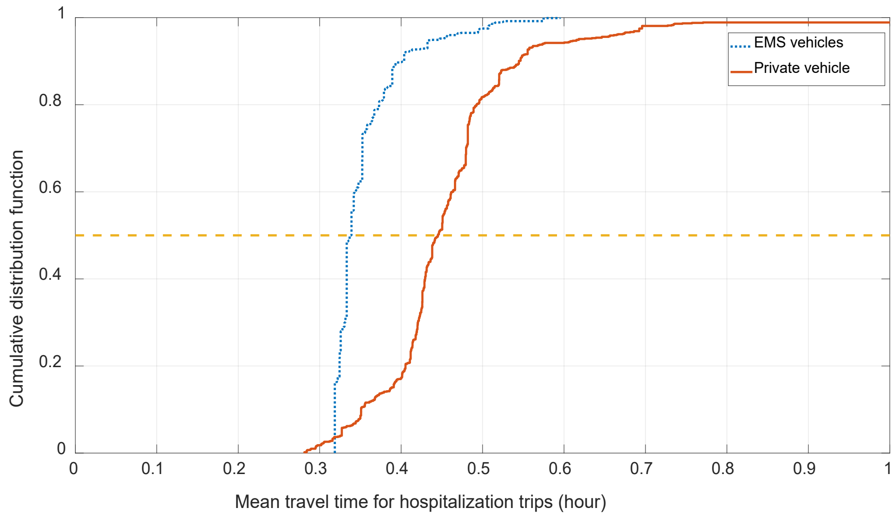

Figure 4.12 Cumulative distribution functions of t_{mean}^{EMSv} and t_{mean}^{pv}

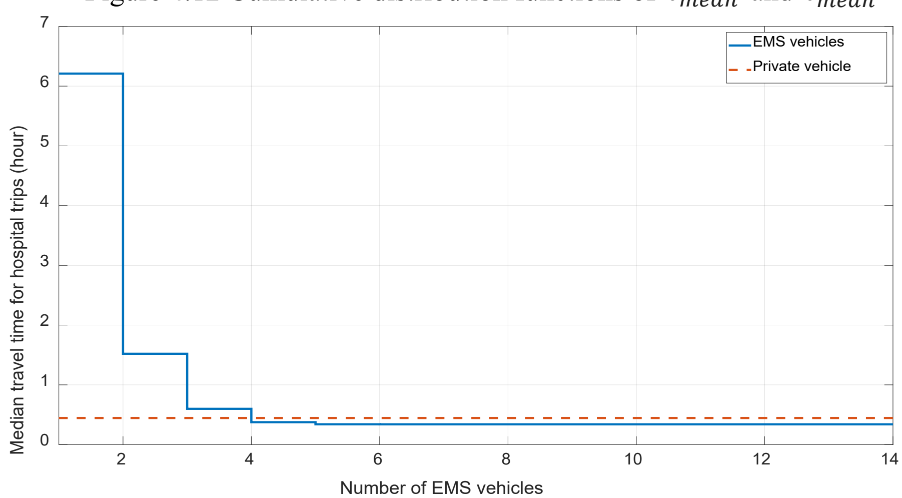

Figure 4.13 t_{mean}^{EMSv} as a function of number of EMS vehicles

A parametric analysis of the minimum reasonable number of EMS vehicles is further conducted to assess its sensitivity to mode choice and ambulance offload delay (Figs. 4.14-4.15). The stair plot in Fig. 4.14 shows the minimum reasonable number of EMS vehicles changes almost linearly with the mode choice percentage. Compared to mode choice, it is found that the minimum reasonable number of EMS vehicles is less sensitive to AOD. It may be due to the relatively small EMS vehicle demand in this demonstrative example and as a result, even a small number of EMS vehicles will suffice the emergency transport demands. When there are sufficient EMS vehicles, AOD is found to have minimal effect on transport efficiency.

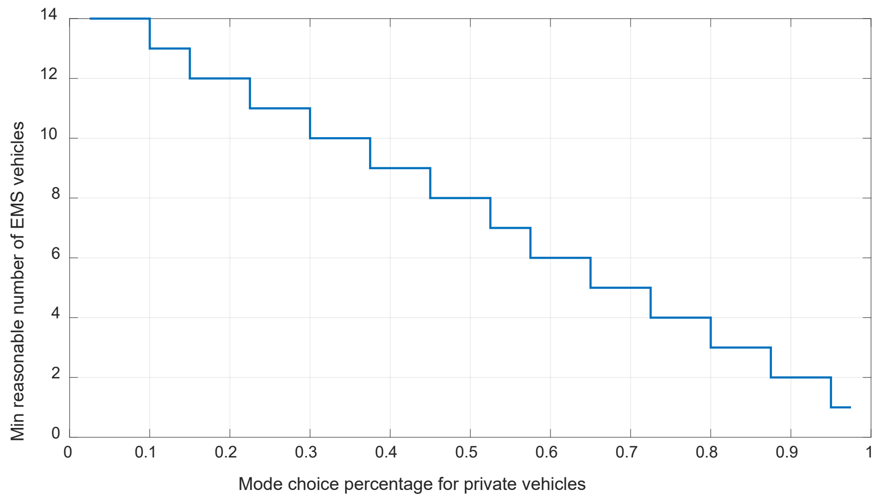

Figure 4.14 Minimum reasonable number of EMS vehicles as a function of mode choice

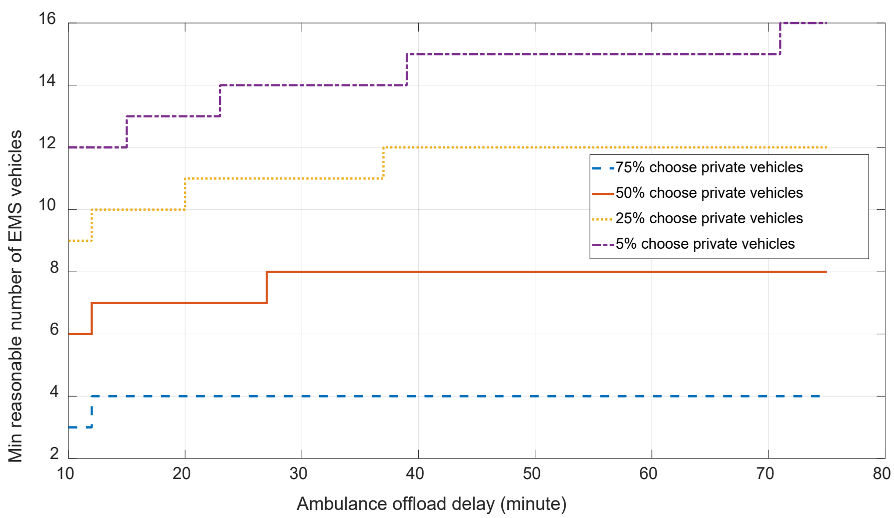

Figure 4.15 Minimum reasonable number of EMS vehicles as a function of AOD

4.5 Conclusion

Emergency response period is very critical and time-sensitive following major earthquakes. A framework to model the resilience performance of transportation systems during the post-earthquake emergency medical response was developed from the EMS perspective with the consideration of emergency dislocation traffic and infrastructure disruption. To simulate various uncertainties in ground motion, infrastructure damage states, debris distribution, and road disruption, the seismic fragility of infrastructures, and Latin Hypercube Sampling method were applied in this study to generate numerous potential scenarios. A dynamic traffic assignment method was adopted to simulate the emergency traffic flow and the time-dependent delays in the private-vehicle-based injury transport system. This study defined a new resilience indicator to quantify the transportation network efficiency and the performance of the emergency medical response of the attacked community based on private vehicles. The model can incorporate uncertainties into road degradation to make the performance quantification more realistic and reliable. The proposed resilience indicator was used to evaluate the efficiency of EMS vehicles during the study time horizon and to derive the reasonable number of EMS vehicles based on transportation efficiency. Finally, the proposed model was demonstrated in a virtual community located in earthquake-prone areas. A comparative study was conducted to investigate the differences between the dynamic and static traffic assignment methods. The results show that the dynamic traffic assignment method has great potential to provide more realistic and reliable results than the static traffic assignment method.

This study proposed a new approach to simulate post-earthquake emergency traffic and quantify the transportation network resilience during the emergency response period after earthquakes. The model is not only more realistic and reliable as compared to traditional connectivity-based methods but also efficient in incorporating various uncertainties. This study still has several limitations: only bridge damage and debris were considered as the factors affecting traffic functionality of those road segments; this study did not consider the spatial correlations of seismic ground motions in the case study area because of the scope limit, which may be improved in future studies; the simplified travel demand in this study doesn't include some emergency trips (e.g., people may immediately return from offices, schools, and stores to their homes); this study did not incorporate the effects of other disruptions on travel time due to the lack of appropriate models and data, such as pavement damages. Instead, a significantly reduced speed limit was approximately applied based on the knowledge gathered from existing studies. Also, this study has adopted various assumptions due to the lack of data, including the search-and-rescue information, the relationship between infrastructure damage states and their performance, and detailed emergency traffic composition. Following the proposed model, more sophisticated and advanced studies on a transportation network can be conducted when more site-specific data becomes available. Finally, although this methodology was presented under earthquakes, it can be adapted and applied to the emergency medical response involving other hazards or incidents causing similar disruptions.

CHAPTER 5 POST-EARTHQUAKE RESILIENCE ASSESSMENT AND LONG-TERM RESTORATION PRIORITIZATION OF TRANSPORTATION NETWORK[4]

5.1 Introduction

An efficient and safe transportation system is essential to communities during the long-term recovery period after earthquakes. A disrupted transportation network due to infrastructure damage or failure affects the functionality of the traffic system and poses increased traffic safety risks. A rational assessment of the traffic network performance in terms of both traffic efficiency and safety cannot only provide comprehensive quantification of system resilience, but also enable more risk-informed post-hazard recovery planning. A new methodology to assess the resilience performance of transportation networks during post-earthquake long-term recovery period is developed in this study with two main innovative contributions: (1) modeling the traffic performance of partially closed road segments in the network simulation and optimization, which offers useful tool to capture the time-progressive recovery process; and (2) integrating both traffic efficiency and safety into the resilience assessment and recovery prioritization. After a resilience indicator is introduced to characterize the overall traffic efficiency and safety of the transportation network using probabilistic sampling method, a new restoration priority measure is proposed to support post-earthquake restoration of damaged bridges. A demonstrative study is conducted on a hypothetical network system located in an earthquake-prone area.

[4] This chapter is adapted from a published paper by the author (Wu et al. 2021) with permission from Elsevier.

This chapter aims to address these limitations by proposing a methodology to assess the time-progressive resilience performance of transportation networks during the post-earthquake long-term recovery period that can consider the traffic performance of partially disrupted roads or bridges. The resulting resilience framework can provide reliable information on travel time and traffic safety of roads with various levels of lane closure on the bridges. This study adopts a microscopic traffic flow simulation model (Hou et al. 2017, 2019) to simulate road travel time, which offers a general approach for any road or bridge with specific lane closure conditions. Moreover, this study adopts statistical methods for transportation data analyses to estimate the traffic accident frequency of roads with different bridge functionality levels. Such a methodology can be applied to different roads with the site-specific traffic crash data (Washington et al. 2010). A resilience indicator is proposed based on the simulated travel time and traffic safety performance to evaluate the performance of regional road networks after major hazards. The model uses existing seismic attenuation laws and bridge fragility data to estimate bridge failure, applies Monte Carlo simulation and Latin Hypercube sampling to consider the uncertainties in earthquake intensity and bridge fragility, and adopts User-Equilibrium (UE) method (Wardrop 1982) and Frank-Wolfe algorithm (Frank & Wolfe 1956; Janson 1991; and Lee & Machemehl 2005) to conduct traffic assignment. Furthermore, this study proposes a bridge restoration prioritization measure based on system resilience and uncertainties to provide critical information for stakeholders to make risk-informed decisions on bridge restoration during post-earthquake long-term recovery period. The Greedy algorithm and probabilistic sampling method are adopted to derive the bridge prioritization measure. The proposed methodology is applied to the transportation network of Centerville (Ellingwood et al. 2016), a hypothetical community located in an earthquake-prone area.

5.2 Resilience assessment framework of disrupted transportation network in long-term recovery stage

The objective of this study is to assess the resilience performance of transportation networks during post-earthquake long-term recovery period, incorporate travel efficiency and safety of disrupted roads and propose a bridge prioritization measure to support decision makings on post-earthquake bridge restoration. As shown in Fig. 5.1, the methodology starts with hazard simulation to generate bridge damage scenarios. The input data includes earthquake information like Richter magnitude, locations of the epicenter and bridges and the output are the earthquake intensities like peak ground acceleration. Seismic attenuation laws and probabilistic sampling methods are applied to estimate earthquake intensities and their uncertainties, respectively. Then the sampled earthquake intensities are used to generate possible bridge damage scenarios based on bridge seismic fragility and probabilistic sampling method.

In Fig. 5.1, when simulating the travel time of roads with different levels of functionalities, the inputs are the road and traffic information. Methods like microscopic traffic flow simulation can be adopted to derive the modified Bureau of Public Road function (US Bureau of Public Roads 1964) to accommodate partial functionality of roads due to bridge damages. For any sampled bridge damage scenario and given travel demand, the travel time and traffic flow of the links and the system can be estimated using traffic assignment methods. For the long-term recovery period, the traffic demand of the system can be recovered to almost the same as the pre-disaster level, and the travel demand of each OD pair can usually be obtained from the transportation department of the region (Chang et al. 2012) or estimated from existing Metropolitan Planning Organization (MPO) models (Kimley-Horn et al., 2007). Without losing generality, it is assumed in this study the travel demand of the community during the long-term recovery period is same as the pre-earthquake level. The traffic flows of different links, together with other traffic safety factors, such as work zone lengths, are the inputs when deriving the traffic safety model using regression models like Poisson regression and Negative Binomial regression (Washington et al. 2010). The total system crash frequency for any sampled scenario can be estimated with the traffic safety model and link traffic flows.

In this study, the resilience index is defined based on the total system travel time and total system crash frequency (Fig. 5.1) to consider both the traffic efficiency and safety performance of the transportation network. By introducing the level-of-performance (LOP) criterion, the system reliability is derived through quantifying the number out of the sampled scenarios under which the performance of the transportation network, in terms of travel time and traffic safety, can meet the selected criterion. The bridge restoration prioritization measure is the indicator for the decision-makers to prioritize the bridge restoration, especially when only limited resources are available. The detailed process and information of the proposed methodology are presented in the following sub-sections.

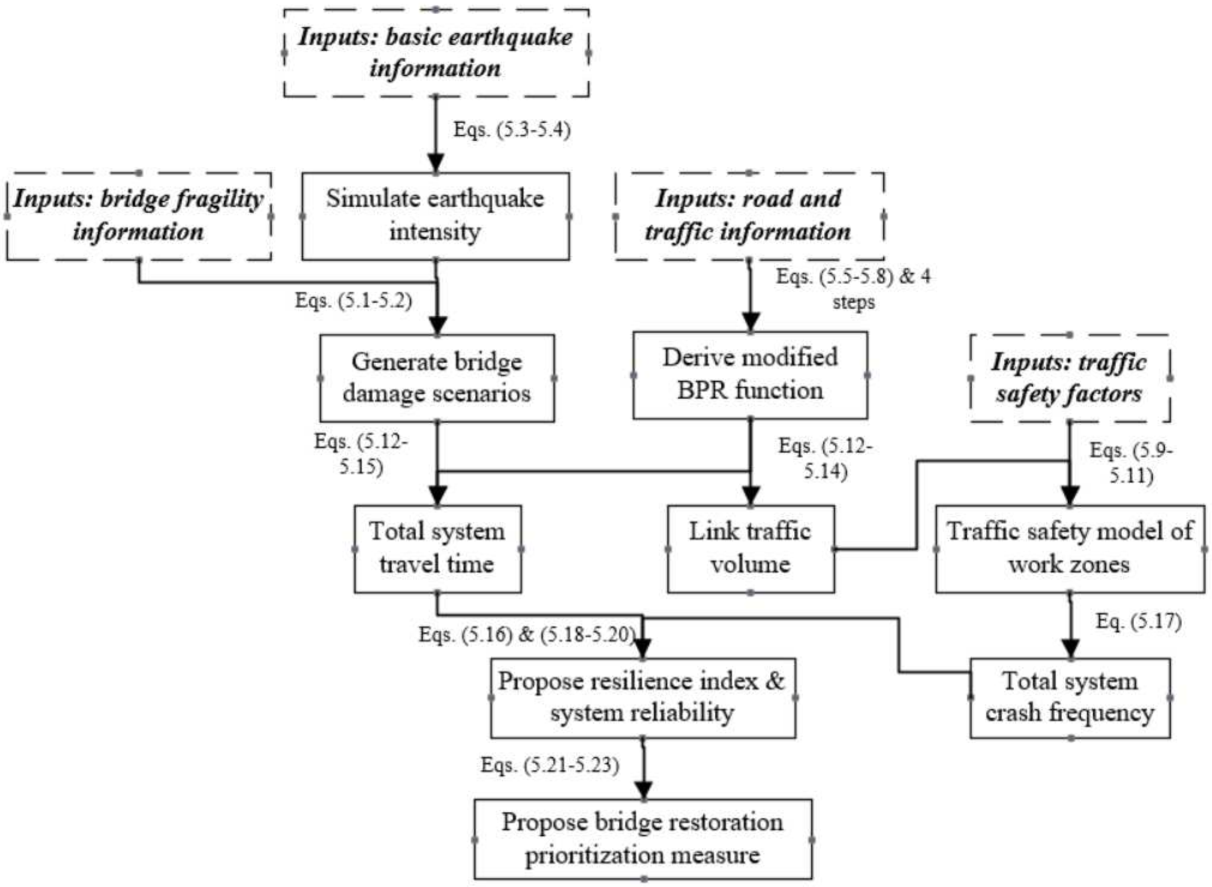

Figure 5.1 Flowchart of the model

5.2.1 Seismic fragility of bridges

The seismic fragility of structures can be defined as the probabilities of a given failure type of the structure under a given intensity level of earthquakes, e.g., spectral acceleration (SA). The failure in terms of a limit state is defined as an excess of the limiting value of the performance indicator, such as stress, displacement, or others. There are many sources of uncertainties affecting the accuracy of the structural capacity and fragility curves are often used to quantify the confidence level for each damage or limit state. For bridge seismic analyses, typically there are several different damage states, for example, no damage or slight/minor damage, moderate damage, extensive damage, and complete damage (Nielson & DesRoches 2007, and Argyroudis et al., 2019). For each damage state, the fragility curve stands for the probability of occurrence under different values of a hazard parameter. The probability of a bridge suffering and exceeding a given damage state is modeled as a cumulative lognormal distribution. For bridge damage, given the peak ground acceleration, PGA, the probability of suffering or exceeding a damage state, i, is modeled as:

$$P[Damage\ State\ i\ or\ greater|PGA] = \Phi\left[\frac{\ln(PGA)-\ln(med_i)}{\zeta_i}\right] \tag{5.1}$$

where med_i is the median PGA value of damage state i; ζ_i is the dispersion of damage state i (Nielson & DesRoches 2007). The damage state of bridge i is defined as:

$$D_i = D_i\left(PGA(\xi_p), \xi_{di}\right) \tag{5.2}$$

where ξ_p is the uncertainty of PGA; ξ_{di} is the uncertainty of structural damage in the fragility curve of bridge i (Chang et al., 2012).

PGA is one of the commonly used seismic intensities when developing seismic fragility of bridges (e.g. Nielson & DesRoches 2007), so it is adopted herein to estimate the bridge damage states in this study. The median of the peak ground acceleration, $\overline{PGA}$, of a given location can be derived by the attenuation laws in terms of Richter magnitude (M_L) and epicentral distance (R_e).

$$\overline{PGA} = f(M_L, R_e) \tag{5.3}$$

The uncertainty of PGA is often assumed to follow a lognormal distribution because the seismic ground motions are estimated with attenuation laws that are usually modeled as the exponential of M_L and R (Campbell 1981). PGA at a given location follows lognormal distribution:

$$\ln PGA = \ln\left(\overline{PGA}\right) + \xi_p \tag{5.4}$$

where ξ_p is the uncertainty of PGA, same as in Eq. (5.2). Following the work by Adachi and Ellingwood (2007), PGA is assumed with a coefficient of variation of 0.6.

5.2.2 Travel time estimate on post-earthquake urban arterials

5.2.2.1 <u>Post-earthquake traffic on urban arterials</u>

In post-earthquake urban transportation networks, road links may be disrupted directly or indirectly. In this study, we only consider the disruption to the traffic flow by damaged bridges given the fact that other temporary or relatively minor disruptions are reasonably assumed to be eliminated by the time of long-term recovery. According to Padgett and DesRoches (2007), a moderately or less damaged bridge can typically be recovered to its original traffic carrying capacity one week after the earthquake, while an extensively damaged bridge can only recover 50% of its capacity while a completely damaged bridge cannot carry any traffic. Considering the long-term recovery period usually begins at least 7 days after the earthquake, the traffic capacity from the survey by Padgett and DesRoches (2007) still can be applied during long-term recovery periods. When site-specific data of traffic capacity of damaged bridges is not available, the generic data from the existing studies (e.g., Padgett & DesRoches 2007) will be adopted.

For demonstration purposes in this study, a bridge which cannot carry any traffic (completely damaged) is deemed to be totally closed; and 50% traffic carrying capacity (extensively damaged) is assumed that half of the lanes are closed on the bridge. This study focuses on urban transportation networks with two-way single-lane and two-way double-lane roads, which are very common in the US. If a bridge on any of the two-way single-lane roads suffers complete damage, the road will be closed to all the through traffic. If a bridge on a two-way single-lane road suffers extensive damage, it is assumed one of the lanes on the bridge will be closed as a “work zone” and the other lane will accommodate traffic with a flag person to direct the traffic of the lane. In this case, it is assumed the free flow travel time on this link is doubled while the capacity remains the same. If a bridge on a two-way double-lane road suffers extensive damage, two lanes on the bridge will be closed as "work zones" and the link will be degraded into a partial two-way single lane road with "work zones". Therefore, for an urban transportation network with two-way single-lane and two-way double-lane roads, there are three typical traffic scenarios after earthquakes (Fig. 5.2): the first one is the normal 1-lane traffic, the second one is the normal 2-lane traffic, and the third one is the disrupted 2-lane traffic, in which one lane is closed for the damaged bridge and the other lane is open.

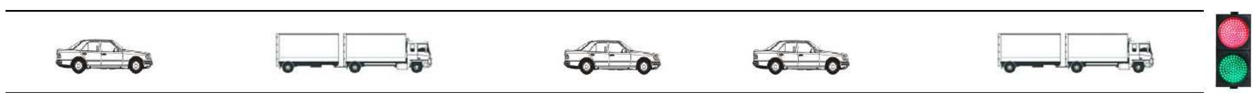

(a) Normal 1-lane traffic

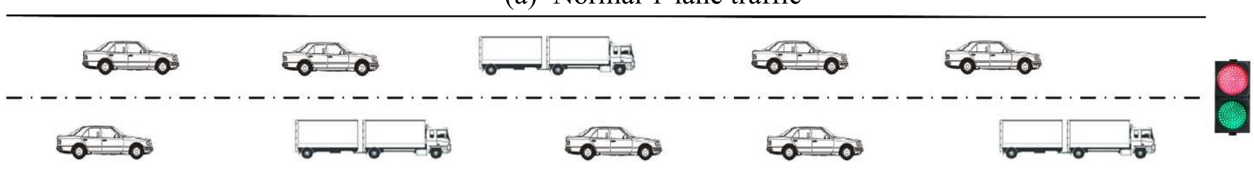

(b) Normal 2-lane traffic

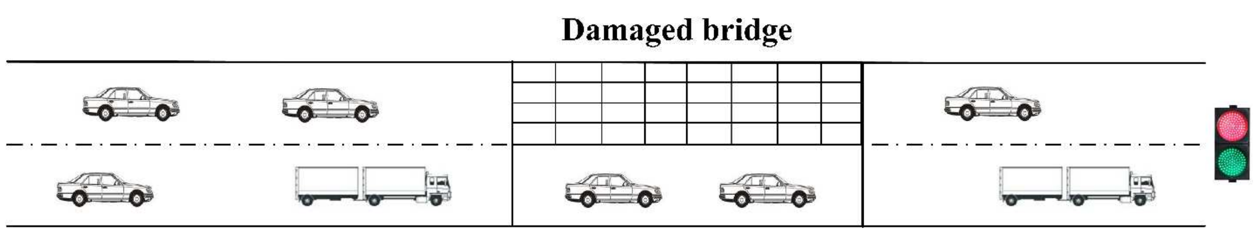

(c) Disrupted 2-lane traffic

Figure 5.2 Post-earthquake traffic scenarios

5.2.2.2 Microscopic traffic flow simulation model

For intact roads shown in Fig. 5.2 (a) and (b), the travel time on a road link has been often predicted with the widely adopted travel time functions for intact roads (e.g., BPR functions). Lane reduction due to damaged bridges shown in Fig. 5.2(c) will reduce the road traffic capacity and increase the travel time. For roads with partial disruptions as shown in Fig. 5.2(c), the corresponding travel time functions are however not available and therefore need to be defined before the traffic performance can be assessed quantitatively.

Traditionally, travel time function for intact roads can be established based on empirical data from traffic monitoring or calibrating the coefficients of BPR functions. Actual post-hazard traffic data, however, has been very rare and as a result, simulation-based approach is often needed to derive the travel time functions for various disruption scenarios. In this study, a Cellular Automaton (CA)-based microscopic traffic flow simulation model developed by Hou et al. (2017, 2019) is used to simulate normal and disrupted traffic flow on post-earthquake arterials and estimate the travel time functions.

The effect of traffic lights must be considered for urban arterials. As shown in Fig. 5.2, there is a traffic light at the right end of a road section, with a cycle length of T and a green ratio of R. The orange light period is ignored. The durations of green-light phase and red-light phase are $T_g = T * R$ and $T_r = T - T_g$, respectively. The CA model used in this study includes forwarding and lane-changing rules. The longitudinal position and velocity of vehicle i are denoted by x_i^t and v_i^t at the time step t. At next time step $t+1$, position x_i^{t+1} and velocity v_i^{t+1} can be updated through the forwarding and lane-changing rules. The forwarding rules can be described as a process of step 1 to 4, which are performed in parallel for all the vehicles.

Step 1 Acceleration: $v_i^{t+1} = min(v_i^t + a_i, v_{i,max})$.

Step 2 Deceleration: $v_i^{t+1} = min(v_i^{t+1}, gap_i^t)$, if the traffic light is green in front of vehicle i; $v_i^{t+1} = min(v_i^{t+1}, gap_i^t, S_i)$, if the traffic light is red in front of vehicle i.

Step 3 Randomization with a probability of p_r: $v_i^{t+1} = max(v_i^{t+1} - d_i, 0)$.

Step 4 Movement: $x_i^{t+1} = x_i^t + v_i^{t+1}$.

where $v_{i,max}$ denotes the maximum velocity of vehicle i; a_i and d_i denote the acceleration rate and deceleration rate of vehicle i; gap_i^t is the clear distance between vehicle i and its front vehicle $i+$

1 on the current lane at time step t, $gap_i^t = x_{i+1}^t - x_i^t - l_i$; l_i is the length of vehicle i; S_i is the clear distance between vehicle i and the traffic light.

For 2-lane traffic as shown in Fig. 5.2 (b) and (c), vehicle i will perform a lane-changing maneuver with a probability of p_{ch}, if the lane-changing rules shown in Eq. (5.4) to (5.6) are satisfied.

$$gap_i^t < min(v_i^t + a_i, v_{i,max}) \tag{5.5}$$

$$gap_{i,f}^t > gap_i^t \tag{5.6}$$

$$gap_{i,b}^t > v_{i,b}^t \tag{5.7}$$

where $gap_{i,f}^t$ is the clear distance between vehicle i and the nearest vehicle on the target lane ahead of vehicle i at time step t; $gap_{i,b}^t$ is the clear distance between vehicle i and the nearest vehicle on the target lane behind vehicle i at time step t; $v_{i,b}^t$ is the velocity of the nearest vehicle on the target lane behind vehicle i.

Open boundary conditions are used in this model. Vehicles are injected into the road section of stimulation from the left end with a flow rate of q, and the time headway h is assumed to follow a displaced exponential distribution, which has a cumulative probability distribution as follows:

$$F(h) = 1 - e^{-\lambda(h-t_m)} \tag{5.8}$$

where $F(h)$ is the cumulative distribution function of h; t_m is the minimum headway between vehicles; $\lambda = \frac{q}{(1-t_m q)}$. If a vehicle reaches the right end of the road section, it will leave when the traffic light is green and will stop when the traffic light is red.

5.2.3 Traffic safety risks of partially disrupted infrastructures

Earthquakes can cause bridge damage or even collapse, which will change the traffic patterns on the whole network. Both the damaged infrastructure and the traffic volume affect car crash frequencies. Whenever a bridge is under repair with partial blockage by providing limited traffic, it can be practically treated as a work zone with increased traffic safety risks (Yang et al. 2015). Poisson Regression is a basic but popular count-data model to simulate traffic crash frequency. If historical crash data is available, statistical analyses with more advanced models (e.g. Negative Binomials, panel data models) can be conducted to capture the site-specific safety performance of the area. If the site-specific crash data is not available or sufficient, Poison model will be an ideal option as the default and baseline analysis model thanks to its minimum data requirement and high popularity. In a Poison regression model, the probability of road i having y_i crashes (where y_i is a non-negative integer) is given by

$$P(y_i) = \frac{EXP(-\lambda_i)\lambda_i^{y_i}}{y_i!} \tag{5.9}$$

where EXP () is the exponential function; $P(y_i)$ is the probability of road i having y_i crashes per year and λ_i is the Poisson parameter for road i, which is equal to the expected number of crashes per unit time on road i, $E[y_i]$ (Washington et al. 2010). Poisson regression models are estimated by specifying the Poisson parameter λ_i (the expected number of events per period) as a function of explanatory variables. For the long-term recovery case, explanatory variables might include the average hourly traffic, length of roads, work zone length, and duration of work zone length. The most common relationship between explanatory variables and the Poisson parameters is the log-linear model,

$$\lambda_i = EXP(\beta x_i) \tag{5.10}$$

where x_i is the vector of explanatory variables and β is the vector of estimable parameters. In this formulation, the expected number of events per period is given by $E[y_i] = \lambda_i = EXP(\beta x_i)$ (Washington et al. 2010). According to Washington et al. (2010), this model is estimated by standard maximum likelihood methods, with the likelihood function given as

$$L(\beta) = \prod_i \frac{EXP[EXP(\beta x_i)][EXP(\beta x_i)]^{y_i}}{y_i!} \tag{5.11}$$

5.2.4 Resilience index and applications

5.2.4.1 <u>Traffic assignment</u>

The static traffic assignment using user equilibrium (UE) model provides a reasonable and efficient prediction of the average travel time and is widely adopted by many transportation agencies and researchers. The mathematical formulation of UE can be given by

$$\text{Minimize} \qquad \sum_i \int_0^{x_i} t_i(\omega)\, d\omega \tag{5.12}$$

subject to

$$x_i = \sum_r \sum_s \sum_k f_k^{rs} \delta_{i,k}^{rs}, \forall i \tag{5.13}$$

$$\begin{cases} \sum_k f_k^{rs} = q_{rs}, & \forall r, s \\ f_k^{rs} \geq 0, & \forall r, s \end{cases} \tag{5.14}$$

where x_i is the traffic flow on link i, $i \in link\ set\ A$; t_i is the travel time on link i; f_k^{rs} is the traffic flow on the k^{th} path connecting origin-destination (OD) pair $r - s$; $\delta_{i,k}^{rs}$ is the indictor variable: $\delta_{i,k}^{rs} = 1$, if link i is part of the k^{th} path connecting OD pair $r - s$, otherwise $\delta_{i,k}^{rs} = 0$. q_{rs} is the travel demand from r (origin) to s (destination) (Wardrop 1982).

5.2.4.2 System resilience index

The total system travel time (TSTT) is proposed to reflect the efficiency of the transportation network and is defined as

$$TSTT = \sum_i t_i(x_i) = \sum_i t_0 \left(1 + \alpha \left[\frac{x_i}{C_i}\right]^{\beta}\right) \tag{5.15}$$

where C_i is the traffic carrying capacity of link i; $t_0 \left(1 + \alpha \left[\frac{x_i}{C_i}\right]^{\beta}\right)$ is from the Bureau of Public Roads (BPR) function; α and β are BPR function parameters with classical values of 0.15 and 4.0, respectively (US Bureau of Public Roads 1964), but their values vary by link types according to recent studies (Hou et al. 2017, 2019). In this study, the travel demand stays the same during the long-term recovery period. So, the smaller TSTT's value is, the more efficient the network will be in terms of travel time. The efficiency indicator of the system is defined as

$$R_t = \frac{TSTT_0}{TSTT} \tag{5.16}$$

where $TSTT_0$ and $TSTT$ are for the pre-disaster period and long-term recovery period respectively.

The expected total system crash frequency (TSCF) is used to quantify the traffic safety risk of the network, which is defined as:

$$TSCF = \sum_i \lambda_i \tag{5.17}$$

The safety indicator of the system is defined as:

$$R_s = \frac{TSCF_0}{TSCF} \tag{5.18}$$

where $TSCF_0$ and $TSCF$ are for the pre-disaster period and long-term recovery period respectively.

The resilience index (RI) in this study is proposed to consider both traffic efficiency and safety performance:

$$RI = m.R_t + (1 - m).R_s \tag{5.19}$$

where m is a weight parameter between [0, 1], which is usually defined by the stakeholders based on the specific scenario and priority.

5.2.5 System reliability and post-earthquake restoration prioritization

5.2.5.1 System reliability

System reliability R is the probability that a system can maintain its functionality while suffering from some extent of disruption. It is an important performance indicator for hazard resilience since it can provide an estimation of the system serviceability including uncertainties and relative importance of different links in terms of resilience performance, which is defined as:

$$R(\varepsilon) = P(RI_M \geq \varepsilon) \tag{5.20}$$

where RI is the resilience index of the system; M is the size of the samples using heuristic method; ε is the level-of-performance (LOP) of the disrupted transportation network specified by stakeholders, and it is a ratio between 0 and 1 being used as a criterion to assess whether the reduced serviceability of the disrupted network is acceptable or not.

5.2.5.2 Resilience-based post-earthquake bridge restoration prioritization

Due to usually limited resources, it is important for decision makers to optimize the resources on pre-disaster preventive strengthening and post-hazard recovery efforts. Accordingly, the stakeholders often would need to know the priorities of bridges in terms of these preventive and recovery efforts before and after hazards. In addition, it is imperative to accommodate the uncertainties related to the seismic intensity, bridge fragility, travel time and safety during the assessment of the priorities. In this study, the restoration priority of a bridge is not only related to the importance of the bridge to the network, which means the difference between the performance indicators of the network when the bridge is intact, partially failed or totally failed, but also affected by the required repair time of the bridge. If a vulnerable bridge has a great impact on the network and takes relatively less time to repair, it should be prioritized during the restoration. When considering the priorities of different bridges under a given state, a rational way is to optimize the reconstruction sequence to maximize the resilience index Z over time:

$$\text{Maximize } Z = \int_0^T RI(t)dt \tag{5.21}$$

where Z is the integration of the resilience index over the recovery time; T is the total recovery time of the system which is defined as the sum of the repair times of all the damaged bridges.

The sequence rankings are direct indicators for the restoration priorities of bridges under a given state. Among the damaged bridges, the smaller a bridge's repair sequence ranking is, the higher prioritization the bridge would receive. Considering the uncertainties in earthquakes and bridge failures, it is important to apply the Monte Carlo Simulation or Latin Hypercube Sampling to generate possible damage states of the bridges and develop the repair sequences of different bridges under each generated state. The mean restoration sequence (MRS) of any bridge i considering uncertainties is defined as:

$$MRS_i = \frac{\sum_1^M Seq_{i,m}}{M} \ , \ m \in [1, M] \tag{5.22}$$

where MRS_i is the MRS of bridge i , M is the size of the samples using heuristic method, and $Seq_{i,m}$ is the restoration sequence of bridge i under scenario m. As discussed earlier, MRS incorporates the failure rates of different bridges. However, when planning the post-hazard restoration of damaged bridges with limited resources, it is more meaningful for stakeholders to know which bridge to repair first, and then which ones would be the next for any given damage scenario. Thus, it is necessary to eliminate the effect of bridge failure rate on MRS when deriving the post-hazard restoration priority of bridges.

Therefore, the bridge priority index is defined as:

$$PR_i = \frac{n*(1-Pf_i)}{MRS_i} \ , \ Pf_i \in (0,1) \tag{5.23}$$

where PR_i is the post-hazard restoration priority index of bridge i, n is the number of bridges in the network, and Pf_i is the failure rate of bridge i. The bigger PR is, the higher prioritization the bridge should receive. As a result, the proposed PR is a comprehensive prioritization indicator related not only to the network topology and bridge locations but also to origin-destination matrix and bridge repair times.

5.3 Case study

5.3.1 Centerville transportation network

Fig. 5.3 shows the basic traffic network of a virtual community called Centerville located in earthquake-prone areas (Ellingwood et al. 2016). Following existing studies on this virtual community, the earthquakes are with Richter Magnitude between 5 and 7.25, depth of 10 kilometers and epicenter longitude and latitude coordinates of [-97.20, 35.20]. Some basic information of the network is shown in Table 5.1 and the length of each link is calculated based on the geographic information of the community. There are 20 zones in the community. Each of the 20 nodes in Fig. 5.3 is the center of a zone in the community. Most of the industry or companies are located in the I zones (industrial areas); most of the schools, universities, markets, shopping centers and recreational facilities are in the P zones (Public areas); and most of the residents live in the R zones (residential areas). In this study, only bridge damages may cause the links to be totally or partially disrupted. Nine out of the thirty-three roads/links are therefore vulnerable to earthquakes due to the existence of bridges (*B1-B9*) on these links (marked in Fig. 5.3). There are nine types of bridges in the community: multi-span continuous (MSC) concrete, slab, and steel bridges; multi-span simple supported (MSSS) concrete girder, concrete box girder, steel girder and slab bridges; and simple supported (SS) concrete girder and steel girder bridges. The parameters in Table 5.1 are determined based on the link information and the parameters in Tables 5.2-5.3 are derived from the microscopic traffic flow simulation model. When comparing Centerville's transportation network to real-world ones, it has the similar size as a small to medium sized city's transportation network. So, the population is assumed to be 120,000 based on the traffic capacity of the network.

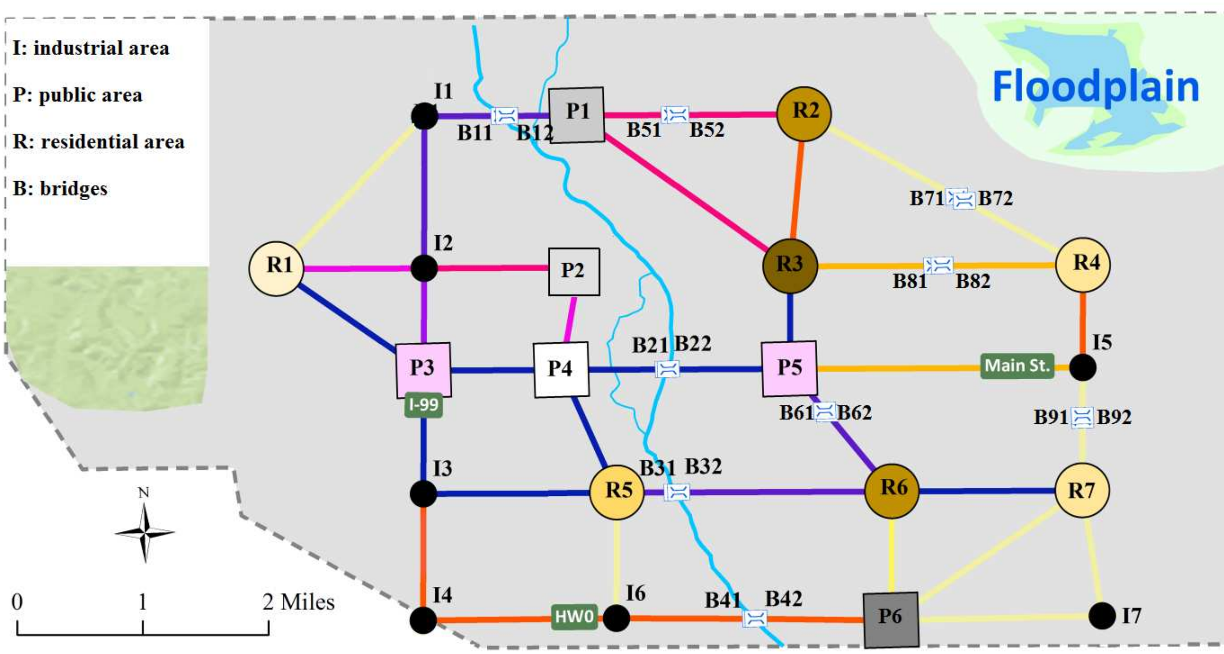

Figure 5.3 Transportation network of Centerville

Table 5.1 Link characteristics

Link#	Zone1	Zone2	Length (km)	No. of lanes	Bridges	Bridge longitudes	Bridge latitude
1	I1	I2	1.94	1	0		
2	I1	P1	1.59	1	MSC Concrete	-97.479543	35.256638
3	I1	R1	2.48	1	0		
4	I2	P2	1.62	1	0		
5	I2	P3	1.31	1	0		
6	I2	R1	1.55	1	0		
7	I3	I4	1.62	1	0		
8	I3	P3	1.57	1	0		
9	I3	R5	2.02	2	0		
10	I4	I6	2.02	1	0		
11	I5	P5	3.07	2	0		
12	I5	R4	1.31	1	0		
13	I5	R7	1.57	1	SS Steel	-97.461509	35.226897
14	I6	P6	2.88	1	MSSS concrete	-97.460889	35.212719
15	I6	R5	1.61	1	0		
16	I7	P6	2.21	1	0		
17	I7	R7	1.62	1	0		
18	P1	R2	2.38	1	MSSS conc box	-97.452268	35.197926
19	P1	R3	2.97	1	0		
20	P2	P4	1.32	2	0		
21	P3	P4	1.44	2	0		
22	P3	R1	2.03	1	0		
23	P4	P5	2.39	2	MSC Slab	-97.459936	35.256156
24	P4	R5	1.68	2	0		
25	P5	R3	1.31	2	0		
26	P5	R6	1.91	2	MSSS slab	-97.443390	35.221606
27	P6	R6	1.65	1	0		
28	P6	R7	2.58	1	0		
29	R2	R3	1.95	1	0		
30	R2	R4	3.52	1	MSSS steel	-97.427446	35.245770
31	R3	R4	3.07	1	SS concrete	-97.430203	35.237922
32	R5	R6	2.88	2	MSC Steel	-97.413721	35.220139
33	R6	R7	1.99	1	0		

Table 5.2 Estimated parameters of BPR functions for normal traffic

Link#	t_0 (min)	α	β	C (veh/h)
1	2.21	0.093	7.397	745
2	1.83	0.111	6.767	745
3	2.63	0.070	7.671	745
4	1.83	0.111	6.767	745
5	1.57	0.100	7.761	745
6	1.83	0.111	6.767	745
7	1.83	0.111	6.767	745
8	1.83	0.111	6.767	745
9	2.21	0.093	7.397	1490
10	2.21	0.093	7.397	745
11	3.11	0.052	8.054	1490
12	1.57	0.100	7.761	745
13	1.83	0.111	6.767	745
14	3.11	0.052	8.054	745
15	1.83	0.111	6.767	745
16	2.21	0.093	7.397	745
17	1.83	0.111	6.767	745
18	2.63	0.070	7.671	745
19	3.11	0.052	8.054	745
20	1.57	0.100	7.761	1490
21	1.57	0.100	7.761	1490
22	2.21	0.093	7.397	745
23	2.63	0.070	7.671	1490
24	1.83	0.111	6.767	1490
25	1.57	0.100	7.761	1490
26	2.21	0.093	7.397	1490
27	1.83	0.111	6.767	745
28	2.63	0.070	7.671	745
29	2.21	0.093	7.397	745
30	3.63	0.066	6.904	745
31	3.11	0.052	8.054	745
32	3.11	0.052	8.054	1490
33	2.21	0.093	7.397	745

Table 5.3 Estimated parameters of BPR functions for disrupted traffic

Link#	t_0 (min)	α	β	C (veh/h)
23	2.67	0.273	4.267	820
26	2.25	0.3063	4.344	820
32	3.15	0.2429	4.106	820

According to Eqs. (5.3-5.4), the peak ground acceleration (PGA) can be estimated using seismic attenuation laws. In this study, we employed the seismic attenuation law developed by Atkinson and Boore (1995). Their ground motion relation works for earthquakes with $4 \leq M_L \leq 7.25$ and epicentral depth of 10km and the mean PGA is estimated as:

$$\log(\mathrm{PGA}) = \mathrm{c}_1 + \mathrm{c}_2(\mathrm{M}_L - 6) + \mathrm{c}_3(\mathrm{M}_L - 6)^2 - \log R_e - \mathrm{c}_4 R_e \tag{5.24}$$

where M_L is the Richter magnitude; R_e is the epicentral distance; c_1, c_2, c_3, and c_4 are parameters from regression analysis. According to the study by Atkinson and Boore (1995), $\mathrm{c}_1 = 3.79$, $\mathrm{c}_2 = 0.298$, $\mathrm{c}_3 = -0.0536$, $\mathrm{c}_4 = 0.00135$ are adopted here primarily for demonstration purposes. For a specific region with sufficient historical data, more site-specific parameters can be used after calibration. It is assumed in this study that M_L is a uniformly distributed random variable.

In Eq. (5.1), Nielson and DesRoches (2007) defined bridge fragility as the probability that the seismic demand meets or exceeds its capacity. The median PGA value med_i and dispersion ζ_i of different damage states are shown in Table 5.4.

Table 5.4 Median and dispersion values for seismic fragility curves of nine bridge classes (Nielson & DesRoches 2007)

Bridge Class	Median PGA Values (g)		Dispersion ζ_i
	Extensive med_i	Complete med_i	
MSC concrete	0.75	1.03	0.7

MSC slab	0.78	1.73	0.7
MSC steel	0.39	0.5	0.55
MSSS concrete	0.83	1.17	0.65
MSSS concrete box	1.19	2.92	0.75
MSSS slab	0.94	1.92	0.75
MSSS steel	0.56	0.82	0.5
SS concrete	2.62	3.64	0.9
SS steel	1.52	2.49	0.55

We take afternoon rush hour (5:00pm-6:00pm) as the study period. The origin-destination data is estimated by the Memphis travel demand model of Metropolitan Planning Organization (MPO) (Kimley-Horn et al., 2007). There are nine trip purposes including journey to work, home based school, home based university, home based shopping, home based social-recreational, home based pickup/drop-off, home based other, non-home based work and non-home based non-work. Some of the travel demand information is presented in Table 5.5. The population of the Memphis area is around 1,000,000. In the Memphis MPO model (Kimley-Horn et al., 2007), a survey was conducted about the transportation modes of people's trips. About 99.8% of the trips are auto-based (drive alone, shared ride, bus, etc.). The average occupancies of a shared ride and a bus are 2.4 and 7.2, respectively, according to Henao and Marshall (2019) and Federal Highway Administration (2018). The number of vehicle trips for every trip purpose of Centerville during the afternoon rush hour is estimated from the MPO model, assuming it has the same demographic properties as the Memphis area except for population size. Table 5.6 lists the nine simplified trip purposes for Centerville. For any trip classification, if there are more than one origin-destination pairs, the trips will be evenly distributed between two different OD pairs due to the lack of more specific information. Table 5.6 is based on people's typical trip behavior, e.g., journey to work trips is classified as trips from industrial areas to residential areas because "go home from work" is very typical during the afternoon rush hour. The origin-destination data is randomly assigned to different OD pairs based on the estimated trips among the residential, industrial, and public areas, and the related information is shown in Table 5.7.

Table 5.5 Memphis area travel demand information (Kimley-Horn et al., 2007)

Trip Purpose	Daily total trips	Intrazonal trip %	PM rush hour %
Journey to work	949,895	0.027	0.123
Home based school	334,407	0.056	0.044
Home based university	50,197	0.057	0.044
Home based shopping	199,141	0.101	0.086
Home based social recreational	218,306	0.056	0.086
Home based pickup/drop-off	182,627	0.074	0.086
Home based other	546,012	0.011	0.086
Non-home based work	122,174	0.075	0.037
Non-home based non-work	457,157	0.055	0.037

Table 5.6 Simplification of nine trip purposes

Trip Purpose	Trip origin and destination	Classification
Journey to work	work to home	Industrial to Residential
Home based school Home based university	public to home	Public to Residential
Home based shopping Home based social recreational	home to/from public	Residential to/from Public
Home based pickup/drop-off Home based other	Between home and any other places	Residential to/from residential, public, and industrial areas
Non-home based work	work to public	Industrial to Public
Non-home based non-work	intra public	Public to Public

Table 5.7 Origin (column 1)-destination (row 1) data of afternoon rush hour

	I1	I2	I3	I4	I5	I6	I7	P1	P2	P3	P4	P5	P6	R1	R2	R3	R4	R5	R6	R7
I1	0	1	0	0	0	1	0	5	5	3	4	5	2	101	98	103	81	90	113	95
I2	2	0	0	0	0	1	1	4	4	4	4	6	3	112	129	91	98	88	99	93
I3	0	0	0	1	0	0	0	5	5	5	4	3	3	68	118	91	109	109	88	82
I4	0	0	1	0	0	0	1	3	5	4	4	5	5	96	78	104	98	84	104	92

I5	1	0	0	0	0	0	0	3	5	4	5	4	6	102	123	105	101	81	76	86
I6	1	0	0	2	2	0	0	4	4	4	4	5	4	77	105	107	99	86	90	101
I7	0	1	0	0	1	0	0	4	4	3	6	5	5	89	90	95	90	60	89	103
P1	1	0	0	0	0	1	0	0	25	16	21	15	21	50	53	48	47	52	42	42
P2	2	1	0	0	1	0	1	31	0	28	22	26	19	31	46	47	47	35	35	31
P3	0	0	0	0	0	0	0	20	12	0	15	23	19	49	43	50	41	42	47	35
P4	0	0	0	0	0	1	1	19	24	13	0	13	14	39	49	45	40	46	32	46
P5	0	0	0	2	1	0	1	25	20	22	21	0	18	41	41	44	51	32	36	32
P6	0	1	1	1	2	1	0	23	16	32	24	18	0	53	40	47	41	45	35	45
R1	9	5	15	5	12	8	12	39	28	18	26	27	35	0	29	31	14	34	15	13
R2	8	9	10	3	8	9	12	39	37	27	29	30	32	18	0	4	23	25	22	20
R3	15	12	6	11	12	7	7	30	39	36	32	35	38	19	9	0	22	25	15	19
R4	8	10	13	10	10	5	6	37	35	33	32	30	25	16	19	11	0	19	13	26
R5	8	7	7	10	8	10	5	28	42	34	34	31	37	10	21	15	16	0	16	17
R6	5	4	8	11	6	9	11	42	30	26	28	40	29	18	17	20	25	16	0	18
R7	8	14	12	12	11	13	18	40	22	35	34	31	30	24	12	19	22	14	21	0

For the virtual community adopted in this study, the traffic crash data as well as detailed traffic volume data are not available. Without losing generality in the demonstration, the assumed observed number of traffic crashes (NTC) during afternoon rush hour over 1 year is shown in Table 5.8, where AHT is the average hourly traffic and it is from the traffic assignment of the OD matrix in Table 5.7; L_{wz} and t_{wz} are the length and the construction time of the work zone; L_{link} is the link length; and t_{ob} is the observation time (1 year for this case). Poisson regression (Eqs. (5.9-5.11)) analysis gives coefficients $\beta = -0.12754; 0.4382; 0.1449; 0.8198; 0.7548$ for *constant*, AHT, L_{link}, L_{wz}/L_{link} and t_{wz}/t_{ob}, respectively. In this study, it is assumed that there is no work zone in the pre-disaster period and the work zones during the long-term recovery period are only caused by the bridges suffering extensive and complete damage states which need repair. The ratios of bridge lengths to their link lengths are randomly generated between [0.05, 0.15].

Table 5.8 Parameters and observed number of crashes of the system

Link #	AHT (k)	L_{link}	L_{wz}/L_{link}	t_{wz}/t_{ob}	NTC(1 year)
1	0.250	1.945	0.037	0.547	2
2	0.993	1.594	0.078	0.139	2
3	0.204	2.482	0.659	0.149	3
4	0.062	1.625	0.556	0.258	2
5	0.529	1.312	0.254	0.841	3
6	0.143	1.548	0.760	0.254	3
7	0.042	1.621	0.028	0.814	2
8	0.687	1.574	0.351	0.244	2
9	0.486	2.023	0.305	0.929	4
10	0.200	2.023	0.612	0.350	3
11	0.341	3.065	0.636	0.197	3
12	0.855	1.312	0.149	0.251	2
13	0.385	1.574	0.392	0.616	3
14	0.423	2.882	0.356	0.473	3
15	0.543	1.605	0.517	0.352	3
16	0.269	2.207	0.567	0.831	4
17	0.376	1.620	0.604	0.585	3
18	0.350	2.376	0.221	0.550	3
19	0.766	2.969	0.544	0.917	6
20	0.338	1.324	0.524	0.286	2
21	1.521	1.441	0.130	0.757	4
22	0.666	2.032	0.095	0.754	3
23	1.750	2.391	0.399	0.380	5
24	0.640	1.680	0.768	0.568	4
25	1.702	1.312	0.272	0.076	3
26	0.943	1.908	0.468	0.054	3
27	0.545	1.651	0.179	0.531	3

28	0.480	2.584	0.601	0.779	5
29	0.228	1.949	0.204	0.934	3
30	0.104	3.519	0.405	0.130	2
31	0.403	3.065	0.559	0.569	4
32	0.608	2.881	0.713	0.469	4
33	0.598	1.992	0.767	0.012	3

With LOP $\varepsilon = 0.8$ and $m = 0.5$, Monte Carlo approach is used to simulate the PGA with 1,000,000 samples and Latin Hypercube sampling is adopted to simulate bridge damage states with 1,000 samples. Applying Eqs. (5.12-5.20) through Matlab simulations, the results are shown in Table 5.9 and Figs. 5.4-5.6. It is found from Table 5.9 that the increase of the $TSTT$ in terms of percentage is similar to but a little less than the increase of $TSCF$ as compared to the respective pre-disaster values, $TSTT_0$ and $TSCF_0$. It is likely because traffic crashes are very sensitive to the presence of work zones, which is in accordance with the large coefficient values for L_{wz}/L_{link} and $t_{wz}\ /t_{ob}$. Figs. 5.4-5.6 show that the post-hazard $TSTT$ and $TSCF$ for most sampled scenarios are concentrated within small ranges near $TSTT_0$ and $TSCF_0$ respectively and the system RI values are mostly close to 1. This phenomenon is mainly due to the low failure rate of the bridges when the Richter magnitude is low. In Fig. 5.4, when TSTT is between 160 and 205, the cumulative distribution function (CDF) increases slowly. It may be because the failures of a certain bridge or specific combinations of bridges just have a very limited impact on the system travel time. If a vulnerable link has some alternative routes with similar travel time, its failure may not significantly impair the traffic efficiency of the system. Compared to Fig. 5.4, Fig. 5.5 has a smoother increase in the curve possibly because TSCF is very sensitive to the existence of work zones, which complies with the coefficient values of the Poisson regression. For instance, if some links as discussed above are partially closed, the system travel time doesn't increase considerably, but the number of traffic crashes may increase because of the existence of work zones.

Fig. 5.6(a) shows that CDF has almost no increase from 0.5-0.65 and 0.9-1, a slow increase from 0.65-0.8, a rapid increase from 0.8-0.9, and a dramatic increase at 1. Since the resilience index is based on both TSTT and TSCF, such phenomena can be explained by the observed trends in the CDF curves of TSTT and TSCF. We fit the system resilience to various probability distributions and found out that Beta distribution had the best fit. Fig. 5.6(b) shows Beta distribution fits the system resilience very well at most points. So, the Beta distribution may be used to estimate the system resilience with the proposed methodology.

Table 5.9 System indices

System index	Value
Pre-disaster $TSTT_0$ (min/hour)	150.85
Pre-disaster $TSCF_0$ (/year)	59.66
Post-hazard mean $TSTT$ (min/hour)	171.50
Post-hazard mean $TSCF$ (/year)	68.80
Increase in $TSTT$ (%)	13.69
Increase in $TSCF$ (%)	15.32
System reliability	0.85

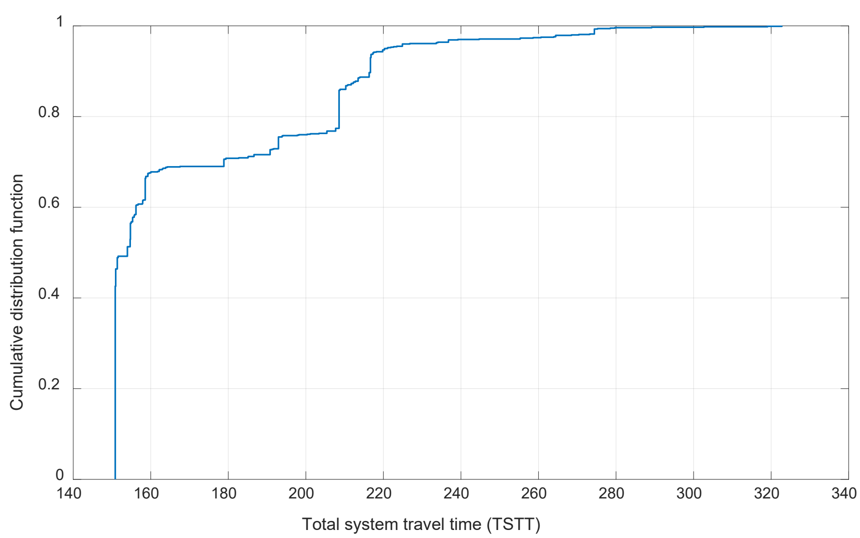

Figure 5.4 Cumulative distribution of TSTT

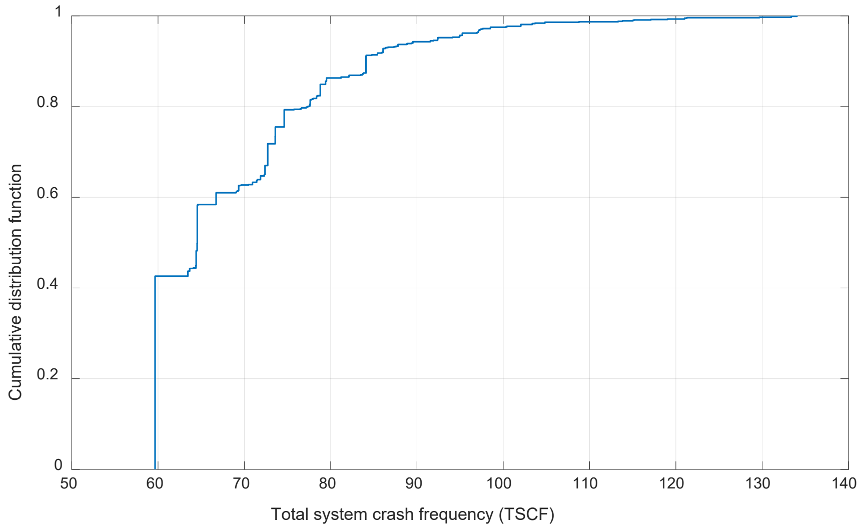

Figure 5.5 Cumulative distribution of TSCF

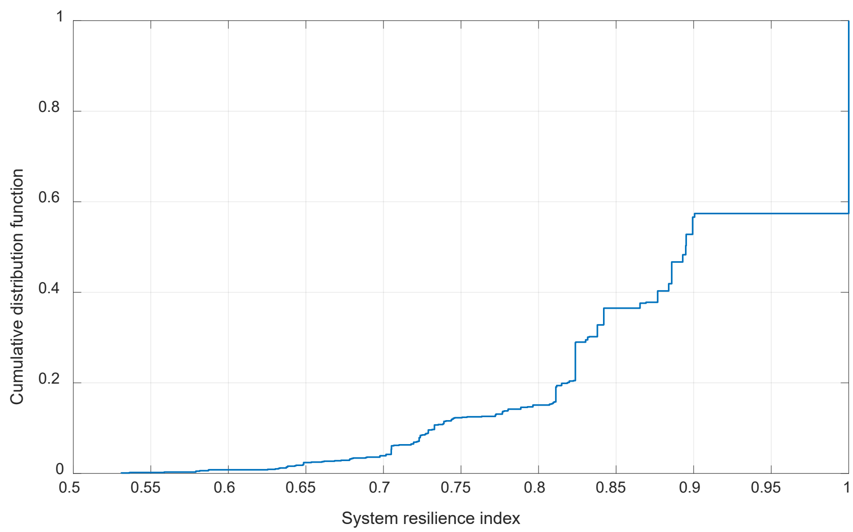

(a) Cumulative distribution of system resilience index

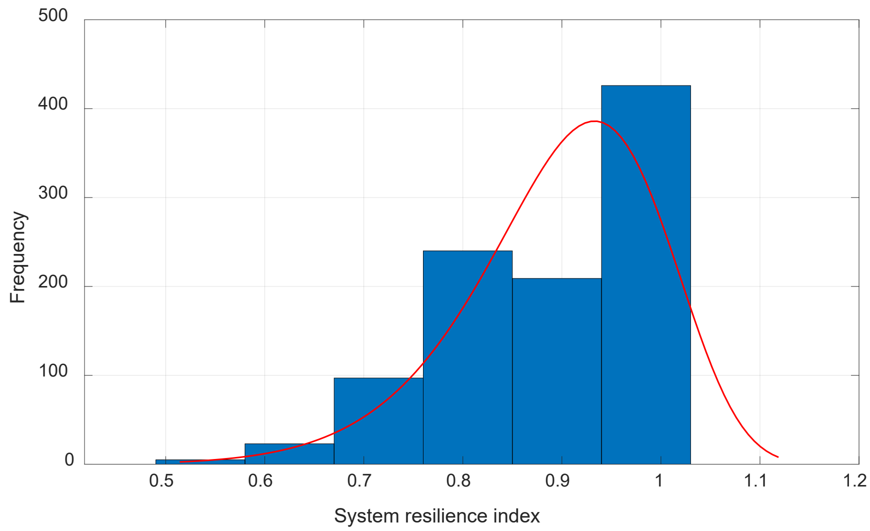

(b) Histogram of system resilience index

Figure 5.6 Distribution of system resilience index

The impacts of earthquake intensity and LOP on the system reliability are also studied and the results are presented in Figs. 5.7-5.8. It is found in Fig. 5.7 that the system reliability R decreases slower at lower earthquake intensities and then decreases faster but almost linearly at higher magnitudes. As expected, a stronger earthquake will cause a higher chance of damages on the bridges, and in turn lower the system resilience index and reliability of the whole system. Apparently when the earthquake intensity is low, almost no bridge fails, which may be the reason for the slower drop in the system reliability at the lower magnitudes. In Fig. 5.8, it is found that the system resilience index remains stable around 1 when the level-of-performance (LOP) is low. It is because the network remains a certain level of functionality, even under the worst bridge damage situations. So, the network meets the low LOP in almost all the sampled damage scenarios. Then system reliability slowly decreases when LOP is between 0.6-0.8. It is because some severely damaged scenarios can no longer meet the increasing LOP. The failures of the most important bridges or bridge combinations happen during this interval, and the damage of any of these bridges or bridge combinations will greatly reduce the system performance. When the LOP is between 0.8-0.9, the system reliability quickly decreases, representing a deteriorating condition from the system resilience perspective. It means when the LOP is high, the network with failures of even a very limited number of bridges cannot maintain the required performance criterion. The selection of LOP value in this interval will ensure the network doesn't suffer any major damage and remains a very high level of functionality.

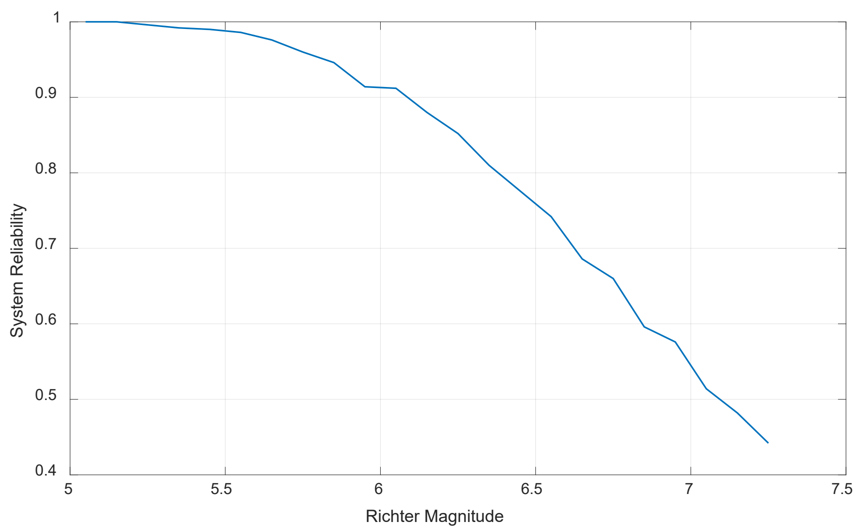

Figure 5.7 System reliability as a function of Richter magnitude

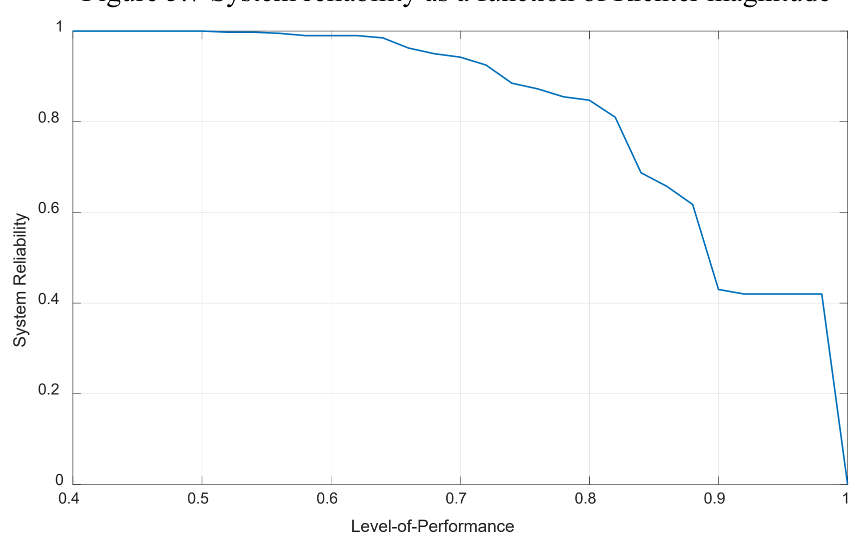

Figure 5.8 System reliability as a function of level-of-performance

5.3.2 Post-earthquake bridge restoration prioritization

Due to the relatively low failure rates for bridges, none or just few of the bridges are damaged in most of the possible states generated from Latin Hypercube sampling. In this case, we would restore the damaged (extensive damage or worse) bridges in the best sequences while the restoration sequences of fully functional (less than extensive damage) bridges are set to be the last- 9 (the total number of bridges in the network). Assuming the repair time for bridges B1 to B9 are 98, 74, 99, 90, 79, 83, 85, 97, and 77 days respectively if they are damaged, the optimization is conducted based on Eqs. (5.21-5.23) following the Greedy Algorithm, and the result is presented in Fig. 5.9. It is found that Bridge 9 on link (I5, R7) has the highest priority due to the network topology, bridge location, etc. From Fig. 5.3 and Table 5.2, we can tell Bridge 9 is very important to the trips between OD pairs including (I5, R7), (R4, R7), (I5-I7), (P6, I5), (P6, R4), (I7, R4) and so on. All these trips don't have alternatives with similar travel time. Among these OD pairs, (I5, R7), (P6, R4), (I7, R4), and (R4, R7) have considerable number of trips. A great increase in the travel time and the number of traffic crashes can be expected when Bridge 9 suffers extensive or complete damages. Similarly, Bridge 3 has the least priority because of the relatively insignificant location in the graph in terms of travel time and safety. Fig. 5.3 and Table 5.2 show trips that need to go through link (R5, R6) have many alternative routes to choose with similar travel times.

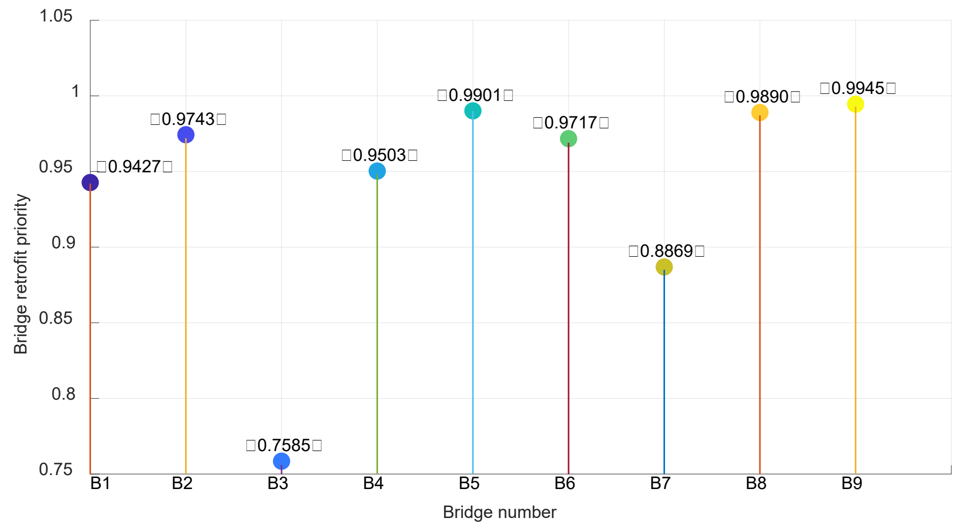

Figure 5.9 Post-hazard restoration priority for different bridges

5.4 Conclusions

Long-term recovery is a very important stage following any major hazard or incident. A framework of modeling resilience-related performance of a transportation network was developed from both travel time and traffic safety perspectives. In the model, uncertainties in the earthquake information and fragility of the bridges were addressed to simulate real-world earthquake scenarios and possible disconnected or partial functioning bridges. A resilience performance indicator was introduced to evaluate the overall travel time and safety performance for the whole network and a bridge restoration prioritization index was proposed to evaluate the relative restoration priorities of different bridges in a traffic network. The priority information of bridges can help developing more efficient post-hazard long-term recovery strategy by keeping those bridges robust and functional in the long-term recovery stage. Based on the long-term recovery performance in terms of travel time and safety, the proposed model can assist on developing rational long-term recovery plan for a community with some partially functional bridges. Finally, the proposed framework was demonstrated in a hypothetical community located in earthquake-prone areas vulnerable to extensive earthquake attacks. This study has two main innovative contributions: (1) simulating the traffic performance of road segments with partially closed bridges in the network performance assessment, which helps capture the time-progressive recovery process; and (2) integrating both travel time and traffic safety into the resilience quantification and recovery prioritization. Despite the approximations and relatively simpler models being adopted, it is noted that the proposed approach is general enough to be extended to more advanced models with more site-specific data without losing generality.

This study also has some limitations. The traffic crash frequency was estimated with Poisson model due to the popularity, simplicity, and low requirement of site-specific data. There are some more advanced traffic crash frequency modeling techniques which can be applied in the proposed framework when more site-specific historical crash data are available. Also, due to the lack of data and computation complexity, we didn't consider the deterioration process of bridges (García-Segura et al., 2017) and the interdependency between the transportation network and other lifeline systems, which can also be important for studying community resilience. Following the proposed methodology, more insightful and advanced studies on a community can be conducted in the future once more site-specific data becomes available. For example, more advanced traffic safety modeling techniques like Negative Binomial model and comprehensive site-specific traffic accident data can be applied to estimate the community's traffic crash frequency. Dynamic traffic assignment algorithms can be adopted to model the changes of travel demand and traffic flow during a day instead of just focusing on the traffic performance during the afternoon rush hour.

CHAPTER 6 TRANSPORTATION RESILIENCE MODELING AND BRIDGE RECONSTRUCTION PLANNING BASED ON TIME-EVOLVING TRAVEL DEMAND DURING POST-EARTHQUAKE RECOVERY PERIOD [5]

6.1 Introduction

After major earthquakes, the communities may experience time-evolving population in terms of size and distribution and varying travel demands along with the displacement and recovery of residents caused by the damage and restoration of dwelling units. The community transportation can be significantly affected if the changes in population size and distribution are considerable. As a result, the post-hazard infrastructure reconstruction process is essentially like urban replanning to meet the realistic traffic needs of the remaining and recovering residents and further maximize the sustainability of the community. To fill the gap in existing studies that considered the travel demand as fixed during the long-term recovery stage, it is important to investigate the effects of time-evolving travel demand on transportation resilience modeling and bridge reconstruction planning during the post-earthquake recovery period. A new methodology is proposed to analyze such impact by assessing the time-dependent resilience performance of transportation networks during the post-earthquake recovery stage. Traffic efficiency and safety are the two resilience performance indicators used to evaluate the transportation network. A post-earthquake infrastructure restoration planning is conducted using a heuristic algorithm based on the time-dependent resilience performance indicator. A demonstrative case study is carried out at Shelby County, Tennessee.

[5] This chapter is submitted to a journal as a paper that is currently under review (Wu and Chen 2023c).

This chapter is to investigate the time-dependent transportation resilience modeling and reconstruction planning during the post-earthquake recovery stage to close existing research gaps. The contributions of this study include (1) modeling more realistic time-dependent travel demand of the community during the post-earthquake recovery stage; (2) conducting the reconstruction planning with a focus on meeting the realistic demands of the current/remaining and future/recovering residents. Specifically, both the time-evolving population size and distribution are simulated based on hazard-induced building damages, public shelter information, community demographics, and building recovery information. The time-evolving travel demand is further estimated based on the time-evolving zone population, community demographics, and a verified travel demand model in the case study area.

6.2 Methodology

This study proposes a methodology to quantify the resilience performance of transportation networks during the post-earthquake recovery stage by incorporating the time-dependent travel demand of the community and support the reconstruction planning of damaged transportation infrastructure. As presented in Fig. 6.1, the model begins with the given earthquake information (location, intensity, etc.) to generate the bridge and building damage scenarios using the seismic attenuation function (Atkinson and Boore 1995) and fragility curves of structures (Nielson and DesRoches 2007). Building damages are used to estimate the total displaced population (Hazus 2020) and the initial travel demand using the trip generation model (Kimley-Horn et al. 2007). Building recovery reflects the restoration progress of dwelling units, which is used to estimate the recovery of the dislocated residents and the time-dependent population size and distribution, and travel demand (Hazus 2020).

In Fig. 6.1, bridge damage scenarios are related to link functionalities based on existing studies (Zhang et al. 2019) and are generated using the Latin Hypercube sampling method. The time-dependent link travel time and traffic flow can be estimated using traffic assignment methods, the sampled link functionality scenarios, and the time-evolving travel demand (Wardrop 1952). The traffic flow and traffic accident models based on the community's historical traffic crash data can be used to derive the expected traffic accident frequency (Washington et al., 2010). The expected time-dependent resilience index is defined based on system travel time, traffic accident frequency, and bridge damage uncertainty. Finally, the optimal bridge reconstruction planning can be derived using heuristic algorithms based on the proposed resilience index. Fig. 6.1 shows the detailed process of the methodology.

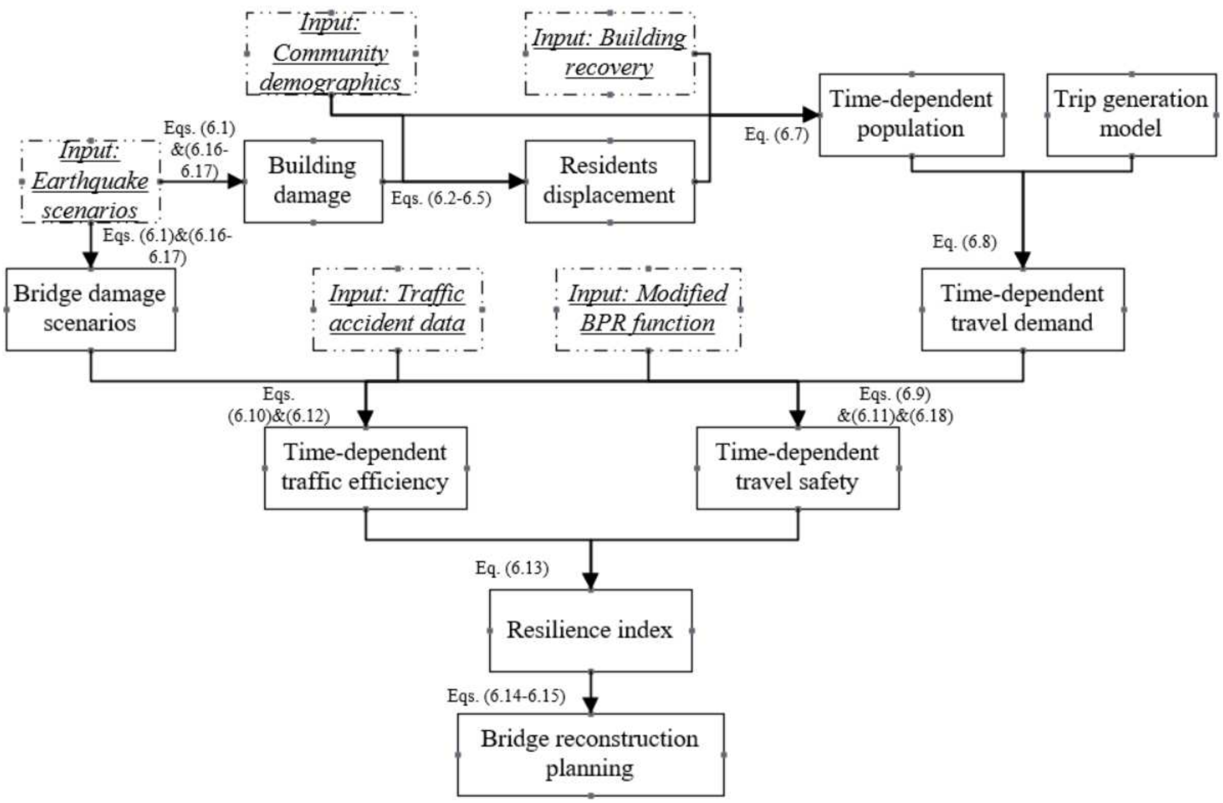

Figure 6.1 Flowchart of the model

Table 6.1 List of notations

Variables	Description
ADT_i	Average daily traffic per lane of road segment i
b_{res}	Resource constraint for reconstruction planning
c_i	Traffic capacity of road i
DH_i	Number of total dislocated households of zone i
HH_i	Total number of households for zone i
$HH_i^{t=0}$	Initial total number of households for zone i at the beginning of recovery
HH_i^t	Number of households of zone i at recovery time t
L_i	Length of link/road segment i
m	Weight parameter
M	The set of all sampled network damage scenarios
med_i	Median peak ground acceleration value of damage state i
$\%MF_i$	Parameter related to multi-family dwelling units damage states
$\%MFC_i$	Possibility for multi-family residential buildings suffering complete damage
$\%MFE_i$	Possibility for multi-family residential buildings suffering extensive damage
$\%MFM_i$	Possibility for multi-family residential buildings suffering moderate damage
MFU_i	Total numbers of multi-family dwelling units in zone i
M_L	Richter magnitude
n_b	Total number of damaged bridges
ND_i	Number of displaced households move to the public shelter in zone i
n_s	Number of shelters in the community
n_z	Number of zones in the community
PGA	Mean peak ground acceleration
POP_{total}^0	Community population at the pre-hazard stage
POP_{total}^t	Community population at recovery time t
q_i	Traffic volume on road i
R	Epicentral distance
$\%RDU_i^t$	Percentage of recovered dwelling units of zone i at time t
RI^t	Time-dependent resilience index
$\%SF_i$	Parameter related to single-family dwelling units damage states
$\%SFC_i$	Possibility for single-family residential buildings suffering complete damage
$\%SFE_i$	Possibility for single-family residential buildings suffering extensive damage
$\%SFM_i$	Possibility for single-family residential buildings suffering moderate damage
SFU_i	Total numbers of single-family dwelling units in zone i
STP_{ij}	Number of people from zone j that are assigned to the public shelters in zone i
STP_j	Number of people moving from zone j to public shelters
T	Total recovery time of the system
TAF	Expected total accident frequency of the system
TAF_0	Expected total accident frequency of the system at the pre-hazard stage
TAF_t	Expected total accident frequency of the system at recovery time t

t_i	Travel time of the road i
t_i^0	Free-flow travel time of road i
t_i^s	Travel time of link i in sampled damage scenario s
TP_i^H	Average household trip production of zone i
TP_i^t	Total trip production of zone i at recovery time t
TTT	Total travel time of all links
TTT_0	Total travel time of all links at the pre-hazard stage
TTT_t	Total travel time of all links at recovery time t
W_{MFC}	Default value for completely damaged multi-family dwelling units
W_{MFE}	Default value for extensively damaged multi-family dwelling units
W_{MFM}	Default value for moderately damaged multi-family dwelling units
W_{SFC}	Default value for completely damaged single-family dwelling units
W_{SFE}	Default value for extensively damaged single-family dwelling units
W_{SFM}	Default value for moderately damaged single-family dwelling units
x_i	Vector of explanatory variables for traffic accident regression
x_i^t	Binomial variable specifying if bridge i is being repaired at time t
α	BPR function parameter
β	Vector of estimable parameters for traffic accident regression
β_c	BPR function parameter
ε_i	Error term for traffic accident regression
ζ_i	Dispersion of damage state i
λ_i	Expected number of accidents per unit time on road i
λ_i^s	The expected number of traffic accidents of link i in sampled damage scenario s

6.2.1 Seismic vulnerability and household displacement

6.2.1.1 Seismic intensity measure and structural damage

As a popular earthquake intensity measure, the peak ground acceleration, PGA, of a given location can be estimated using the attenuation laws in existing studies based on the fault information such as Richter magnitude (M_L) and epicentral distance (R) (Campbell 1981). Typical attenuation laws are expressed as:

$$PGA = f(M_L, R) \tag{6.1}$$

The seismic fragility of structures (buildings and bridges, etc.) can be defined as the probability of occurrence of a given infrastructure damage state under given intensities of earthquakes, e.g., PGA. The failure in terms of a limit state is defined as the excess of the limiting values of the structural performance indicators. Based on the failure severity level, the damage states for bridges and buildings are usually divided into five types: no damage, slight/minor damage, moderate damage, extensive damage, and complete damage (Nielson and DesRoches 2007; and Hazus 2020). The damage states of buildings and bridges can be used to estimate building habitability and link functionality. The population size and distribution and the initial travel demand at the beginning of the recovery stage can be calculated based on the building damage states.

6.2.1.2 Household displacement

The damaged dwelling units may result in an estimable number of displaced households. These households may need immediate shelters such as family or friends' houses, rental homes, and public shelters. For the convenience of estimation, two types of displaced households are assumed in this study: those moving to temporary homes out of the community and those moving to public shelters within the community. Households moving out of the community are considered to relocate to and live in their new communities/cities, while households moving to shelters within the community are assumed to have the same travel habits as the residents in those zones where the public shelters locate. The public shelters may be in different zones from those before the hazard. For both types of displaced households, it is assumed they will move back when their pre-hazard dwelling units are repaired. For each zone, the number of total displaced households is estimated as (Hazus 2020):

$$DH_i = (SFU_i \times \%SF_i + MFU_i \times \%MF_i) * (\frac{HH_i}{SFU_i + MFU_i}) \tag{6.2}$$

where for zone i, DH_i is the number of total displaced households; SFU_i is the total number of single-family dwelling units; MFU_i is the total number of multi-family dwelling units; HH_i is the total number of households. All these data are included in the demographics of a community (U.S. Census Bureau 2019). $\%SF_i$ and $\%MF_i$ are parameters related to the building damage states (Hazus 2020), which are defined as:

$$\%SF_i = W_{SFM} \times \%SFM_i + W_{SFE} \times \%SFE_i + W_{SFC} \times \%SFC_i \tag{6.3}$$

$$\%MF_i = W_{MFM} \times \%MFM_i + W_{MFE} \times \%MFE_i + W_{MFC} \times \%MFC_i \tag{6.4}$$

where $\%SFM_i$, $\%SFE_i$, and $\%SFC_i$ are the probabilities of single-family residential buildings suffering moderate, extensive, and complete damage states, respectively. Similarly, $\%MFM_i$, $\%MFE_i$, and $\%MFC_i$ are the probabilities for multi-family residential buildings suffering moderate, extensive, and complete damage states, respectively. W_{SFM}, W_{SFE}, W_{SFC}, W_{MFM}, W_{MFE}, and W_{MFC} are the default values for moderately, extensively, and completely damaged single- and multi-family dwelling units with values of 0, 0, 1, 0, 0.9, and 1, respectively.

According to Hazus (2020), the number of households displaced to public shelters within the community for a given zone can be estimated based on its population size and the income, ethnicity, home ownership, and age distribution of the residents in the zone. Thus, the number of households displaced to other cities can be estimated by deducting the households displaced to public shelters from the total displaced households. The estimated household displacement information can be used to derive the initial population size and distribution of the community at the beginning of the post-earthquake recovery stage.

6.2.2 Time-evolving population and travel demand

6.2.2.1 Time-evolving population

To estimate the time-evolving population size and distribution of the community and further derive the travel demand, the reconstruction of damaged dwelling units needs to be introduced to simulate the recovery of the displaced residents. After an earthquake, restoring damaged buildings is part of the community's recovery process. Given the distributions of the recovery time of buildings with different damage states, the population of each zone at any given recovery time t can be estimated by assuming residents will move back immediately after their damaged dwelling units are restored. Based on Eq. (6.2), the initial total households for zone i after dislocation is:

$$HH_i^{t=0} = \begin{cases} HH_i - DH_i, & Zone\ i\ has\ 0\ public\ shelter \\ HH_i - DH_i + ND_i, & Zone\ i\ has\ public\ shelter(s) \end{cases} \tag{6.5}$$

$$\textstyle\sum_1^{n_z} STP_j = \sum_1^{n_s} ND_i \tag{6.6}$$

where ND_i is the number of displaced households that move to the public shelter in zone i; n_z is the number of zones in the community; STP_j is the number of people moving from zone j to public shelters; n_s is the number of shelters in the community. Considering distance can be a significant factor for the shelter choice of displaced residents, this study reasonably assumes that the residents who need public shelters will seek temporary housing at the closest public shelter until it is full. Based on this assumption, ND_i is calculated using linear programming.

According to Hazus (2020), the mean recovery time of single-family and multi-family dwelling units is listed in Table 6.2. Following existing studies, this study assumes the recovery time of dwelling units follows a lognormal distribution with a covariance of 0.4 (Lin and Wang 2017).

Table 6.2 Building recovery times in days (Hazus 2020)

Occupancy class	Recovery time				
	Structural damage state				
	None	Slight	Moderate	Extensive	Complete
Single-family dwelling	0	5	120	360	720
Multi-family dwelling	0	10	120	480	960

As assumed above, the displaced residents will return to their pre-hazard dwelling units soon after the buildings are restored to the habitability criterion. The total households of zone i at time recovery time t can be estimated as:

$$HH_i^t = \begin{cases} HH_i^{t=0} + \%RDU_i^t * DH_i, & Zone\ i\ has\ 0\ public\ shelter \\ HH_i^{t=0} + \%RDU_i^t * DH_i - \sum_j \%RDU_j^t * STP_{ij}\ , & Zone\ i\ has\ public\ shelter(s) \end{cases} \tag{6.7}$$

where HH_i^t is the number of households of zone i at recovery time t; $\%RDU_i^t$ is the percentage of recovered dwelling units of zone i at time t; and STP_{ij} means the number of people from zone j that are assigned to the public shelters in zone i. $\%RDU_i^t$ can be derived based on the recovery time (Table 6.2) and the specified distribution information. The time-dependent number of households, HH_i^t, can be used to estimate the travel demands of the community at any time during the recovery stage.

6.2.2.2 <u>Time-dependent travel demand</u>

The recovery stage can last up to several years after major earthquakes. Unlike the usually sudden, short, and intense post-earthquake emergency response stage that can easily disrupt almost all regular travel plans (Wu and Chen 2023b), the relatively long-lasting recovery stage may allow the remaining residents to keep up their daily activities despite the ongoing reconstruction of the damaged infrastructures (Chang et al. 2012). The Memphis Metropolitan Planning Organization (MPO) developed a travel demand model in the Long-Range Transportation Plan for the Memphis region. They used trip generation, trip attraction, and the trip distribution matrix based on the gravity model to derive the travel demand of the region, the model settings of which have been verified to be reliable (Kimley-Horn et al., 2007).

According to the Memphis MPO travel demand model (Kimley-Horn et al. 2007), there are nine typical trip purposes, including journey to work, home-based school, home-based university, home-based shopping, home-based social-recreational, home-based pickup/drop-off, home-based other, non-home-based work, and non-home-based non-work. For household trip production, the numbers of trips generated for different purposes are related to at least two of the following parameters: number of persons in a household, number of persons aged 0-17 in a household, number of workers in a household, and number of vehicles in a household (Kimley-Horn et al. 2007). Based on the Memphis MPO model, the total trip production of a given zone at any recovery time can be estimated as:

$$TP_i^t = TP_i^H * HH_i^t \tag{6.8}$$

where TP_i^t is the total trip production of zone i at recovery time t; TP_i^H is the average household trip production of zone i derived using the Memphis MPO model (Kimley-Horn et al. 2007) with the demographics of the zone (U.S. Census Bureau 2019).

For the trip attraction of each zone, the number of attracted trips for each purpose is related to one or more of the following parameters of the zone: total employment, school enrollment, university enrollment, retail employment, service employment, total households, and office employment (Kimley-Horn et al. 2007). All the above-mentioned zone information is available in the demographics of a community (U.S. Census Bureau 2019). This study follows the Memphis MPO model for travel demand estimation. A commonly used method, the gravity model (Erlander and Stewart 1990), is adopted for trip distribution.

The factors used to determine the trip distribution matrix are travel distances and production-attraction dummies.

Based on the estimated daily travel demand, the origin-destination (OD) matrix will be derived during the study period according to the historical time-of-day travel data of the Memphis area. Similarly, a mode choice logit model is adopted to estimate the percentage of vehicle-based trips. The factors considered in the mode choice logit model are origin-destination highway distance, production-attraction zone types (e.g., CBD, urban, suburban, and rural), and household auto ownership. The derived time-dependent OD demand during the study period can be used with various traffic assignment methods (e.g., Wardrop 1952) to get the link travel time and traffic accident frequency of the community.

6.2.3 Travel time and safety for roads with work zones

6.2.3.1 Modified Bureau of Public Roads function

Damaged bridges may disrupt road links following earthquakes and create work zones. According to Padgett and DesRoches (2007), bridges with extensive damage can recover 50% of their capacities in one week after the disaster. Considering the recovery stage usually does not start immediately after earthquakes, the results from their research will be applied in this study. We focus on two-way two-lane roads (two lanes in each direction), which are common in the US. In this study, a two-way two-lane bridge is deemed fully closed if it is completely damaged; and one lane in each direction remains open if the bridge suffers extensive damage to reflect the 50% capacity. With extensive damage, since one lane in each direction on the bridge will be closed, the link will be degraded into a road essentially with "work zones" in both directions (Fig. 6.2). As a result, there are three typical traffic scenarios for two-way double-lane roads:

normal four-lane traffic, disrupted traffic with work zones on the bridge (Fig. 6.2), and fully closed to traffic.

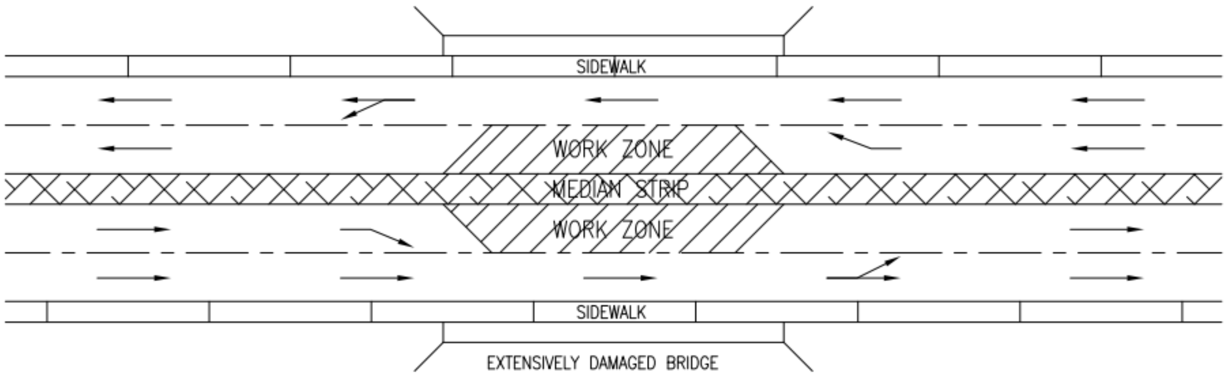

Figure 6.2 Traffic pattern for a road with work zones

Significant difference exists between the travel patterns of normal roads and those with work zones. To consider the impact of work zones on travel time, a modified Bureau of Public Roads (BPR) function is adopted from an existing study (Zhang et al. 2019) to estimate the travel time of roads i in Fig. 6.2. The travel time function for road i can be expressed as:

$$t_i = t_i^0[1 + \alpha\left(\frac{q_i}{c_i}\right)^{\beta_c}] \tag{6.9}$$

where t_i is the travel time of the road i; t_i^0 is the free-flow travel time of the road; q_i is the traffic volume on the road; c_i is the traffic capacity of the road; α and β_c are BPR function parameters. Different from the default values of 0.15 and 4.0 for α and β_c for normal roads, these parameters have values of 1.429 and 4.293, respectively, for road i with the traffic pattern as specified in Fig. 6.2 (Zhang et al. 2019). According to the US Highway Capacity Manual (TRB 2010), the ideal capacity of one intact lane is usually assumed to be 2,000 vehicles. Zhang et al. (2019) have confirmed that Eq. (6.9) works when the ratio of heavy vehicles is not higher than 10%. Since trucks and heavy vehicles account for 4.2% of the highway vehicles (Sprung 2018), the BPR function can be applied in this study.

6.2.3.2 Work-zone traffic accident estimation

For the road scenario in Fig. 6.2, the changed traffic pattern will affect traffic accident frequency (Garber and Zhao, 2002; La Torre et al., 2017; Pigman and Agent, 1990; Weng and Meng, 2011; and Yang et al., 2015). As an important topic that has been widely investigated, work zone traffic safety can be as important as traffic efficiency to travelers. The Poisson regression model has been used for traffic accident counts but with a significant limitation: the mean and standard deviation of accidents need to be close. To handle the over-dispersed accident data, negative binomial regression is often used as an alternative for discrete and nonnegative events. According to Washington et al. (2010), for the negative binomial distribution, the expectation of the number of accidents on road i is:

$$\lambda_i = e^{\beta x_i + \varepsilon_i} \tag{6.10}$$

where λ_i is the Poisson parameter for road i, which is equal to the expected number of accidents per unit time on road i; x_i is a vector of explanatory variables; β is a vector of estimable parameters; $EXP(\varepsilon_i)$ is a gamma-distributed error term (Washington et al. 2010). For work zone traffic accidents, the explanatory variables may include link length, light conditions (daytime or nighttime), adjusted traffic volume, posted speed limit, speed reduction to the normal speed limit, the number of open lanes, the number of lane closures, road type, the number of ramps, and the number of intersections within the work zone (Ozturk et al., 2013). It should be noted that the explanatory variables for normal roads are usually different from those of work zones.

6.2.4 Resilience index and reconstruction planning

6.2.4.1 Time-dependent resilience index

The expected total travel time (TTT) is one of the commonly used system performance metrics in transportation engineering to characterize the efficiency of a transportation network:

$$TTT = \frac{\sum_s \sum_i t_i^s}{|M|} \tag{6.11}$$

where t_i^s is the travel time of link i derived from Eq. (6.9) and traffic assignment methods in sampled damage scenario s; and M is the set of all sampled network damage scenarios. Similarly, the expected total accident frequency (TAF) of the system is used to quantify the traffic safety risk of the network, which is defined as:

$$TAF = \frac{\sum_s \sum_i \lambda_i^s}{|M|} \tag{6.12}$$

where λ_i^s is the expected number of traffic accidents of link i derived from Eq. (6.10) in sampled damage scenario s. The integrated resilience index (RI) at time t is proposed to consider both traffic efficiency and travel safety performances. Considering that travel demand and community population are both functions of the recovery time, a time-dependent integrated resilience index of the transportation system to offset the effect of population change can be defined as:

$$RI^t = m.\frac{TTT_0}{{POP_{total}^0}^{\delta}} \Bigg/ \frac{TTT_t}{{POP_{total}^t}^{\delta}} + (1-m).\frac{TAF_0}{{POP_{total}^0}^{\delta}} \Bigg/ \frac{TAF_t}{{POP_{total}^t}^{\delta}} \tag{6.13}$$

where m is a weight parameter between [0, 1] usually defined by decision-makers based on the specific scenarios and preferences; TTT_0, TAF_0, POP_{total}^0 and TTT_t, TAF_t, POP_{total}^t are the TTT, TAF and community populations at the pre-disaster period and recovery time t respectively; δ is an adjustment factor for RI. Considering both TTT and TAF may change exponentially with recovery time, a proper δ will keep RI between 0 to 1. For demonstrative purposes, this study let $m = 0.5$ to evenly distribute the importance to travel time and traffic safety and use $\delta = 2$.

6.2.4.2 <u>Reconstruction planning of transportation infrastructure</u>

According to the above-mentioned characteristics of the post-earthquake recovery stage, the post-earthquake reconstruction planning can be deemed as an urban replanning if the population size and distribution changes are significant. Compared to the reconstruction planning of the damaged infrastructures with a fixed travel demand that is usually derived based on the pre-hazard population in existing studies, the infrastructure restoration in this study is based on the time-evolving travel demand of the community. Therefore, the reconstruction planning in this study focuses on serving the remaining and recovering residents instead of the pre-hazard residents in most existing studies.

Considering the common situation of limited resources that would impede the repairing efforts of all damaged infrastructures simultaneously, this study focuses on developing the optimal reconstruction planning of the damaged bridges to improve transportation resilience. For long-term recovery, minor damages are not critical and there are two types of bridge damage scenarios according to Subsection 6.2.3: a completely damaged bridge that is fully closed to traffic, and an extensively damaged bridge that partially opens to traffic with work zones. Other than the bridge damage state, the reconstruction time of a bridge is also an important factor affecting its repair priority and effect on system performance. In this study, the performance indicator is based on the proposed time-dependent resilience index in Section 6.2.4.1. The optimal bridge reconstruction plan is to maximize the system resilience. The objective function of the reconstruction optimization is defined as:

$$\text{Objective } Z = \max\left(\int_0^T RI^t dt\right) \quad (6.14)$$

$$\text{Subject to: } \sum_{i=1}^{n_b} x_i^t \leq b_{res} \quad (6.15)$$

where T is the total recovery time of the system; x_i^t is a binomial variable specifying if bridge i is being repaired at time t; n_b is the total number of damaged bridges; and b_{res} is the resource constraint.

6.3 Case study

6.3.1 Shelby County, Tennessee

Shelby County, Tennessee is in an earthquake-prone area. There are 37 zip codes in Shelby County and the demographics of each zip code area are available from the US Census Bureau (Figs. 6.3-6.4) (U.S. Census Bureau 2019). Among all the zip codes, 38054, 38058, 38131 and 38132 are not considered in this study because of their special functionalities (e.g., PO box, local airport). To better fit Shelby County in the model with a reasonable scope, every main road network intersection is considered as a single node/zone (Fig. 6.5). The basic information for the zip codes and zones is presented in Tables 6.2 and 6.3, respectively.

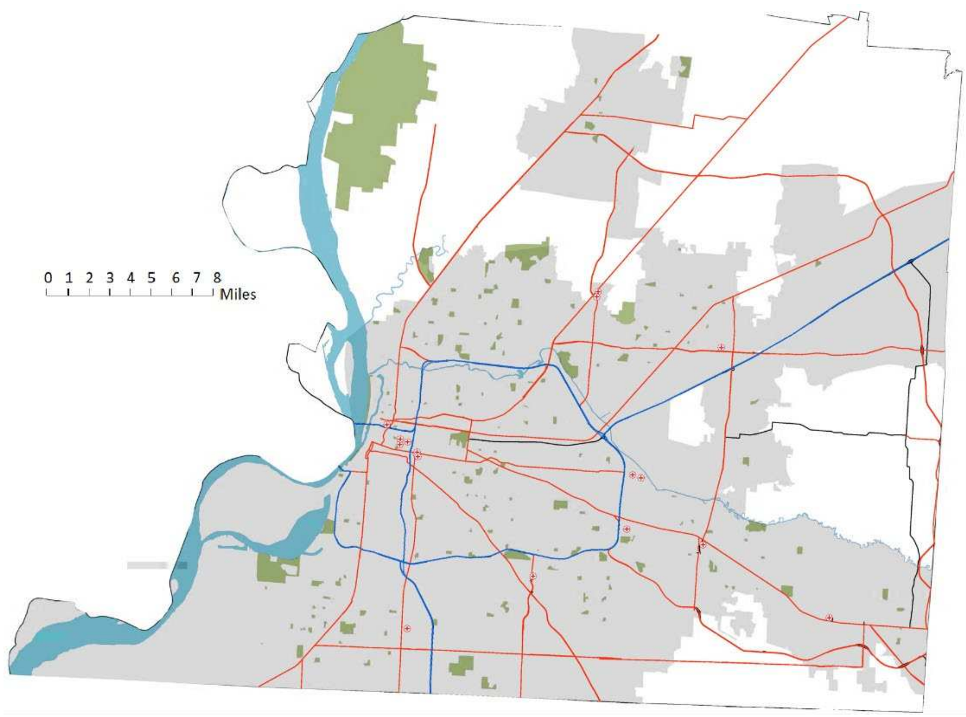

Figure 6.3 Main road network of Shelby County

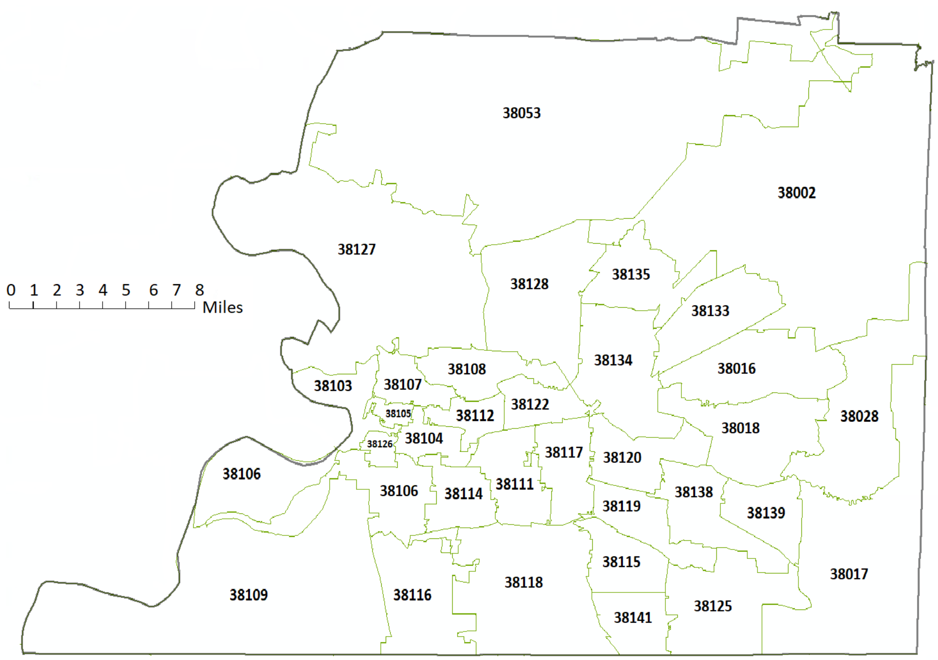

Figure 6.4 Zip code border of Shelby County

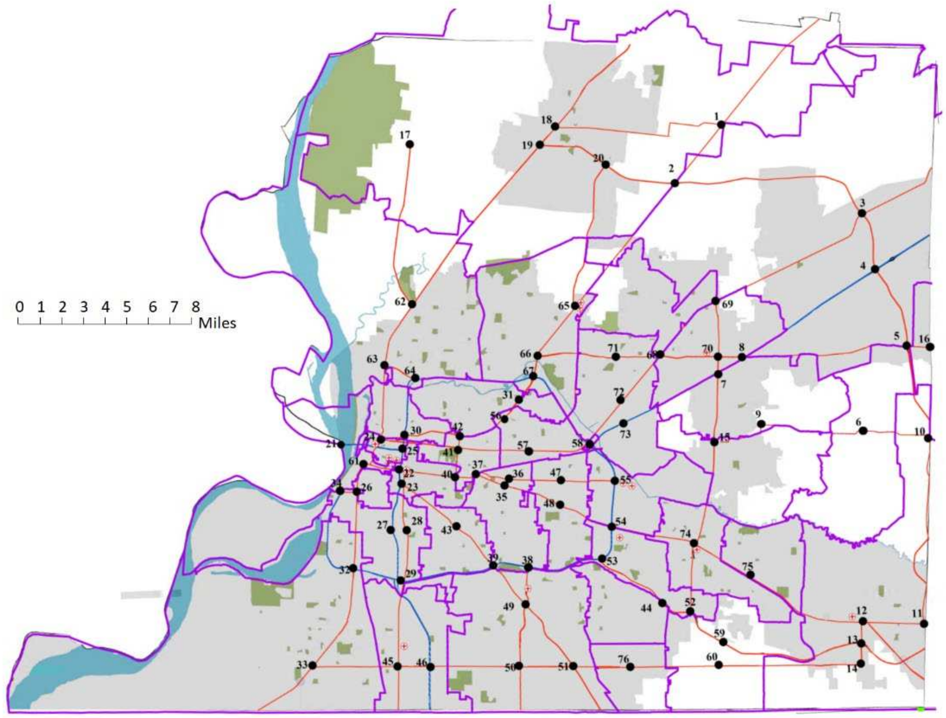

Figure 6.5 Nodes/ zones distribution of Shelby County

The main road network of Shelby County comprises 78 nodes and 115 links. This study evenly distributed the population of each zip code to the nodes inside it. It is assumed there are eight different types of buildings in the community according to the building classification in Hazus (2020): 1-2 stories wood frame, other wood frame, 1-3 stories steel moment frame, 4-7 stories steel moment frame, 1-3 stories concrete moment frame, 4-7 stories concrete moment frame, 1-3 stories concrete shear wall, and 4-7 stories concrete shear wall. Due to the lack of detailed and reliable data, the percentages of different building types are randomly generated for each zone for demonstrative purposes. Among all the links, it is assumed 31 of them have bridges on them (Fig. 6.6). There are five different types of bridges in the network: multi-span continuous (MSC) concrete, slab, and steel girder bridges, and multi-span simply supported (MSSS) concrete girder and steel girder bridges. In this study, it is assumed only bridge damage may cause the failure or degradation of a link. 31 out of 115 links are, therefore, vulnerable to earthquakes due to the existence of bridges (*B1-B31*) on them (Fig. 6.6). The geographic information of the nodes and bridges is available on Google Maps and ArcGIS database. The households of each zone are divided into single-family and multi-family households. The percentage of single-family households is 70% according to the demographics of Shelby County (Census profile 2018).

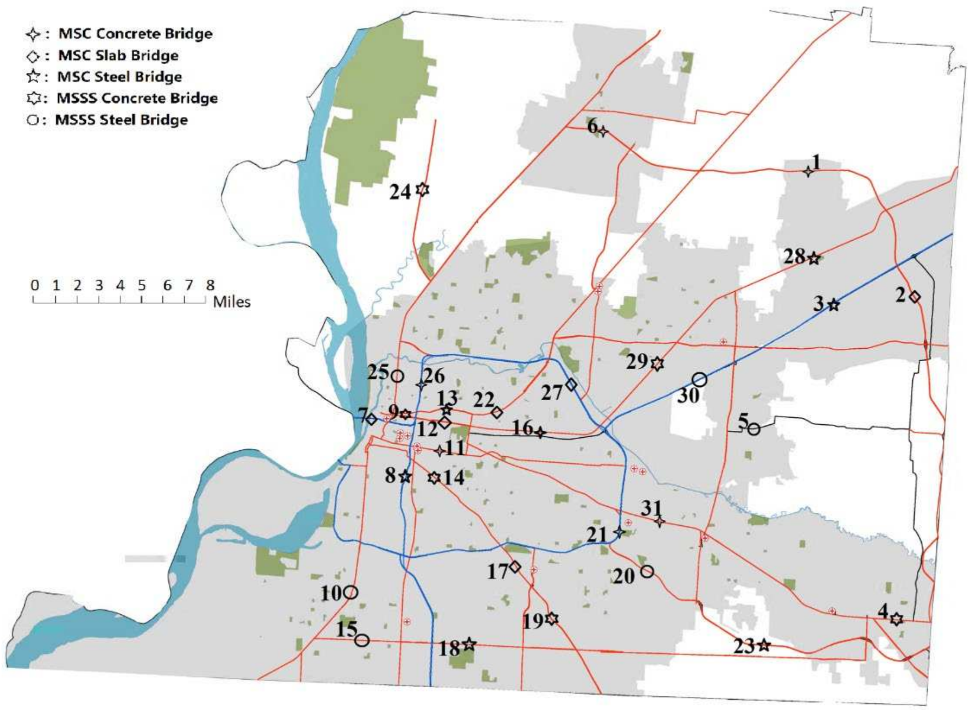

Figure 6.6 Bridge locations and types of Shelby County

Table 6.3 Zip code information of Shelby County

Zip code	TDP*	Avg*	Households
38002	25802	1.84	14053
38016	33445	1.78	18801
38017	48012	2.67	17980
38018	29209	2.04	14317
38028	4696	1.77	2646
38053	23981	2.29	10490
38103	35566	5.08	7005
38104	37758	3.02	12517
38105	17336	6.48	2676

38106	28019	2.69	10429
38107	15159	2.14	7073
38108	19164	2.85	6729
38109	43959	2.59	16989
38111	38634	2.16	17860
38112	18764	2.75	6826
38114	25507	2.4	10624
38115	37249	2.32	16053
38116	43802	2.96	14793
38117	37887	3.15	12029
38118	101321	7.21	14062
38119	28514	2.83	10065
38120	42874	6.28	6827
38122	23456	2.34	10044
38125	33446	2.27	14722
38126	10891	4.18	2607
38127	35673	2.33	15320
38128	35595	2.21	16080
38133	35919	4.67	7689
38134	42981	2.86	15053
38135	18557	1.66	11170
38138	34024	3.37	10082
38139	10335	1.84	5629
38141	19847	2.58	7678

Note: [1]TDP means total daily time population, including daytime workers and daytime residents; [2]Avg means average daily household size.

Table 6.4 Zonal information of Shelby County

Zones	Longitude	Latitude	Households	Zone type
1	35.343022	-89.788899	3513	Rural
2	35.308079	-89.822665	2098	Rural
3	35.288887	-89.686639	3513	Rural
4	35.2561	-89.676892	3513	Rural
5	35.210145	-89.653792	3513	Rural
6	35.158731	-89.694493	1323	Rural
7	35.195068	-89.792187	9401	Suburban
8	35.20436	-89.77236	2563	Suburban
9	35.156498	-89.774194	9401	Suburban
10	35.156446	-89.638166	3596	Rural
11	35.044817	-89.637635	3596	Rural

12	35.046272	-89.689285	3596	Rural
13	35.033613	-89.689272	3596	Rural
14	35.020894	-89.689143	3596	Rural
15	35.157881	-89.794974	14317	Suburban
16	35.211229	-89.63495	1323	Rural
17	35.332123	-90.015529	2098	Rural
18	35.34534	-89.906004	2098	Rural
19	35.331266	-89.920981	2098	Rural
20	35.319164	-89.873442	2098	Rural
21	35.153188	-90.059146	7005	Suburban
22	35.137466	-90.024084	6259	CBD
23	35.130376	-90.023955	6259	Urban
24	35.155747	-90.037473	3537	CBD
25	35.151606	-90.040735	2676	CBD
26	35.124652	-90.054897	2086	Suburban
27	35.10264	-90.029534	2086	Suburban
28	35.103061	-90.019985	2086	Suburban
29	35.071525	-90.023332	2086	Suburban
30	35.158338	-90.020242	3537	CBD
31	35.182929	-89.932609	6729	Suburban
32	35.07939	-90.057321	8495	Rural
33	35.020647	-90.08822	8495	Rural
34	35.124294	-90.067707	2086	Suburban
35	35.131173	-89.956728	5953	Urban
36	35.133559	-89.956127	5953	Urban
37	35.135243	-89.968143	1707	Urban
38	35.079982	-89.930549	5953	Urban
39	35.080578	-89.955869	5312	Urban
40	35.133766	-89.984064	1707	Urban
41	35.150891	-89.98136	1707	Urban
42	35.158259	-89.980416	1707	Urban
43	35.108035	-89.98827	5312	Urban
44	35.057674	-89.833646	16053	Urban
45	35.021095	-90.025306	7397	Suburban
46	35.020989	-90.002561	7397	Suburban
47	35.131269	-89.901452	6015	Suburban
48	35.11449	-89.901795	6015	Suburban
49	35.057248	-89.932866	4687	Suburban
50	35.021407	-89.937372	4687	Suburban
51	35.020528	-89.898062	4687	Suburban
52	35.052222	-89.812832	5033	Suburban

53	35.084536	-89.878106	5033	Suburban
54	35.101952	-89.870081	3414	Suburban
55	35.130947	-89.867721	3414	Suburban
56	35.171825	-89.943552	3348	Urban
57	35.149089	-89.927158	3348	Urban
58	35.152387	-89.884629	3348	Urban
59	35.037425	-89.795708	7361	Suburban
60	35.020556	-89.795966	7361	Suburban
61	35.142383	-90.051141	2607	CBD
62	35.236202	-90.014406	5107	Rural
63	35.199458	-90.034662	5107	Rural
64	35.191005	-90.016037	5107	Rural
65	35.235393	-89.895316	4020	Suburban
66	35.205276	-89.923297	4020	Suburban
67	35.192791	-89.926172	4020	Suburban
68	35.205485	-89.834333	11170	Suburban
69	35.237388	-89.793563	2563	Suburban
70	35.204362	-89.791932	2563	Suburban
71	35.204642	-89.867163	3763	Suburban
72	35.180442	-89.860168	3763	Suburban
73	35.168234	-89.85416	3763	Suburban
74	35.093018	-89.808541	10082	Suburban
75	35.075809	-89.774767	5629	Suburban
76	34.994567	-89.84841	7678	Suburban
77	35.207011	-89.894558	4020	Suburban
78	35.169095	-89.90233	3763	Suburban

6.3.2 Data analysis

In this study, an earthquake with an epicentral depth of 10 km is assumed to happen in the community being investigated. Atkinson and Boore (1995) developed the seismic attenuation law for earthquakes with an epicentral depth of 10 km. So, it is applied in this study to derive the ground motion at different zones and bridges. According to Atkinson and Boore (1995), the peak ground acceleration at a certain distance from the epicenter can be estimated as:

$$\log(\mathrm{PGA}) = \mathrm{c}_1 + \mathrm{c}_2(\mathrm{M}_L - 6) + \mathrm{c}_3(\mathrm{M}_L - 6)^2 - \log \mathrm{R} - \mathrm{c}_4\mathrm{R} \tag{6.16}$$

where M_L is the Richter magnitude of the earthquake; R is the epicentral distance (km) of the location; and c_1, c_2, c_3, and c_4 are the parameters from regression analyses. According to the study by Atkinson and Boore (1995), the following parameters are used: $c_1 = 3.79$, $c_2 = 0.298$, $c_3 = -0.0536$, and $c_4 = 0.00135$.

As mentioned in Section 6.2.1, the peak ground accelerations derived from Eq. (6.16) can be used to evaluate the building and bridge damage. According to Nielson and DesRoches (2007), the probability of a given infrastructure damage state is defined as:

$$P[Damage\ State\ i\ or\ greater|PGA] = \Phi[\frac{\ln(PGA) - \ln(med_i)}{\zeta_i}] \tag{6.17}$$

where med_i and ζ_i are the median PGA value and the dispersion of damage state i, respectively. For certain damage states of buildings and bridges, the med_i and ζ_i are shown in Tables 6.5-6.6. Moderate med_i, extensive med_i, and complete med_i in Tables 6.5-6.6 are the mean PGA values for moderate, extensive, and complete damages, respectively. Per Hazus (2020), typical buildings are designed based on four seismic standards: high-code, moderate-code, low-code, or not seismically designed (also called pre-code). Buildings designed based on codes with higher seismic standards are more robust under earthquakes. This study assumes all the buildings in Table 6.6 were designed based on the moderate-code seismic standards.

Table 6.5 Seismic fragility parameters of five bridge types (Nielson and DesRoches. 2007)

	Median PGA values (g)		ζ_i
Bridge Type	Extensive med_i	Complete med_i	
MSC concrete	0.75	1.03	0.7
MSC slab	0.78	1.73	0.7
MSC steel	0.39	0.5	0.55

MSSS concrete	0.83	1.17	0.65
MSSS steel	0.56	0.82	0.5

Table 6.6 Median and dispersion values for seismic fragility of eight building types (Hazus 2020)

Building Type	Stories	Moderate med_i	Extensive med_i	Complete med_i	ζ_i
Wood frame	1 – 2	0.43	0.91	1.34	0.64
	all other	0.35	0.64	1.13	0.64
Steel moment frame	1 – 3	0.22	0.42	0.8	0.64
	4 – 7	0.21	0.44	0.82	0.64
Concrete moment frame	1 – 3	0.23	0.41	0.77	0.64
	4 – 7	0.21	0.49	0.89	0.64
Concrete shear wall	1 – 3	0.3	0.49	0.87	0.64
	4 – 7	0.26	0.55	1.02	0.64

According to the historical traffic data of the Memphis/Shelby County area, the morning rush hour (7:00 am-8:00 am) has the heaviest traffic during the day (Kimley-Horn et al., 2007). The resilience assessment of this study is based on the traffic performance of the morning rush hour during the recovery stage. The percentages of different trip purposes as introduced in Section 6.2.2.2 of the morning rush hour over total daily trips are presented in Table 6.7 (Kimley-Horn et al., 2007). In this study, due to insufficient information, the percentages of different trip purposes during the morning rush hour are assumed to be the same as the pre-earthquake period throughout the recovery stage.

Table 6.7 Percentages of trips by purpose

Time period	Percentages of trips by purpose over daily trips				All purposes
	Journey to work	Home-based school / Home based university	Other home-based purposes	Non-home based	
7:00-8:00 AM	16.7%	23.6%	7%	3.8%	12.52%

This study assumes the earthquake has an epicenter latitude and longitude of (35.107757, -89.940678). For comparison purposes, the data analysis also explored earthquakes with four Richter Magnitudes: 6.0, 6.5, 7.0, and 7.25. Given the demographic data, earthquake information, and building fragility, the community population during the recovery stage can be estimated using Eqs. (6.2)-(6.7). The total auto-mode OD demand during the morning rush hour at any recovery time can be derived from the household information, community population, and zone information using the Memphis MPO model (Kimley-Horn et al., 2007). The community population and OD demand are shown in Figs. 6.7-6.8 as functions of recovery time. The figures show both the community population and OD demand increase with the recovery time, which conforms to the reality that the displaced residents keep moving back to their original zones due to the restoration of their pre-hazard dwelling units. The percentage increments in the community population and OD demand are similar. It is because the community OD demand is a rough product of the community household number and the average household trips considering the latter may only vary slightly among different zones within the community. As shown in Figs. 6.7-6.8, the higher the earthquake magnitude is, the smaller the community population and OD demand are, and the faster they recover. The lower starting point is consistent with the common understanding that higher magnitude generally causes more damaged housing units, more displaced residents, and higher reduced travel demand. The faster increase is caused by the lognormal distribution of the building recovery time. In this case, most damaged houses will recover within the mean recovery time (Table 6.2). Figs. 6.7-6.8 also show the changes in the community population and OD demand can be around 10%, which may significantly affect the transportation performance of the community. The considerable difference underscores the necessity to consider the time-dependent population and OD demand when simulating transportation resilience during the post-earthquake recovery stage.

The displaced population was estimated based on the information of the buildings (Table 6.6) designed according to the moderate-code seismic standards. However, there are many countries and regions where some or even most dwelling units were designed based on low-code or even pre-code seismic standards

(Bilham 2010; Ilki and Celep 2012; Wang 2008). Under major earthquakes, the communities under attack may experience extensive infrastructure damages, a significantly displaced population, substantially decreased travel demands, and a long-lasting recovery stage (Naddaf 2023).

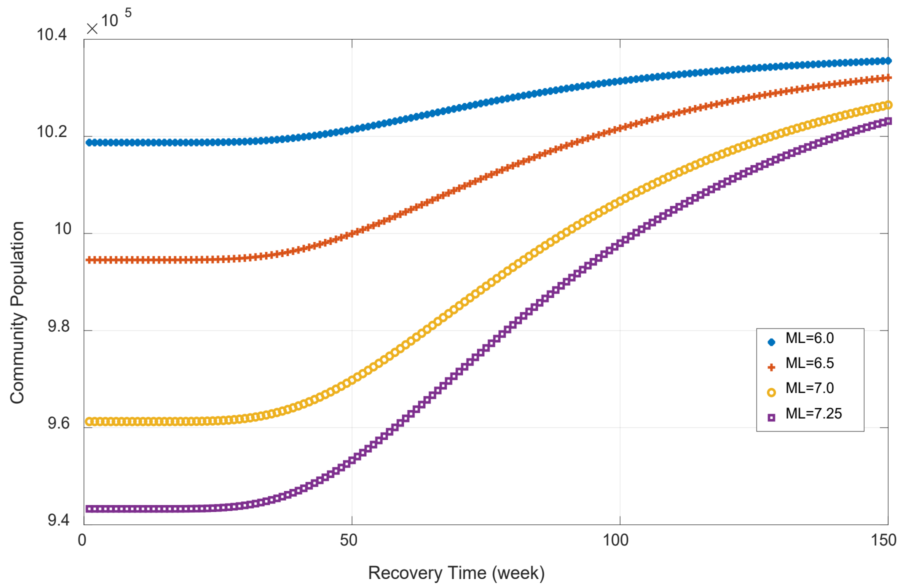

Figure 6.7 Community population over time

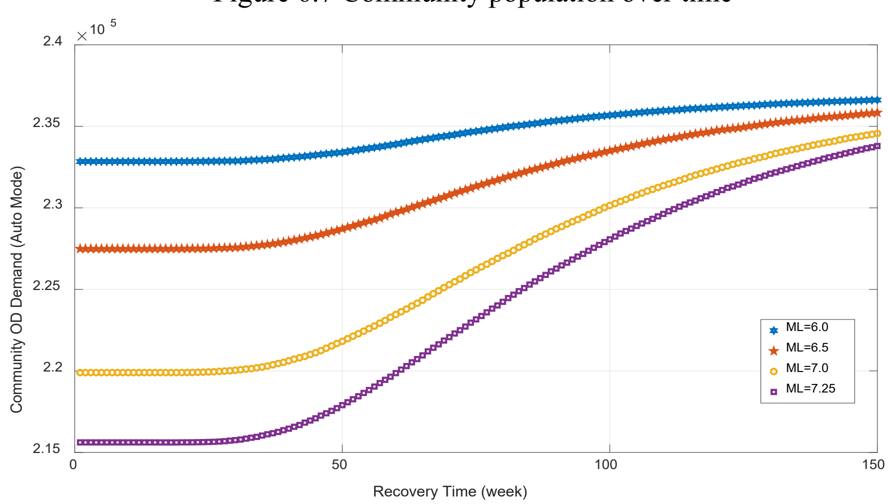

Figure 6.8 Community OD demand over time

Considering the lack of the specific work-zone traffic accident data in the Memphis area, this study uses the work-zone traffic accident model by Ozturk et al. (2013) to model the traffic safety in work zones.

Their model uses the Negative Binomial regression based on the observed data in the State of New Jersey. The traffic accident model of fully functioning roads adopted in this study is based on the observed data in Tennessee to estimate the travel safety of roads with moderate or lower damages (Kiattikomol 2005). Based on the existing studies, the case study assumes the speed limits are 55 mph and 45 mph for fully functional roads and work zones, respectively (Mannering 2007; Mekker et al. 2016). Considering the trivial effects of ramps and intersections on traffic accidents according to the studies summarized by Ozturk et al. (2013), this case study assumes no ramp and intersection on the links. Since all roads are typical 4-lane roads, the numbers of operating and closed lanes are both two for the road situation in Fig. 6.2. Based on the available information, the traffic accident frequency of road i is expressed as:

$$\lambda_i = \begin{cases} 2 \times 10^{-10} \cdot {L_i}^{0.7856} {ADT_i}^{2.26}, & Fully\ functional\ roads \\ 0.0799 \cdot {L_i}^{0.477} {ADT_i}^{0.512}, & Road\ with\ work\ zones \end{cases} \tag{6.18}$$

where L_i is the length of link/road segment i ; ADT_i is the average daily traffic per lane of road segment i. ADT_i can be derived from the community travel demand and the traffic assignment method. The link lengths can be estimated from the longitudes and latitudes (Table 6.4) of the links' starting and ending nodes.

6.3.3 Results

This study assumes that only bridge reconstruction will generate work zones during the post-earthquake recovery period. Assuming the above-mentioned earthquake has a Richter Magnitude of 7.25, Latin Hypercube sampling is used to simulate bridge damage scenarios with 10,000 samples. Based on the estimated travel demand (Fig. 6.8), the traffic simulation for the morning rush hour is conducted during the post-earthquake recovery stage through static traffic assignment. The expected system total travel time, total accident frequency, and resilience index are calculated using Eqs. (6.11-6.13 & 6.18). They are presented in Figs. 6.9-6.11 as functions of recovery time.

The box plots in Figs. 6.9-6.10 suggest both the expected total travel time and total accident frequency increase with time. Such phenomena are caused by the increasing travel demand along with the recovery process of the population and thus are in accordance with reality. The increased percentages of expected TTT and TAF are 3.49% and 14.02%, respectively. The smaller increase in TTT may be caused by the fact that the traffic volumes on most links are lower than their capacities, which reflects trivial increase in their travel time. Only a few links with high traffic volumes have significant traffic delays and contribute to the increase in TTT. The larger increase in TAF may result from the increased traffic volume. Unlike link travel time, traffic accident frequency is more sensitive to link traffic volume, no matter if it is below the link traffic capacity or not (Eq. (6.18)). Fig. 6.11 shows the expected RI also increases with the recovery time despite the increase in TTT and TAF. It is because the resilience index is related to not only the expected total travel time and accidents on the transportation network, but also the community population it serves. As a result, the system resilience index of the transportation network gradually increases during the recovery period.

The pre-hazard TTT and TAF are 1389 and 4888, respectively, assuming no link damage. Figs. 6.9-6.10 show TTT and TAF for most sampled network damage scenarios fall in ranges of [1555, 1684] and [5494, 7145], respectively. The results show TAF is more sensitive to bridge damages with larger variations as compared to TTT. The less deviated TTT may be caused by the existence of many redundant links, so there are always alternative paths with similar travel time in case of link damage. The larger variations in TAF may result from partially functional bridges with work zones. It corroborates the traffic accident model in Eq. (6.18), which shows roads with work zones tend to have higher traffic accident frequencies than fully functional roads unless the traffic is very heavy. This observation also proves the significance of considering work-zone traffic accidents when simulating transportation resilience during the post-earthquake recovery stage, especially when the recovery takes a very long time. Although the expected TTT in this case study is relatively stable, TAF presents a time-evolving difference of 14.02%, which is non-negligible. Like traffic efficiency, traffic safety is also critical to the travel experience of the remaining and recovering residents. The considerable difference in TAF throughout the recovery stage confirms the significance of simulating the time-evolving community population and travel demand. Also, as mentioned above, many countries and regions have many older buildings designed using codes with lower standards or even pre-code seismic standards (Bilham 2010; Ilki and Celep 2012; and Wang 2008). For those areas, the impact of earthquakes on population, travel demand, and traffic patterns can be more significant so that both TTT and TAF may show considerable changes during the recovery stage.

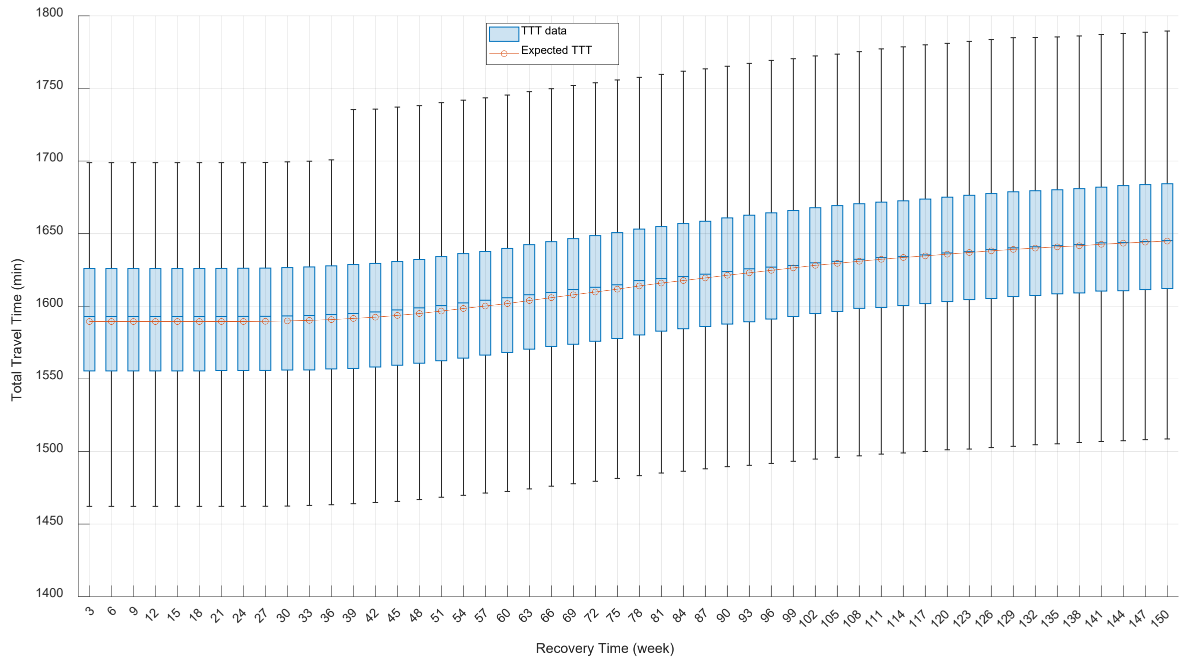

Figure 6.9 The total travel time of the system

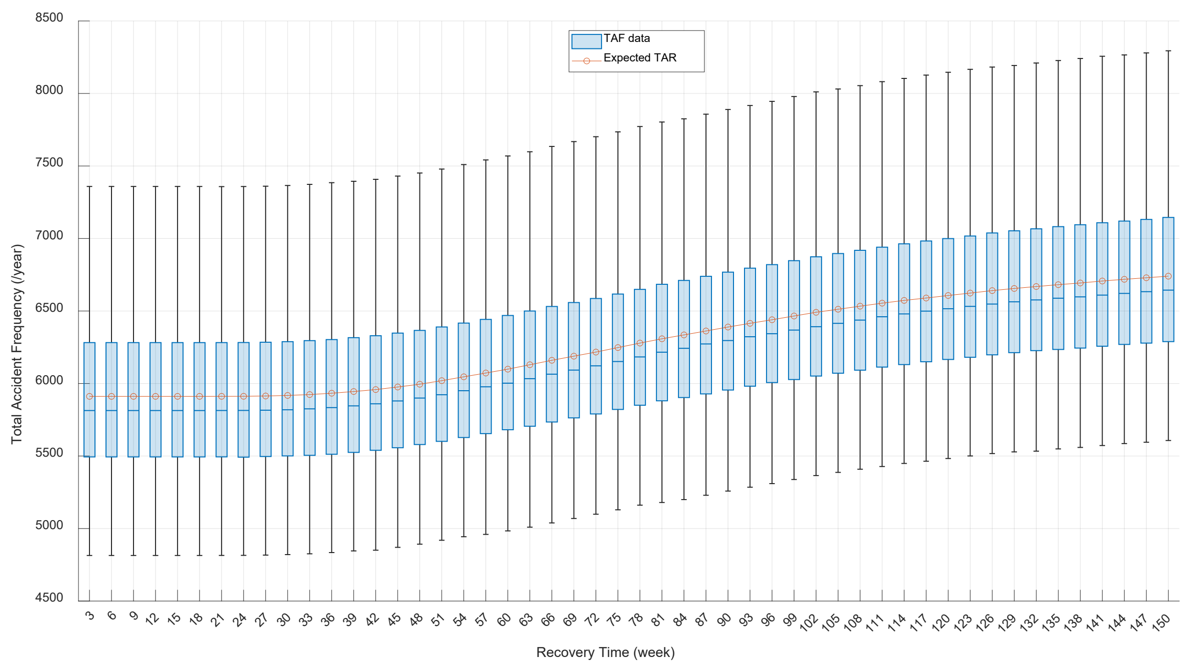

Figure 6.10 The total accident frequency of the system

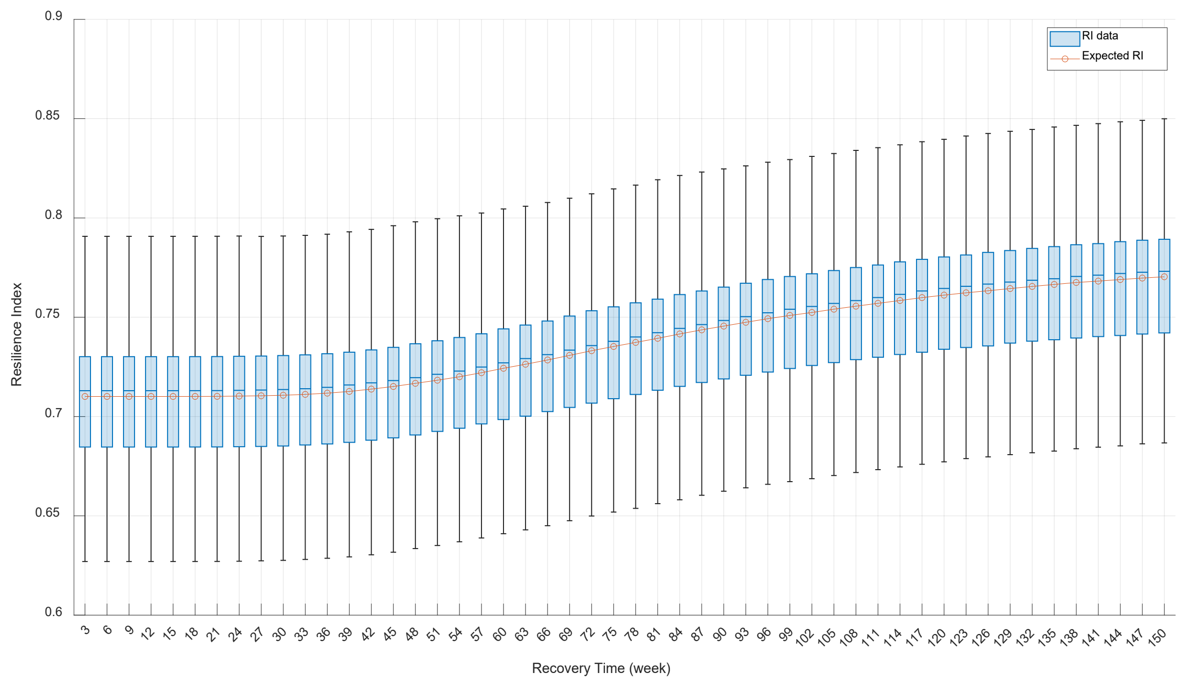

Figure 6.11 System resilience index

6.3.4 Post-earthquake bridge reconstruction planning

Due to the usually limited resources, it is not realistic to reconstruct all the damaged bridges simultaneously. Without losing generality, this study assumes that only one bridge can be repaired at a time for demonstrative purposes. So, it is meaningful to repair the most critical bridges first. In this study, the most critical bridges will be identified based on their impacts on the system resilience index. Considering the computational complexity to include the bridge damage uncertainties in the optimization, a specific bridge damage scenario was assumed in Table 6.8 to demonstrate the reconstruction planning. Since moderately or less damaged bridges will fully recover their traffic-carrying capacities (Padgett and DesRoches 2007) before the recovery stage, all bridges to be repaired have suffered either extensive or complete damage. Due to the lack of reconstruction information and the highly discrete bridge reconstruction time, the repair time of different bridges is randomly assumed for demonstrative purposes. The post-earthquake time-evolving travel demand after the Richter Magnitude 7.25 earthquake (Fig. 6.8) is used to carry out the reconstruction planning optimization. The effect of an intuitive reconstruction sequence (simply following the order of bridge numbers) on system resilience index is also investigated for comparison purposes. The goal here is to identify which plan is better in terms of meeting the demands of the remaining and recovering residents in the community.

Based on Eqs. (6.14-6.15), the bridge reconstruction optimization is derived using the Greedy Algorithm. The optimal reconstruction sequence of the bridges is 3, 9, 11, 14, 7, 28, 10, 18, 25, 16, 24, 13, 26, 8. For both the optimal and intuitive reconstruction plans, their corresponding resilience indexes as functions of recovery time are presented in Fig. 6.12. Fig. 6.12 shows both curves start and end at the same values, which conforms to the reality that the two reconstruction plans have the same starting and ending bridge damage situations. The curve of the resilience index for the optimal plan increases fast at the beginning and slows down at $t = 140\ weeks$. The curve of the resilience index for the intuitive plan rises slowly during the first 50 weeks, has similar increasing speed as the optimal plan after that, and boosts at $t = 179\ weeks$. The curve of the resilience index for the optimal plan has higher values throughout the recovery stage, which means the optimal reconstruction plan provides a better transportation experience to the remaining and recovery residents. This phenomenon is likely because the critical bridges have received priority in the optimal plan. It is also found that all seven bridges with "extensive" damage states except bridge 16 will be fixed first. Although bridges losing full functionality may have more significant impact on the capacity of the transportation network than those only losing partial functionality, extensively damaged bridges have bigger impacts on the overall system resilience since TAF is very sensitive to the existence of work zones. In contrast, TTT is more stable than TAF due to many redundant links according to the above analysis.

Table 6.8 Bridge repair times by damage states

Bridge #	Damage state	Repair time (week)
3	Extensive	10
7	Extensive	12
8	Complete	16
9	Extensive	10
10	Complete	13
11	Extensive	12
13	Complete	15
14	Extensive	11
16	Extensive	13
18	Complete	14
24	Complete	10
25	Complete	13
26	Complete	16
28	Extensive	14

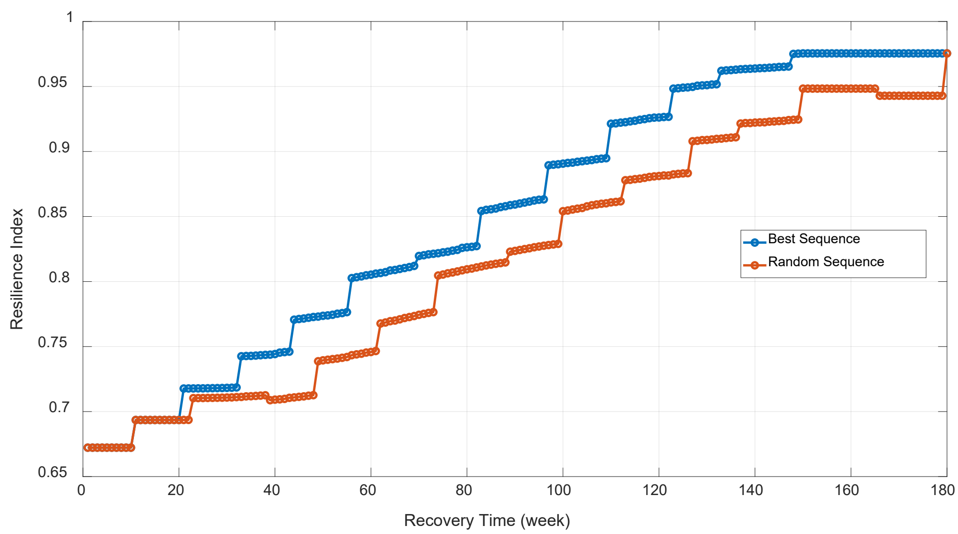

Figure 6.12 Resilience index for two repair sequences

6.4 Conclusions

Transportation networks may remain disrupted for years and significantly affect the traffic efficiency and safety of the community's remaining and recovering residents during the post-earthquake recovery stage. A framework to model the time-dependent resilience performance of transportation networks during the post-earthquake recovery stage was developed with a focus on the transportation experience of the current and future residents of the attacked community. To simulate the uncertainties in bridge damage scenarios, the seismic attenuation law, bridge fragility functions, and Latin Hypercube sampling method were adopted in this study to generate numerous network disruption scenarios. The building fragility functions, building recovery information, community demographics, and the MPO model were applied to estimate the time-evolving community population and travel demand. The modified BPR function for work zones, static traffic assignment method, and work-zone traffic accident model derived based on Negative Binomial regression were applied to simulate the traffic efficiency and travel safety during the morning rush hour throughout the recovery stage. This study defined a new time-dependent integrated resilience index to assess the transportation performance experienced by the time-evolving community residents. The methodology incorporates uncertainties into link degradation to make the resilience modeling more reliable. The proposed resilience index was used to derive the optimal bridge construction plan to maximize the overall benefits of the time-evolving community residents. Finally, the proposed methodology was demonstrated in Shelby County, Tennessee, which belongs to an earthquake-prone area. A comparative analysis was conducted in the reconstruction planning to investigate the effects of the optimal reconstruction plan on transportation resilience during the post-earthquake recovery stage.

It is found that earthquakes may significantly affect the community population and travel demand and, in turn, impact the time-dependent travel time, traffic accident, and system resilience index. Therefore, the model is more realistic and reliable than traditional methodologies that did not reasonably consider the time-evolving population and travel demand. The reconstruction planning emphasized the significance of focusing on the needs of adopting a more realistic population group instead of a fixed resident group derived from the pre-hazard population. This study still has some limitations: due to the lack of reliable data, some assumptions had to be made, including some specific parameters related to buildings and bridges, the bridge reconstruction time, the travel behavior of residents, etc.; some factors that may affect the traffic simulation were not incorporated in this study, including traffic signal lights and the correlation between traffic delay and accidents; and the reconstruction planning was scenario-based due to the computational complexity when both time-evolving feature and uncertainty get involved at the same time. However, despite these assumptions and simplifications in the demonstrative study, the proposed methodology is general enough to be applied to conduct a more advanced study once more reliable and site-specific data and more powerful computational technologies becomes available in the future. Finally, although this methodology was proposed based on earthquakes, it can be easily adapted and applied to the long-term recovery stage involving other hazards or incidents causing similar disruptions and time-evolving population and travel demand.

CHAPTER 7 SUMMARY OF THE DISSERTATION AND FUTURE STUDIES

7.1 Summary and conclusions

The contributions and findings of this dissertation are summarized in the following, which correspond to Chapters 2 - 6:

Chapters 2 - 4 were about transportation resilience during post-earthquake emergency response stage with focuses on emergency medical response based on EMS vehicles, private vehicles, and the combined service of both, respectively. These three chapters introduced new resilience indicators related to transportation efficiency and accessibility to assess the transportation performance resilience. Risk-informed hazard mitigation plans were developed in these chapters, including link importance factor, pre-hazard bridge reinforcement planning, and the reasonable number of EMS vehicles. The specific contributions of each chapter are summarized in the following.

Chapter 2 built a framework to consider the interactions between infrastructure, people, and hazards. The proposed framework was demonstrated in a virtual community. Also, a parametric study and the location optimization of a new medical center were conducted. The results indicate that seismic magnitudes significantly affect the number of severely injured individuals requiring emergency medical assistance. The proportion of different bridge types plays a vital role in total rescue time of the network. The locations and number of EMS medical centers notably impact the total rescue time as they influence the accessibility of emergency medical services.

Chapter 3 introduced methods to fully consider the network redundancy, search and rescue activities, and life vitality decay on the way to hospitals. The proposed methodology was demonstrated in Shelby

County, Tennessee. Through a parametric study, the effects of Richter magnitude on multiple parameters were investigated. The pre-hazard bridge strengthening planning was optimized based on the resilience index, using detailed budget information. The results revealed a significant impact of Richter magnitude on the aforementioned factors, including the number of injured individuals, the potential for saving lives, and network redundancy. Consequently, seismic magnitude played a notable role in determining the connectivity between different zones and their designated hospitals, as well as the overall performance of emergency medical response.

Chapter 4 proposed a methodology to reasonably estimate the emergency travel demand and quantify the functionality of damaged links during the post-earthquake emergency response stage. The proposed model was applied to a virtual community. To examine the disparities between dynamic and static traffic assignment methods, a comparative study was conducted. The findings demonstrate the superior potential of the dynamic traffic assignment method in delivering more realistic and reliable outcomes compared to the static traffic assignment method.

Chapters 5 and 6 were about transportation resilience during post-earthquake recovery stage, focusing on the effects of partially damaged road segments and time-evolving travel demand, respectively. Both chapters introduced new resilience indicators related to transportation efficiency and safety to assess transportation performance resilience. Post-earthquake bridge reconstruction planning was induced in these chapters to assist risk-informed decision-making. Specifically, Chapter 5 introduced a method to model the traffic performance on roads with work zones and incorporated traffic accident models to investigate travel safety. Chapter 6 proposed a methodology to reasonably estimate the time-evolving community population and travel demand during the post-earthquake recovery stage. All these contributions can help make the transportation resilience modeling during the post-earthquake recovery stage and the risk-informed reconstruction planning more rational and dependable.

The methodologies in Chapters 5 and 6 were applied to communities situated in earthquake-prone areas. It was found in Chapter 5 that the existence of work zones may greatly affect travel time and traffic accidents, and therefore it is significant to simulate the partially functional roads caused by bridge damage in transportation resilience modeling. It was found in Chapter 6 that the community population and travel demand can be significantly affected by earthquakes, subsequently impacting the time-dependent travel time, traffic accident rates, and system resilience index. In the reconstruction planning, a comparative analysis was conducted in Chapter 6 to investigate the effects of the optimal reconstruction plan on transportation resilience during the post-earthquake recovery stage. The reconstruction planning emphasized the significance of focusing on the needs of adopting a more realistic population group instead of a fixed resident group derived from the pre-hazard population.

7.2 Directions for future research

Some possible improvements and extensions in the future based on the current research are discussed in the following.

a) Resilience of transportation networks during post-earthquake emergency response stage

The studies have adopted various assumptions due to the lack of data, including search-and-rescue information, the relationship between infrastructure damage states and their performance, and detailed emergency traffic composition. More sophisticated and advanced studies on a transportation network can be conducted in the future when more site-specific data becomes available.

The studies in this dissertation only considered bridge damage and building debris as causes of link degradation. Future studies need to incorporate all types of link damages to simulate the network degradation more accurately, including bridge damages, building debris, obstacles, and pavement damages.

Also, the studies did not consider the interactions between EMS vehicles and private vehicles, functionality of hospitals, and extreme situations when almost all links are damaged in the network. Future studies can be conducted to improve these aspects.

b) Resilience of transportation networks during post-earthquake recovery stage

Like the studies about the post-earthquake emergency response stage, many assumptions have been made, including some specific parameters related to buildings and bridges, the bridge reconstruction times, the travel behavior of residents, etc. So, some specific observations may not be accurate for the case study communities. Once more data becomes available in the future, more insightful and advanced studies on a community can be conducted in the future.

Some factors that may affect the traffic simulation were not incorporated in this dissertation, e.g., the correlation between traffic delays and accidents, which can be considered in future studies to make the simulation more reliable.

REFERENCES

Adachi, T., & Ellingwood, B. (2007). Impact of infrastructure interdependency and spatial correlation of seismic intensities on performance assessment of a water distribution system. In Proceedings of the 10th International Conference on Applications of Statistics and Probability in Civil Engineering.

Akiyama, M., Frangopol, D. M., & Ishibashi, H. (2020). Toward life-cycle reliability-, risk-and resilience-based design and assessment of bridges and bridge networks under independent and interacting hazards: emphasis on earthquake, tsunami and corrosion. Structure and Infrastructure Engineering, 16(1), 26-50.

Alipour, A., & Shafei, B. (2016). Seismic resilience of transportation networks with deteriorating components. Journal of Structural Engineering, 142(8), C4015015.

Argyroudis, S. A., Mitoulis, S. A., Hofer, L., Zanini, M. A., Tubaldi, E., & Frangopol, D. M. (2020). Resilience assessment framework for critical infrastructure in a multi-hazard environment: Case study on transport assets. Science of The Total Environment, 714, 136854.

Argyroudis, S. A., Mitoulis, S. A., Winter, M. G., & Kaynia, A. M. (2019). Fragility of transport assets exposed to multiple hazards: State-of-the-art review toward infrastructural resilience. Reliability Engineering & System Safety, 191, 106567.

Atkinson, G. M., & Boore, D. M. (1995). Ground-motion relations for eastern North America. Bulletin of the Seismological Society of America, 85(1), 17-30.

Atkinson, G. M., & Boore, D. M. (2006). Earthquake ground-motion prediction equations for eastern North America. Bulletin of the seismological society of America, 96(6), 2181-2205.

Aydin, N. Y., Duzgun, H. S., Heinimann, H. R., Wenzel, F., & Gnyawali, K. R. (2018). Framework for improving the resilience and recovery of transportation networks under geohazard risks. International journal of disaster risk reduction, 31, 832-843.

Beamon, B. M., & Kotleba, S. A. (2006). Inventory modelling for complex emergencies in humanitarian relief operations. International Journal of Logistics: Research and Applications, 9(1), 1-18.

Bell, M. (2000). "A game theory approach to measuring the performance reliability of transport networks". Transportation Research Part B: Methodological, 34(6), 533-545.

Berdica, K. (2002). An introduction to road vulnerability: what has been done, is done and should be done. Transport policy, 9(2), 117-127.

Bilham, R. (2010). Lessons from the Haiti earthquake. Nature, 463(7283), 878-879.

Blackman, D., Nakanishi, H., & Benson, A. M. (2017). Disaster resilience as a complex problem: Why linearity is not applicable for long-term recovery. Technological Forecasting and Social Change, 121, 89-98.

Boakye, J., Guidotti, R., Gardoni, P., & Murphy, C. (2022). The role of transportation infrastructure on the impact of natural hazards on communities. Reliability Engineering & System Safety, 219, 108184.

Bocchini, P., & Frangopol, D. M. (2012a). Restoration of bridge networks after an earthquake: Multicriteria intervention optimization. Earthquake Spectra, 28(2), 426-455.

Bocchini, P., & Frangopol, D. M. (2012b). Optimal resilience-and cost-based postdisaster intervention prioritization for bridges along a highway segment. Journal of Bridge Engineering, 17(1), 117-129.

Bruneau, M., Chang, S. E., Eguchi, R. T., Lee, G. C., O'Rourke, T. D., Reinhorn, A. M., ... & Von Winterfeldt, D. (2003). A framework to quantitatively assess and enhance the seismic resilience of communities. Earthquake spectra, 19(4), 733-752.

Campbell, K. W. (1981). Near-source attenuation of peak horizontal acceleration. Bulletin of the Seismological Society of America, 71(6), 2039-2070.

Casotto, C., Silva, V., Crowley, H., Nascimbene, R., & Pinho, R. (2015). Seismic fragility of Italian RC precast industrial structures. Engineering Structures, 94, 122-136.

Chandrasekaran, S., & Banerjee, S. (2016). Retrofit optimization for resilience enhancement of bridges under multihazard scenario. Journal of Structural Engineering, 142(8), C4015012.

Chang, L., Peng, F., Ouyang, Y., Elnashai, A. S., & Spencer Jr, B. F. (2012). Bridge seismic retrofit program planning to maximize postearthquake transportation network capacity. Journal of Infrastructure Systems, 18(2), 75-88.

Chang, L., Elnashai, A. S., & Spencer Jr, B. F. (2012). Post-earthquake modelling of transportation networks. Structure and infrastructure Engineering, 8(10), 893-911.

Chang, S. E., & Nojima, N. (2001). Measuring post-disaster transportation system performance: the 1995 Kobe earthquake in comparative perspective. Transportation Research Part A: Policy and Practice, 35(6), 475-494.

Chang, S. E., & Shinozuka, M. (2004). Measuring improvements in the disaster resilience of communities. Earthquake spectra, 20(3), 739-755.

Chen, A., Yang, H., Lo, H., and Tang, W. (2002). Capacity reliability of a road network: an assessment methodology and numerical results. Transportation Research Part B: Methodological, 36(3), 225-252.

Chen, Y. W., & Tzeng, G. H. (1999). A fuzzy multi-objective model for reconstructing the post-quake road-network by genetic algorithm. International Journal of Fuzzy Systems, 1(2), 85-95.

Choi, E., DesRoches, R., and Nielson, B. (2004). Seismic fragility of typical bridges in moderate seismic zones. Engineering Structures, 26(2), 187-199.

Cho, S., Gordon, P., Richardson, H. W., Moore, J. E., & Shinozuka, M. (2000). Analyzing transportation reconstruction network strategies: a full cost approach. Review of Urban & Regional Development Studies, 12(3), 212-227.

Cimellaro, G. P., Reinhorn, A. M., & Bruneau, M. (2010). Seismic resilience of a hospital system. Structure and Infrastructure Engineering, 6(1-2), 127-144.

Clark, S., and Watling, D. (2005). Modelling network travel time reliability under stochastic demand. Transportation Research Part B: Methodological, 39(2), 119-140.

Coburn, A. W., Spence, R. J. S., and Pomonis, A. (1992). Factors determining human casualty levels in earthquakes: mortality prediction in building collapse. In Proceedings of the 10th World Conference on Earthquake Engineering, 5989-5994.

Cooney, D. R., Wojcik, S., Seth, N., Vasisko, C., & Stimson, K. (2013). Evaluation of ambulance offload delay at a university hospital emergency department. International Journal of Emergency Medicine, 6(1), 1-4.

Costa, C., Figueiredo, R., Silva, V., & Bazzurro, P. (2020). Application of open tools and datasets to probabilistic modeling of road traffic disruptions due to earthquake damage. Earthquake Engineering & Structural Dynamics, 49(12), 1236-1255.

Day, J. M. (2014). Fostering emergent resilience: the complex adaptive supply network of disaster relief. International Journal of Production Research, 52(7), 1970-1988.

Dalal, J., & Üster, H. (2017). Combining Worst Case and Average Case Considerations in an Integrated Emergency Response Network Design Problem. Transportation Science.

D'este, G. M., and Taylor, M. A. (2003). Network vulnerability: an approach to reliability analysis at the level of national strategic transport networks. In: The Network Reliability of transport Proceedings of the first international symposium of transportation network reliability (INSTR), 23-44.

Di Ludovico, D., D'Ovidio, G., & Santilli, D. (2020). Post-earthquake reconstruction as an opportunity for a sustainable reorganisation of transport and urban structure. Cities, 96, 102447.

Dijkstra, E. (1959). A note on two problems in connexion with graphs. Numerische Mathematik, 1(1), pp.269-271.

Djalali, A., Khankeh, H., Öhlén, G., Castrén, M., & Kurland, L. (2011). Facilitators and obstacles in pre-hospital medical response to earthquakes: a qualitative study. Scandinavian journal of trauma, resuscitation and emergency medicine, 19(1), 1-9.

Dong, Y., & Frangopol, D. M. (2015). Risk and resilience assessment of bridges under mainshock and aftershocks incorporating uncertainties. Engineering Structures, 83, 198-208.

Du, Z., and Nicholson, A. (1997). Degradable transportation systems: Sensitivity and reliability analysis. Transportation Research Part B: Methodological, 31(3), 225-237.

Eckstein, M., & Chan, L. S. (2004). The effect of emergency department crowding on paramedic ambulance availability. Annals of emergency medicine, 43(1), 100-105.

Edrissi, A., Nourinejad, M., and Roorda, M. (2015). Transportation network reliability in emergency response. Transportation Research Part E: Logistics and Transportation Review, 80, 56-73.

EMS Statistics. (2017). Naemt.org, http://www.naemt.org/About_EMS/statistics.aspx (May 19, 2017).

El-Anwar, O., Ye, J., & Orabi, W. (2015). Efficient optimization of post-disaster reconstruction of transportation networks. Journal of Computing in Civil Engineering, 30(3), 04015047.

Ellingwood, B, Cutler, H., Gardoni, P., Peacock, W., van de Lindt, J. and Wang, N. (2016). The Centerville virtual community: a fully integrated decision model of interacting physical and social infrastructure systems, Journal of Sustainable and Resilient Infrastructure, 1, 3-4, 95-107.

Erlander, S., & Stewart, N. F. (1990). The gravity model in transportation analysis: theory and extensions (Vol. 3). Vsp.

Federal Highway Administration. (2018). Average Vehicle Occupancy Factors for Computing Travel Time Reliability Measures and Total Peak Hour Excessive Delay Metrics. Retrieved from https://www.fhwa.dot.gov/tpm/guidance/avo_factors.pdf

Feng, K., Li, Q., & Ellingwood, B. R. (2020). Post-earthquake modelling of transportation networks using an agent-based model. Structure and Infrastructure Engineering, 16(11), 1578-1592.

FHWA. (2002). Bicycle Lanes. Retrieved February 25, 2022, from https://www.safety.fhwa.dot.gov/ped_bike/univcourse/pdf/swless15.pdf

Frank, M., & Wolfe, P. (1956). An algorithm for quadratic programming. Naval research logistics quarterly, 3(1-2), 95-110.

Freckleton, D., Heaslip, K., Louisell, W., & Collura, J. (2012). Evaluation of resiliency of transportation networks after disasters. Transportation Research Record: Journal of the Transportation Research Board, (2284), 109-116.

Ganin, A. A., Kitsak, M., Marchese, D., Keisler, J. M., Seager, T., & Linkov, I. (2017). Resilience and efficiency in transportation networks. Science advances, 3(12), e1701079.

García-Segura, T., Yepes, V., & Frangopol, D. M. (2017). Multi-objective design of post-tensioned concrete road bridges using artificial neural networks. Structural and Multidisciplinary Optimization, 56(1), 139-

150.

Garber, N. J., & Zhao, M. (2002). Distribution and characteristics of crashes at different work zone locations in Virginia. Transportation Research Record, 1794(1), 19-25.

Gardoni, P., Der Kiureghian, A., & Mosalam, K. M. (2002). Probabilistic capacity models and fragility estimates for reinforced concrete columns based on experimental observations. Journal of Engineering Mechanics, 128(10), 1024-1038.

Gardoni, P., Mosalam, K. M., & der Kiureghian, A. (2003). Probabilistic seismic demand models and fragility estimates for RC bridges. Journal of Earthquake Engineering, 7(spec01), 79-106.

Gauthier, P., Furno, A., & El Faouzi, N. E. (2018). Road network resilience: how to identify critical links subject to day-to-day disruptions. Transportation research record, 2672(1), 54-65.

Guo, J., Huang, W., and Williams, B. (2015). Real time traffic flow outlier detection using short-term traffic conditional variance prediction. Transportation Research Part C: Emerging Technologies, 50, 160-172.

Hadjidemetriou, G., Herrera Fernandez, M. H., & Parlikad, A. (2021). Road Network Layout Planning based on Evaluation of Connectivity and Asset Criticality.

Hafeez, G., Doudak, G., & McClure, G. (2018). Establishing the fundamental period of light-frame wood buildings on the basis of ambient vibration tests. Canadian Journal of Civil Engineering, 45(9), 752-765.

Han, K., Eve, G., & Friesz, T. L. (2019). Computing dynamic user equilibria on large-scale networks with software implementation. Networks and Spatial Economics, 19(3), 869-902.

Hassan, E. M., & Mahmoud, H. (2019). Full functionality and recovery assessment framework for a hospital subjected to a scenario earthquake event. Engineering Structures, 188, 165-177.

Hazus, E. L. E. M. (1997). Technical manual. National Institute of Building for the Federal Emergency

Management Agency, Washington (DC).

Hazus, E. L. E. M. (2020). Technical manual. National Institute of Building for the Federal Emergency Management Agency, Washington (DC).

Henao, A., & Marshall, W. E. (2019). The impact of ride-hailing on vehicle miles traveled. Transportation, 46(6), 2173-2194.

Holguín-Veras, J., Taniguchi, E., Jaller, M., Aros-Vera, F., Ferreira, F., and Thompson, R. (2014). The Tohoku disasters: Chief lessons concerning the post disaster humanitarian logistics response and policy implications. Transportation Research Part A: Policy and Practice, 69, 86-104.

Hou, G., Chen, S., Zhou, Y., & Wu, J. (2017). Framework of microscopic traffic flow simulation on highway infrastructure system under hazardous driving conditions. Sustainable and Resilient Infrastructure, 2(3), 136-152.

Hou, G., & Chen, S. (2019). An Improved Cellular Automaton Model for Work Zone Traffic Simulation Considering Realistic Driving Behavior. Journal of the Physical Society of Japan, 88(8), 084001.

Hou, G., Chen, S., & Bao, Y. (2022). Development of travel time functions for disrupted urban arterials with microscopic traffic simulation. Physica A: Statistical Mechanics and its Applications, 126961.

Horner, M. W., & Widener, M. J. (2011). The effects of transportation network failure on people's accessibility to hurricane disaster relief goods: a modeling approach and application to a Florida case study. Natural hazards, 59(3), 1619-1634.

Hsu, Y. T., & Fu, C. C. (2004). Seismic effect on highway bridges in Chi Chi earthquake. Journal of performance of constructed facilities, 18(1), 47-53.

Hu, Z. H., Sheu, J. B., & Xiao, L. (2014). Post-disaster evacuation and temporary resettlement considering panic and panic spread. Transportation research part B: methodological, 69, 112-132.

Huo, J.-R and Hwang, H. (1996). Attenuation of ground motions in central and eastern United States and its application, Technical report, Center for Earthquake Research and Information, The University of Memphis, Memphis, TN.

Husdal, J. (2004). Reliability and vulnerability versus cost and benefits. In Proc. 2nd Int. Symp. Transportation Network Reliability (INSTR). Christchurch, New Zealand ,180-186.

Hwang, H. H. M., Lin, H., & Huo, J. R. (1997). Site coefficients for design of buildings in eastern United States. Soil Dynamics and Earthquake Engineering, 16(1), 29-40.

Hwang, H., & Huo, J. R. (1997). Attenuation relations of ground motion for rock and soil sites in eastern United States. Soil Dynamics and Earthquake Engineering, 16(6), 363-372.

Hwang, S. J., Shu, K. H., Lain, J. D., & Yang, W. C. (2001). Renal replacement therapy at the time of the Taiwan Chi-Chi earthquake. Nephrology Dialysis Transplantation, 16(suppl_5), 78-82.

Ilki, A., & Celep, Z. (2012). Earthquakes, existing buildings and seismic design codes in Turkey. Arabian Journal for Science and Engineering, 37, 365-380.

Ip, W. H., & Wang, D. (2011). Resilience and friability of transportation networks: evaluation, analysis and optimization. IEEE Systems Journal, 5(2), 189-198.

Jaiswal, K., Wald, D., and D'Ayala, D. (2011). Developing Empirical Collapse Fragility Functions for Global Building Types. Earthquake Spectra, 27(3), 775-795.

Janson, B. N. (1991). Dynamic traffic assignment for urban road networks. Transportation Research Part B: Methodological, 25(2-3), 143-161.

Jenelius, E., Petersen, T., and Mattsson, L. (2006). Importance and exposure in road network vulnerability analysis. Transportation Research Part A: Policy and Practice, 40(7), 537-560.

Kagan, M. (2015). On equivalent resistance of electrical circuits. American Journal of Physics, 83(1), 53-63.

Kameshwar, S., Misra, S., & Padgett, J. E. (2020). Decision tree based bridge restoration models for extreme event performance assessment of regional road networks. Structure and Infrastructure Engineering, 16(3), 431-451.

Kang, P., Tang, B., Liu, Y., Liu, X., Liu, Z., Lv, Y., & Zhang, L. (2015). Medical efforts and injury patterns of military hospital patients following the 2013 Lushan earthquake in China: a retrospective study. International journal of environmental research and public health, 12(9), 10723-10738.

Kiattikomol, V. (2005). Freeway crash prediction models for long-range urban transportation planning. The University of Tennessee.

Kilanitis, I., & Sextos, A. (2019a). Integrated seismic risk and resilience assessment of roadway networks in earthquake prone areas. Bulletin of earthquake engineering, 17(1), 181-210.

Kilanitis, I., & Sextos, A. (2019b). Impact of earthquake-induced bridge damage and time evolving traffic demand on the road network resilience. Journal of traffic and transportation engineering (English edition), 6(1), 35-48.

Kimley-Horn and Associates, Inc., Cambridge Systematics, Inc., and HNTB. Technical Memorandum: Memphis Travel Demand Model Prepared for Memphis MPO, 2007.

Kiremidjian, A., Moore, J., Fan, Y. Y., Yazlali, O., Basoz, N., & Williams, M. (2007). Seismic risk assessment of transportation network systems. Journal of Earthquake Engineering, 11(3), 371-382.

Kondo, R., Shiomi, Y., and Uno, N. (2012). Network evaluation based on connectivity reliability and accessibility. In Network reliability in practice, 131-149.

Kozin, F., & Zhou, H. (1990). System study of urban response and reconstruction due to earthquake. Journal of Engineering Mechanics, 116(9), 1959-1972.

La Torre, F., Domenichini, L., & Nocentini, A. (2017). Effects of stationary work zones on motorway crashes. Safety science, 92, 148-159.

Lee, C., & Machemehl, R. B. (2005). Combined traffic signal control and traffic assignment: algorithms, implementation and numerical results. Southwest Region University Transportation Center, Center for Transportation Research, University of Texas at Austin.

Li, M., Vanberkel, P., & Carter, A. J. (2019). A review on ambulance offload delay literature. Health care management science, 22(4), 658-675.

Li, J., & Zhou, Y. (2020). Optimizing risk mitigation investment strategies for improving post-earthquake road network resilience. International journal of transportation science and technology, 9(4), 277-286.

Li, Z., Jin, C., Hu, P., & Wang, C. (2019). Resilience-based transportation network recovery strategy during emergency recovery phase under uncertainty. Reliability Engineering & System Safety, 188, 503-514.

Liao, T. Y., Hu, T. Y., & Ko, Y. N. (2018). A resilience optimization model for transportation networks under disasters. Natural Hazards, 1-21.

Lin, P., & Wang, N. (2017). Stochastic post-disaster functionality recovery of community building portfolios II: Application. Structural Safety, 69, 106-117.

Liu, K. (2022). GIS-based MCDM framework combined with coupled multi-hazard assessment for site selection of post-earthquake emergency medical service facilities in Wenchuan, China. International Journal of Disaster Risk Reduction, 73, 102873.

Liu, Z., Chen, H., Liu, E., & Hu, W. (2022). Exploring the resilience assessment framework of urban road network for sustainable cities. Physica A: Statistical Mechanics and its Applications, 586, 126465.

Liu, Z., Jacques, C. C., Szyniszewski, S., Guest, J. K., Schafer, B. W., Igusa, T., & Mitrani-Reiser, J. (2016). Agent-based simulation of building evacuation after an earthquake: coupling human behavior with structural response. Natural Hazards Review, 17(1), 04015019.

Liu, Y., McNeil, S., Hackl, J., & Adey, B. T. (2020). Prioritizing transportation network recovery using a resilience measure. Sustainable and Resilient Infrastructure, 1-12.

Liu, L., Yang, D. Y., & Frangopol, D. M. (2020). Network-level risk-based framework for optimal bridge adaptation management considering scour and climate change. Journal of Infrastructure Systems, 26(1), 04019037.

Liu, K., Zhai, C., & Dong, Y. (2021). Optimal restoration schedules of transportation network considering resilience. Structure and Infrastructure Engineering, 17(8), 1141-1154.

Lu, X., Cheng, Q., Xu, Z., Xu, Y., & Sun, C. (2019). Real-time city-scale time-history analysis and its application in resilience-oriented earthquake emergency responses. Applied Sciences, 9(17), 3497.

Mackie, K. R., & Stojadinović, B. (2006). Post-earthquake functionality of highway overpass bridges. Earthquake engineering & structural dynamics, 35(1), 77-93.

Mannering, F. (2007, January). Effects of interstate speed limits on driving speeds: Some new evidence. In Compendium of papers CD-ROM, Transportation Research Board 86th Annual Meeting.

Mannering, F. L., & Washburn, S. S. (2020). Principles of highway engineering and traffic analysis. John Wiley & Sons.

Manual, H. C. (2010). HCM2010. Transportation Research Board, National Research Council, Washington, DC, 1207.

Mahmassani, H., Hou, T., and Saberi, M. (2013). Connecting Networkwide Travel Time Reliability and the Network Fundamental Diagram of Traffic Flow. Transportation Research Record: Journal of the Transportation Research Board, 2391, 80-91.

Meisel, Z. F., Pines, J. M., Polsky, D., Metlay, J. P., Neuman, M. D., & Branas, C. C. (2011). Variations in ambulance use in the United States: the role of health insurance. Academic Emergency Medicine, 18(10), 1036-1044.

Mekker, M. M., Remias, S. M., Bunnell, W. A., Krohn, D. W., Cox, E. D., & Bullock, D. M. (2016). Variable speed limit study upstream of an Indiana work zone with vehicle matching. Transportation Research Record, 2555(1), 53-64.

Mete, H., and Zabinsky, Z. (2010). Stochastic optimization of medical supply location and distribution in disaster management. International Journal of Production Economics, 126(1), 76-84.

Merschman, E., Doustmohammadi, M., Salman, A. M., & Anderson, M. (2020). Postdisaster decision framework for bridge repair prioritization to improve road network resilience. Transportation research record, 2674(3), 81-92.

Miller-Hooks, E., Zhang, X., and Faturechi, R. (2012). Measuring and maximizing resilience of freight transportation networks. Computers & Operations Research, 39(7), 1633-1643.

Moya, L., Mas, E., Yamazaki, F., Liu, W., & Koshimura, S. (2020). Statistical analysis of earthquake debris extent from wood-frame buildings and its use in road networks in Japan. Earthquake Spectra, 36(1), 209-231.

Municode Library. (2022). Downtown District. Retrieved February 25, 2022, from https://library.municode.com/co/fort_collins/codes/land_use?nodeId=ART4DI_DIV4.16DODID

Muntasir Billah, A. H. M., & Shahria Alam, M. (2015). Seismic fragility assessment of highway bridges: a state-of-the-art review. Structure and Infrastructure Engineering, 11(6), 804-832.

Murakami, H., Takemoto, T., & Sakamoto, K. (2000, January). Study of search and rescue operations in the 1995 Hanshin-Awaji earthquake: analysis of labor work in relation with building types. In Proceedings of the 12th World Conference on Earthquake Engineering (Vol. 272, pp. 1-8).

Musson, R., Grünthal, G., and Stucchi, M. (2009). The comparison of macroseismic intensity scales. Journal of Seismology, 14(2), 413-428.

Naddaf, M. (2023). Turkey-Syria earthquake: what scientists know. Nature.

National Association of State EMS Officials. (2020). The 2020 National Emergency Medical Services Assessment. Falls Church, VA: NASEMSO.

Nia, M. S., Nafissi, N., & Moharamzad, Y. (2008). Survey of Bam earthquake survivors' opinions on medical and health systems services. Prehosp Disaster Med, 23(3), 263-268.

Nicholson, A. (2003). Transport Network Reliability Measurement and Analysis. TRANSPORTES, 11(2).

Nielson, B. G., & DesRoches, R. (2007). Analytical seismic fragility curves for typical bridges in the central and southeastern United States. Earthquake Spectra, 23(3), 615-633.

Nogal, M., Martinez-Pastor, B., O'Connor, A., & Caulfield, B. (2015). Dynamic restricted equilibrium model to determine statistically the resilience of a traffic network to extreme weather events. In Proceedings of the 12th International Conference on Applications of Statistics and Probability in Civil Engineering, ICASP12, Vancouver, Canada.

Nogal, M., O'Connor, A., Caulfield, B., & Brazil, W. (2016a). A multidisciplinary approach for risk analysis of infrastructure networks in response to extreme weather. Transportation Research Procedia, 14, 78-85.

Nogal, M., O'Connor, A., Caulfield, B., & Martinez-Pastor, B. (2016b). Resilience of traffic networks: From perturbation to recovery via a dynamic restricted equilibrium model. Reliability Engineering & System Safety, 156, 84-96.

Nogal, M., O'Connor, A., Martinez-Pastor, B., & Caulfield, B. (2017). Novel probabilistic resilience assessment framework of transportation networks against extreme weather events. ASCE-ASME Journal of Risk and Uncertainty in Engineering Systems, Part A: Civil Engineering, 3(3), 04017004.

Novak, D., and Sullivan, J. (2014). A link-focused methodology for evaluating accessibility to emergency services. Decision Support Systems, 57, 309-319.

Orabi, W., El-Rayes, K., Senouci, A. B., & Al-Derham, H. (2009). Optimizing postdisaster reconstruction planning for damaged transportation networks. Journal of Construction Engineering and Management, 135(10), 1039-1048.

Orabi, W., Senouci, A. B., El-Rayes, K., & Al-Derham, H. (2010). Optimizing resource utilization during the recovery of civil infrastructure systems. Journal of management in engineering, 26(4), 237-246.

Osei-Asamoah, A., & Lownes, N. E. (2014). Complex network method of evaluating resilience in surface transportation networks. Transportation Research Record, 2467(1), 120-128.

Ozturk, O., Ozbay, K., Yang, H., & Bartin, B. (2013, January). Crash frequency modeling for highway construction zones. In Transportation Research Board 92nd Annual Meeting (pp. 13-4555).

Padgett, J. E., & DesRoches, R. (2007). Bridge functionality relationships for improved seismic risk assessment of transportation networks. Earthquake Spectra, 23(1), 115-130.

Padgett, J. E., & DesRoches, R. (2009). Retrofitted bridge fragility analysis for typical classes of multispan bridges. Earthquake Spectra, 25(1), 117-141.

Padgett, J. E., Dennemann, K., & Ghosh, J. (2010). Risk-based seismic life-cycle cost–benefit (LCC-B) analysis for bridge retrofit assessment. Structural Safety, 32(3), 165-173.

Pan, X., Dang, Y., Wang, H., Hong, D., Li, Y., & Deng, H. (2022). Resilience model and recovery strategy of transportation network based on travel OD-grid analysis. Reliability Engineering & System Safety, 223, 108483.

Pigman, J. G., & Agent, K. R. (1990). Highway accidents in construction and maintenance work zones. Transportation Research Record, (1270).

Population in the U.S.-Google Public Data Explorer. (2017). Google.com, https://www.google.com/publicdata/explore?ds=kf7tgg1uo9ude_&met_y= population &idim=country:US&hl=en&dl=en (May 19, 2017).

Qian, Y., Wang, M., Kang, H., Zeng, J., and Liu, Y. (2012). Study on the Road Network Connectivity Reliability of Valley City Based on Complex Network. Mathematical Problems in Engineering, 2012, 1-14.

Radun, I., Radun, J., Kaistinen, J., Wedenoja, J., & Lajunen, T. (2022). Using personal cars for emergency transport of patients with life-threatening medical conditions: A pilot study. Journal of Transport & Health, 24, 101339.

Reinhorn, A. M., Barron-Corverra, R., and Ayala, A. G. (2001). Spectral evaluation of seismic fragility of structures". In Proceedings ICOSSAR,1-8.

Scott, D., Novak, D., Aultman-Hall, L., and Guo, F. (2006). Network Robustness Index: A new method for identifying critical links and evaluating the performance of transportation networks. Journal of Transport Geography, 14(3), 215-227.

Shinozuka, M., Zhou, Y., Kim, S., Murachi, Y., Banerjee, S., Cho, S., & Chung, H. (2008). Socio-economic effect of seismic retrofit implemented on bridges in the Los Angeles highway network (No. CA06-0145). California. Dept. of Transportation.

Somy, S., Shafaei, R., & Ramezanian, R. (2021). Resilience-based mathematical model to restore disrupted road-bridge transportation networks. Structure and Infrastructure Engineering, 1-16.

Sprung, M. J. (2018). Freight facts and figures 2017.

Statista. (2022). Average size of households in the U.S. 2021. Retrieved February 22, 2022, from https://www.statista.com/statistics/183648/average-size-of-households-in-the-us/

Stein, W. J., & Neuman, T. R. (2007). Mitigation strategies for design exceptions (No. FHWA-SA-07-011). United States. Federal Highway Administration. Office of Safety.

Steelman, J., & Hajjar, J. F. (2008). Capstone scenario applications of consequence-based risk management for the Memphis Testbed.

Sun, W., Bocchini, P., & Davison, B. D. (2020). Resilience metrics and measurement methods for transportation infrastructure: the state of the art. Sustainable and Resilient Infrastructure, 5(3), 168-199.

Tamima, U., & Chouinard, L. (2016). Development of evacuation models for moderate seismic zones: A case study of Montreal. International Journal of Disaster Risk Reduction, 16, 167-179.

Tamima, U., & Chouinard, L. (2017). Systemic seismic vulnerability of transportation networks and emergency facilities. Journal of Infrastructure Systems, 23(4), 04017032.

Tanaka, H., Iwai, A., Oda, J., Kuwagata, Y., Matsuoka, T., Shimazu, T., & Yoshioka, T. (1998). Overview of evacuation and transport of patients following the 1995 Hanshin-Awaji earthquake. The Journal of emergency medicine, 16(3), 439-444.

Tani, A., Yamamura, T., Waridashi, Y., Kawamura, H., & Takizawa, A. (2004, August). Simulation on rescue in case of earthquake disaster by multi-agent system. In Proceedings of the 13th World Conference on Earthquake Engineering, Vancouver, BC, Canada (pp. 1-6).

TRB (2010). Highway Capacity Manual. Transportation Research Board, National Research Council, Washington, DC, 1207.

US Bureau of Public Roads. Office of Planning. Urban Planning Division. (1964). Traffic Assignment Manual for Application with a Large, High Speed Computer. US Department of Commerce.

U.S. Census Bureau (2019). QuickFacts: Shelby County, Tennessee. Retrieved from: https://www.census.gov/quickfacts/shelbycountytennessee

U.S. Census Bureau (2021). American Community Survey 1-year estimates. Retrieved from Census Reporter Profile page for Shelby County, TN http://censusreporter.org/profiles/05000US47157-shelby-county-tn/

Üster, H., & Dalal, J. (2017). Strategic emergency preparedness network design integrating supply and demand sides in a multi-objective approach. IISE Transactions, 49(4), 395-413.

U.S. Population. Place Explorer - Data Commons. Retrieved November 5, 2022, from https://datacommons.org/place/country/USA?utm_medium=explore&mprop=count&popt=Person&hl=en#

Viriyasitavat, W., Bai, F., and Tonguz, O. (2011). Dynamics of Network Connectivity in Urban Vehicular Networks. IEEE Journal on Selected Areas in Communications, 29(3), 515-533.

Wakabayashi, H., & Kameda, H. (1992). Network performance of highway systems under earthquake effects: A case study of the 1989 Loma Prieta earthquake. In Proceedings of the US-Japan Workshop on

Earthquake Disaster Prevention for Lifeline Systems. Tsukuba Science City, Japan (Vol. 215232).

Wardrop, J. G. (1982). Some theoretical aspects of road traffic research. Proceedings of the Institute of Civil Engineers, (Part II), 325-378.

Washington, S. P., Karlaftis, M. G., & Mannering, F. (2010). Statistical and econometric methods for transportation data analysis. Chapman and Hall/CRC.

Wang, W. L., & van de Lindt, J. W. (2021). Quantitative modeling of residential building disaster recovery and effects of pre-and post-event policies. International Journal of Disaster Risk Reduction, 59, 102259.

Wang, W. L., & van de Lindt, J. W. (2022). Quantifying the effect of improved school and residential building codes for tornadoes in community resilience. Resilient Cities and Structures, 1(1), 65-79.

Wang, W., van De Lindt, J. W., Rosenheim, N., Cutler, H., Hartman, B., Sung Lee, J., & Calderon, D. (2021). Effect of residential building wind retrofits on social and economic community-level resilience metrics. Journal of Infrastructure Systems, 27(4), 04021034.

Wang, W. L., van De Lindt, J. W., Hartman, B., Cutler, H., Kruse, J. L., McAllister, T. P., & Hamideh, S. (2022). Determination of individual building performance targets to achieve community-level social and economic resilience metrics. Journal of Structural Engineering, 148(5), 04022045.

Wandling, M. W., Nathens, A. B., Shapiro, M. B., & Haut, E. R. (2018). Association of prehospital mode of transport with mortality in penetrating trauma: a trauma system–level assessment of private vehicle transportation vs ground emergency medical services. JAMA surgery, 153(2), 107-113.

Wandelt, S., Shi, X., & Sun, X. (2021). Estimation and improvement of transportation network robustness by exploiting communities. Reliability Engineering & System Safety, 206, 107307.

Wald, D., Quitoriano, V., Heaton, T., and Kanamori, H. (1999). Relationships between Peak Ground

Acceleration, Peak Ground Velocity, and Modified Mercalli Intensity in California. Earthquake Spectra, 15(3), 557-564.

Wakabayashi, H., and IIDA, Y. (1992). Upper and lower bounds of terminal reliability of road networks: an efficient method with Boolean algebra. Journal of Natural Disaster Science, 14(1), 29-44.

Wang, Z. (2008). A preliminary report on the Great Wenchuan Earthquake. Earthquake engineering and engineering vibration, 7(2), 225-234.

Wang, Z., & Jia, G. (2020). Efficient sample-based approach for effective seismic risk mitigation of transportation networks. Sustainable and Resilient Infrastructure, 5(6), 349-364.

Wang, W. L., & van de Lindt, J. W. (2021). Quantitative modeling of residential building disaster recovery and effects of pre-and post-event policies. International Journal of Disaster Risk Reduction, 59, 102259.

Wang, N., & Yuen, K. F. (2022). Resilience assessment of waterway transportation systems: Combining system performance and recovery cost. Reliability Engineering & System Safety, 108673.

Wardrop, J. G. (1952). Some theoretical aspects of road traffic research. Proceedings of the Institute of Civil Engineers, (Part II), 325-378.

Washington, S. P., Karlaftis, M. G., & Mannering, F. (2010). Statistical and econometric methods for transportation data analysis. Chapman and Hall/CRC.

Wen, T., Gao, Q., Chen, Y. W., & Cheong, K. H. (2022). Exploring the vulnerability of transportation networks by entropy: A case study of Asia–Europe maritime transportation network. Reliability Engineering & System Safety, 108578.

Weng, J., & Meng, Q. (2011). Analysis of driver casualty risk for different work zone types. Accident Analysis & Prevention, 43(5), 1811-1817.

Wu, Y., & Chen, S. (2019). Resilience modeling of traffic network in post-earthquake emergency medical response considering interactions between infrastructures, people, and hazard. Sustainable and Resilient Infrastructure, 4(2), 82-97.

Wu, Y., & Chen, S. (2023a). Resilience modeling and pre-hazard mitigation planning of transportation network to support post-earthquake emergency medical response. Reliability Engineering & System Safety, 230, 108918.

Wu, Y., & Chen, S. (2023b). Traffic resilience modeling for post-earthquake emergency medical response and planning considering disrupted infrastructure and dislocated residents. International Journal of Disaster Risk Reduction, 103754.

Wu, Y., Hou, G., & Chen, S. (2021). Post-earthquake resilience assessment and long-term restoration prioritization of transportation network. Reliability Engineering & System Safety, 211, 107612.

Xu, X., Chen, A., Jansuwan, S., Heaslip, K., & Yang, C. (2015). Modeling transportation network redundancy. Transportation Research Procedia, 9, 283-302.

Xu, X., Chen, A., Xu, G., Yang, C., & Lam, W. H. (2021). Enhancing network resilience by adding redundancy to road networks. Transportation research part E: logistics and transportation review, 154, 102448.

Yang, H., Ozbay, K., Ozturk, O., & Xie, K. (2015). Work zone safety analysis and modeling: a state-of-the-art review. Traffic injury prevention, 16(4), 387-396.

Yeh, C. T., Lin, Y. K., Yeng, L. C. L., & Huang, P. T. (2021). Reliability evaluation of a multistate railway transportation network from the perspective of a travel agent. Reliability Engineering & System Safety, 214, 107757.

Yi, F., & Tu, Y. (2018). An evaluation of the paired assistance to disaster-affected areas program in disaster recovery: The case of the Wenchuan earthquake. Sustainability, 10(12), 4483.

Yoon, S., Suh, W., & Lee, Y. J. (2021). Optimal decision making in post-hazard bridge recovery strategies for transportation networks after seismic events. Geomatics, Natural Hazards and Risk, 12(1), 2629-2653.

Zamanifar, M., & Seyedhoseyni, S. M. (2017). Recovery planning model for roadways network after natural hazards. Natural Hazards, 87(2), 699-716.

Zhang, N., & Alipour, A. (2020). Two-Stage Model for Optimized Mitigation and Recovery of Bridge Network with Final Goal of Resilience. Transportation Research Record, 2674(10), 114-123.

Zhang, C., Qin, J., Zhang, M., Zhang, H., & Hou, Y. (2019). Practical Road-Resistance Functions for Expressway Work Zones in Occupied Lane Conditions. Sustainability, 11(2), 382.

Zhang, W., & Wang, N. (2016). Resilience-based risk mitigation for road networks. Structural Safety, 62, 57-65.

Zhang, W., Wang, N., Nicholsonc, C., & Tehrani, M. H. (2018). A stage-wise decision framework for transportation network resilience planning. arXiv preprint arXiv:1808.03850.

Zhang, M., Yang, X., Zhang, J., & Li, G. (2022). Post-earthquake resilience optimization of a rural "road-bridge" transportation network system. Reliability Engineering & System Safety, 225, 108570.

Zhao, T., & Zhang, Y. (2020). Transportation infrastructure restoration optimization considering mobility and accessibility in resilience measures. Transportation Research Part C: Emerging Technologies, 117, 102700.

Zheng, S., Liu, Y., Lin, Y., Wang, Q., Yang, H., & Chen, B. (2022). Bridging Strategy for the Disruption of Metro Considering the Reliability of Transportation System: Metro and Conventional Bus

Network. Reliability Engineering & System Safety, 108585.

Zhou, Y., Banerjee, S., & Shinozuka, M. (2010). Socio-economic effect of seismic retrofit of bridges for highway transportation networks: a pilot study. Structure and Infrastructure Engineering, 6(1-2), 145-157.

Zhou, Y., Wang, J., & Sheu, J. B. (2019). On connectivity of post-earthquake road networks. Transportation Research Part E: Logistics and Transportation Review, 123, 1-16.

Zou, Q., & Chen, S. (2019). Enhancing resilience of interdependent traffic-electric power system. Reliability Engineering & System Safety, 191, 106557.

Zou, Q., & Chen, S. (2021). Resilience-based recovery scheduling of transportation network in mixed traffic environment: a deep-ensemble-assisted active learning approach. Reliability Engineering & System Safety, 215, 107800.

CURRICULUM VITAE

Yangang Wu

Education

Ph.D. Civil Engineering, 2015-2023
Colorado State University, Fort Collins, CO
Dissertation title: Resilience of transportation network during post-earthquake emergency and recovery stages
Advisor: Professor Suren Chen

M.S. Civil Engineering, 2012-2015
Tongji University, Shanghai, China
Thesis title: A method to optimize composite fore-fulcrum form travelers in single plane cable-stayed bridges
Advisor: Professor Dewei Chen

B.Eng. Civil Engineering, 2008-2012
Jilin University, Changchun, China

Publications

- ◻ Wu, Y., and Chen, S. (2023). Transportation resilience modeling and bridge reconstruction planning based on time-evolving travel demand during the post-earthquake recovery period. Sustainability, under review.
- ◻ Wu, Y., & Chen, S. (2023). Traffic resilience modeling for post-earthquake emergency medical response and planning considering disrupted infrastructure and dislocated residents. International Journal of Disaster Risk Reduction, 103754.
- ◻ Wu, Y., & Chen, S. (2023). Resilience modeling and pre-hazard mitigation planning of transportation network to support post-earthquake emergency medical response. Reliability Engineering & System Safety, 230, 108918.
- ◻ Wu, Y., Hou, G., & Chen, S. (2021). Post-earthquake resilience assessment and long-term restoration prioritization of transportation network. Reliability Engineering & System Safety, 211, 107612.
- ◻ Wu, Y., & Chen, S. (2019). Resilience modeling of traffic network in post-earthquake emergency medical response considering interactions between infrastructures, people, and hazard. Sustainable and Resilient Infrastructure, 4(2), 82-97.